DELIVERY OF PHOSPHONOFORMATE PRODRUGS

IAN WALKER

Doctor of Philosophy

UNIVERSITY OF ASTON IN BIRMINGHAM

December 1992

The University of Aston in Birmingham

DELIVERY OF PHOSPHONOFORMATE PRODRUGS

by

IAN WALKER

A thesis submitted for the degree of Doctor of Philosophy
1992

SUMMARY

AIDS dementia complex is a common neurological syndrome thought to result from the invasion of the CNS by HIV. Phosphonoformate has anti-HIV activity but due to its charged nature is excluded from the CNS by the blood-brain barrier. Lipophilic triesters of phosphonoformate designed to improve transport properties are unsuitable prodrugs due to their rapid and complicated hydrolysis, involving competitive P-O and P-C bond cleavage. Diesters, though hydrolytically stable, are considered too polar to passively diffuse into the CNS. Hydophilic drugs mimicking endogenous nutrients are known to be actively transported across the blood-brain barrier. In this thesis the possibility that diesters of phosphonoformate may be actively transported is investigated.

Triesters of phosphonoformate with labile aryl carboxyl esters were synthesised and their hydrolysis followed by ^{31}P NMR spectroscopy. The triesters were found to undergo rapid hydrolysis *via* P-C bond cleavage to the phosphite. Phosphonoformate diesters designed to be analogues of actively transported α-keto acids have been synthesised and fully characterised. Tyrosine-phosphonoformate and lipid-phosphonoformate conjugates have also been synthesised and characterised.

An *in vitro* model of the blood-brain barrier utilising confluent monolayers of porcine brain microvessel endothelial cells grown on a permeable support has been established. The presence of enzyme and antigen markers specific to the blood-brain barrier has been demonstrated for the endothelial cells and the diffusional properties of the model investigated with hydrophilic and lipophilic compounds. Active transport systems for α-keto acids and large amino acids have been identified in the endothelial cell monolayers using ^{14}C-pyruvate and ^{3}H-L-tyrosine respectively. Temperature and concentration dependence of the two systems have been demonstrated and transport constants calculated. Competition with ^{14}C-pyruvate transport was shown with other monocarboxylic acids including the anti-epileptic drug valproate. Stereospecificity was shown in that L-lactate inhibited pyruvate transport while D-lactate did not. Sodium methyl methoxycarbonylphosphonate, a phosphonoformate diester was shown not to compete for ^{14}C-pyruvate transport indicating that this compound has no affinity for the carrier. Competition with ^{3}H-L-tyrosine transport was shown with other large amino acids, including the anti-Parkinsonian agent L-dopa. Stereospecificity was shown using L- and D-tyrosine and L- and D-dopa. The tyrosine-phosphonoformate conjugate, which was stable under the experimental conditions, was shown to compete with ^{3}H-L-tyrosine transport indicating that it may be actively transported at the blood-brain barrier.

Thirty two triesters, diesters and monoesters of phosphonoformate, showed no activity in an anti-HIV screen above that attributable to hydrolysis to the parent compound.

Key words: Phosphonoformate, Prodrug, Blood-Brain Barrier, Active Transport.

DEDICATION

To Claire with all my love.

ACKNOWLEDGEMENTS

I would like to thank my supervisor, Dr Sally Freeman, for all her hard work, guidance and encouragement. When faced with confusion or failure, talking to Sally always made things appear clearer and gave me new enthusiasm.

I would like to thank my advisor, Dr William Irwin, for his invaluable assistance.

I would like to thank Dr Dave Nicholls for his guidance and practical assistance in the establishment of the cell culture system used in this research. I would not have been able to do this work without Dave and I am indebted to him.

Thanks also to Graham Smith for his excellent artwork.

I acknowledge and appreciate the financial support of the Medical Research Council AIDS-Directed Programme.

Finally, I would like to thank my family for their encouragement and support throughout my education and especially Claire for the last three years.

CONTENTS

ABBREVIATIONS AND SYMBOLS

A	Surface area
ABC	Avidin biotin complex
ADC	AIDS dementia complex
AIDS	Acquired immune deficiency syndrome
AO	Antisense oligonucleotides
Ar	Aryl
ARC	AIDS-related complex
A-System	Alanine-preferring system
ATP	Adenosine triphosphate
AZT	Zidovudine
BBB	Blood-brain barrier
BMEC	Brain microvessel endothelial cell
bp	Boiling point
bs	Broad singlet
BUI	Brain uptake index
cAMP	Cyclic adenosine monophosphate
C_{brain}	Brain concentration
cm	Centimetres
C_{plasma}	Plasma concentration

C_{ref}	Concentration of reference substance
C_{test}	Concentration of test substance
^{11}C	Carbon-11 isotope
^{14}C	Carbon-14 isotope
^{o}C	Degrees celsius
C_o	Concentration in donor chamber
C_r	Concentration in receiver chamber
$CDCl_3$	Deuterated chloroform
CI	Chemical ionisation (mass spectrometry)
CMV	Cytomegalovirus
^{13}C NMR	Carbon nuclear magnetic resonance spectroscopy
CNS	Central nervous system
d	Doublet
ddC	2',3'-Dideoxycytidine
ddI	2',3'-Dideoxyinosine
D	Membrane diffusion coefficient
D,L-NAM	D,L-2-Amino-7-bis[(2-chloroethyl)amino]-1,2,3,4-tetrahydro-2-naphthoic acid
DMSO-D_6	Deuterated dimethyl sulphoxide
DNA	Deoxyribonucleic acid
D_2O	Deuterated water

DPM	Decays per minute
E	Fractional loss of test substance
EC_{50}	Concentration of drug which reduces cell culture infection by 50%
EI	Electron impact (mass spectrometry)
ER	Electrical resistance
FAB	Fast-atom bombardment (mass spectrometry)
g	Grammes
GABA	γ-Aminobutyric acid
h	Membrane thickness
^3H	Tritium Isotope
HEPES	N-(2-Hydroxyethyl)piperazine-N'-(2-ethane sulphonic acid)
HIV	Human immunodeficiency virus
^1H NMR	Proton nuclear magnetic resonance
HSV	Herpes simplex virus
Hz	Hertz
IR	Infra-red
IV	Intravenous
J	Flux (Chapter 3) or Coupling constant (Chapters 2 and 4)
J_m	Flux across membrane alone
J_t	Flux across membrane and cell monolayer

K	Constant of relative diffusion of two solutes
K'	Partition coefficient
K_d	Non-saturable diffusion constant
K_m	Concentration at half maximal velocity (Michaelis constant)
Kp	Permeability coefficient
Kp_c	Permeability coefficient of cell monolayer
Kp_t	Permeability coefficient of cell monolayer and permeable support
Kp_m	Permeability coefficient of permeable support
LAA	Large amino acid
lit	Literature
LNAA	Large neutral amino acid
L-System	Leucine-preferring system
m	Multiplet
M	Molar
MCA	Monocarboxylic acid
MEM	Minimum essential medium
MHz	Megahertz
min	Minute
ml	Millilitre
mm	Millimetre

mM	Millimolar
mm Hg	Measurement of pressure in millimetres of mercury
mmol	Millimoles
mol	Moles
mp	Melting point
mw	Molecular weight
m/z	Mass divided by charge
n	Number
nmol	Nanomoles
NMR	Nuclear magnetic resonance
^{15}O	Oxygen-15 isotope
P	Permeability coefficient
P-C	Phosphorus carbon bond
PET	Positron emission tomography
PFA	Phosphonoformate
pH	Negative log of hydrogen ion concentration
pK_a	Negative log of dissociation constant
^{31}P NMR	Phosphorus nuclear magnetic resonance
PBS	Phosphate-buffered saline
PMEA	9-(2-Phosphonylmethoxyethyl)adenine

ppm	Parts per million
q	Quartet
Q	Blood flow
R_f	Retention factor
RNA	Ribonucleic acid
s	Singlet
sept	Septet
t	Triplet
$t_{1/2}$	Half-life
TC_{50}	Concentration of drug which reduces cell growth by 50%
TLC	Thin-layer chromatography
UV	Ultra-violet
V	Rate of solute uptake
V_{max}	Maximal velocity of transport
WHO	World Health Organisation
δ	Chemical shift measured in parts per million
µl	Microlitres
µCi	MicroCuries
Ω	Ohms

LIST OF FIGURES

LIST OF TABLES

LIST OF PHOTOGRAPHS

CHAPTER 1 - INTRODUCTION

1.1 The Human Immunodeficiency Virus (HIV)

In the early 1980's numerous reports of previously rare and unusual infections and tumours in homosexual men appeared in the United States. These became linked by the impaired immune responses measured in the patients and in 1983 the isolation of a virus, later to be termed HIV, completed the picture of a newly emerging health threat.

Evidence to date indicates transmission of HIV *via* blood, sexual activity and perinatal events only. After infection, an individual normally remains apparently well for a number of years (mean = 9.8 years)[1] although progression of the disease may be followed using serological markers. The term aquired immunodeficiency syndrome (AIDS) defines the later stages of this long-term chronic HIV infection. AIDS-related complex (ARC) describes the period of HIV infection characterised by symptoms such as weight loss, chronic diarrhoea, fever and minor infections. ARC is indicative of a progression towards AIDS itself; a diagnosis satisfied by the presence of a major opportunistic infection or tumour. The World Health Organisation (WHO) has been notified of 501,272 cases of AIDS by 2nd July 1992,[2] however, due to under-recognition and late reporting, it is accepted that this is a gross underestimate of the true number. The asymptomatic nature of HIV infection before AIDS becomes apparent means that the incidence of HIV infection can only be estimated.

Owing to the development of effective vaccines and WHO programmes, the prevalence of viral infections such as smallpox, yellow fever and poliomyelitis has rapidly declined. In contrast, HIV presents serious difficulties in the quest for a vaccine due to its ability to rapidly change surface protein antigens; the first target for a protective immune response.[3] Independent HIV isolates have been found to vary from one another by 20-25% of the nucleic acid sequence.[4] Such mutations are introduced during the three conversion steps of replication (see section 1.1.2). Moreover, viral DNA is made in the cytoplasm while the cellular repair enzymes which recognise mismatched nucleotides are located in the nucleus. Although many mutations will be lethal to the virus, others will induce the antigenic variation that frustrates vaccine development.[5] The seriousness of HIV infection also prevents the use of live attenuated or inactivated virus vaccines due to the possibility of incomplete inactivation.[3] In the absence of a vaccine and considering the large numbers of infected individuals, anti-HIV chemotherapy and control of opportunistic infections, which afflict AIDS patients, are of primary importance.

1.1.1 The Structure of HIV

HIV is a retrovirus, that is, an RNA virus replicating through DNA generated by a virally encoded RNA-directed DNA polymerase. The virus consists of a protein capsid containing the RNA genome and DNA polymerase and integrase enzymes.[4] This is surrounded by a lipoprotein membrane or envelope, the surface of which contains the glycoprotein gp120 which binds to the cellular CD4 antigen leading to attachment of the virus to its host cell.[6]

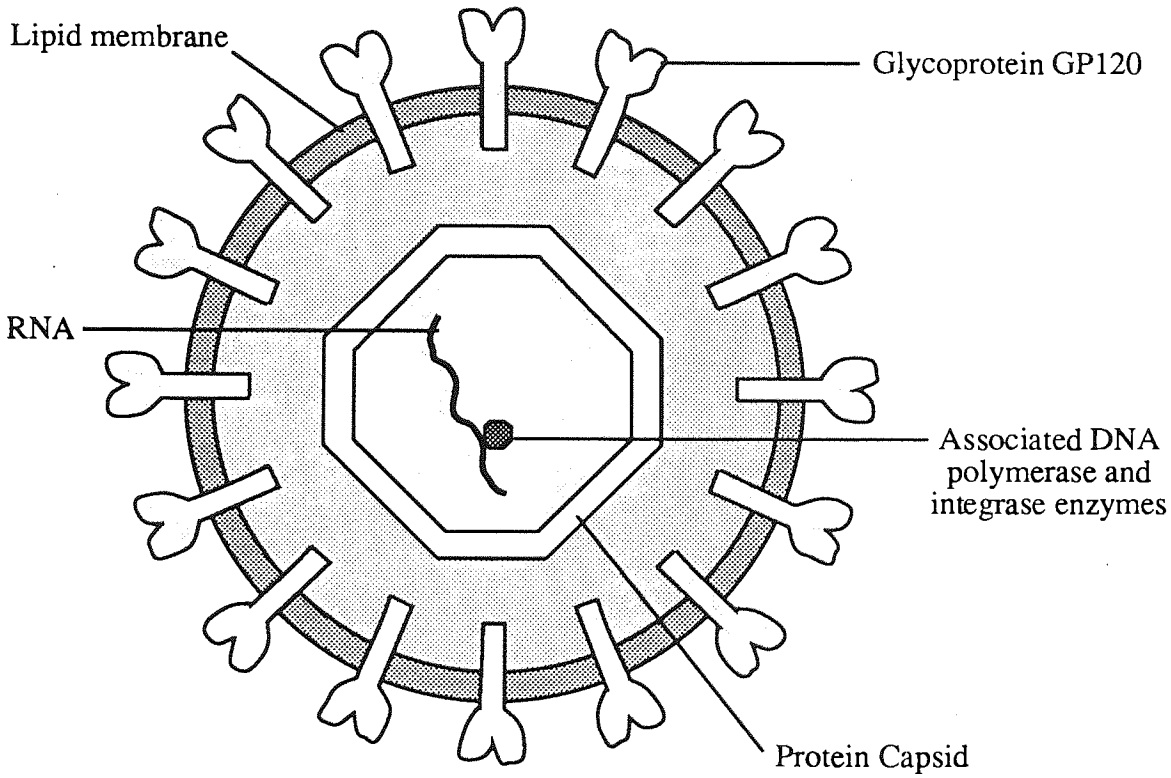

Figure 1.1 - Schematic Diagram of HIV

1.1.2 HIV Life Cycle

After binding to the CD4 receptor, the viral envelope fuses with the cell membrane of the host cell and the capsid enters the cell cytoplasm (1). The viral RNA and associated DNA polymerase and integrase enzymes are then released from the capsid (2). The term DNA polymerase refers to two enzymes; first reverse transcriptase which generates a DNA strand complementary to the viral RNA (3), and second ribonuclease which then destroys the original RNA strand (4), so that a second DNA strand complementary to the first can be synthesised (5). The double-stranded DNA and associated integrase enzyme, termed a provirus, then enters the cell nucleus and is inserted into the host cell chromosomes at a random site by the viral integrase enzyme (6). Once the viral genome is incorporated into the host cell DNA the virus may become latent until expression is triggered by a cellular stimulus. Replication leads to the formation of RNA and viral proteins (7), which undergo post-translational modification by HIV protease (see section 1.1.3.3). Assembly occurs at the cell surface and the virions leave the cell by budding (8).[7]

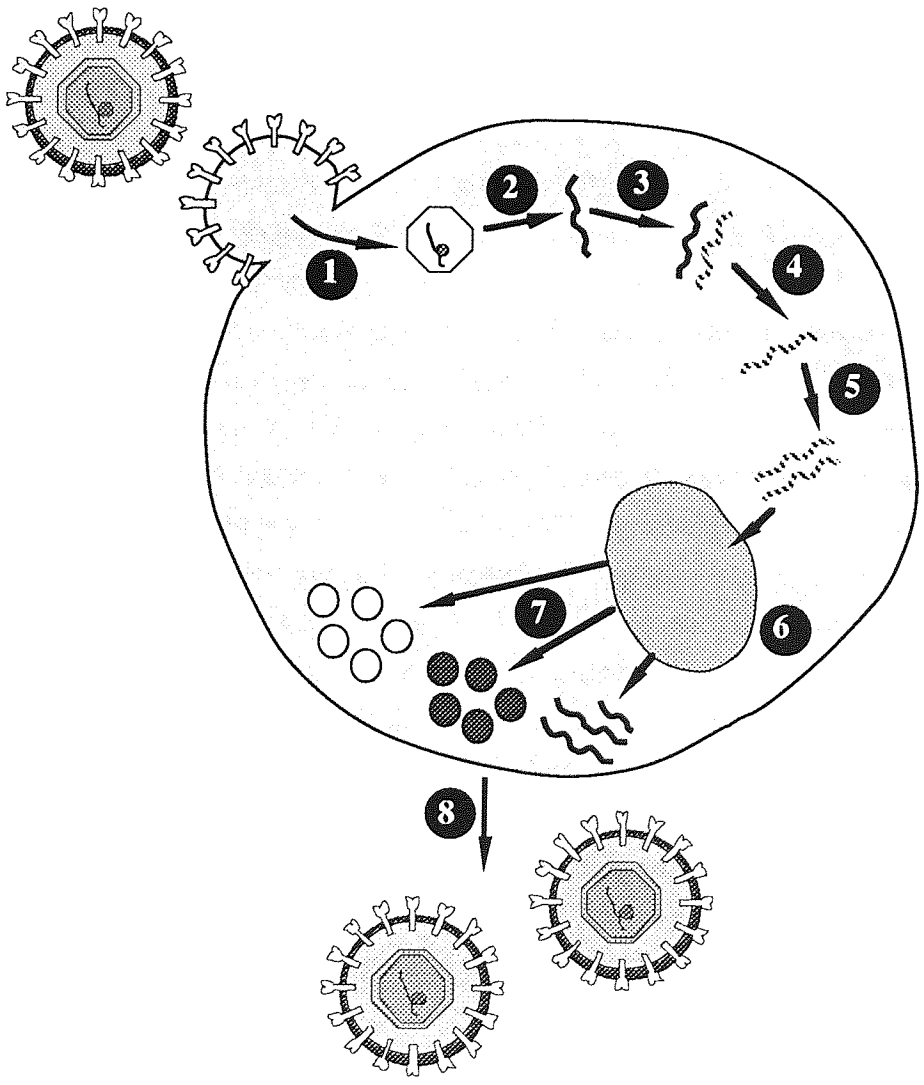

Figure 1.2 - Schematic Diagram of HIV Life Cycle

1.1.3 Anti-HIV Chemotherapy

The life cycle of HIV provides numerous potential targets for chemotherapy, some of which have given rise to promising anti-HIV agents.

1.1.3.1 Soluble CD4

Receptor-mediated attachment of HIV to the host cell may be prevented by the use of a soluble form of the CD4 receptor. This agent coats the viral particles preventing attachment to cellular CD4 receptors and has been found to have a potent inhibitory effect on HIV replication *in vitro*.[8] However, its therapeutic use has not, as yet, been realised due to its very short plasma half-life (15 minutes).[9] In an attempt to overcome this, CD4 has been linked with the immunoglobulin IgG to form a conjugate termed an Immunoadhesin which has a far longer half-life (48 hours).[9] CD4 has also been linked to toxins designed to selectively kill infected cells expressing viral gp 120.[10]

1.1.3.2 Reverse Transcriptase Inhibitors

Viral nucleic acid synthesis and, in particular, inhibition of reverse transcriptase has provided the only clinically useful agents to date. Zidovudine (3'-azido-3'-deoxythymidine, AZT, Retrovir, Wellcome Medical Division, **1**) is currently the only agent licensed in the United Kingdom for the management of manifestations of HIV infection.[11] Reverse transcriptase produces a DNA strand from nucleoside triphosphates with the release of pyrophosphate (see Figure 1.3). Zidovudine is phosphorylated to zidovudine triphosphate by host kinases and competes with endogenous nucleoside triphosphates. When incorporated into a DNA strand, it causes chain termination, as it lacks a 3'-hydroxyl, thereby inhibiting viral DNA synthesis.[12] Zidovudine has been shown to reduce mortality and the incidence of opportunistic infections, leading to weight gain and increased feeling of well being in AIDS patients.[13] Other dideoxynucleoside analogues such as 2',3'-dideoxycytidine (ddC, **2**) and 2',3'-dideoxyinosine (ddI, **3**) are in clinical trials and may soon be licensed.[13] However, problems encountered with nucleoside antiviral agents include side effects such as bone marrow depression and, with ddC and ddI, painful peripheral neuropathy which necessitates discontinuation of therapy.[13] Zidovudine-resistant HIV isolates have also appeared in the clinic, which is a problem of prolonged monotherapy against an organism with of a high degree of genetic mutation.[13,14]

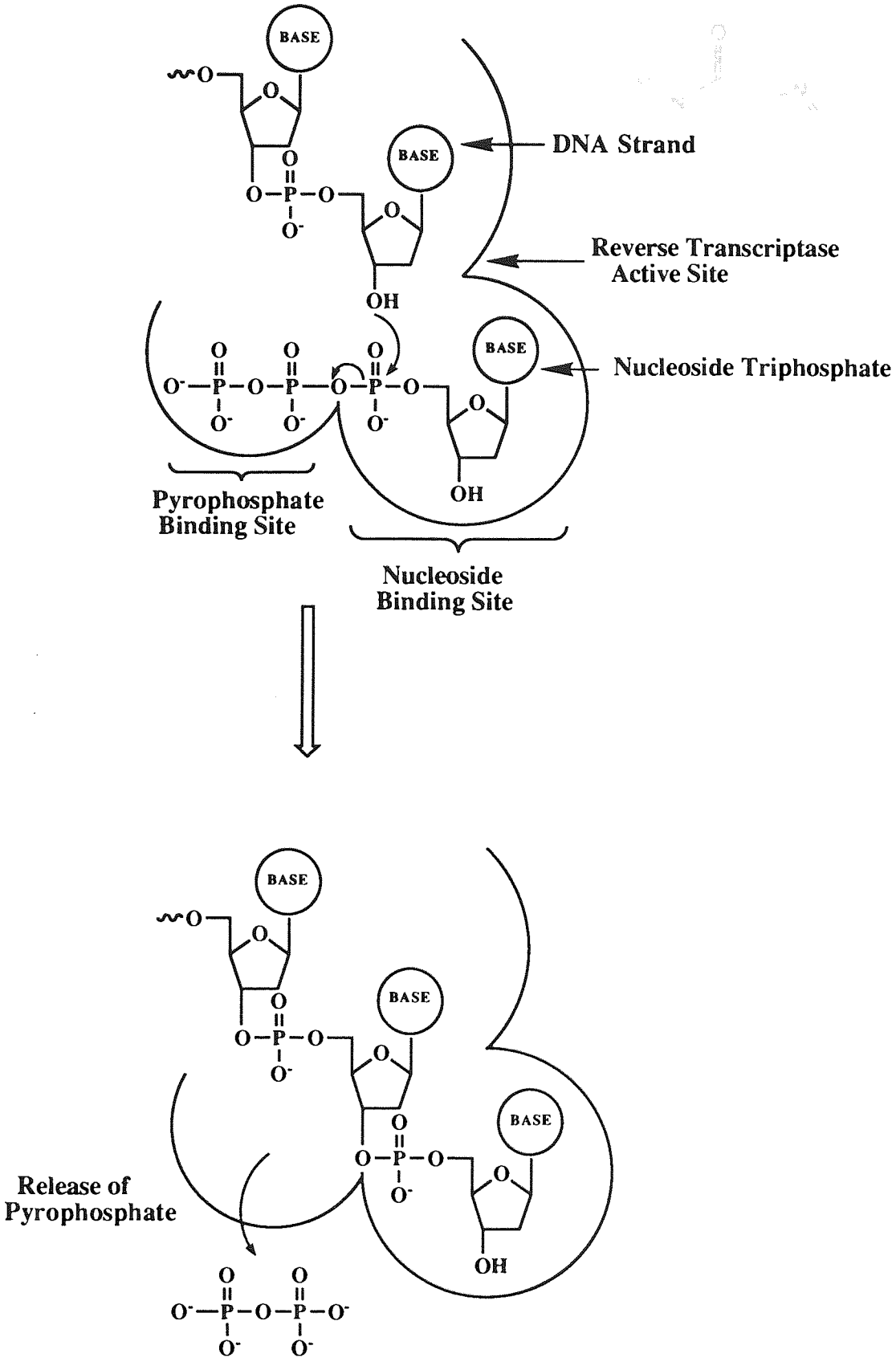

Figure 1.3 - Production of DNA by Reverse Transcriptase

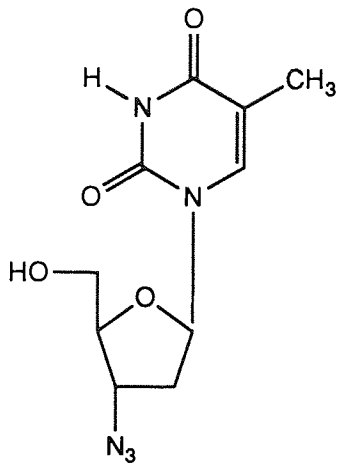

(1)

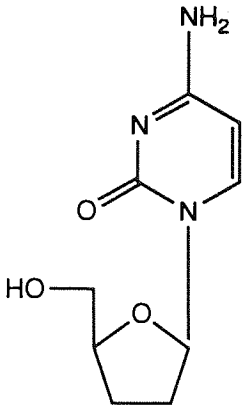

(2)

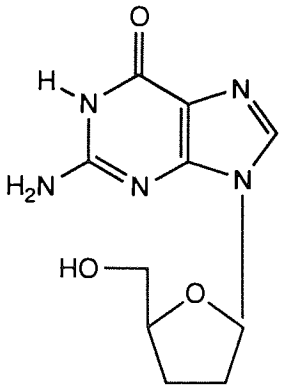

(3)

9-(2-Phosphonylmethoxyethyl)adenine (PMEA, **4**), an acyclic nucleotide has been identified as a potent and selective inhibitor of HIV and herpes viruses.[12] The phosphonate function provides enzymatic stability giving a longer duration of action as compared with zidovudine and other dideoxynucleosides.[15] However, the polar nature of PMEA limits oral bioavailability. Phosphonoformate (foscarnet, PFA, Foscavir, **5**), a pyrophosphate analogue shows a broad spectrum of antiviral activity inhibiting herpes simplex and cytomegalovirus as well as HIV, however, as with PMEA, oral bioavailability is low.[16]

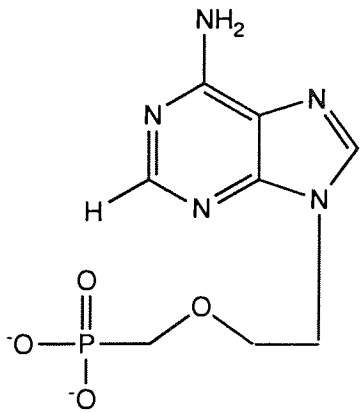

(4)

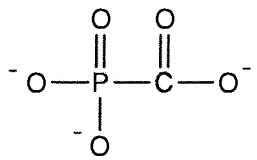

(5)

A novel series of tetrahydro-imidazo[4,5,-jk][1,4]-benzodiazepin-2-(1H)-one and -thione (TIBO) derivatives, unrelated to other antivirals, have been found to inhibit HIV-1 reverse transcriptase. However, TIBO derivatives have been found not to inhibit HIV-2; the virus isolated from West African patients. Some derivatives such as R82913 (**6**) have comparable potencies to zidovudine but are far less toxic.[17] However, the emergence of resistance to TIBO derivatives has been identified as a problem.[18]

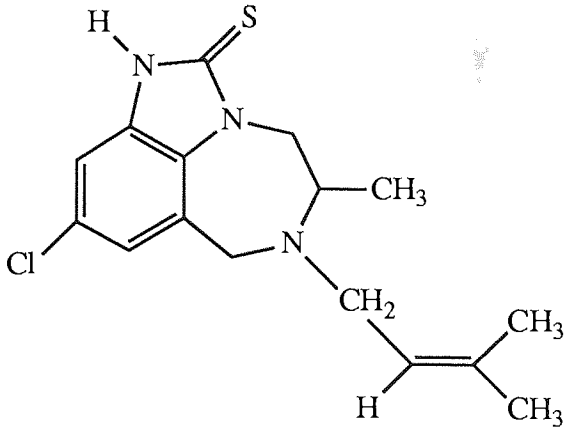

(6)

1.1.3.3 HIV Protease Inhibitors

During or subsequent to virus assembly the modification of gag and gag-pol derived polyproteins is required for virions to be infective. This modification is mediated by a specific HIV protease enzyme related to the aspartyl proteases pepsin and renin. HIV protease has been isolated and its symmetrical dimeric structure elucidated by crystallography.[19] The availability of this structural information has lead to the synthesis of a variety of highly potent and specific inhibitors which inhibit HIV replication in cell culture at nanomolar concentrations. The peptide character of the most potent inhibitors has given rise to problems with metabolism, distribution and oral bioavailability, which prevent clinical use at present.[19]

1.1.3.4 Glycosylation Inhibitors

Glycosylation of env-derived HIV proteins results in the envelope glycoproteins, such as gp120, which is critical to the binding of HIV to its host cell. Therefore, the inhibition of the glycosidase enzyme involved appears a rational target for anti-HIV chemotherapy. The natural plant alkaloids 1-deoxynojirimycin (**7**, N-(n-butyl) derivative shown) and castanospermine **(8)** are known glycosidase inhibitors and have been found to possess anti-HIV activity.[20] N-Alkylation as in (**7**) has been shown to increase activity of some alkaloids, although concentrations approaching 1mM are still required to inhibit HIV *in vitro*.[21] No toxicity was detected but it is unlikely that such concentrations could be obtained *in vivo*.[12] More potent inhibitors are yet to be developed.

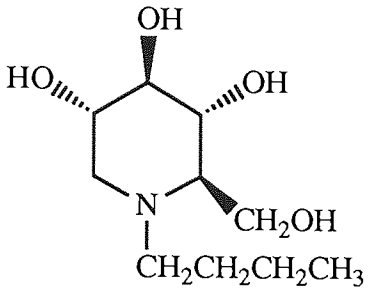

(7)

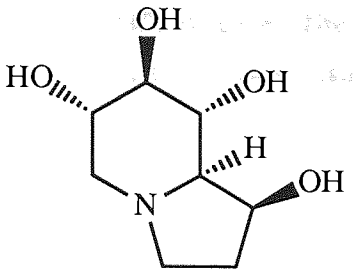

(8)

1.1.3.5 Antisense Oligonucleotides

Zamecnik *et al* have used antisense oligonucleotides (AO) to selectively inhibit the production of HIV-encoded proteins in HIV infected cells.[22] AO are short lengths (12-25 nucleotides) of single stranded nucleic acid with base sequences either complementary or antisense to those in a region of target nucleic acid. AO could potentially interfere at three stages in the HIV life cycle.[23] They may bind to the viral RNA preventing DNA production by reverse transcriptase (see Figure 1.2, step 3) or bind to the single strand DNA product of reverse transcriptase stopping synthesis of a complimentary strand (see Figure 1.2, step 5). AO may also bind to viral mRNA preventing manufacture of viral proteins at the ribosome (see Figure 1.2, step 7). Delivery of AO is frustrated by their rapid degradation *in vivo* and their polar nature limiting membrane permeability. Modification of the phosphodiester linkage of AO and use of molecular and particulate carriers are methods currently under investigation for improving cell delivery.[24]

1.1.4 The Pathogenesis of HIV

The affinity of HIV for the CD4 molecule guides its pathogenesis. T-Helper lymphocytes, macrophages, monocytes and astrocytes are CD4-positive and are target cells for HIV. The T-helper lymphocytes have a high expression of the CD4 molecule on their surface and are the main target for HIV infection. However, expression of HIV proteins and RNA only occurs in activated T-helper lymphocytes and as only 1 in 10,000 are replicating at any one time, infection, at least initially, is largely latent in these cells. When activation of infected lymphocytes does occur, it results in prolific viral expression, the release of virus and cell death. Activation of infected macrophages and monocytes will also propagate infection and as these cells are less susceptible to the cytopathic effects of HIV they may serve as a reservoir for the virus.[25] Over a prolonged period, the numbers of latently infected T-helper lymphocytes will increase and random activation will result in further infection and reduction in CD4 lymphocyte numbers leading eventually to immunosuppression. This gradual process is reflected in the slow

progression and long asymptomatic period before active HIV disease. The destruction of cellular immunity can be followed in otherwise asymptomatic patients using serological markers. CD4-positive lymphocyte counts have been shown to be useful in the prediction of the onset of symptomatic disease. CD4 lymphocyte counts fall by 60-100 /mm^3 per year of HIV infection, from a normal value of 800-900 /mm^3. Counts below 200 are associated with progression to symptomatic disease.[1] T-helper lymphocytes initiate the destruction of virally infected or cancerous cells and their increasing loss gives rise to the proliferation of virally transformed tumour cells and loss of control of endogenous viral, fungal and protozoal infections,[7] presenting as opportunistic infections (Table 1.1).[26]

Table 1.1 - Opportunistic Infections Common to HIV Infection

Organism	Group	Common Site or Presentation
Pneumocystis	**Protozoal**	**Pneumonia**
Toxoplasma	**Protozoal**	**Cerebral Abscesses**
Cryptococcus	**Fungal**	**Meningitis**
Histoplasma	**Fungal**	**Lungs, Liver, Lymph Nodes, Spleen and Bone marrow**
Candida	**Fungal**	**Oral, Oesophageal and Vaginal**
Cytomegalovirus	**Viral**	**Retinitis, Gastrointestinal Tract, Pneumonitis and Encephalitis**
Herpes	**Viral**	**Facial, Genital and Meningitis**
Mycobacterium	**Bacterial**	**Lungs**

1.1.5 HIV Infection of the CNS

A major and common cause of morbidity in HIV infection is a neurological syndrome termed AIDS dementia complex (ADC) which is characterised by an impairment of cognitive, motor and behavioural functions.[27] Neurological disease is apparent in 20-40% of AIDS patients while upon autopsy 70-80% of patients have CNS pathology.[28] The timing of onset of ADC is controversial with some reports of neurological changes being the first presentation of symptomatic HIV disease in one third of patients.[29] Table 1.2 shows the progression of ADC.[30]

Table 1.2 - A Staging Scheme of ADC

Stage 0	**Normal mental and motor function.**
Stage 0.5	**Minimal or equivocal symptoms of motor or cognitive dysfunction.**
Stage 1 (Mild)	**Unequivocal dysfunction but still able to perform all but the most demanding aspects of work.**
Stage 2 (Moderate)	**Cannot work, may require aid in walking, but can perform basic self-care activities.**
Stage 3 (Severe)	**Major intellectual incapacity, movement slow and clumsy, unable to walk unaided.**
Stage 4 (End Stage)	**Only rudimentary comprehension and responses, paraplegic with double incontinence.**

Viral invasion of the CNS, probably through a macrophage vector, frequently occurs at an early stage in HIV infection.[29] ADC, rather than resulting from an opportunistic infection, is thought to relate to the effects of HIV itself.[28] The impairment of neuronal function is thought to be due to a viral or host product released by infected macrophages rather than direct neuronal infection.[31] In addition, it is possible that the CNS may act as a sanctuary for HIV, in a similar way that it does for leukaemic cells. Therefore, it can be seen that delivery of anti-retroviral agents to the brain is a worthwhile aim.[27]

1.2 Phosphonoformate (PFA, Foscarnet, Foscavir, 5)

1.2.1 Mode of Action and Activity

The anti-viral activity of PFA against herpes simplex virus was first reported in 1978.[32] PFA is an inhibitor of reverse transcriptase and has been shown to have a dose-related inhibitory effect on HIV replication in the H9 cell line *in vitro*.[33] Replication was eliminated at a concentration of 680 μM, a non-cytotoxic dose, and 98% inhibition was achieved at 132 μM.[33] PFA blocks the inorganic pyrophosphate binding site (Figure 1.3), inhibiting HIV reverse transcriptase by a non-competitive mechanism with respect to nucleoside triphosphate.[16] This prevents polymerisation of the nucleoside triphosphates and hence blocks viral DNA formation and viral replication.[26]

1.2.2 Administration and Absorption

Oral absorption of PFA is poor in humans (12-22% of a 4g dose)[34] and it can cause diarrhoea with higher doses.[26] At present this precludes oral therapy against HIV. *In vitro* synergism has been demonstrated between PFA and zidovudine, in the treatment of HIV,[35] and pulse intravenous PFA therapy in conjunction with oral zidovudine has been advocated as a more practical alternative regime.[36] However, this is also difficult to envisage as acceptable on a long term basis. PFA is now licensed as Foscavir (Astra Pharmaceuticals) for the intravenous treatment of cytomegalovirus retinitis in patients with AIDS in whom ganciclovir is contraindicated or inappropriate.[11]

1.2.3 Metabolism, Distribution, Excretion and Toxicity

PFA undergoes no significant metabolism.[16] Bone uptake of between 10 and 28% of an intravenous dose is believed to occur and plasma protein binding varies between 14 and 17%.[37] The high correlation between plasma clearance of PFA and renal function indicates that PFA is excreted mainly *via* the kidneys.[16] Doses therefore need to be based on serum creatinine as well as body weight.[26] Elimination half-life studies indicate more than one half-life. Given normal renal function mean initial half-lifes are 1.4 and 6.8 hours with a longer terminal half-life of 88 hours.[37] Nephrotoxicity,[26] hypocalcaemia[11] and genital and oral ulceration[38] are common hazards of such therapy, however the bone marrow suppression associated with anti-viral nucleosides[26] is not apparent. This difference in toxicity profiles and the emergence of resistance to zidovudine[14] gives further credibility to combination therapy, particularly if PFA administration could be improved.

1.2.4 Brain Penetration

To combat ADC, penetration of the blood-brain barrier is a highly desirable property of an anti-HIV drug. It is unclear whether zidovudine crosses the blood-brain barrier. It is claimed that AIDS patients given continuous infusions have achieved a cerebrospinal fluid / plasma ratio of 0.24[39] while Pardridge has concluded from brain perfusion studies that zidovudine does not cross the blood-brain barrier significantly.[40] This conflict of data was recently reviewed.[41] Patients with ADC have improved when treated with zidovudine,[42] but this could be due either to a reduction in the concentration of the virus in blood-borne mononuclear cells that enter the brain or to a reduction in meningeal proliferation of the virus.[40] PFA is predominantly a trianionic molecule at pH 7.4 with pK_a values of 0.49, 3.41 and 7.27[43] and therefore does not possess the necessary lipophilic character to penetrate the blood-brain barrier by passive diffusion.[16]

1.3 Prodrug Design

A promising strategy for the delivery of hydrophilic drugs through physiological barriers is drug latentiation or the formation of lipid-soluble prodrugs by masking hydrophilic functional groups.[44] Once transport across the barrier has occurred, enzymatic cleavage is required to regenerate the active drug. The enzymes required for the hydrolysis of prodrug bonds are generally non-specific and ubiquitous. This is of benefit to prodrugs designed to enhance corneal or gastrointestinal uptake, as they are crossing from an environment of low enzyme activity to one of high activity. However, prodrugs designed to enhance blood-brain barrier penetration must be stable in areas of high enzyme activity such as blood and the liver, yet still be sufficiently labile to regenerate active drug in the brain. Prodrugs that are too labile will never reach the brain while those that are too stable may achieve high brain concentrations of the prodrug but never become active.[45] Diacetylmorphine (heroin, **9**) has a greater lipid solubility than its parent drug morphine due to the masking of the two hydroxyl functions. This greatly enhances the rate of brain penetration of diacetylmorphine which is then rapidly hydrolysed to monoacetylmorphine and morphine which exert their pharmacological action.[45] The widespread abuse and addictive nature of diacetylmorphine is an unfortunate reflection of its success as a brain-directed prodrug.

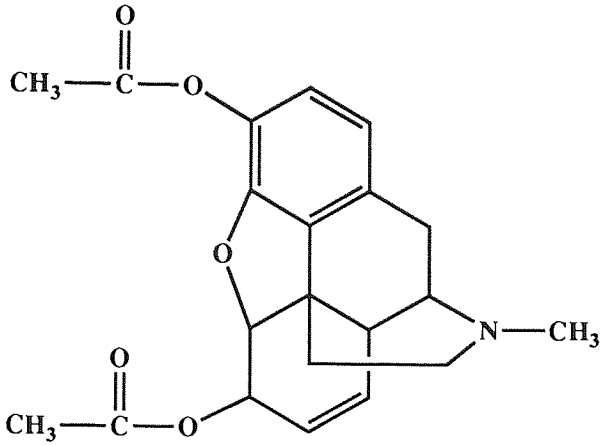

(9)

When considering prodrugs that involve the ester group, the affinity and reactivity of esterases are dependent on the shapes and sizes of the substituents on either side of the ester bond. The rate of hydrolysis can therefore be manipulated by varying the ester moiety.[45] For example, the stability of various ester prodrugs of the dopaminergic molecule 2-(N-propyl-N-2-thienylethylamino)-5-hydroxytetralin (**10**) were assessed in rat serum (Table 1.3).[46]

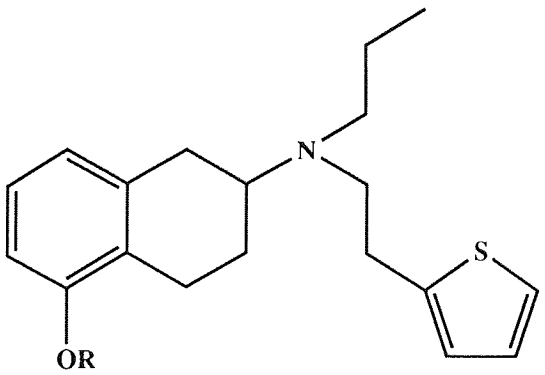

(R = H, 10)

Table 1.3 - Esterase Stability of Various Hydroxyl Ester Moieties of (10)

Nature of Ester Moiety (R)	Rat Serum Half Life
acetyl	3 minutes
isobutyryl	21 minutes
pivaloyl	92 minutes
benzoyl	42 minutes
2-methylbenzoyl	16 hours
2,4-dimethylbenzoyl	31 hours

It can be seen that increasing the size of the aliphatic ester group increases the half-life. This is due to the steric crowding around the carbonyl function making the ester a poorer substrate for the esterase. This trend can also be seen for aromatic esters where ring substitution increases the half-life. The electron-donating nature of the methyl groups is also responsible for stabilising the carbonyl bond.[46] Where interference from the drug moiety itself causes the ester to be a very poor substrate, the use of double esters, such as acyloxymethyl derivatives, moves the site of esterase action away from the drug moiety. The acyloxymethyl ester is a good substrate and is enzymatically cleaved to give the unstable hydroxymethyl ester which rapidly degrades to give the parent drug and formaldehyde. For example, simple carboxyl esters of ampicillin were synthesised to improve oral absorption but were found to be poor substrates of esterases and were therefore inactive, as the free carboxyl anion is essential for activity. Pivampicillin is the pivaloyloxymethyl ester of ampicillin and being more lipophilic has a far higher oral bioavailability than ampicillin. The pivaloyloxymethyl ester is readily cleaved by plasma esterases to give the active drug (Figure 1.4).[45]

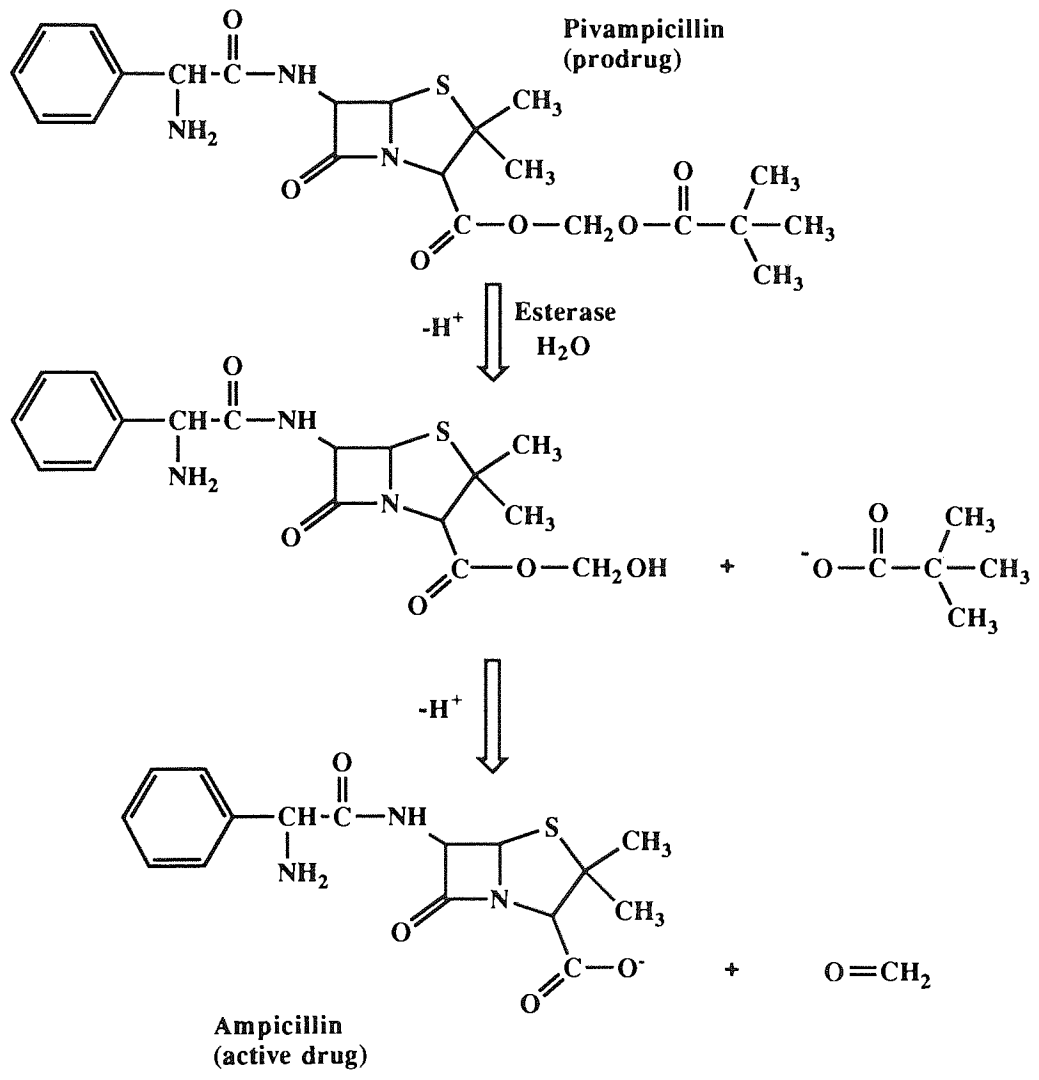

Figure 1.4 - Plasma Hydrolysis of Pivampicillin

The plasma half-life of various esters of benzoic acid was evaluated as a reference for designing ester prodrugs of carboxylic acids (Table 1.4).[47]

Table 1.4 - Esterase Stability of Various Carboxyl Ester Moieties of Benzoic acid (C_6H_5COOR)

Nature of Ester Moiety (R)	Half-Life in 80% Human Plasma (pH 7.4, 37°C)
CH_3	108 minutes
C_2H_5	210 minutes
n-C_3H_7	46 minutes
n-C_4H_9	40 minutes
n-C_5H_{11}	24 minutes
$CH_2C_6H_5$	19 minutes

It can be seen that the ethyl ester appears to be the most stable ester in plasma. As the length of the straight alkyl chain increases, the esters become better substrates of esterases as they have shorter half-lives. This is in contrast to increasing branched chain length which decreases esterase affinity due to steric hinderance around the carbonyl function (see Table 1.3). The benzyl ester can be seen to be less stable than simple alkyl esters.

In an attempt to achieve a greater degree of site-specific delivery than previous prodrug approaches, Bodor *et al* [48-50] have investigated the dihydropyridine group as a carrier for delivery to the CNS. This group has been attached to amino and hydroxyl functions of drugs conferring lipophilic nature, rapid distribution and BBB penetration. The dihydropyridine function is then enzymatically oxidised to the quaternary salt (see Figure 1.5) trapping the carrier-drug conjugate behind the BBB. However, it should be appreciated that the oxidative enzymes involved are far from exclusive to brain and conversion in the periphery will occur. This approach has been applied to the delivery of 2',3'-dideoxynucleosides and zidovudine for the treatment of AIDS dementia.[51-53]

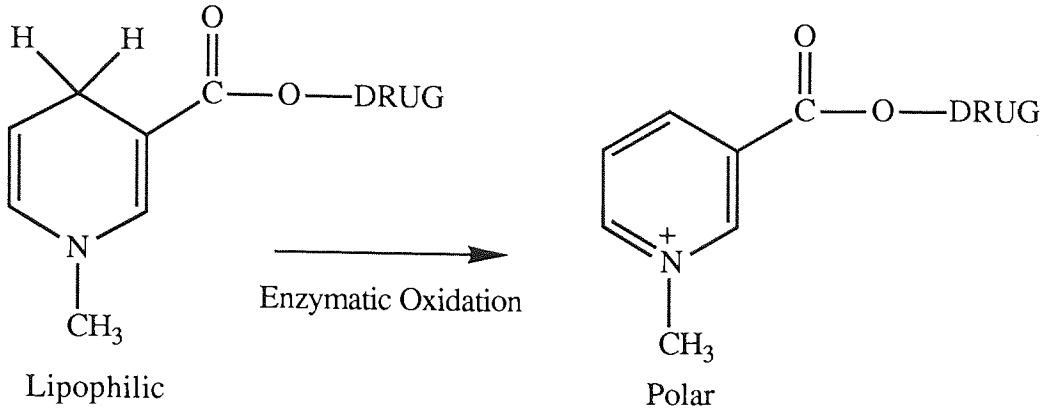

Lipophilic

Polar

Figure 1.5 - Oxidation of Dihydropyridine Carrier

Prodrug design has also been applied to improve the CNS delivery of phosphonate and phosphate drugs. Diprotected lipophilic compounds have been produced but removal of the second protecting group, to achieve activity, is non-trivial as the second chemical cleavage is 1,000,000-fold slower than the first. The relative stability of the monoanionic species is due to the reaction proceeding by P-O bond cleavage. Srivastva and Farquhar[54-55] have produced bioreversible phosphate protecting groups by the use of acyloxymethyl esters. These lipophilic esters degrade smoothly to the corresponding phosphate. Moreover, hydolysis occurs by C-O bond cleavage and is catalysed by carboxyesterases. This methodology has recently been used in the CNS delivery of dideoxyuridine 5'-monophosphate.[56] Within this department, a similar approach using acyloxybenzyl protecting groups has been extended to phosphonates, in particular, methylphosphonate[57] and phosphonoacetate.[58] More recently, the di(4-acetoxybenzyl) derivative of zidovudine 5'-monophosphate (**11**) has also been investigated.[59]

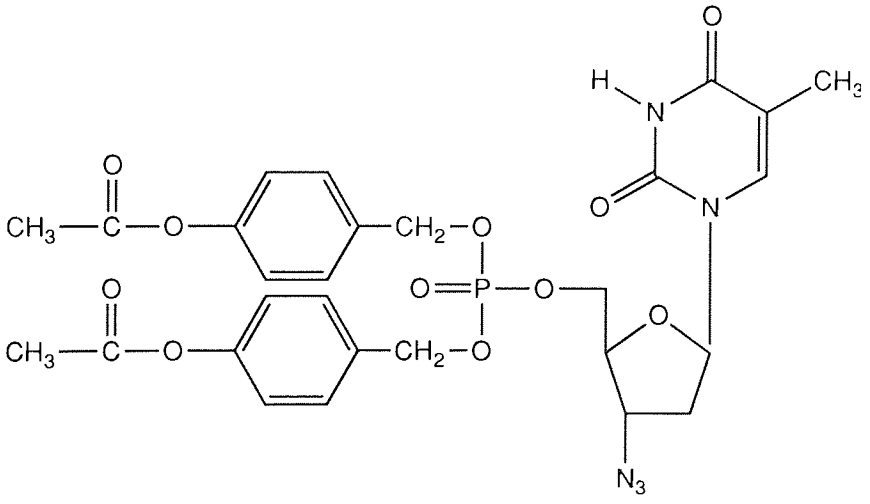

(11)

1.3.1 Prodrugs of PFA

Aliphatic and aromatic mono-, di-, and tri-esters of PFA have been reported.[60] None of these compounds were found to have anti-herpes activity greater than PFA and no attempt was made to evaluate brain penetration. Several PFA derivatives of nucleosides have been synthesised.[61-63] Activity against herpes simplex has been shown for some compounds but no evaluation of their penetration of the blood-brain barrier was made. A PFA ester of zidovudine (**12**) was synthesised in an attempt to either give a better inhibitor of reverse transcriptase or to improve the cell membrane penetration of PFA by acting as a prodrug. However, anti-HIV activity of (**12**) was found to be less than that of zidovudine.[64] Acyloxymethyl esters of PFA, for example di(acetoxymethyl) methoxycarbonylphosphonate (**13**), have recently been synthesised as lipophilic prodrugs.[65] These were made in an attempt to improve the cell membrane transport of PFA and increase oral bio-availability. However, their anti-HIV activity was found to be low and it was reported that they were only stable in the concentrated form or in aprotic solvents at -20°C.[65]

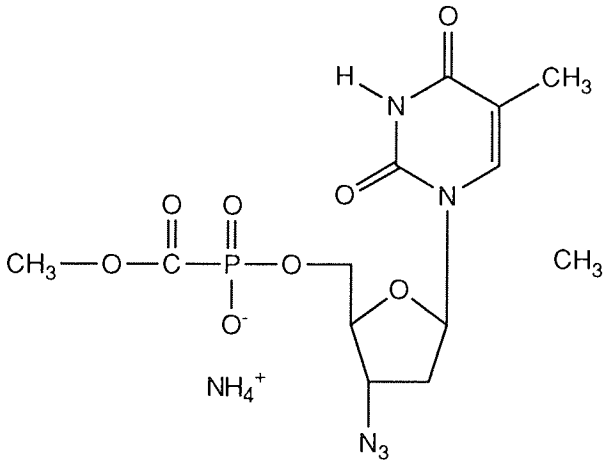

(**12**)

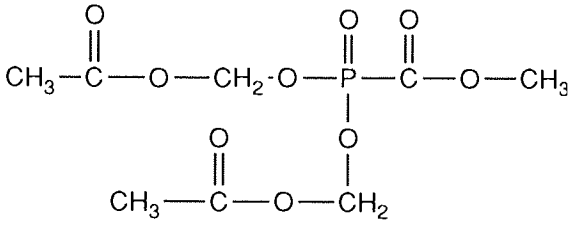

(**13**)

Dibenzyl methoxycarbonylphosphonate (**14**)[66] and a series of similar para-substituted dibenzyl triesters[67] have been synthesised as prodrugs to facilitate brain penetration of PFA. However the chemical hydrolysis of (**14**), the most stable of these analogues, was rapid ($t_{1/2}$ = 60 minutes) under physiological conditions.[66] Moreover it was very complex with the formation of four products, two by P-C bond cleavage, indicating that these triesters are unsuitable prodrugs (see section 2.1). The work of Krol *et al* is in agreement with these findings.[68]

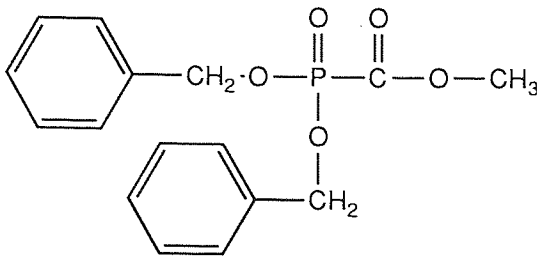

(14)

Neto *et al* have prepared the palmityl phosphonate monoester of PFA. This monoester **(15)** was designed as a fatty acid analogue to improve oral absorption and increase the half-life in plasma by binding to serum proteins.[69]

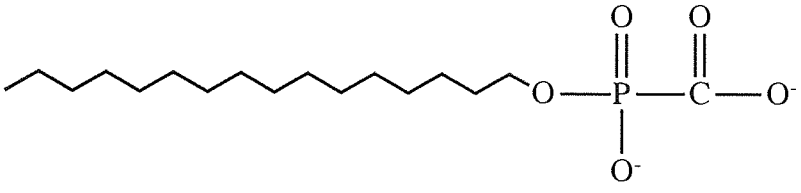

(15)

1.4 The Blood-Brain Barrier (BBB)

There are two physiological barriers protecting the brain, the BBB and the blood-cerebrospinal fluid barrier. The surface area of the BBB vastly exceeds that of the blood-cerebrospinal fluid barrier (5000 : 1), therefore the BBB should be considered the principal route of entry of drugs into the brain.[70] The BBB is made up of brain capillary endothelial cells which differ anatomically from the capillary endothelial cells of other organs. General capillaries possess open endothelial clefts, pore-like fenestra and numerous vesicles involved in pinocytic transport (see Figure 1.6).[71] In contrast brain capillary endothelial cells have tight junctions, no fenestra and few vesicles.

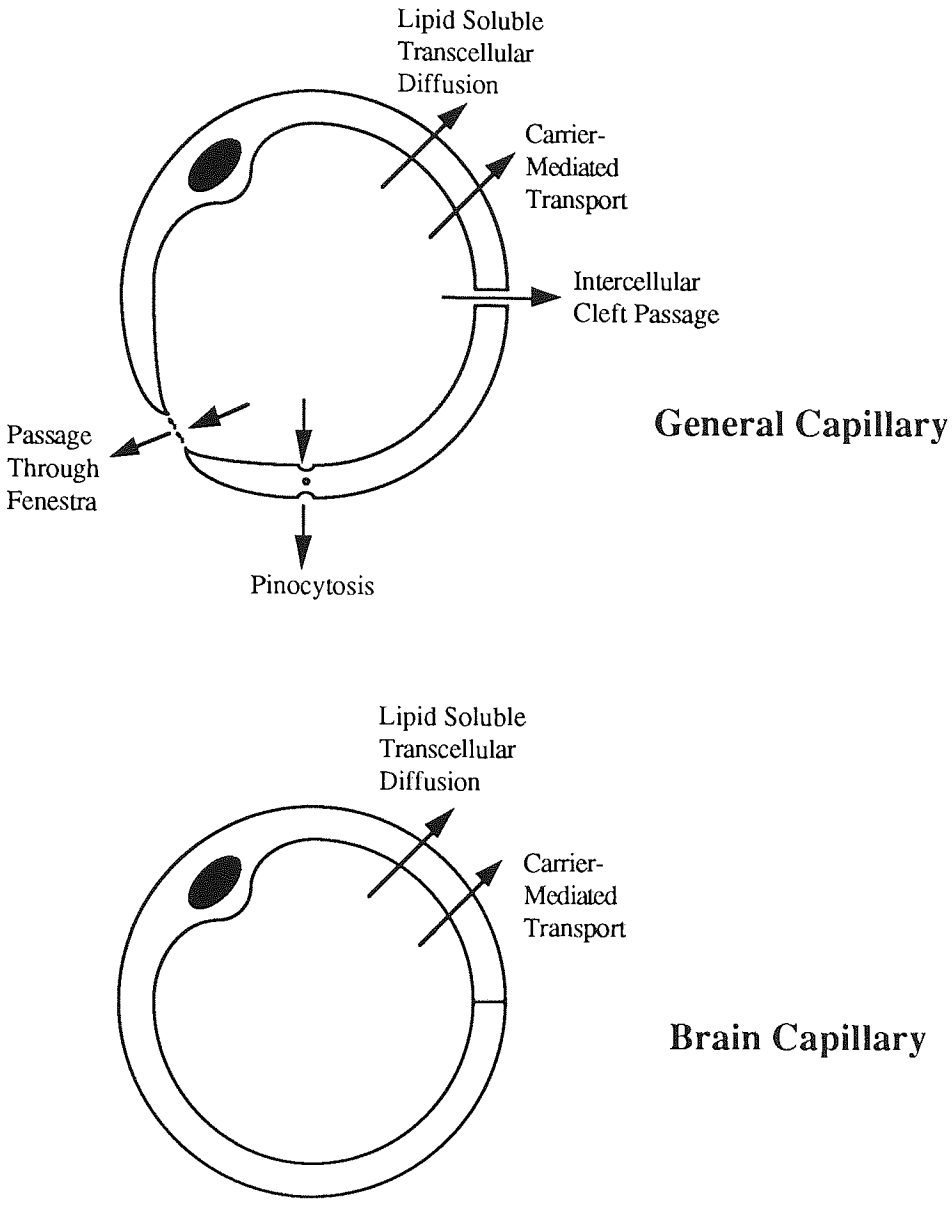

Figure 1.6 - Anatomical Differences Between General and Brain Capillaries

1.4.1 Passive Transport

In order for a drug to enter the brain by passive transport it must be sufficiently lipophilic to diffuse through, first the luminal endothelial cell membrane, traverse the cell cytoplasm, and then through the antiluminal cell membrane to reach the brain extracellular fluid. Passive transport of drugs at the BBB correlates with their lipophilicity and in particular with their log P value. A log P value of 2 has been found to be optimal for brain penetration.[45] The plateau or decline in BBB penetration of drugs of log P > 2 may be explained as being due to partitioning into lipid-rich sites (eg. adipose tissue) and / or insufficient aqueous solubility of the drug to traverse the endothelial cell cytoplasm. The transport of poorly lipid-soluble molecules (log P < -2) is restricted by the BBB, except nutrients, for which specific carrier-mediated systems exist.[71]

1.4.2 Active Transport

Numerous nutrient-specific carrier-mediated transport systems located in both the luminal and antiluminal membranes of brain capillaries have been described (Table 1.5).[70-72]

Table 1.5 - Carrier Systems at the BBB

Carrier	Representative Substrate	K_m (mM)	V_{max} (nmol min^{-1} g^{-1})	K_d (ml min^{-1} g^{-1})
Hexose	Glucose	11.0 ± 1.4	1420 ± 140	0.017 ± 0.003
Monocarboxylic acid	Pyruvic acid	0.57 ± 0.16	88 ± 26	0.034 ± 0.008
Neutral amino acid	Tyrosine	0.15 ± 0.01	31 ± 8	0.016 ± 0.004
Basic amino acid	Arginine	0.088 ± 0.011	7.8 ± 0.9	0.0044 ± 0.0016
Amine	Choline	0.34 ± 0.07	11.3 ± 0.7	0.0069 ± 0.0059
Nucleoside	Adenosine	0.025 ± 0.003	0.75 ± 0.08	0.0066 ± 0.0003
Purine base	Adenine	0.011 ± 0.003	0.50 ± 0.09	0.0024 ± 0.001

Synthesis of substrate analogues with an affinity for one of these specific carrier mediated transport systems provides a strategy for the uptake of hydrophilic drugs into the brain.[72] Examples of drugs penetrating the BBB by this mechanism are methyl-DOPA,[73] L-DOPA,[74] phenylalanine mustard (melphalan)[75] and D,L-NAM[76] (for structures see section 2.2.2) all of which have an affinity for the neutral amino acid carrier. One aspect of this research is concerned with exploring methods of actively transporting PFA. In particular, focusing on α-keto acid and amino acid transport, with the synthesis and evaluation of simple diesters of PFA as α-keto acid analogues and an amino acid linked ester of PFA to potentially utilise active amino acid transport systems.

1.4.3 Transport of Lipids

A lipid prodrug of L-dopa (**16**) has been synthesised which is selectively absorbed from the intestinal tract into the lymphatic circulation without degradation. It achieves a prolonged increase in L-dopa and dopamine levels in the brain when compared with L-dopa itself.[77] Such lipid prodrugs have been shown to bind readily to high density lipoproteins and low density lipoproteins (LDL) and are thought to be carried in this manner in the circulation.[78] Receptors for LDL have been characterised on the luminal surface of brain microvessel endothelial cells. Subsequently, receptor-mediated and non-receptor mediated endocytosis, leading to transport of LDL to the abluminal membrane, has been shown *in vitro*.[79] Jacob *et al* have shown brain uptake and pharmacological

activity of a lipid prodrug of γ-amino butyric acid (GABA)(**17**).[80-82] Phospholipids are known to be transported across the BBB and hydrolysed within brain tissue.[83,84] Therefore the incorporation of PFA into a phospholipid prodrug appears to be a logical rationale for oral and CNS delivery. One aspect of this research will be to link PFA to a diacyl glycerol in a similar manner to L-dopa and γ–amino butyric acid in (**16**) and (**17**).

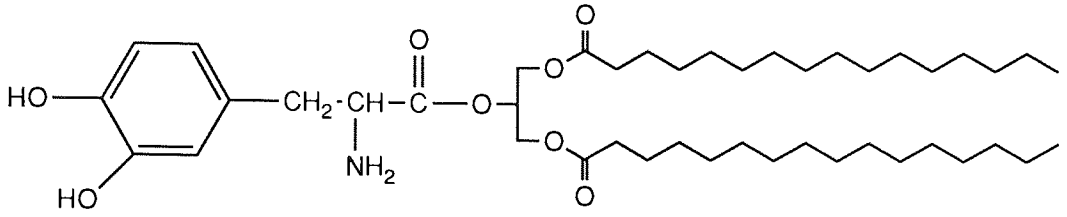

(**16**)

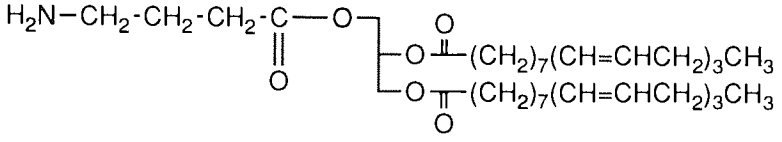

(**17**)

Diglyceride prodrugs have also been prepared for zidovudine monophosphate[85]and melphalan.[86] Lipophilic glycosyl phosphotriesters of zidovudine monophosphate have also been synthesised to improve membrane transport. For example (**18**).[87]

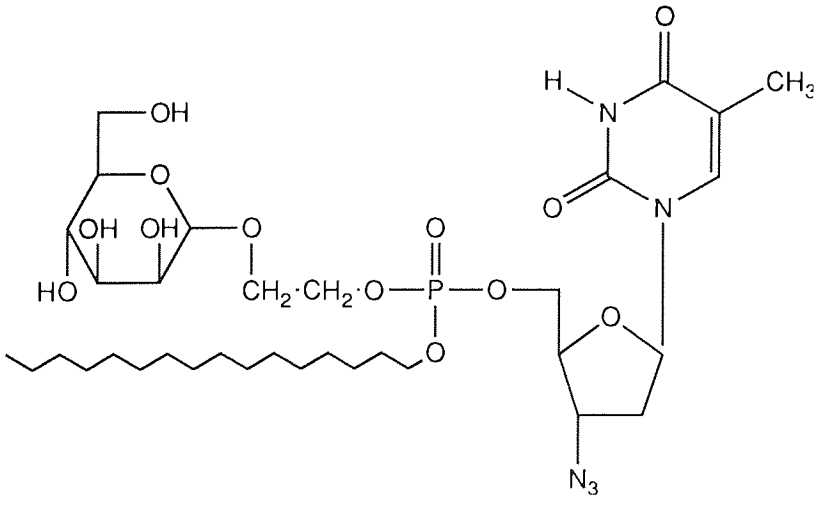

(**18**)

1.5 Strategies for Brain Delivery

Chemical modification or prodrug design, as a strategy for CNS delivery has been discussed in section 1.3. However, other methods of circumventing the BBB to enable the delivery of CNS active agents have been investigated.

Cytotoxic agents, such as methotrexate, have been administered by intralumbar and intraventrical injection into the CSF. While this has been effective in treating neoplasm associated with the meninges it is generally accepted that brain penetration is minimal and ineffective in the treatment of tumours lying within the cortex.[45,88] Therefore, intrathecal administration of water-soluble drugs does not circumvent the BBB. Osmotic opening of the BBB by the intraarterial injection of a hypertonic solution of mannitol (1.5-2.0 M) has been applied successfully in the clinic. This technique shrinks the brain microvessel endothelial cells pulling apart the tight junctions and allowing increased passage of water-soluble agents. This process appears reversible and innocuous although prolonged opening may prove deleterious to the brain.[88] Inducing arterial hypertension to 180-200 mmHg is known to increase BBB permeability, but doubts about the safety of such a technique will probably preclude use in the clinic.[45] Use of solvents, such as dimethyl sulphoxide, to act as a carrier for hydophilic drugs at the BBB has been shown to be largely ineffective and associated with neurotoxicity and changes in bladder and skin permeability.[45] Metrazol, a CNS stimulant, has been shown to reversibly open the BBB. However, use of pentobarbitone is also required to reduce the seizure activity of metrazol. Intracarotid injection of cytotoxic agents, such as etoposide, 5-fluorouracil and hydroxyurea has also been reported to increase BBB permeability but, unlike metrazol, BBB integrity is slow to return and may be associated with neurotoxicity.[45] The incorporation of agents into liposomes containing the glycolipid, sulfatide, has been investigated as a method of CNS delivery. While liposomes without sulfatide have negligible brain penetration, uptake of sulfatide liposomes was approximately 5% of the injected dose. However approximately 25% of the liposomes were sequestered by the liver.[89]

1.6 Evaluation of BBB Transport

An outline of methods used to study mechanisms and quantify transport of solutes at the BBB is given here. A fuller discussion of individual methods follows in Chapter 3.

1.6.1 *In Vivo* Studies

A number of *in vivo* techniques for the quantification of solute transport across the BBB have been developed. These can be divided into single pass and continuous uptake methods.

Single pass techniques involve injection of the solute into the carotid artery and analysis of brain uptake after a single, 5-15 second, passage through the cerebral capillaries. The indicator diffusion technique[90] assesses uptake indirectly by venous sampling, the solute uptake being derived from the difference in arterial and venous concentrations. The brain uptake index technique[91-94] is terminated by decapitation and removal of the brain to assess uptake, while single injection external registration[95] is a non-invasive technique utilising a γ- or positron-emitting radionuclide and an external detector. The disadvantage of these techniques is that they are too insensitive to study the transport of poorly penetrating solutes. This problem is overcome by continuous uptake methods. Intravenous adminstration allows numerous passes of the solute through the cerebral capillaries before uptake is assessed either by removal and analysis of the brain, or by techniques such as positron emission tomography[96] which allows accurate, sensitive and regional determination of solute transport into the brain of human subjects. The brain perfussion technique[97,98] involves infusion of the right hemisphere of an anaesthetised rat *via* the right external carotid over a period exceeding the 5-15 second single pass of the brain capillaries. The advantage of this technique is that the composition of the perfusate can be totally controlled. Analysis of brain uptake follows decapitation.

1.6.2 *In Vitro* Studies

The active transport of amino acids has been studied using cerebral slices[99] and isolated brain capillaries.[100,101] Amongst the *in vitro* techniques most attention has been given to the culture of brain microvessel endothelial cell (BMEC) monolayers as a model of the blood-brain barrier. BMECs can be isolated in good yield, with high viability and grown as a monolayer on a permeable support.[102] The active transport of amino acids[103] and monocarboxylic acids[104] has been characterised using BMEC monolayers. One aspect of this research is concerned with establishing an *in vitro* model of the BBB using cultured BMEC monolayers on permeable supports. This system could then be used to investigate the transport of PFA esters designed to utilise active transporters present at the BBB.

CHAPTER 2 - CHEMISTRY - RESULTS AND DISCUSSION

2.1 Triesters of PFA

Triesters of PFA have been synthesised as lipophilic prodrugs to improve the membrane diffusion properties of this antiviral agent and to aid targeting to the CNS.[65-68] However, the work of Mitchell *et al*,[66] illustrated the instability of triesters of PFA in aqueous media. They have shown that dibenzyl methoxycarbonylphosphonate (**19**) undergoes hydrolysis with a half-life of approximately 60 minutes, in phosphate buffer at pH 7.4 at 37°C. The major products of the hydrolysis are benzyl methoxycarbonylphosphonate diester (**20**) and dibenzyl phosphite (**21**) which in turn undergoes hydrolysis to benzyl phosphite (**22**). Minor products are the rearranged diester (**23**) and dibenzyl phosphate (**24**).

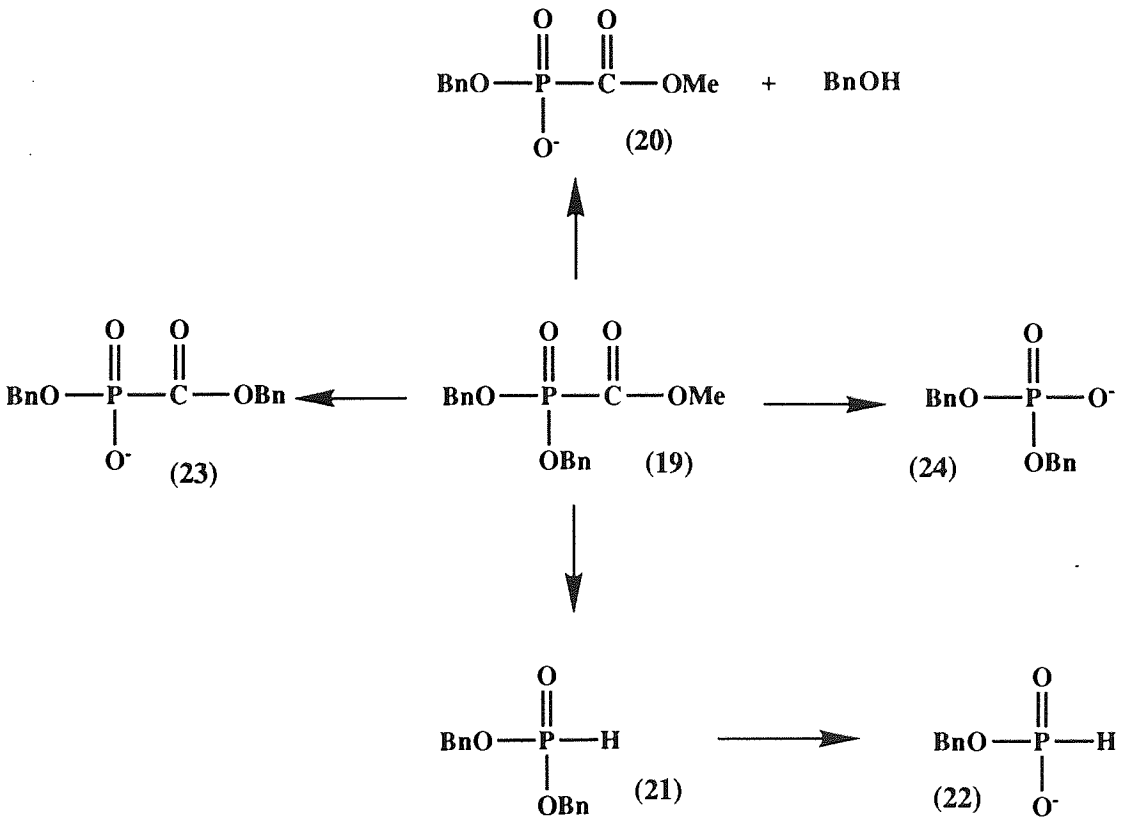

Figure 2.1 - Hydrolyses of Dibenzyl Methoxycarbonylphosphonate

The formation of (**20**) was shown to occur by nucleophilic attack of water at phosphorus in contrast to dibenzyl methylphosphonate and tetrabenzyl pyrophosphate which lose a benzyl group by C-O bond cleavage. This change in mechanism and the high reactivity of (**19**) towards chemical hydrolysis is attributed to the electron-withdrawing effect of the

methoxycarbonyl group making phosphorus sensitive to nucleophilic attack. No hydrolysis of the diester (**20**) was observed, presumably due to the anion discouraging further nucleophilic attack. The formation of dibenzyl phosphite (**21**), and the absence of a species with a free carboxyl group, may be due to either rapid decarboxylation following carboxyl ester hydrolysis or the direct cleavage of the P-C bond. The rearranged diester (**23**) was shown not to be formed *via* transesterification with benzyl alcohol and an intramolecular migration of the benzyloxy group from phosphorus to carbon was proposed.[42] The phosphate (**24**) was thought to be formed *via* an epoxide intermediate following attack at phosphorus.

To produce a successful prodrug of PFA, hydrolysis involving P-C bond cleavage needs to be minimised. As a mechanistic probe, the effect of a good carboxyl ester leaving group on product distribution was evaluated. Dimethyl phenoxycarbonylphosphonate (**25**), and dimethyl (4-nitrophenoxy)carbonylphosphonate (**26**), were synthesised by a published procedure[60] using an Arbuzov reaction between trimethyl phosphite and phenyl or 4-nitrophenyl chloroformate (see Figure 2.2).

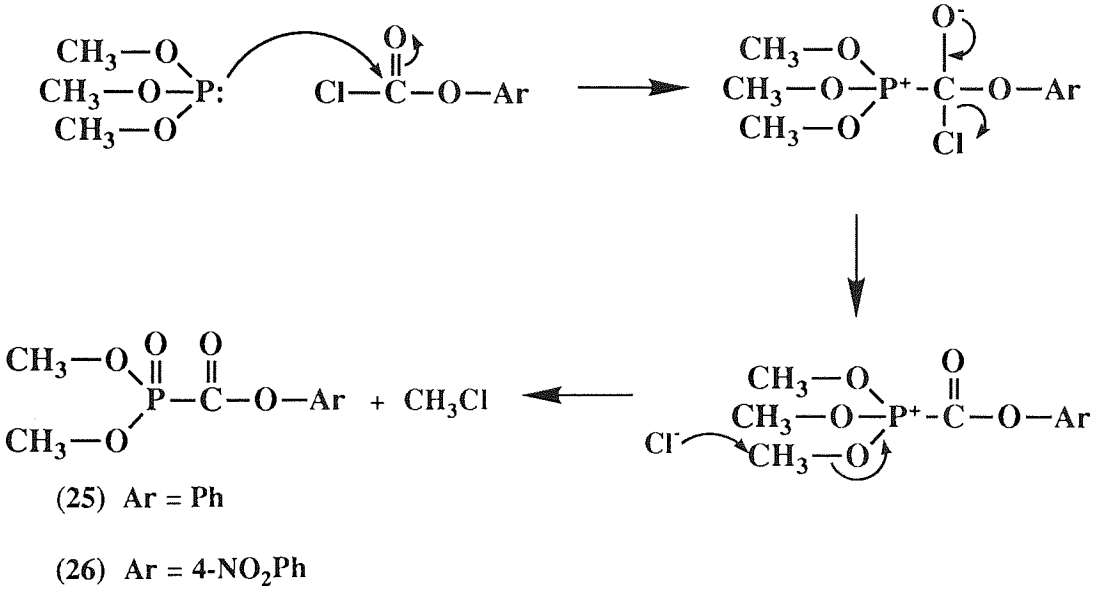

(**25**) Ar = Ph

(**26**) Ar = 4-NO_2Ph

Figure 2.2 - Arbuzov Reaction Mechanism

The phenyl triester (**25**) was distilled and characterised spectroscopically. For example ^{1}H NMR (300 MHz, $CDCl_3$) δ 3.90 (6H, d, J_{PH}=11 Hz, 2xOCH_3), ^{13}C NMR (75.5 MHz, $CDCl_3$) δ 166.23 (d, J_{PC}=275 Hz, C=O), ^{31}P NMR (121.5 MHz, ^{1}H decoupled, $CDCl_3$) δ -3.18 (sept, J_{PH}=11Hz) and IR (liquid film) 1720cm^{-1} (C=O). The 4-nitrophenyl triester (**26**) was recrystallised from toluene and data included, ^{1}H NMR (60 MHz, $CDCl_3$) δ 3.9 (6H, d, J_{PH}=11 Hz, 2xOCH_3) and IR (liquid film) 1720cm^{-1} (C=O). However, it readily decomposed at room temperature to give 4-nitrophenol [^{1}H NMR (60 MHz, $CDCl_3$) δ 9.3 (^{1}H, s, OH, D_2O exchangeable), 8.3 (2H, d, J_{HH}=9 Hz,

aromatic), 7.2 (2H, d, J_{HH}=9 Hz, aromatic)] and a compound still bearing the $POCH_3$ group [δ 3.8 (d, J_{PH}=11 Hz, 2xOCH_3)]. In an attempt to gain more information about the phosphorus-containing product, the hydrolysis of the more stable phenyl ester (**25**) was followed by ^{31}P NMR spectroscopy. In acetonitrile, (**25**) had a chemical shift of 1.9 ppm. Five minutes after the addition of an equal volume of phosphate buffer at pH 7.4 only a single peak at 14.6 ppm could be observed. A proton-coupled spectrum, two hours after the addition, showed the peak at 14.6 ppm as a doublet of septets with a very large J_{PH}=718 Hz for a P-H group and J_{PH}=12 Hz for a $P(OCH_3)_2$ group, characteristic of dimethyl phosphite. This was later confirmed by the addition of a commercially available authentic sample. The coupled spectrum also showed the emergence of a doublet of quartets at 8.2 ppm with coupling constants of J_{PH}=626 Hz and J_{PH}=12 Hz. This is consistent with methyl phosphite, the product of hydrolysis of dimethyl phosphite. From these results, it is suggested that the electron-withdrawing leaving group promotes nucleophilic attack at the carbonyl to give the intermediate (**27**) (see Figure 2.3). Dimethyl phosphite (**29**) can be formed by direct P-C bond cleavage, as in (**i**), or loss of the phenol to give, transiently, dimethyl carboxyphosphonate (**28**) which undergoes decarboxylation, as in (**ii**). Precedence for decarboxylation is provided by Warren and Williams who showed that, in the presence of acid, PFA undergoes decarboxylation to phosphorous acid.[43] Further hydrolysis of (**29**) gives methyl phosphite (**30**). In comparison to the hydrolysis of dibenzyl methoxycarbonyl-phosphonate (**19**), it can be seen that P-C bond cleavage is favoured by a good leaving group on the carboxyl and therefore should be avoided in the design of triester prodrugs of PFA.

Krol *et al* [68] also investigated the hydrolysis of PFA triesters. They concluded that to minimise P-C bond cleavage, the phosphate ester must be a better leaving group than the carboxylate ester. Mitchell *et al* have also synthesised para-substituted benzyl derivatives of (**19**) which minimised the production of phosphite on hydrolysis but further reduced the hydrolytic stability of the triesters.[67] Iyer *et al* [65] examined acyloxymethyl triesters of PFA which were reported to be stable either in the concentrated form or in aprotic solvents at -20°C and were highly unsuitable as prodrugs (see section 1.3.1). The use of such leaving groups to minimise P-C bond cleavage is therefore likely to result in triesters with short chemical half-lives, unsuitable as prodrug forms. Triesters are therefore unlikely to be suitable as prodrugs of PFA and diesters will now be considered.

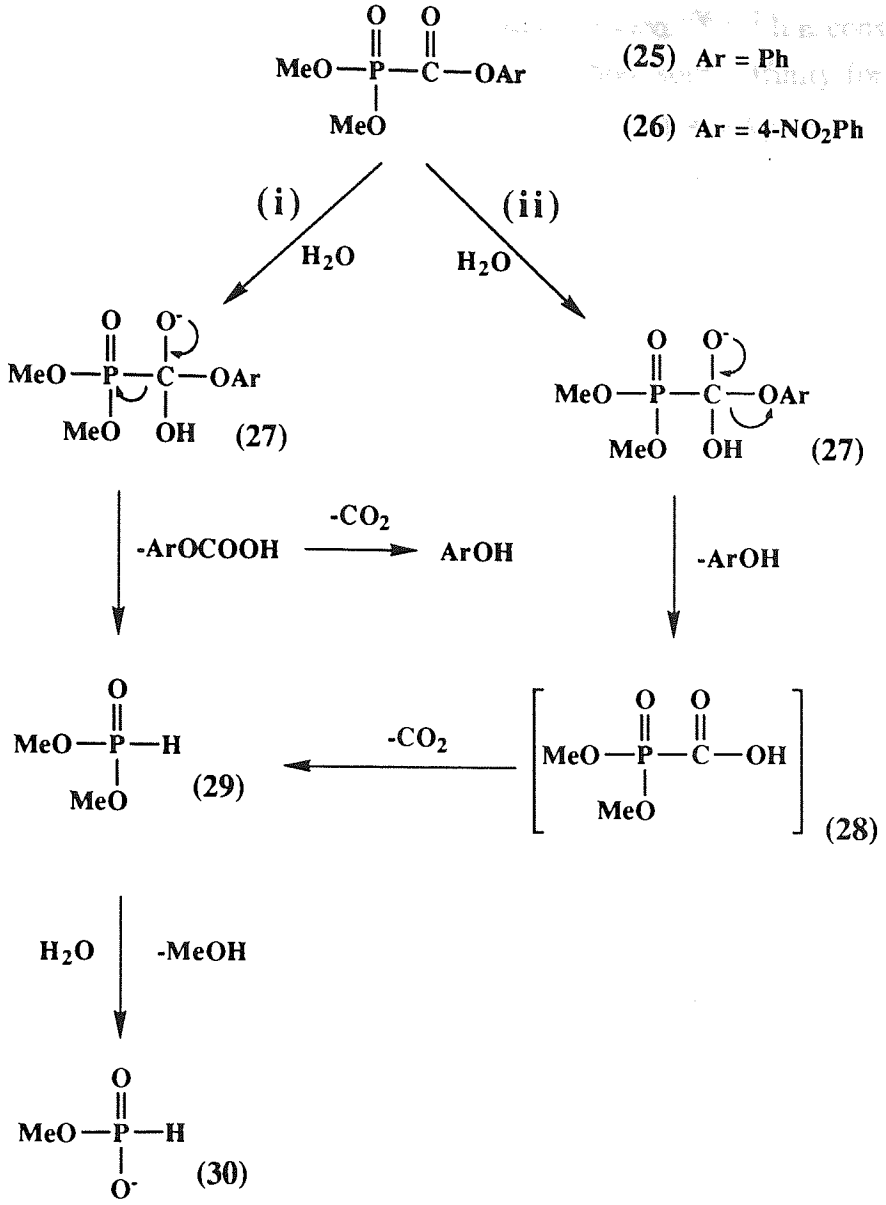

Figure 2.3 - Hydrolysis of (25) Ar = Ph and (26) Ar = 4-NO_2Ph

2.2 Diesters of PFA

In contrast to the uncharged lipophilic triesters of PFA, diesters of PFA are monoanionic at physiological pH, making them hydrophilic. It is anticipated that this will preclude significant brain penetration of these molecules by simple lipophilic diffusion, and methods of actively transporting PFA as a diester are considered.

2.2.1 α-Keto Acids Analogues of PFA

The carrier-mediated BBB transport of short chain mono-carboxylic acids (MCAs) was first described by Oldendorf.[105] α-Keto acids, for example pyruvate (**31**), show the

highest affinity for the monocarboxylic acid transport system.[106,107] It is considered that diesters of PFA as analogues of α-keto acids may show some affinity for the MCA system and achieve brain penetration. Two types of PFA alkyl diesters may be envisaged, both of which could be analogues of α-keto acids. They are the sodium alkyl methoxycarbonyl-phosphonates (**32**) and the sodium dialkyl carboxyphosphonates (**33**). However, as discussed for the hydrolysis of triesters, the latter type with a free carboxylate group will readily decarboxylate.

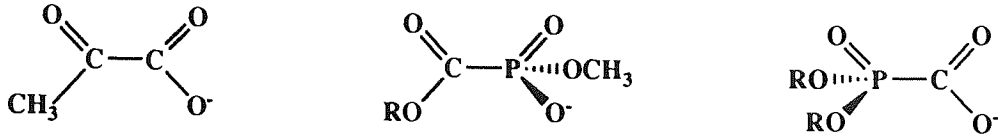

Pyruvate (31) (32) (33)

R = alkyl or aryl group

Figure 2.4 - PFA Diesters as α-Keto Acid Analogues

The substitution of a phosphonate group for a carboxylate, as in (**32**), is a common isosteric replacement in medicinal chemistry. A recent example of this is use of phosphonates as N-methyl-D-aspartate receptor antagonists.[108] Indeed PFA, as a pyrophosphate analogue, indicates the interchangable nature of carboxylates and phosphonates. A range of compounds of type (**32**) were prepared from the corresponding triesters (see Figure 2.5). A series of dimethyl alkyloxycarbonylphosphonate triesters (**34-42**) of varying carboxyl ester were synthesised by published procedures[60] as described earlier for (**25**) and (**26**) (see Figure 2.2). The triesters were distilled and characterised by ^{1}H, ^{13}C and ^{31}P NMR and IR spectroscopy. They were treated with one equivalent of sodium iodide in acetone to give the diesters (**43-51**), which were also characterised by ^{1}H, ^{13}C and ^{31}P NMR spectroscopy, IR spectroscopy and elemental analysis. The corresponding monoesters (**52-59**), were prepared by treatment of the triester with trimethylsilyl bromide followed by hydrolysis of the bis(trimethylsilyl) ester (**60**).[60] They were prepared as possible standards for stability studies and for anti-HIV testing. The disodium salts of the monoesters were characterised by ^{1}H, ^{13}C and ^{31}P NMR and IR spectroscopy. ^{31}P NMR, ^{1}H coupled spectra were highly characteristic, giving septets for triesters, quartets for diesters and singlets for monoesters. The typical coupling constant of 11 Hz, seen in these spectra, was also observed in the doublets given by P-methoxy groups in ^{1}H NMR spectra.

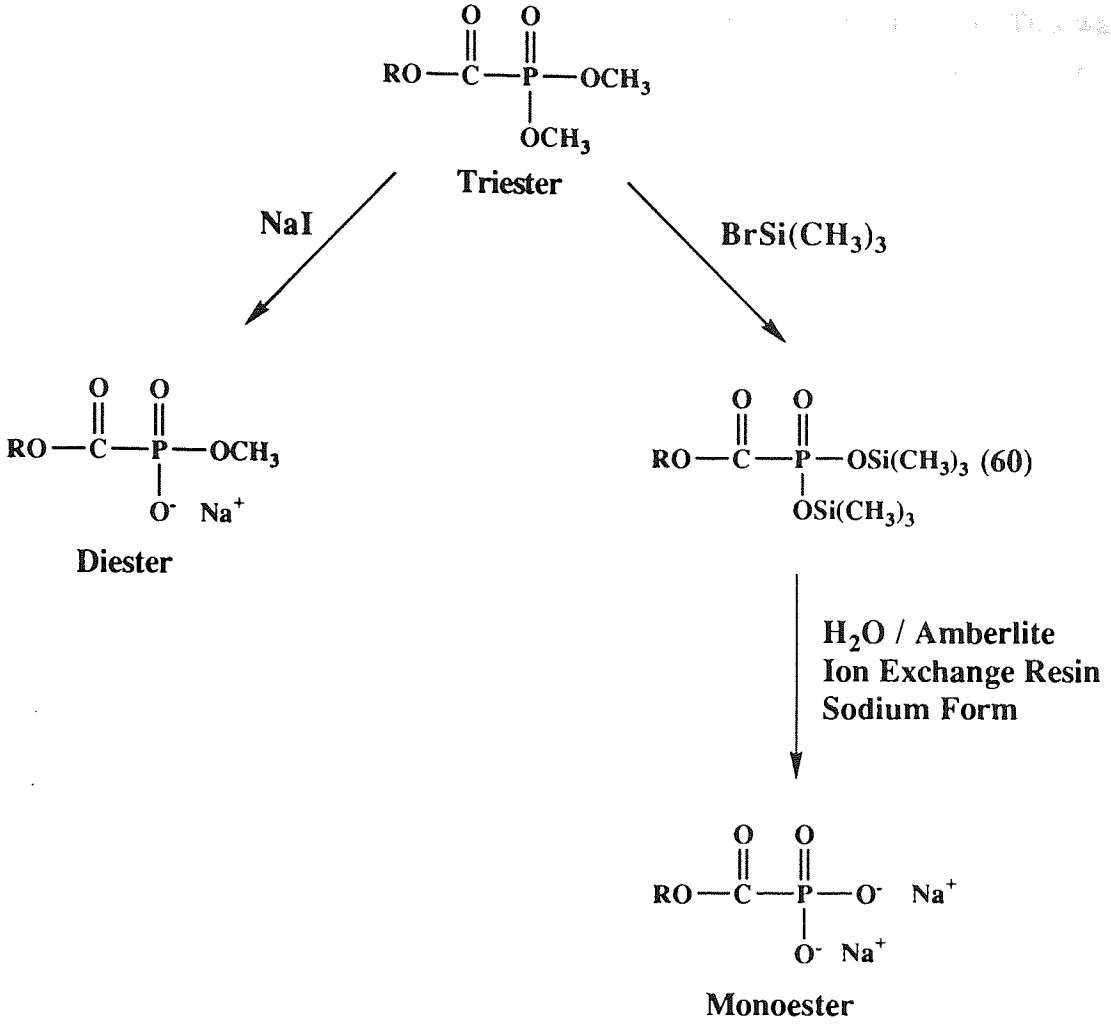

Nature of R Group	Triester	Diester	Monoester
Methyl	(34)	(43)	(52)
Ethyl	(35)	(44)	(53)
n-Propyl	(36)	(45)	(54)
n-Butyl	(37)	(46)	(55)
2-Methylpropyl	(38)	(47)	(56)
n-Octyl	(39)	(48)	(57)
Benzyl	(40)	(49)	(58)
Phenyl	(41)	(50)	(59)
4-Nitrophenyl	(42)	(51)	-

Figure 2.5 - Synthesis of Diesters and Monoesters of PFA

In my hands the literature procedure for the preparation of methyl disodium carboxyphosphonate (**61**)[60] which required the reacting of dimethyl butyloxy-carbonylphosphonate with 50% aqueous sodium hydroxide yielded only PFA. This was shown by no signals in the ^{1}H NMR (60 MHz) spectra and an IR spectra comparable to that of an authentic sample of PFA. Milder hydrolysis conditions using sodium carbonate gave the desired compound (**61**) which was characterised by ^{1}H NMR, ^{13}C NMR [signals including δ 180.23 (d, J_{PC}=230 Hz, C=O)], ^{31}P NMR [signals including δ 4.79 (q, J_{PH}=11 Hz)] and IR spectroscopy.

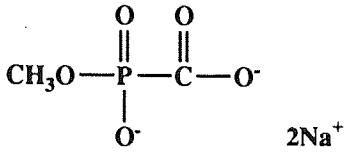

(**61**)

In contrast to the high reactivity of the triesters, by ^{31}P NMR spectroscopy the diester sodium methyl methoxycarbonylphosphonate (**43**) was shown to be completely stable over 24 hours in phosphate buffer at pH 7.4 at 37°C

2.2.2 Amino Acids Analogues of PFA

Following the synthesis of a series of α-keto acid analogues, the design of a prodrug of PFA that may have some affinity for the large amino acid (LAA) transport system of the BBB was considered. The structures of the amino acids and drugs transported into the brain by the LAA transport system are shown in Figure 2.6. From the stereochemistry of these compounds the primary structural requirement for the transporter system, appears to be, an α-amino acid group in the L-configuration. Structural variations such as the bulky alkylating group in melphalan (**66**) and D, L-NAM (**67**) and the basic nature of histidine (**63**), appear to be acceptable to the transporter protein receptor.

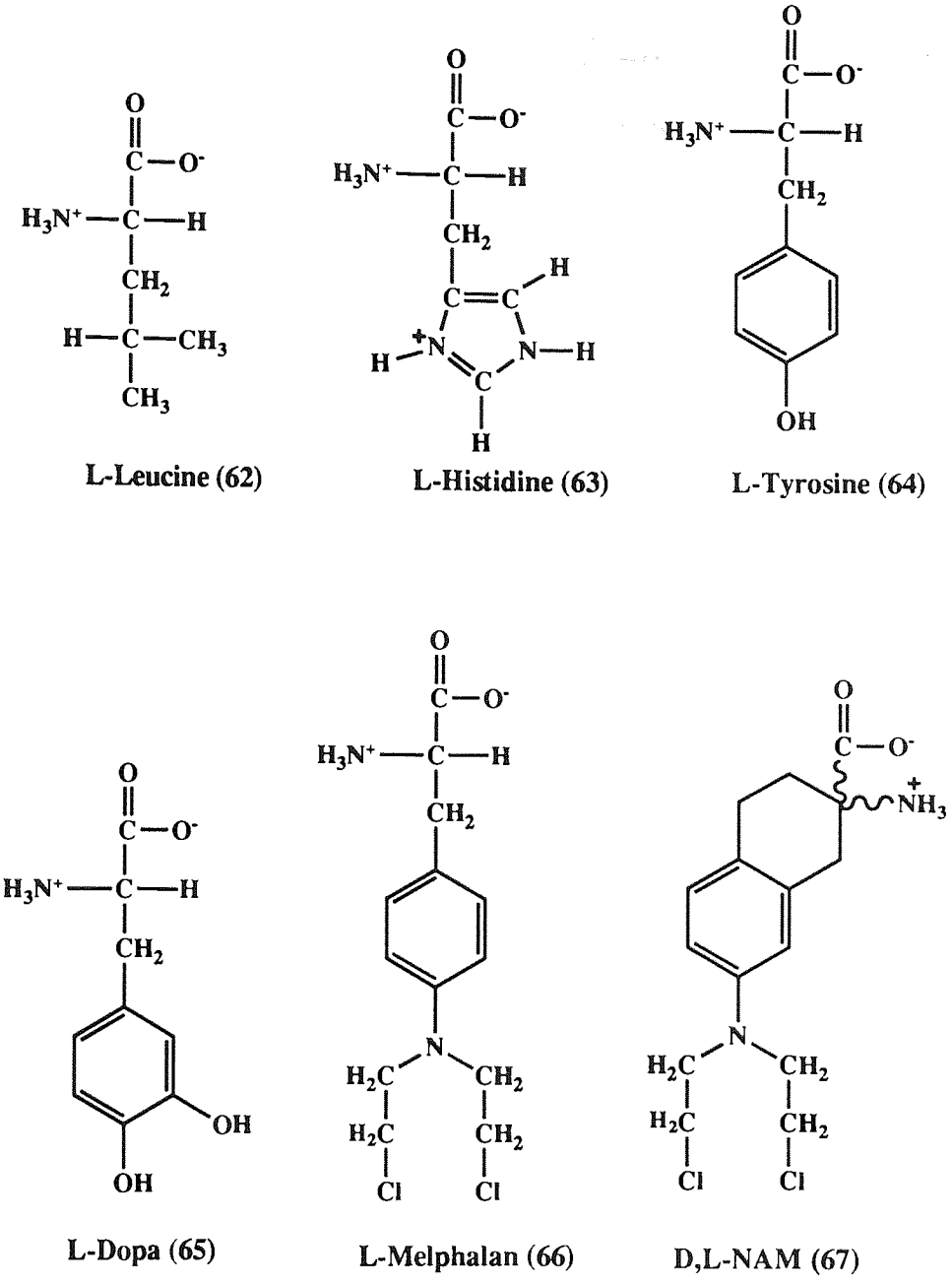

Figure 2.6 - Amino Acids and Drugs Transported by the LAA Transporter as Depicted by their Fischer Projection

Two structures in which L-tyrosine could be used as a carrier for PFA are **(68)** and **(69)**. It is anticipated that passage into the brain will occur *via* the LAA transport system, the ester linkage between PFA and the carrier will then be hydrolysed together with the other ester to give PFA.

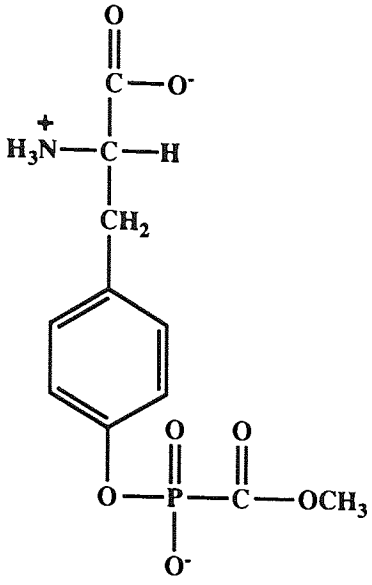

(68)

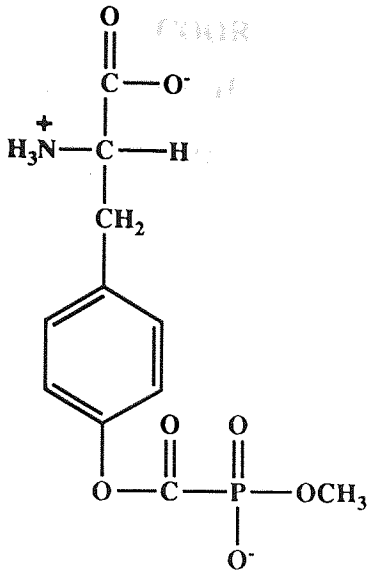

(69)

A synthetic strategy to obtain the diester (**69**), involves treating a suitably protected tyrosine (**70**) with triphosgene to give the chloroformate (**71**) and proceeds *via* an Arbuzov reaction with trimethyl phosphite. The resulting triester (**72**) could then be mono demethylated by reaction with sodium iodide to give the corresponding diester. Removal of the protecting groups on the carboxyl and amino terminals of the tyrosine residue would give the product (**69**) (see Figure 2.7).

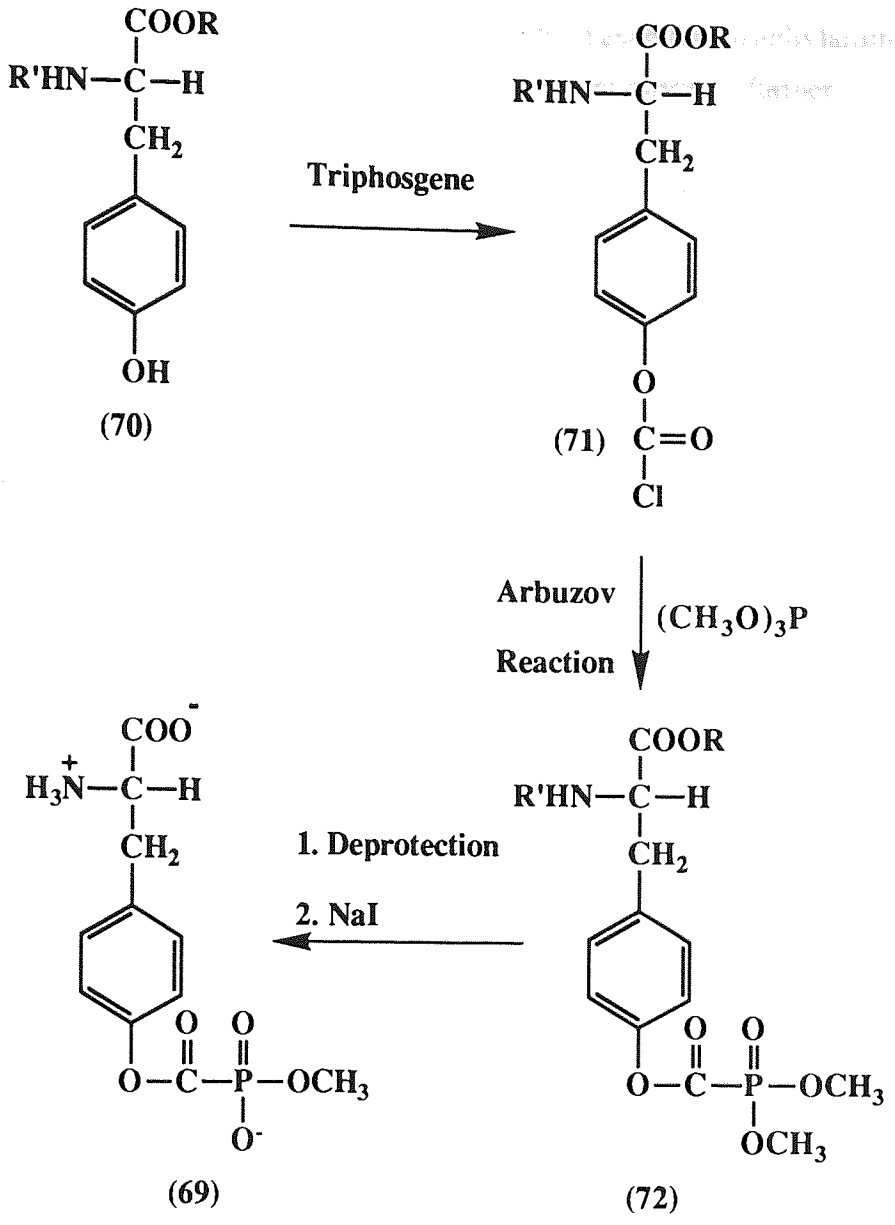

Figure 2.7 - Proposed Synthesis of a Tyrosine-Linked PFA Diester Prodrug (69) (R and R' = Protecting Groups)

As a model compound, phenyl chloroformate was prepared from phenol by a method similar to that described by Zabik and Schuetz for the preparation of aryl chloroformates,[109] but with the replacement of liquid phosgene and benzene with the far less hazardous triphosgene and dichloromethane. It was hoped that this method could be extended to the reaction of N-acetyl tyrosine ethyl ester (73) with triphosgene to give the chloroformate. Although a trace amount of the anticipated chloroformate was produced, as shown by an infra-red peak at 1780cm^{-1}, the reaction largely proceeded to give 5-ethoxy-4-(4'-hydroxyphenylmethyl)-2-methyl oxazole (74). Data leading to this conclusion included, the absence of an α-H in the ^{1}H NMR spectra, absence of ester and amide carbonyls in the IR spectra and the required molecular formula for (74) given by mass spectrometry and elemental analysis. This finding was supported by the reported

reaction of α-amino carbonyl compounds with phosgene and triethylamine to give substituted oxazoles.[110] The synthesis of (**69**) was not investigated further.

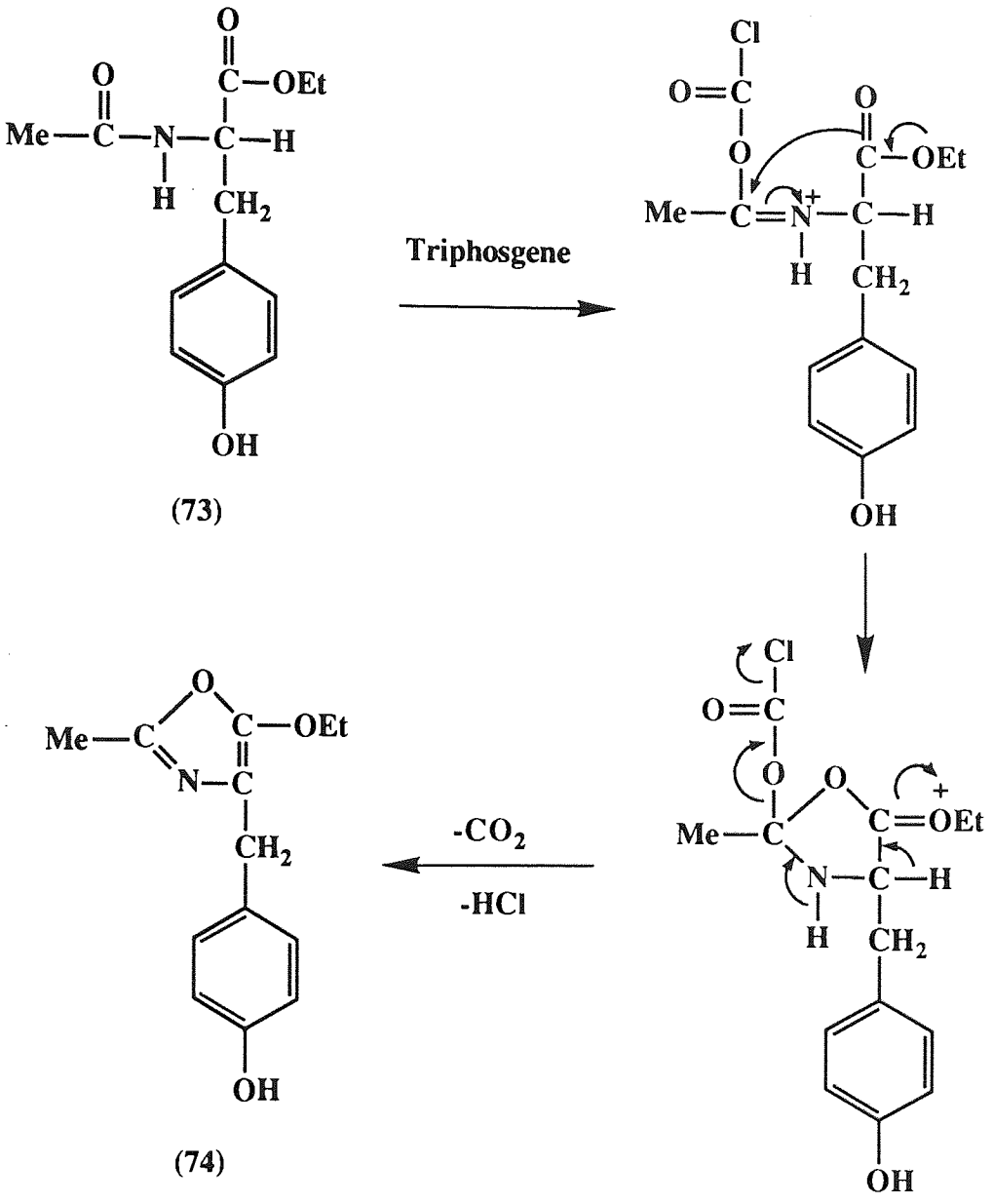

Figure 2.8 - Mechanism of Substituted Oxazole Formation

The synthesis of diester (**68**) was then investigated. Methoxycarbonylphosphonic dichloride (**75**) was synthesised according to the method of Morita *et al* [111] by first treating dimethyl methoxycarbonylphosphonate (**34**) with two equivalents of trimethylsilyl bromide to give the bis(trimethylsilyl) ester (**76**) which was then reacted with phosphorus pentachloride. As a model reaction, one mole of the dichloride (**75**) was treated with two moles of phenol to give diphenyl methoxycarbonylphosphonate (**77**) in high yield (73%), as a colourless oil. This electron-withdrawing effect of the phenyl groups in (**77**) resulted in a characteristic ^{31}P NMR shift of -13.10 ppm.

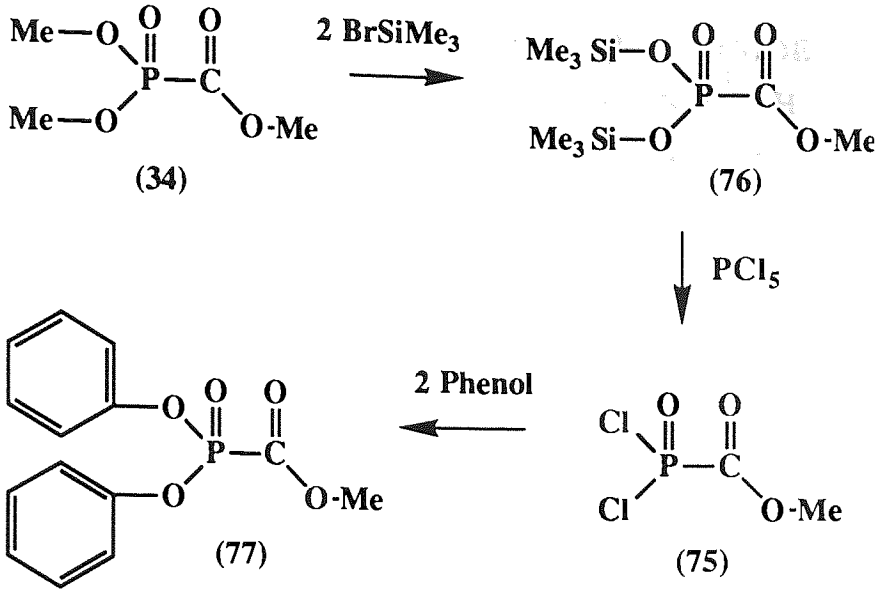

Figure 2.9 - Synthesis of Diphenyl Methoxycarbonylphosphonate (77)

This procedure was then extended by reacting one equivalent of the dichloride (**75**) with two equivalents of N-acetyl L-tyrosine ethyl ester (**73**). This reaction was followed by TLC, eluting with ethyl acetate to detect the formation of triester and eluting with propan-2-ol - water - concentrated ammonium hydroxide (7:2:1) to detect the formation of diester. The reaction did not to go to completion and it is possible, that due to steric hindrance, only one mole of substituted phenol (**73**) will react with one mole of the dichloride (**75**). The reaction was repeated with the reactants in equimolar quantities to give (**78**) which was then subjected, without isolation, to hydrolysis in the presence of a cation-exchange resin in the sodium form to give sodium 4-(2'-ethoxycarbonyl-2'-acetamidoethyl)phenyl methoxycarbonylphosphonate (**79**) (see Figure 2.10). Purification of this product proved difficult. Washing with ether removed (**73**) but ^{31}P NMR showed the presence of disodium methoxycarbonylphosphonate (**52**). Anion-exchange chromatography was attempted and a fraction thought to be the product was collected, however, it was impure and degradation was thought to occur during concentration. Eventually, a pure sample was prepared by preparative TLC using silica plates and eluting with methanol - dichloromethane (1:4). The product was characterised spectroscopically and by elemental analysis. For example ^{1}H NMR (250 MHz, D_2O) δ 3.76 (3H, s, OCH_3), ^{13}C NMR (63 MHz, D_2O) δ 55.14 (d, J_{PC}=4.5 Hz, OCH_3) and ^{31}P NMR (101 MHz, ^{1}H coupled, D_2O) δ -7.38 (s).

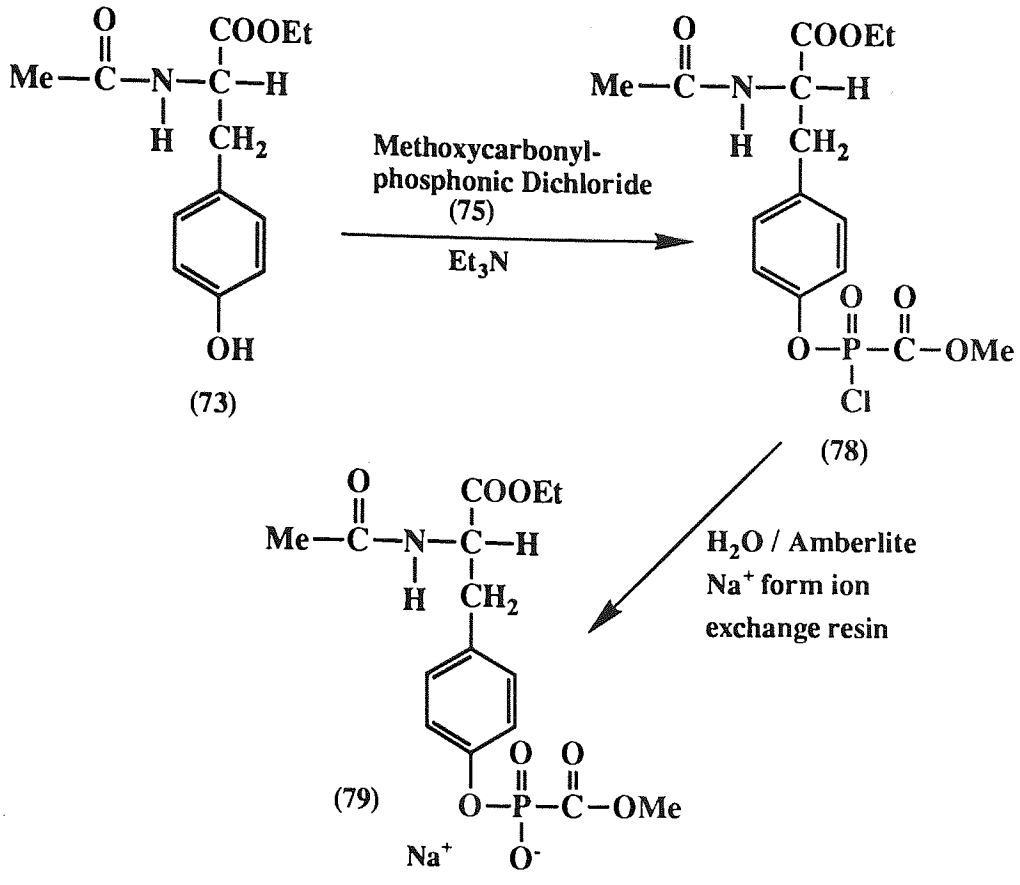

Figure 2.10 - The Synthesis of (79)- a Protected Tyrosine-Linked PFA Diester

Hydrolysis of the ethyl ester and of the amide group of (**79**) was not considered possible without hydrolysis of the PFA ester linkages. Basic hydrolysis to remove the ethyl ester would probably result in cleavage of the methyl ester and the phosphonate ester as previously seen in the attempted synthesis of disodium methyl carboxyphosphonate (**61**) (see section 2.2.1). Acidic hydrolysis may also result in ester cleavage and possibly in P-C bond cleavage.[43] Therefore, a protected tyrosine which could be selectively deprotected was sought. N-Carbonyloxybenzyl L-tyrosine benzyl ester (**80**) with protecting groups removable by catalytic hydrogenation was considered appropriate. The preparation of this protected tyrosine was first attempted by synthesising N-carbonyloxybenzyl L-tyrosine (**81**) by a standard procedure using L-tyrosine and benzyl chloroformate.[112] However, attempted esterification with benzyl alcohol in the presence of thionyl chloride gave a precipitate which by IR spectroscopy indicated an anhydride with peaks at 1820 and 1750cm^{-1}. Formation of L-tyrosine N-carboxyanhydride (**82**) was supported by ^{1}H NMR spectroscopy, in particular the absence of the benzyl group. The synthesis of an N-carboxyanhydride from the reaction of di-N-carbonyloxybenzyl lysine with phosphorus pentachloride was consistent with this assignment. [112]

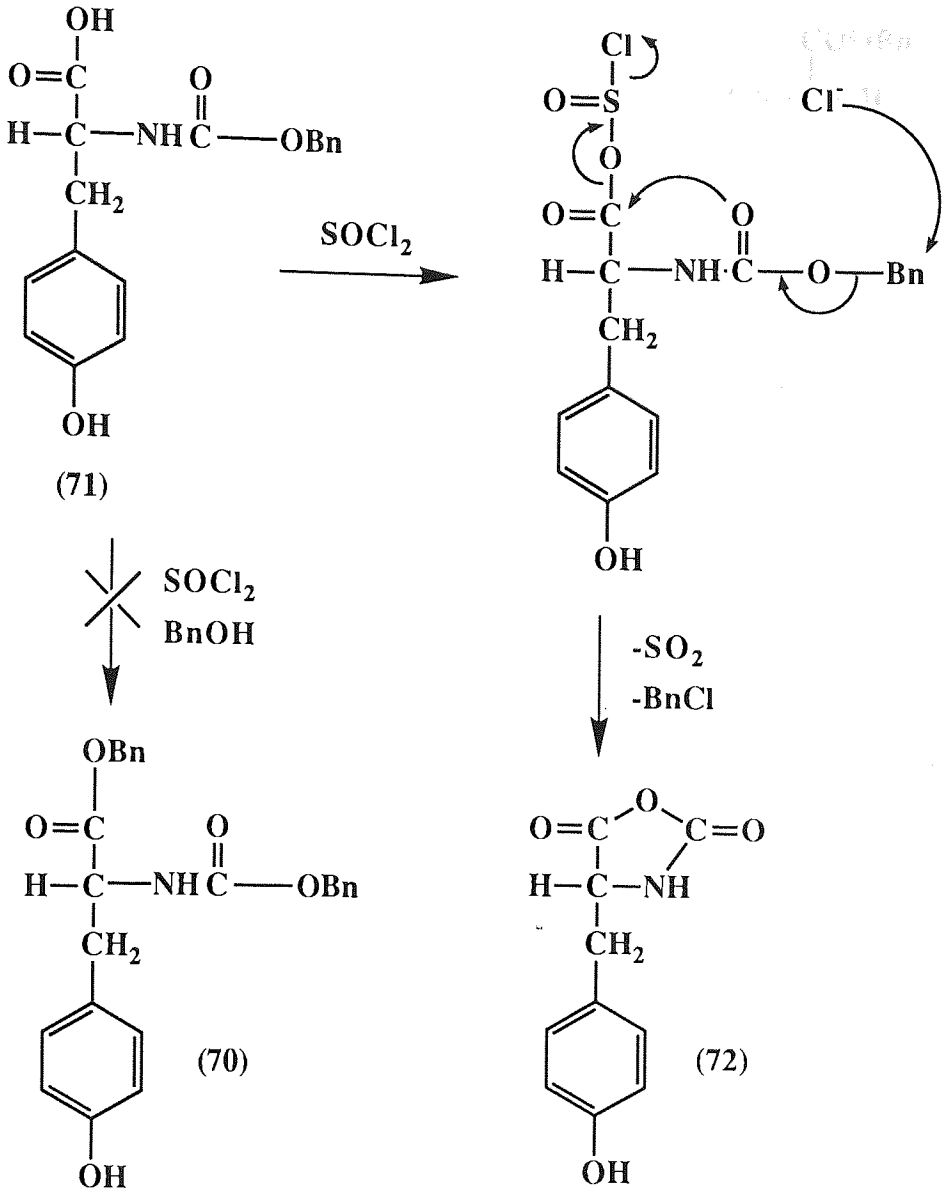

Figure 2.11 - The Synthesis of Tyrosine N-Carboxyanhydride (82)

The successful synthesis of N-carbonyloxybenzyl tyrosine benzyl ester (**80**) was achieved by first preparing the benzyl ester of L-tyrosine. The esterification was performed by the method of Erlanger and Hall[113] which involved stirring L-tyrosine in excess benzyl alcohol at 90-95°C with polyphosphoric acid as a dehydrating agent to give L-tyrosine benzyl ester (**83**). The benzyl ester (**83**) was then dissolved in ice cold acetonitrile, and benzyl chloroformate was added. As well as the required product (**80**), some O-benzyl carbonate formation also occurred to give (**84**), but this was minimised by using a slight excess of benzyl ester, maintaining the temperature at 0°C and adding the benzyl chloroformate dropwise. Separation of the required product was performed by flash chromatography.[114]

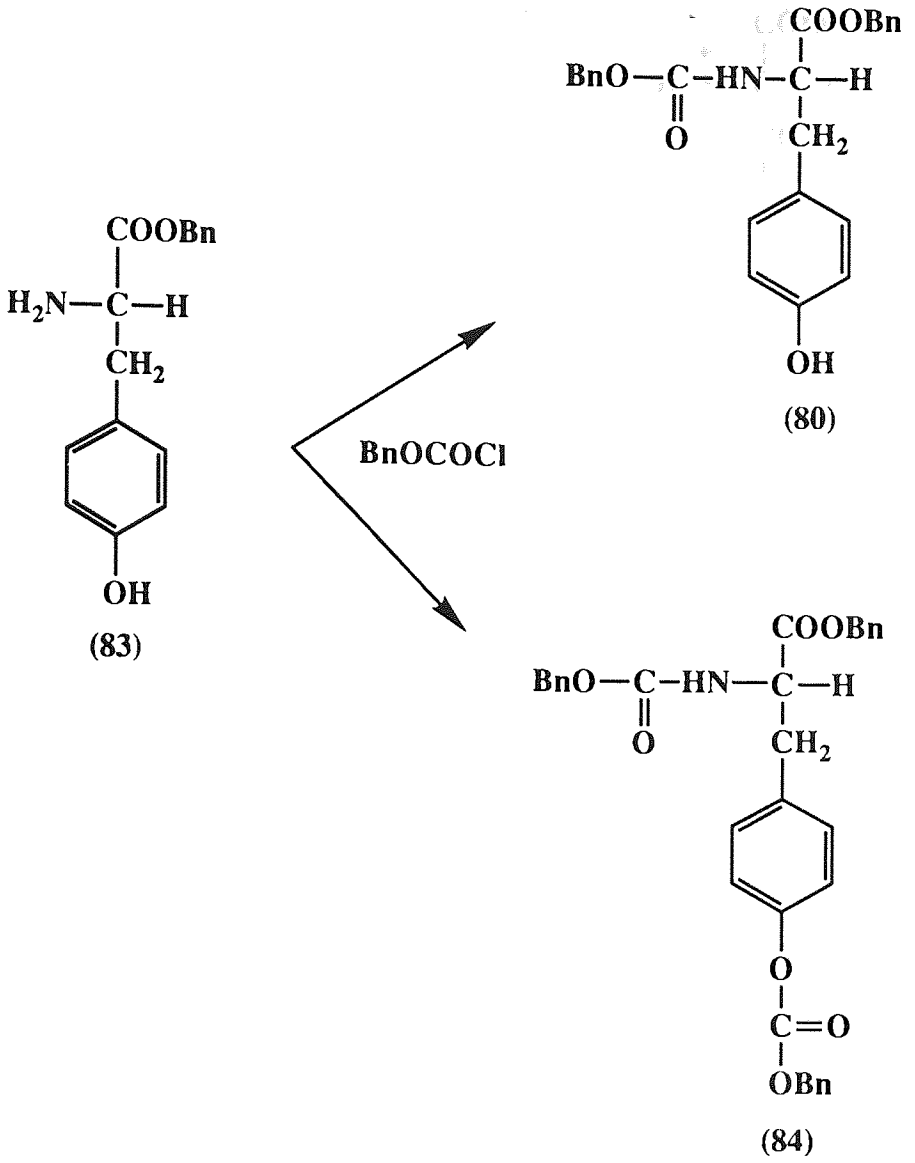

Figure 2.12 - Synthesis of N-Carbonyloxybenzyl-L-Tyrosine Benzyl Ester (80) and Carbonate By-Product (84)

One equivalent of N-carbonyloxybenzyl-L-tyrosine benzyl ester (**80**) was then treated with one equivalent of methoxycarbonylphosphonic dichloride (**75**), in a manner similar to that descibed for N-acetyl-L-tyrosine ethyl ester (**73**) (see Figure 2.10). The product, sodium 4-[2'-(benzyloxycarbonyl)-2'-(N-carbonyloxybenzylcarbamate)ethyl]phenyl methoxycarbonylphosphonate (**85**) was then purified by preparative TLC using silica plates and eluting with methanol - dichloromethane (3:17). The product was fully characterised by ^{1}H, ^{13}C, ^{31}P NMR, and IR spectroscopy and by elemental analysis. For example, ^{1}H NMR (250 MHz, CD_3OD) δ 3.68 (3H, s, OCH_3), ^{13}C NMR (63 MHz, CD_3OD) δ 51.84 (d, J_{PC}=4.5Hz, OCH_3), ^{31}P NMR (101 MHz, ^{1}H coupled, CD_3OD) δ -6.96 (s) and IR (Nujol mull) 1710cm^{-1} (C=O, methyl ester). Deprotection with hydrogenation using a palladium catalyst gave sodium 4-(2'-carboxyl-2'-aminoethyl)phenyl methoxycarbonylphosphonate (**68**) (see Figure 2.13).

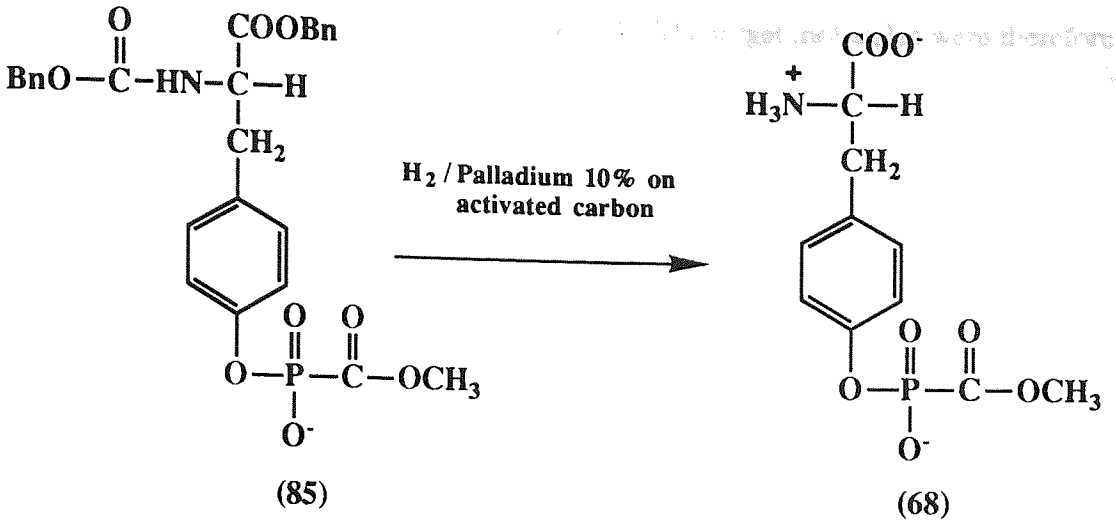

Figure 2.13 - Hydrogenation of (85) to give (68)

The diester (68) was then fully characterised by ^{1}H, ^{13}C and ^{31}P NMR and IR spectroscopy, mass spectrometry and elemental analysis. For example, ^{1}H NMR (250 MHz, CD_3OD) δ 3.86 (3H, s, OCH_3), ^{13}C NMR (63 MHz, CD_3OD) δ 55.23 (d, J_{PC}=4.5Hz, OCH_3), ^{31}P NMR (101 MHz, ^{1}H coupled, CD_3OD) δ -7.35 (s) and IR (Nujol mull) 1700cm^{-1} (C=O, methyl ester). Monitoring by ^{31}P NMR spectroscopy, diester (68) was shown to be completely stable over 24 hours in phosphate buffer at pH 7.4, at 37°C.

2.2.3 Lipid Analogues of PFA

Hydrophilic drugs, for example, L-dopa,[77] GABA[80-82] and nucleosides,[78] have been targeted to the brain by derivatisation with lipid molecules (see section 1.4.3). Conjugation of PFA with a lipid molecule may provide a method of enhancing both oral and brain delivery. The masking of polar groups of the parent drug does not appear necessary for enhanced delivery of lipid analogues, therefore diesters and monoesters of PFA may be suitable prodrug forms. In designing the PFA-lipid conjugate, the positioning of PFA on the glycerol backbone and the nature of the acyl chains was considered. PFA was attached to the 1-position on the glycerol, similar to the GABA and nucleoside lipids reported, although substitution at the 2-position may possibly afford more protection from lipases.[77] GABA-containing lipids have been reported to have varying brain uptake depending on the nature of the acyl groups of the lipids,[80-82] but the significance and mechanism of this effect is unclear. A fully saturated acyl chain was considered preferable to keep the synthesis as straight-forward as possible. Palmitoyl chains, as used in the L-dopa and nucleoside lipids, were selected. The final consideration in the designing the PFA-lipid conjugate was whether PFA should be linked by a phosphonate or carboxylate ester. For ease of synthesis, it was considered

preferable to link through the carboxyl end of PFA. The target molecules were therefore (**86**) and (**87**).

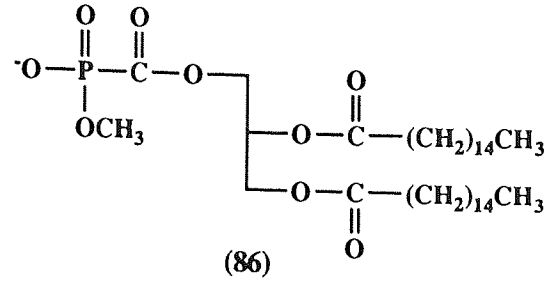

(**86**)

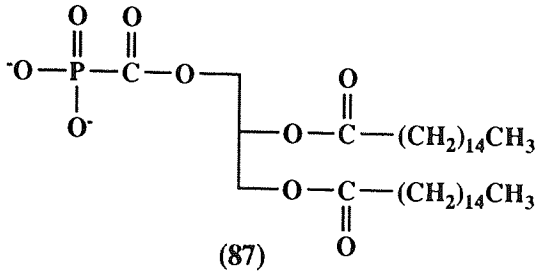

(**87**)

The preparation of (**86**) and (**87**) from 1,2-dipalmitoyl glycerol (**92**) is shown in Figure 2.15. The synthesis first required the preparation of 1,2-dipalmitoyl glycerol (**92**) and the route employed is shown in Figure 2.14. 1,2-Dipalmitoyl glycerol (**92**) was prepared in a four-step synthesis from solketal (1,2-isopropylidene-*rac*-glycerol) (**88**). The benzyl ether of solketal (**89**) was prepared using the method of Vogel.[115] The isopropylidene group was removed by refluxing in acid using the method of Sowden and Fischer[116] to give 1-benzyl glycerol (**90**). Esterification with palmitoyl chloride[116] gave compound (**91**). The benzyl group of (**91**) was removed by hydrogenation to give (**92**). All compounds were characterised by ^{1}H, ^{13}C, ^{31}P NMR and IR spectroscopy. Compounds (**86**), (**87**) and (**94**) were also characterised by elemental analysis

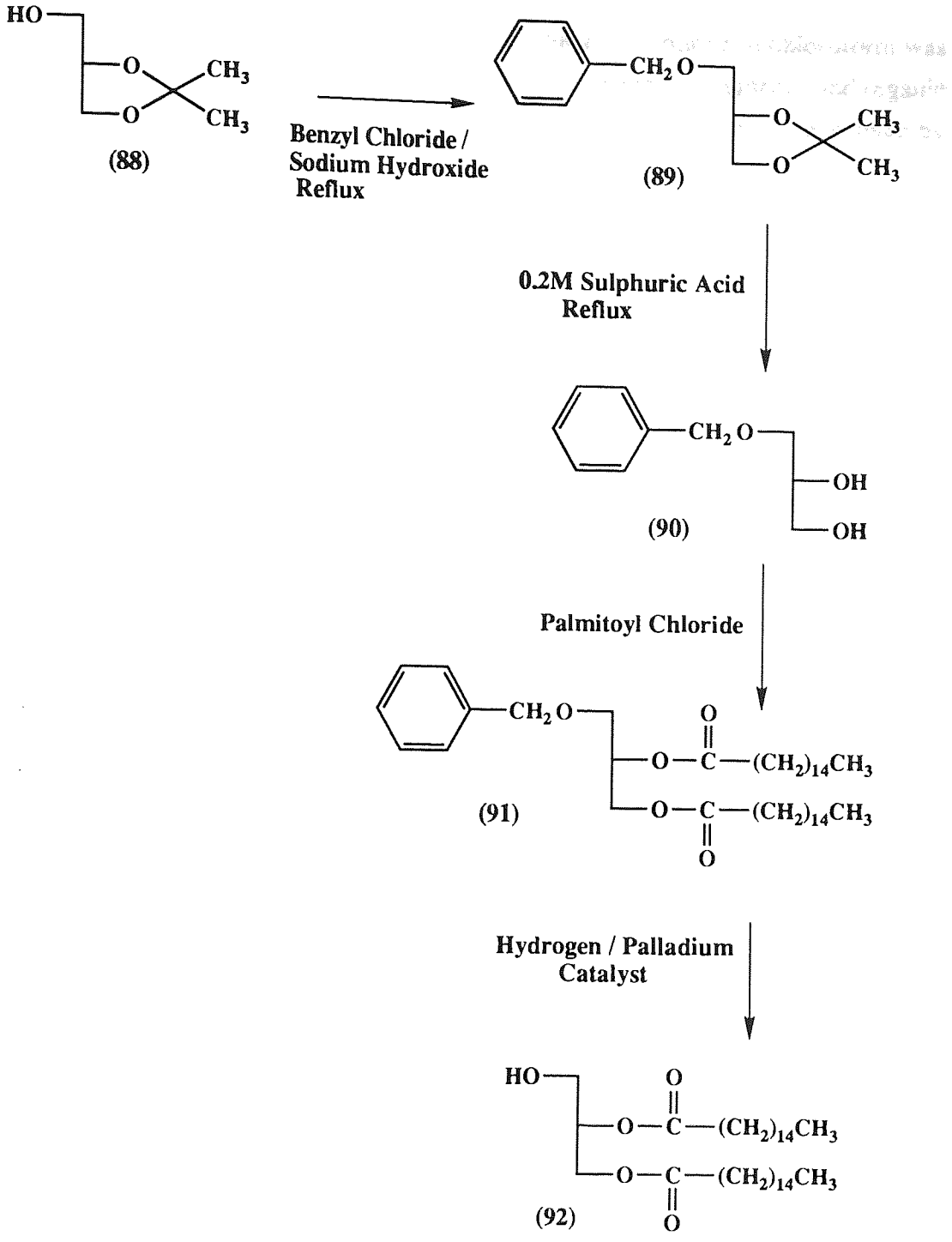

Figure 2.14 - Synthesis of Dipalmitoyl Glycerol (92)

The chloroformylation of (92) was performed using triphosgene and triethylamine in dichloromethane. The success of this step was indicated by IR spectroscopy (1775cm^{-1}, C=O, chloroformate). The chloroformate (93) was then reacted with trimethyl phosphite to give the triester (94) which was purified by flash chromatography eluting with ethyl acetate - hexane (1:1). Data for (94) included a septet in the ^{1}H coupled ^{31}P NMR spectra. Selective mono-demethylation of (94) was achieved using sodium iodide to give the diester (86). Treatment with 2 equivalents of trimethylsilyl bromide followed by hydrolysis of the bis(trimethylsilyl) ester using cyclohexylamine-water[117] gave the

monoester (87). The cyclohexylammonium salt which was soluble in chloroform was prepared because the sodium salt was found to be insoluble in both aqueous and organic solvents. ^{1}H and ^{31}P NMR coupling patterns were hidden by the broad peaks given by compounds (86) and (87).

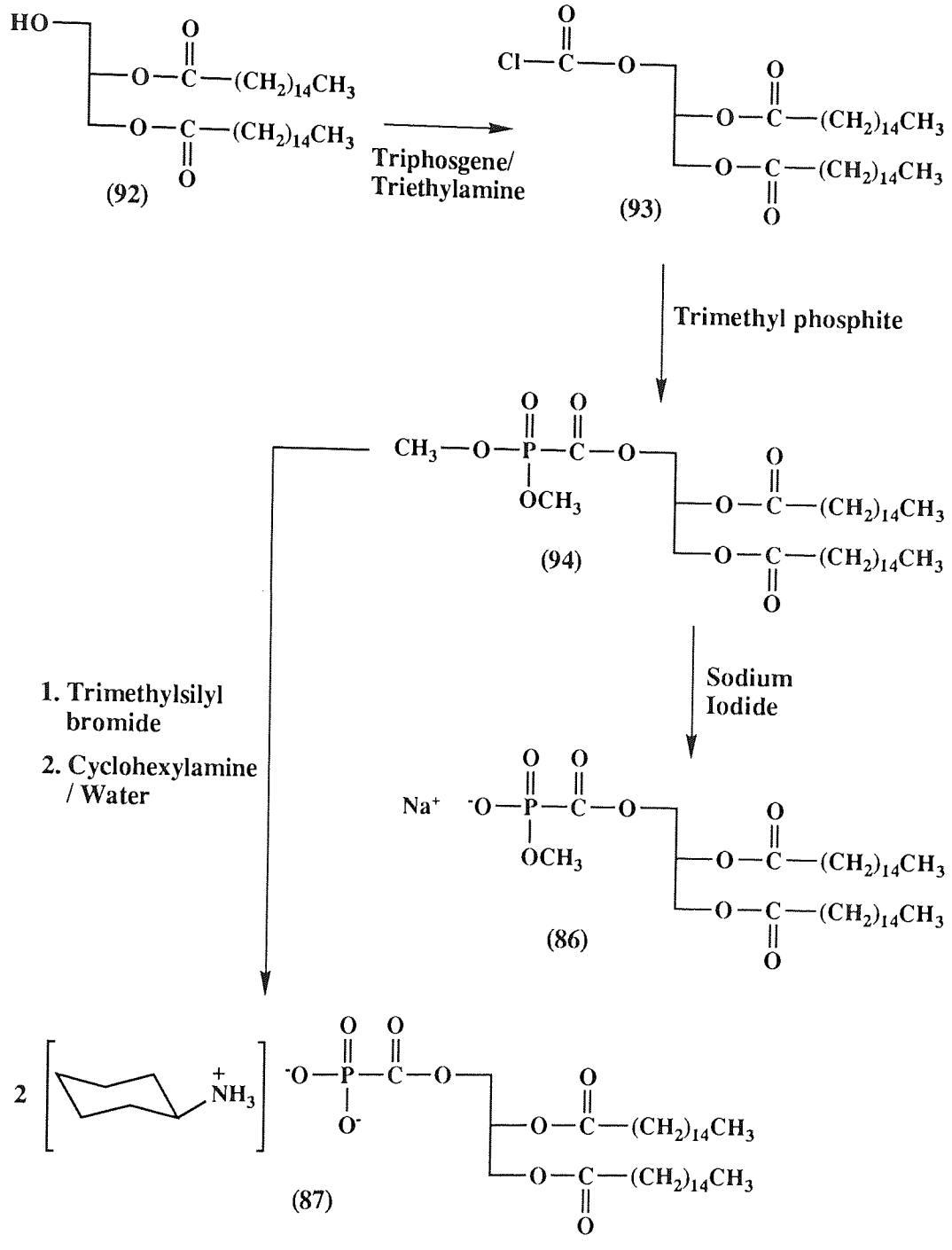

Figure 2.15 - Synthesis of Lipid-PFA Triester (94), Diester (86) and Monoester (87)

2.3 Anti-HIV Testing

Compounds synthesised containing the PFA moiety were tested for anti-HIV activity. PFA was used as a control. The results listed in Tables 2.1, 2.2 and 2.3 were supplied by Dr. A. Hay, National Institute for Medical Research, Mill Hill, London. The EC_{50} values represent the concentration of compound which reduces the HIV antigen (either gp120 or p24) by 50% in HIV-infected C8166 T-lymphoblastoid cell cultures and is therefore an expression of anti-HIV activity. Values in excess of 1000 μM indicate that no activity was observed. The TC_{50} values represent the concentration of drug which reduces cell growth by 50% and is therefore an expression of toxicity. Values in excess of 1000 μM indicate that no toxicity was observed. This method is summarised in section 4.3.

From Table 2.1 it can be seen that very low activity is shown by sodium methyl benzyloxycarbonylphosphonate (**49**) and disodium benzyloxycarbonylphosphonate (**58**). Only disodium phenoxycarbonylphosphonate (**59**) shows activity comparable to that of PFA. It may be concluded that none of the compounds submitted have intrinsic anti-HIV activity. Hydrolysis to active PFA would not be expected for the majority of esters under the assay conditions and therefore the results follow expectations. The activity attributed to disodium phenoxycarbonylphosphonate (**59**) is thought to derive from hydrolysis to PFA, given the labile nature of this ester. These results are in line with the work of Noren *et al.* who found anti-HSV activity for (**59**) and also for di- and triphenyl esters of PFA.[60] Toxicity was noted for the 4-nitrophenyl esters. This is thought to be due to the labile nature of this ester resulting in the release of 4-nitrophenol which is responsible for the toxicity observed. The compounds listed in Table 2.1 were also submitted to Dr. A. Karpas, University of Cambridge Clinical School, Department of Haematological Medicine and Dr. D. Kinchington, Department of Virology, St. Bartholomews Hospital, London. Results from these centres were in general agreement with those of Dr. A. Hay, although results from Dr. A. Karpas did not show any activity for (**59**).

Table 2.1 - Anti-HIV Activities and Toxicities of Triesters, Diesters and Monoesters of PFA with PFA and Zidovudine for Comparison

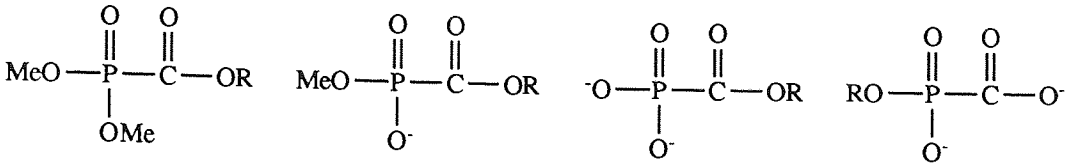

(A) (B) (C) (D)

Type of Ester	Nature of R	Compound No.	EC_{50} (μM)	TC_{50} (μM)
Triester (A)	methyl	(34)	>1000	>1000
"	ethyl	(35)	>1000	500
"	propyl	(36)	>1000	500
"	butyl	(37)	>1000	1000
"	2-methylpropyl	(38)	>1000	>1000
"	octyl	(39)	>1000	500
"	benzyl	(40)	>1000	1000
"	phenyl	(41)	>1000	>1000
"	4-nitrophenyl	(42)	>1000	100
Diester (B)	methyl	(43)	>1000	>1000
"	ethyl	(44)	>1000	>1000
"	propyl	(45)	>1000	>1000
"	butyl	(46)	>1000	>1000
"	2-methylpropyl	(47)	>1000	>1000
"	octyl	(48)	>1000	500
"	benzyl	(49)	500	>1000
"	phenyl	(50)	>1000	>1000
"	4-nitrophenyl	(51)	>1000	150
Monoester (C)	methyl	(52)	>1000	>1000
"	ethyl	(53)	>1000	>1000
"	propyl	(54)	>1000	>1000
"	butyl	(55)	>1000	>1000
"	2-methylpropyl	(56)	>1000	>1000
"	octyl	(57)	>1000	>1000
"	benzyl	(58)	1000	>1000
"	phenyl	(59)	20	>1000
Monoester (D)	methyl	(61)	>1000	>1000
PFA		(5)	10	>1000
Zidovudine		(1)	0.01	>1000

Table 2.2 - Anti-HIV Activities and Toxicities of Protected and Deprotected Amino Acid-Linked PFA Compounds

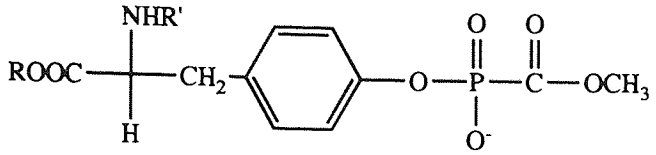

Nature of R	Nature of R'	Compound No.	EC_{50} (μM)	TC_{50} (μM)
CH_2CH_3	$COCH_3$	(79)	>1000	>1000
$CH_2C_6H_5$	$COOCH_2C_6H_5$	(85)	50	250
H	H	(68)	500	>1000

Table 2.2 shows some activity, but also a degree of toxicity, for the benzyl-protected derivative (**85**). The reason for this is unclear given the expected stability of this PFA diester. The very low activity of (**68**) indicates that hydrolysis to PFA does not occur under assay conditions. This is in line with expectations as (**68**) was shown to be hydrolytically stable (see section 2.2.2). The deprotected compound (**68**) was also submitted to Dr. A. Karpas who demonstrated no activity or toxicity.

Table 2.3 - Anti-HIV Activities and Toxicities of Lipid-PFA Compounds

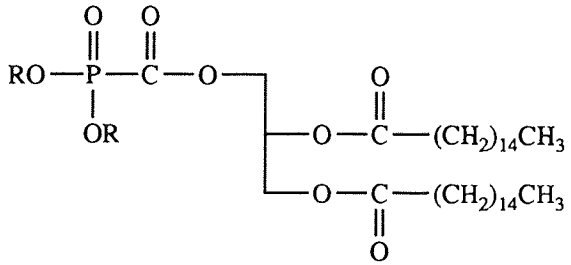

Nature of R	Compound No.	EC_{50} (μM)	TC_{50} (μM)
methyl	(94)	>1000	100
cyclohexylammonium salt	(87)	>1000	>200

Table 2.3 shows no activity for the lipid conjugates of PFA, however these compounds were toxic. Results from Dr. A. Karpas indicated (**94**) and (**87**) to be toxic and have low activity. The toxicity of (**87**) may be due to its surfactant properties interferring with cell membrane structure. Similarly, hydrolysis of (**94**) to the diester (**86**) or to dipalmitoyl glycerol (**92**) may result in toxic surfactant properties.

CHAPTER 3 - BLOOD-BRAIN BARRIER TRANSPORT

3.1 Determination of BBB Transport of Drugs

3.1.1 *In Vivo* Techniques

Prior to the work of Crone[90] the most commonly used method to investigate flux across the BBB was the tissue analysis technique. This involved the intravascular injection of solutes followed by analysis of brain slices to determine brain penetration. The low time resolution of this method only allowed the grouping of test substances into high and low penetrating categories.[90] Crone's indicator diffusion technique gives high time resolution as solute flux is investigated within seconds of a rapid carotid arterial injection. This method involves the simultaneous injection of a non-diffusable reference substance (to indicate blood dilution) and a test substance. By comparing the concentrations of the two substances in the injected fluid with those of venous samples collected every 2-3 seconds for 20-30 seconds after injection the fractional loss of test substance (E) can be calculated as $(C_{ref} - C_{test}) / C_{ref}$, where C_{ref} = relative concentration of reference substance and C_{test} = relative concentration of test substance. From (E), and given the capillary surface area (A) and the blood flow (Q), the permeability coefficient (P) can be calculated:

$$P = - Q/A \times \ln(1-E)$$

The limitations of this method include the underestimation of penetration of highly diffusible solutes (due to back diffusion from brain to blood) and a lack of sensitivity for poorly diffusible substances. This lack of sensitivity is a reflection of this single pass methodology and is inherent in the brain uptake index and single injection external registration techniques that were developed from this initial technique.

The brain uptake index technique developed by Oldendorf[91-94] involves a rapid injection into the carotid artery followed by decapitation after a single passage of the solute through the cerebral capillaries. The brain is immediately removed and direct analysis of the tissue for radiolabelled solute is performed. Tritiated water (to act as a freely diffusable internal reference) is simultaneously injected with a ^{14}C-labelled test substance . The brain uptake index is then calculated as follows:

$$\text{brain uptake index} = \frac{^{14}\text{C DPM (brain)} / ^{14}\text{C DPM (injection)}}{^{3}\text{H DPM (brain)} / ^{3}\text{H DPM (injection)}} \times 100$$

The advantages of the Brain Uptake Index technique are its speed and its simplicity. In Oldendorf's laboratory alone 10,000 animals (usually adult rats) have been used to examine the BBB transport of 200 different compounds.

The Single Injection External Registration Technique[95] is a non-invasive technique utilising γ- or positron-emitting radionuclides, such as ^{11}C and ^{15}O, detected by an external sodium iodide scintillation detector. After injection, into the carotid artery, brain radioactivity rapidly reaches a peak and then decreases with time. The fall-off in activity can be divided into two components (see Figure 3.1). Initially, a rapid decline attributable to the movement of tracer through the vasculature, followed by a slower decline reflecting tracer efflux from the brain. Extrapolating the slow component back to the time of peak activity (B) gives the total radioactivity entering the brain. Unidirectional extraction may then be calculated as the ratio of brain radioactivity (B) divided by the total activity (A) at the peak of the curve.

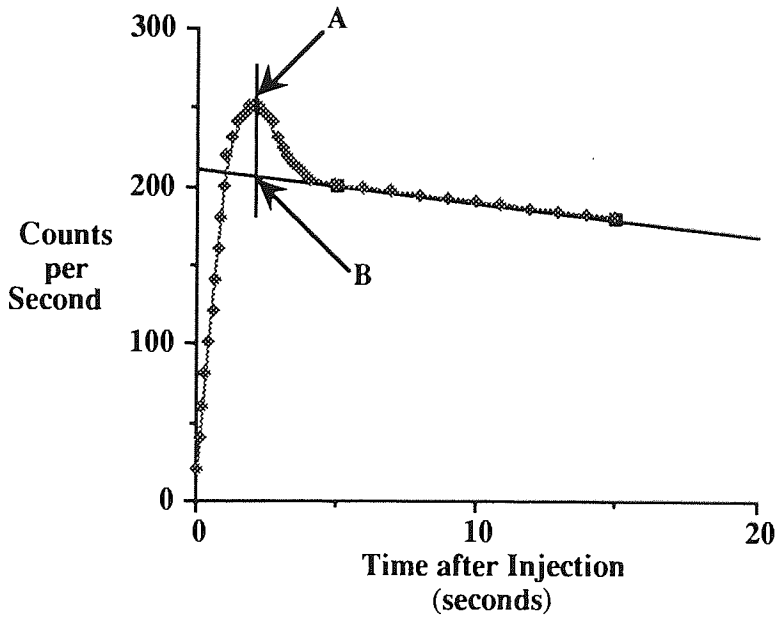

Figure 3.1 - Typical Time Course of Tracer in Brain after Intracarotid Injection

The advantages of this technique are that no reference is required and its non-invasive nature permits possible use in the study of human BBB transport.

As discussed, these single-pass techniques share the disadvantage of poor sensitivity in studying poorly diffusable solutes. This is overcome by the use of continuous uptake techniques. The Intravenous (IV) Administration technique used to determine BBB permeability allows numerous cerebral capillary passages and is therefore more sensitive than single passage techniques. With this technique, solute is given

parenterally and plasma concentrations of the solute monitored. When using small animals, analysis of solute content of the brain follows removal. For humans and larger animals, non-invasive techniques such as Positron Emission Tomography (PET)[96] can be used to follow the transport of solutes labelled with positron-emitting isotopes such as ^{11}C. A kinetic model is used to calculate the brain-uptake rate of the solute.

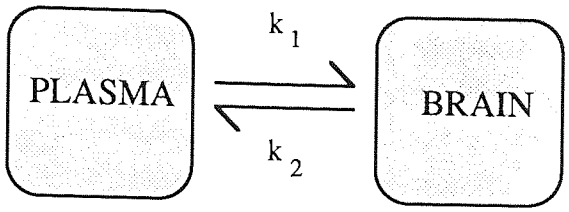

Figure 3.2 - Two Compartment Model

The most frequently used and simplest kinetic model is the two compartment model (Figure 3.2). The rate of solute-uptake into brain (V) after parenteral administration is given as:

$$V = (k_1 \times C_{plasma}) - (k_2 \times C_{brain})$$

where C_{plasma} = arterial plasma concentration of solute and C_{brain} = brain concentration of solute. More complex models are required to describe binding and metabolism of the solute, intracerebral distribution and brain - cerebrospinal fluid exchange. The advantages of the IV administration technique are high sensitivity and, due to the use of PET, the ability to study regional brain uptake with human subjects.

Another continuous uptake technique is the brain perfusion technique developed by Takosato *et al.*[97,98] The right hemisphere of an anaesthetised rat is perfused *via* the right external carotid artery after occluding normal blood flow. The period of perfusion is typically 60 to 300 seconds (in excess of the 5-15 seconds required for a single passage of the cerebral capillaries) giving greater sensitivity than single pass techniques. The perfusion rate is controlled to maintain a perfusion pressure similar to systemic blood pressure. After perfusion, the brain is removed to allow direct analysis of solute in brain tissue. Regional uptake of solute can be derived from analysis of individually dissected areas of brain. In contrast to other *in vivo* techniques, the composition of the perfusate is totally controllable, allowing solute concentration to be manipulated to examine saturation, competition and inhibition of carrier-mediated transport processes. The limitations of this technique include its non-suitability for human studies and the developement of hypoxia if the brain is perfused with saline for longer than 30 seconds.

3.1.2 *In Vitro* Techniques

Active transport of amino acids into cerebral slices has been studied.[99] However, with this technique, no attempt is made to isolate the processes occurring at the microvessel endothelium from the activities in the rest of the tissue preparation. Human brain capillaries have been mechanically isolated and active transport of amino acids described.[100,101] The metabolic status of these capillaries was shown to differ from the situation *in vivo*. The capillaries were shown to be leaky using trypan blue and cellular ATP was found to be only 5-10% of normal levels. Despite this, active amino acid transport was comparable to that observed previously. For example, K_m values for various amino acids correlated with those obtained from *in vivo* rat brain studies.[100]

The successful enzymatic isolation of BMEC, producing good yields and high viability in comparison to previous mechanical methods, has lead to much interest in the culture of BMEC monolayers as a convenient model of the BBB. *In vitro* cell culture as a method of studying the BBB may have a number of advantages over conventional techniques:

1 Allows rapid assessment of BBB permeability and metabolism of drugs.
2 Allows the investigation of transport mechanisms.
3 Reduces slow, expensive and controversial animal experiments.
4 Provides the opportunity to use human tissue.

Metabolic and transport properties of an *in vitro* BBB model must closely mimick those found in the *in vivo* situation. This will be dependent on the cell type chosen, whether the cells are primary cultures or passaged lines and the culture conditions used. The transport properties of the model will also be dependent upon the permeable membrane used as a support for the BMEC monolayer. Ideally the permeable support should be translucent to allow microscopic examination of the cell monolayer. It must also be freely permeable to the solutes being investigated, such that the transport properties of the cell monolayer are studied and not those of the support. Control experiments using the support without the cell monolayer are necessary to ensure solute permeability.[118] The apparatus used in transport experiments will also affect the transport properties of the model. Two main types of apparatus have been employed. Firstly, the unstirred cell culture insert and secondly, mechanically stirred diffusion chambers as used by Audus *et al.*[119] Stirring reduces the aqueous diffusion layers above the cell monolayer on the apical side and below the permeable support on the basolateral side. This is of particular importance in the transport of hydrophobic solutes where diffusion across this aqueous layer may be rate-limiting.[118]

Primary cultures of BMEC retain many of the characteristics of BMEC *in vivo*. Tight junctions, although not as extensive as *in vivo*, are retained. BBB markers such as γ-glutamyl transpeptidase, alkaline phophatase, angiotensin-converting enzyme and Factor VIII antigen have also been identified in BMEC primary culture.[102] In contrast, passaged BMEC lose many such characteristics.[118] The diffusion of various molecules across BMEC monolayers has been correlated with log of partition coefficient / (molecular weight)$^{1/2}$ (see Figure 3.3)[120] and transport *in vivo*.[121]

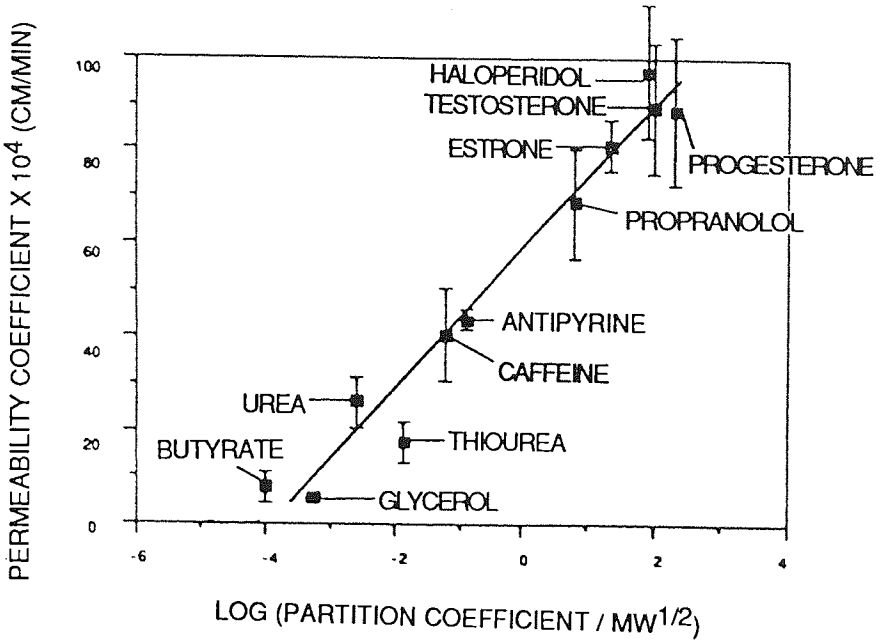

Figure 3.3 - The Relationship Between Permeability Coefficients of Solutes crossing Monolayers of Bovine BMEC and Partition Coefficient / (Molecular Weight)$^{1/2}$

However, in a comparison of *in vivo* rat brain perfusion studies and *in vitro* BMEC monolayers grown in continuous culture, the rate of diffusion *in vitro* has been said to be 150-fold greater than that *in vivo*.[122] Using the diffusion of impermeant markers, such as sucrose, Audus *et al* have corrected their data for this leakage. For example, in the study of amino acid transport, leucine and sucrose flux was followed simultaneously using dual labelling. The corrected value for leucine transport was obtained by subtracting the flux of sucrose (multiplied by a factor allowing for the difference in molecular weight of sucrose and leucine) from the apparent flux of leucine.[103] Active transport across BMEC monolayers has been successfully studied and is discussed in sections 3.3 and 3.4.[102,103] However, expression of active transporters has been reported to be reduced from that seen *in vivo* and Pardridge *et al* could not demonstrate a correlation between the flux of actively transportable compounds *in vitro* using BMEC monolayers and *in vivo*.[122]

The effect of trophic factors released by astrocytes appears to be important in the maintenance of BBB properties.[123] *In vivo*, astrocytic foot processes are closely associated with BMEC and interactions between these two cell types is the subject of much interest. The co-culture of passaged BMEC with astrocytes or growth in astrocyte-conditioned medium, thought to contain trophic factors, has been shown to re-establish and retain BBB markers.[124,125] Also, an increase in tight junction integrity, monolayer electrical resistance and consequent reduction in the permeability of BMEC monolayers has been reported.[125,126] This reduction of permeability has been determined to be approximately 50%.[127] Astrocyte-conditioned medium has also been reported to increase the expression of hexose transporters.[128,129] Dehouck *et al* have established a correlation between *in vivo* brain uptake index studies and transport across BMEC monolayers grown in co-culture with astrocytes. It is claimed that this correlation extends to actively transported compounds such as glucose and leucine.[130,131] The use of agents that elevate cellular cAMP concentrations have been shown to increase the electrical resistance of BMEC monolayers with or without astrocyte co-culture.[132]

3.2 Characterisation of an *In Vitro* Model of the BBB

To assess the transport of PFA prodrugs, an *in vitro* BBB model using BMEC monolayers was established. Porcine BMEC were isolated by the method of Audus *et al* for the isolation of bovine BMEC.[102] Porcine brains were utilised as bovine brains were unavailable due to restrictions applied in the wake of bovine spongiform encephalitis. No significant differences in the culture of bovine and porcine BMEC were apparent from the literature.[133] The isolation procedure is described in section 5.2 and schematically presented in Figure 3.4. Porcine brains were obtained from a local abattoir as soon after death as possible and transported in ice-cold medium. Removal of meninges and surface vessels was performed to eliminate large vessel endothelial cells from the isolation. Grey matter was collected and white matter discarded as microvessels are found in higher concentration in grey matter. During these procedures, the brains were kept at 0-4°C to aid manipulation and avoid degradation. Enzyme incubations using dispase and collagenase/dispase were performed to free the microvessels from their extra-cellular matrix. The dextran centrifugation removed fat, cell debris and myelin from the isolation. Finally, the Percoll gradient centrifugation isolated the BMEC from erythrocytes and any remaining cell debris. BMEC were frozen in medium containing 10% DMSO and stored at -70°C for up to 6 weeks. BMEC stored for in excess of 6 weeks failed to produce monolayers of sufficient integrity despite no apparent loss of viability. The viability of isolated BMEC was determined as being greater than 85% using trypan blue exclusion. This is consistent

with reports of high viability (around 90%) from the enzymatic isolation of BMEC.[102,133] Cell counts were performed using crystal violet nuclei staining. Cell density in freezing medium was typically 3 million cells / ml with a total yield of approximately 150 million cells from 7 porcine brains, comparable with 30-40 million BMEC isolated from one porcine brain by Mischeck *et al* [133]. Growth surfaces were coated with rat-tail collagen, which was cross-linked under an atmosphere of ammonia before sterilisation under UV light. The collagen coated surface was wetted with fibronectin and again sterilised under UV light . Cells were seeded, at 50,000 cells / cm^2, on coated Falcon cell culture inserts and grew to form small clusters of cells after 2 days and confluent monolayers in 4 to 5 days (see Photograph 3.1), faster than the 7 days previously reported.[133] Under phase-contrast microscopy, the BMEC exhibited a spindle-shaped morphology typical of BMEC in primary culture.[133] Cellular features, such as nuclei, were not easily decernable. Angiogenesis, indicated by defined concave edges to cell growth, was observed occasionally in days 2 to 5 of culture but did not prevent confluency and, importantly, growth of BMEC up to the edges of the permeable support was apparent.

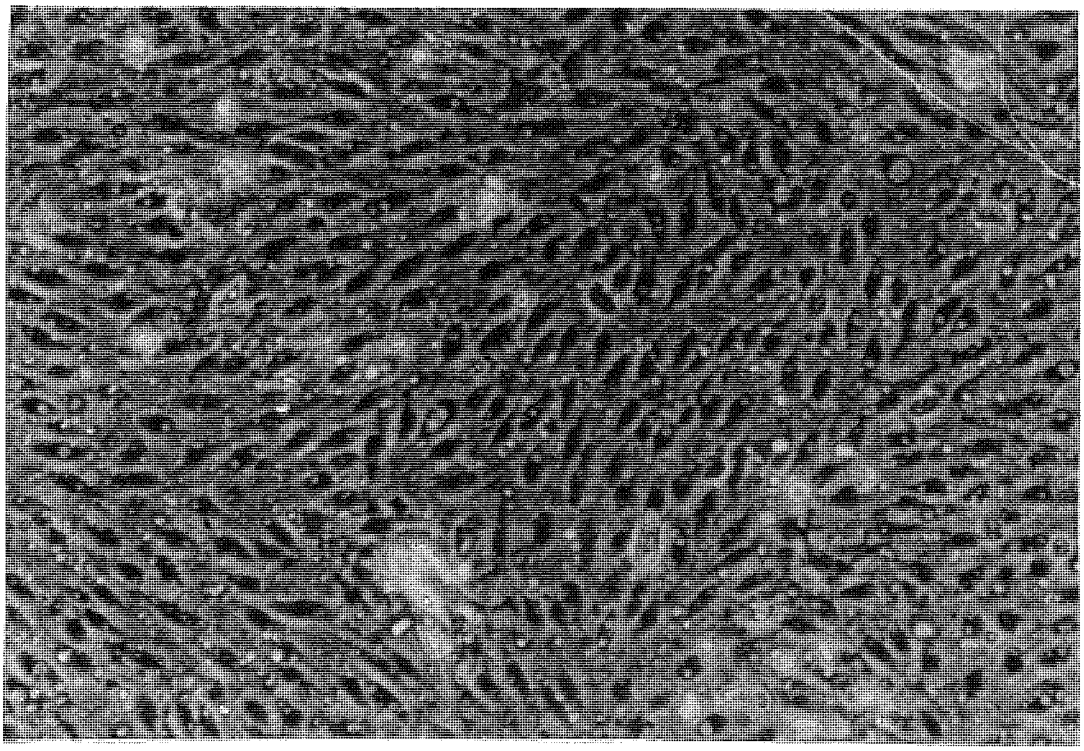

Photograph 3.1 - A 5-Day Old Confluent BMEC Monolayer

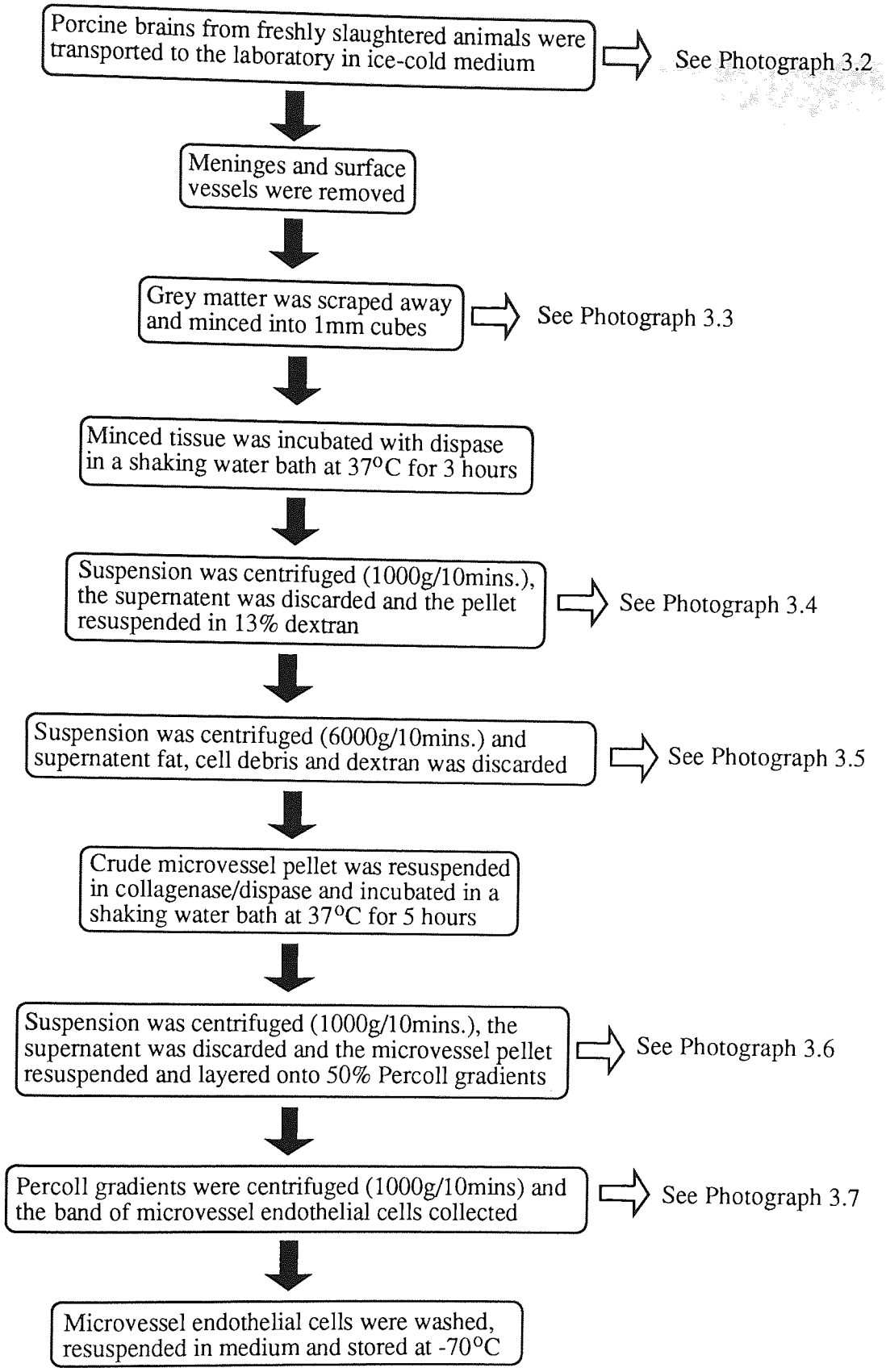

Figure 3.4 - Schematic Representation of the Isolation of Porcine BMEC

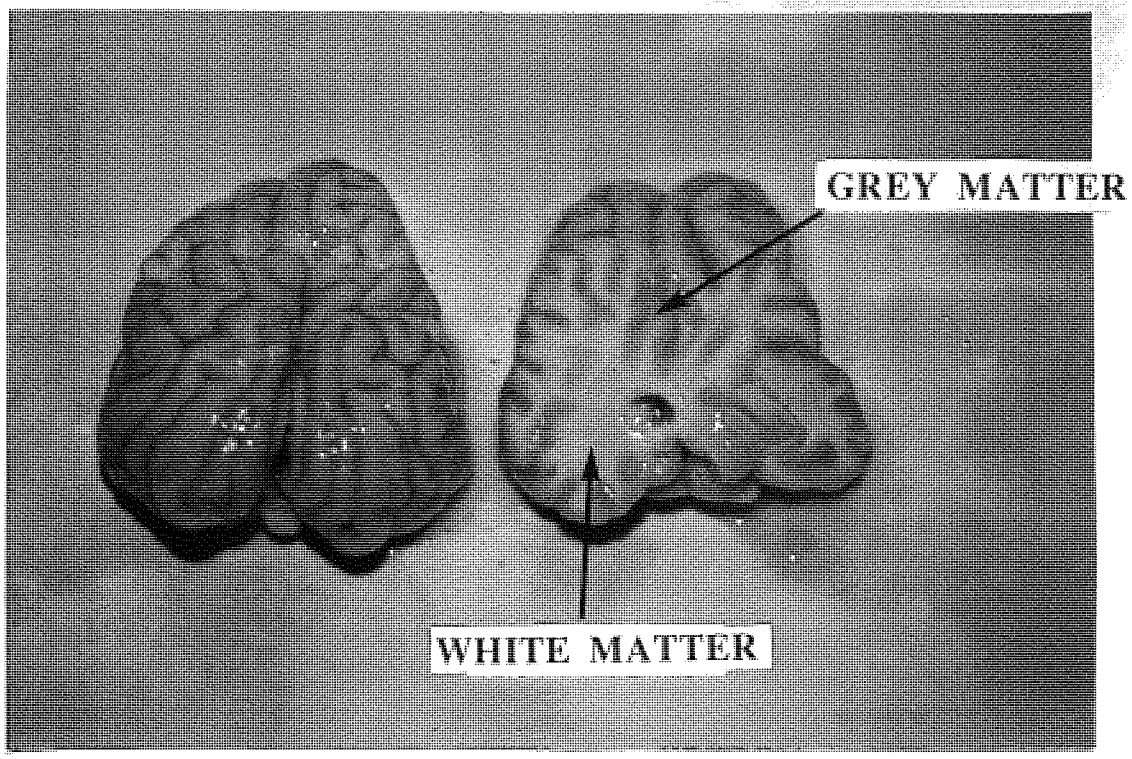

Photograph 3.2 - Porcine Brains Prior to Isolation

Photograph 3.3 - Grey Matter, Scraped from the Brains, Prior to Mincing

Photograph 3.4 - Pellet obtained from Centrifugation after Dispase Incubation

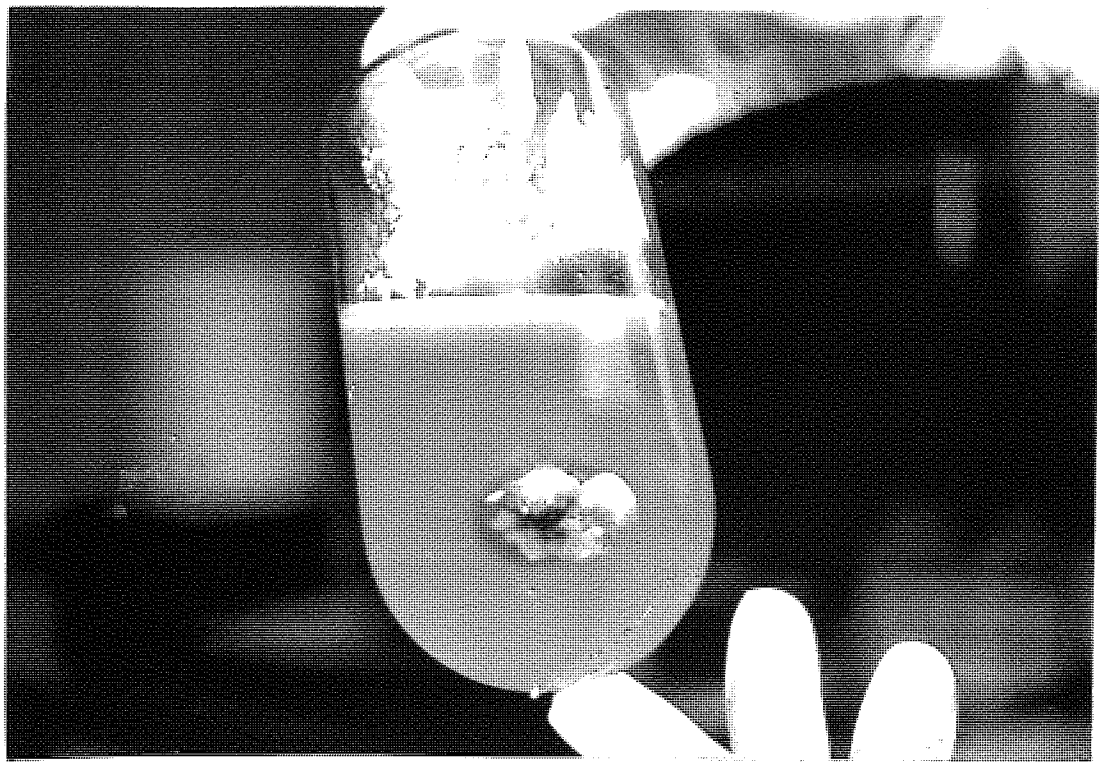

Photograph 3.5 - Pellet obtained from Dextran Centrifugation

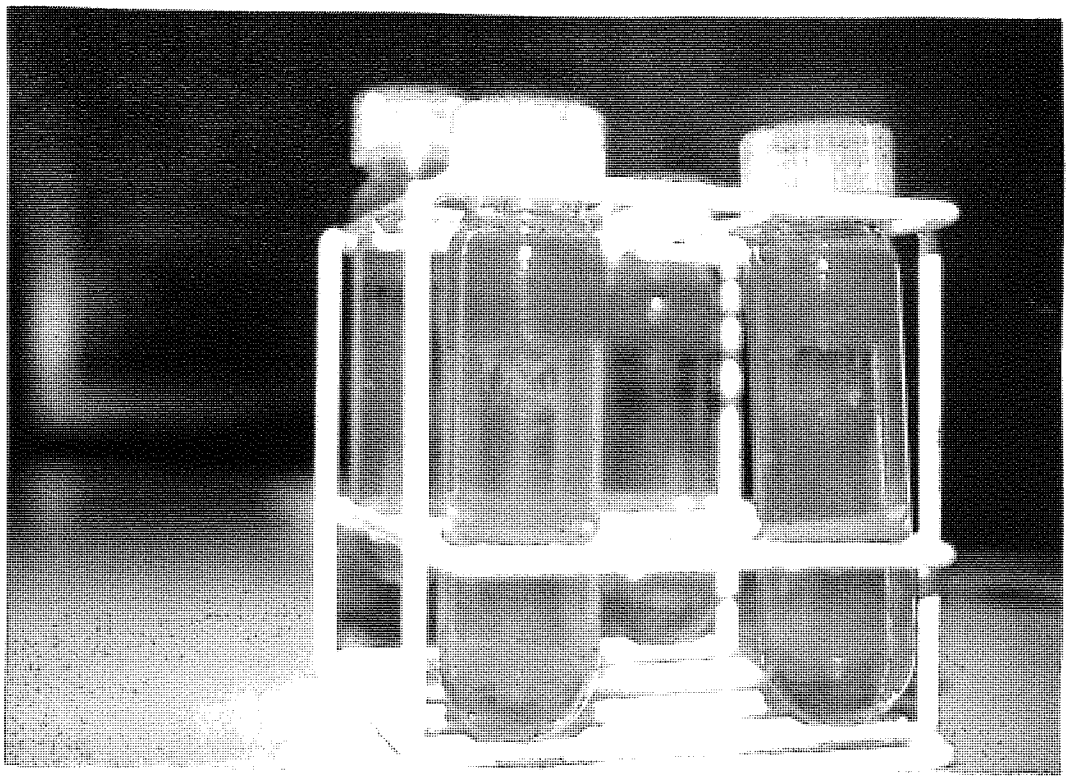

Photograph 3.6 - Microvessel Suspension layered onto 50% Percoll Gradients

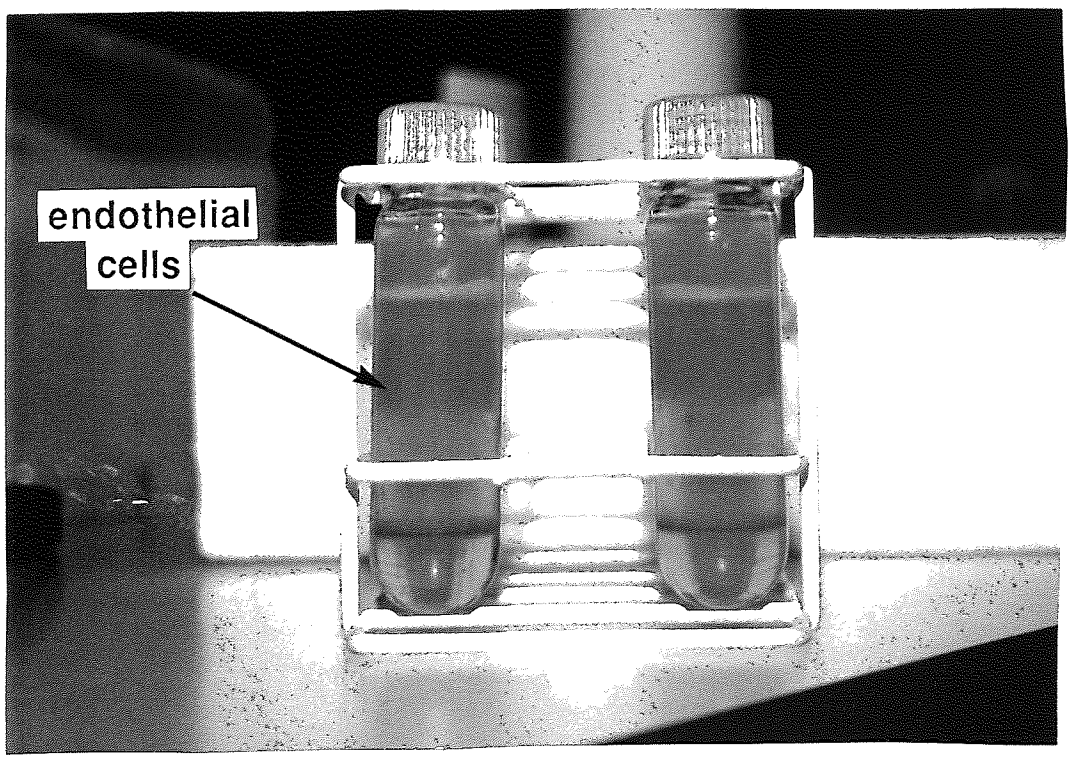

Photograph 3.7 - Position of BMEC following Centrifugation of Percoll Gradients

3.2.1 Alkaline Phosphatase Activity

Alkaline phosphatase activity, although not exclusive to BMEC, is an important enzyme marker often used to characterise BMEC isolations. Alkaline phosphatase activity was demonstrated in seven day old BMEC monolayers as shown by characteristic dark purple perinuclear granular staining (see Photograph 3.8). This is consistent with reports of BMEC in culture[102] although a decline in alkaline phosphatase activity in BMEC with time in culture has also been reported.[132]

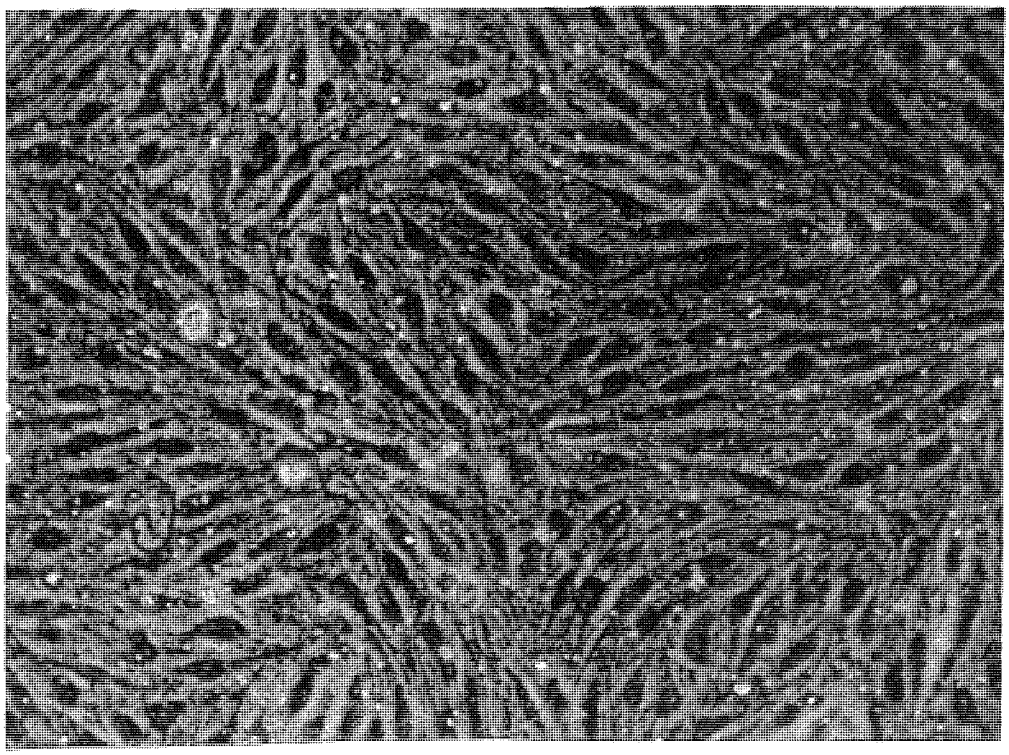

Photograph 3.8 - Alkaline Phosphatase Staining of a 7-Day Old BMEC Monolayer

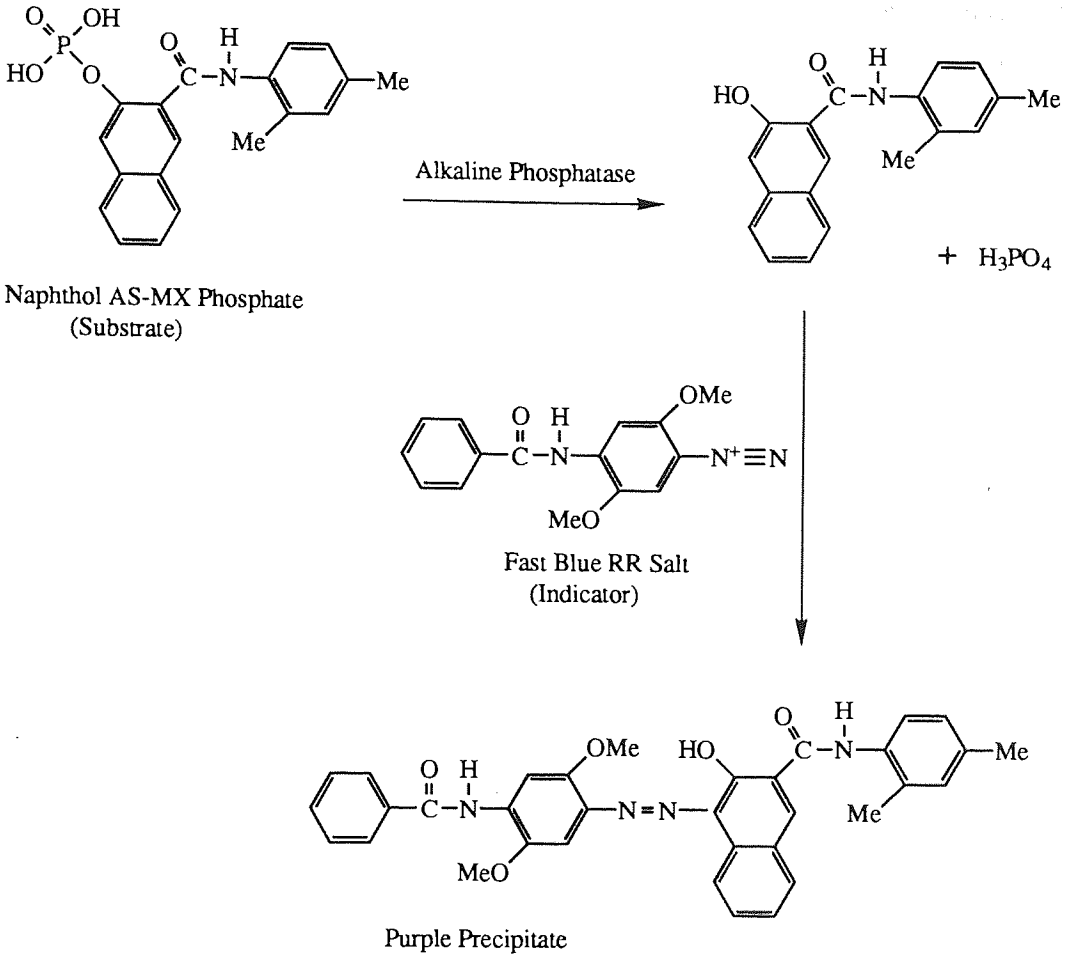

Figure 3.5 - Histochemical Detection of Alkaline Phosphatase

A scheme of the formation of the characteristic dark purple stain is shown in Figure 3.5. Alkaline phosphatase hydrolyses the phosphate function of the substrate naphthol AS-MX phosphate. The resulting phenolic compound undergoes an electrophilic aromatic substitution reaction, coupling with the diazonium salt indicator, to produce a purple precipitate at the site of enzyme action.

3.2.2 γ-Glutamyl Transpeptidase Activity

γ-Glutamyl transpeptidase activity is also not exclusive to BMEC. The majority of activity found in brain capillaries appears to be associated with pericytes and astrocytes which due to their close association with BMEC are possible contaminants of BMEC isolations.[133,134] Despite this, γ-glutamyl transpeptidase activity is widely used as an identifying marker for BMEC. γ-Glutamyl transpeptidase activity in seven day-old BMEC monolayers could not be demonstrated by the method of DeBault and Cancilla.[124] This is in contrast to the work of Audus and Borchardt[102] but in agreement with that of other workers[124,135] who indicate a rapid decline in γ-glutamyl transpeptidase activity with time in culture. It is believed that BMEC proliferating in culture do not express γ-glutamyl transpeptidase and any residual activity is due to original cells.[135] This was confirmed by photographs taken of attempts to show γ-glutamyl transpeptidase activity in which original pieces of microvessel are stained while proliferating cells are not (see Photograph 3.9).

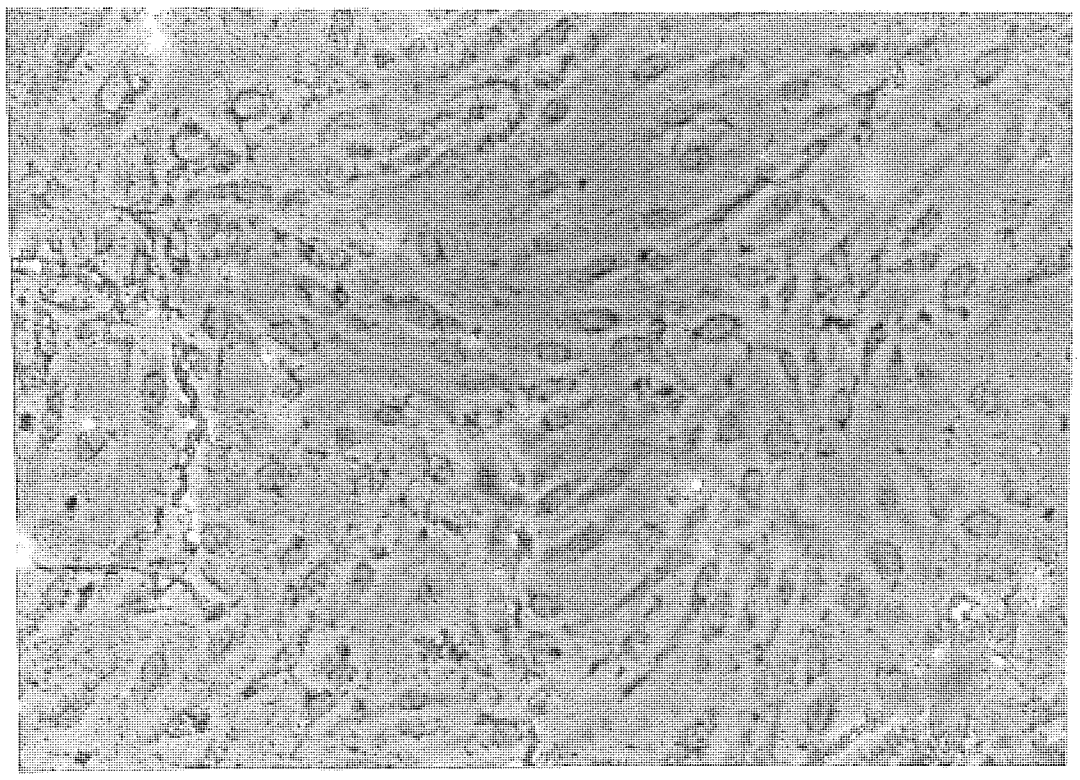

Photograph 3.9 - Attempted γ-Glutamyl Transpeptidase Staining of a 7-Day Old BMEC Monolayer

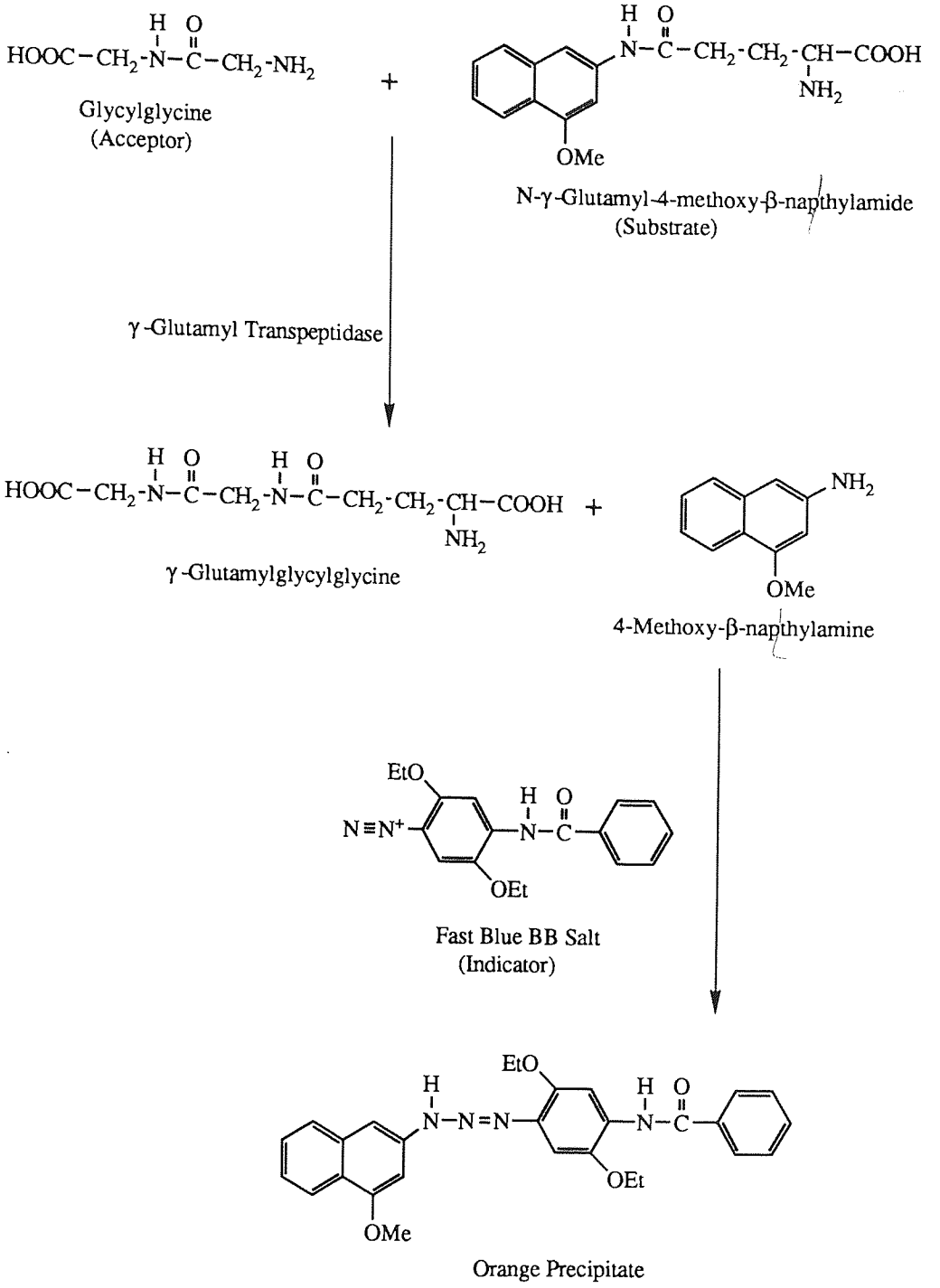

Figure 3.6 - Histochemical Detection of γ-Glutamyl Transpeptidase

A scheme of the formation of the characteristic orange stain is shown in Figure 3.6. γ-Glutamyl transpeptidase transfers the γ-glutamyl function from, the substrate, N-γ-glutamyl-4-methoxy-β-napthylamide to, the acceptor, glycylglycine. The resulting aromatic amine couples with the diazonium salt indicator to give an orange precipitate at the site of enzyme action.

3.2.3 Factor VIII Antigen

Factor VIII antigen is a specific marker of endothelial cells and is used to characterise BMEC isolations. The presence of Factor VIII antigen was demonstrated using seven day old BMEC monolayers as shown by characteristic black perinuclear staining. This is consistent with reports of BMEC in culture.[102]

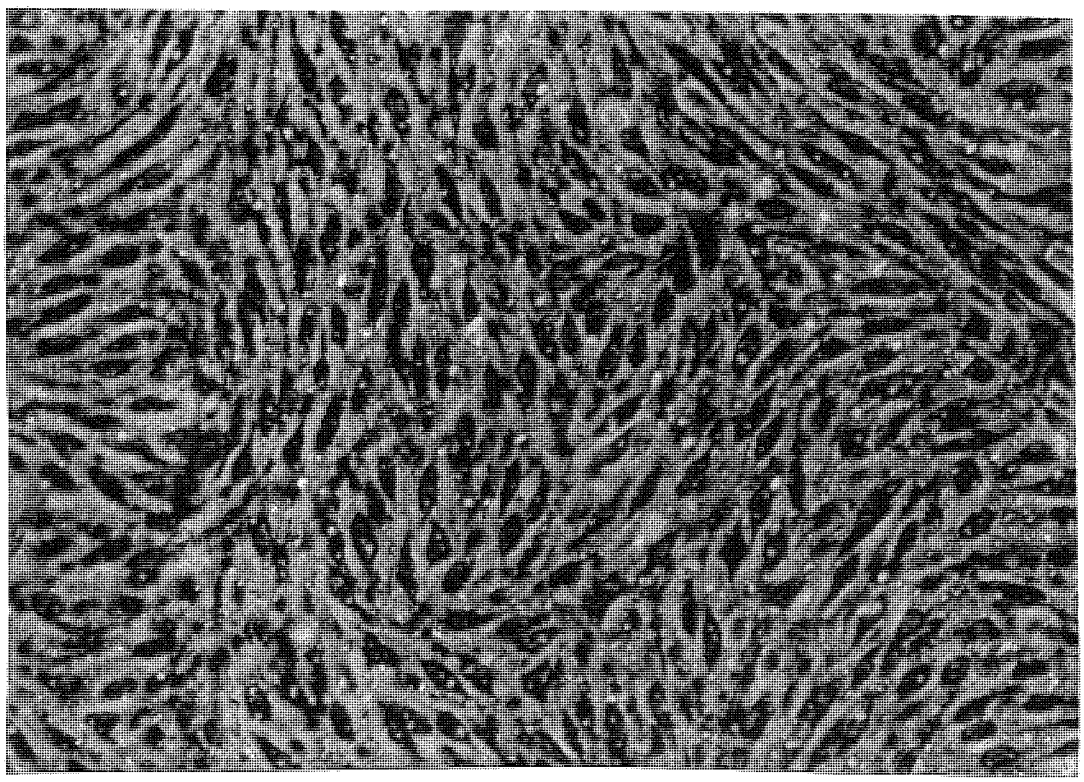

Photograph 3.10 - Factor VIII Staining of a 7-Day Old BMEC Monolayer

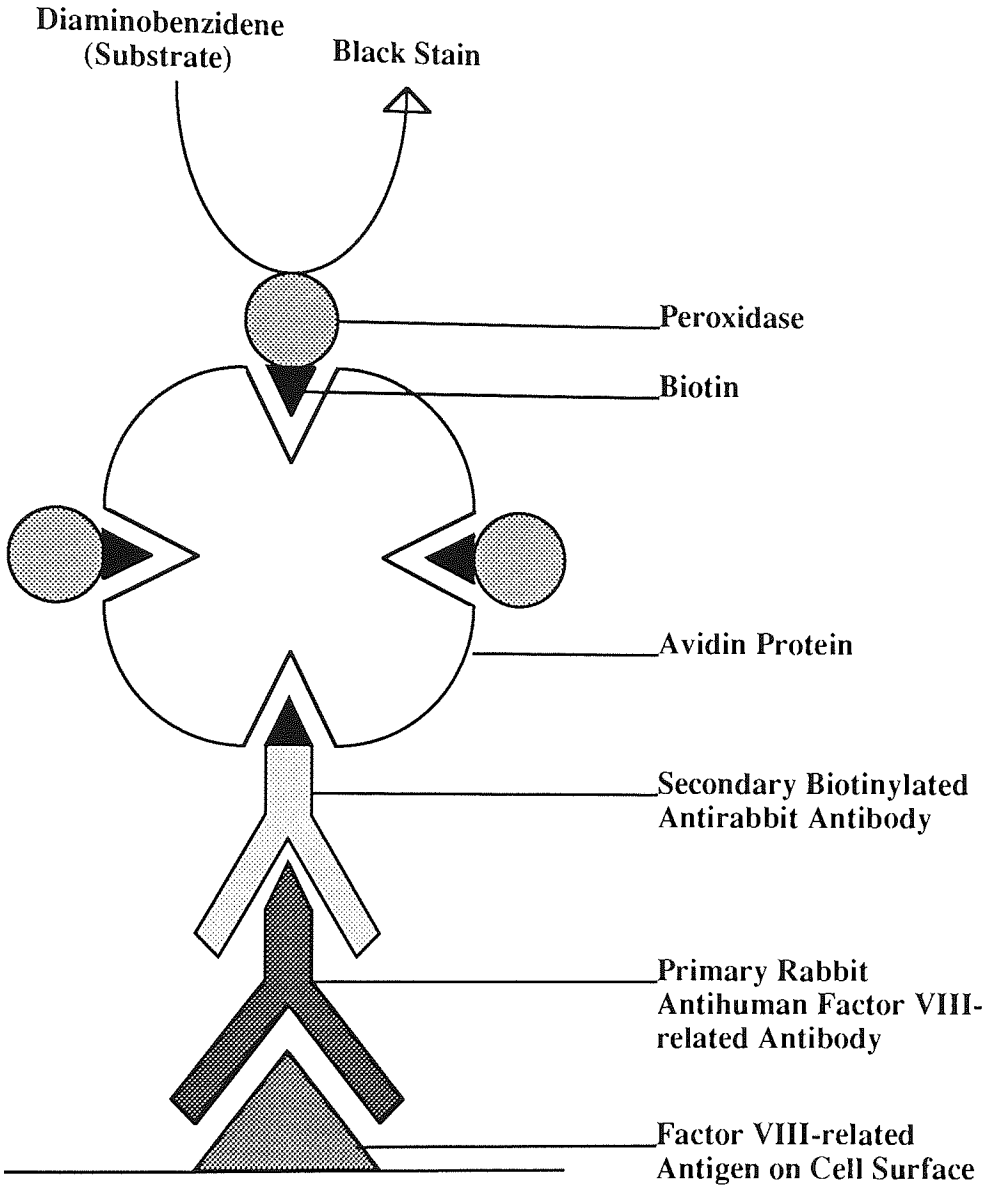

Figure 3.7 - Schematic Representation of the Histochemical Detection of Factor VIII-related Antigen

A scheme for the formation of a black stain in the presence of factor VIII-related antigen is shown in Figure 3.7. The cells are incubated with a primary antibody to factor VIII-related antigen which adheres to the antigen. Unattached antibody is removed by washing the cells, before incubating with a biotinylated secondary antibody which binds to the primary antibody. An avidin-biotin-peroxidase complex is added which binds to the biotinylated portion of the secondary antibody. Following washing, the cells are incubated with the substrate which is oxidised to a black precipitate by the peroxidase at the site of the factor VIII-related antigen.

3.2.4 Mannitol Transport

Mannitol is a highly hydrophilic molecule that does not possess the necessary lipid solubility to allow transcellular diffusion. Mannitol is therefore a marker of paracellular diffusion. The transport of ^{3}H-mannitol across 7-day old BMEC monolayers was investigated using the system shown in Figure 3.8. The transport protocol is detailed in section 5.4.4. Briefly, transport buffer containing ^{3}H-Mannitol was added to the apical chamber and the system incubated at 37°C. The insert was transferred to another outer well containing fresh buffer at 30 minute intervals. After 180 minutes, the ^{3}H-label content of the apical and basolateral samples was determined using liquid scintillation spectroscopy.

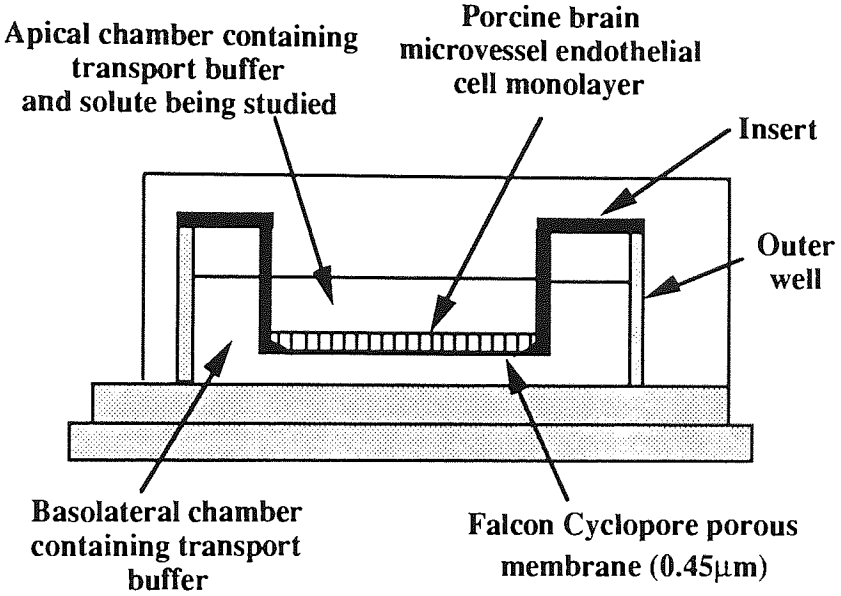

Figure 3.8 - Cell Culture Insert System used for Transport Studies

The results of mannitol transport studies performed across BMEC monolayers and the permeable support alone are recorded in Table 3.1.and illustrated in Figure 3.9.

Table 3.1 - The Effect of BMEC Monolayers on ^{3}H-Mannitol Transport

Time (minutes)	% Mannitol Transport Across BMEC Monolayer	% Mannitol Transport Across Membrane Alone
30	1.90 (0.24)	12.81 (1.57)
60	3.52 (0.30)	24.98 (1.67)
90	5.14 (0.31)	35.49 (2.51)
120	6.82 (0.41)	44.46 (2.86)
150	8.46 (0.39)	53.20 (2.94)
180	10.31 (0.13)	58.99 (2.94)

Standard deviations in parentheses, n=3 for all time points.

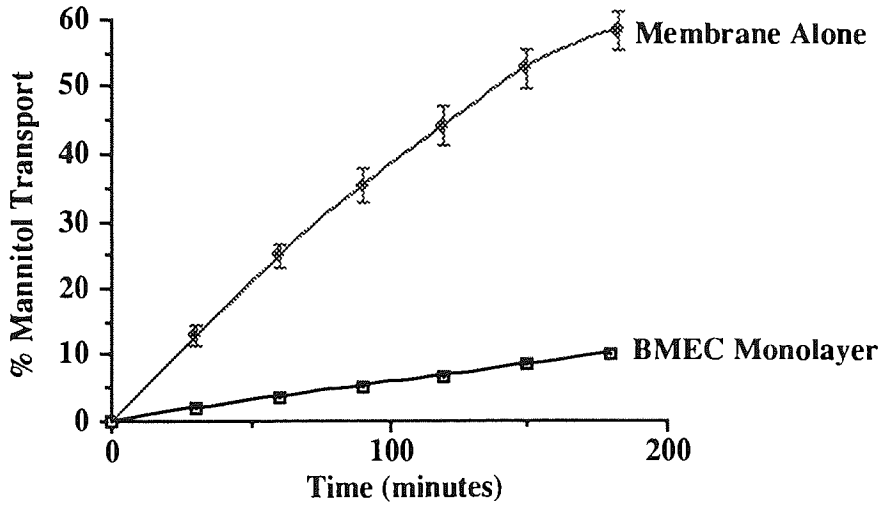

Figure 3.9 - The Effect of BMEC Monolayers on ^{3}H-Mannitol Transport

Figure 3.9 shows a reduction in ^{3}H-mannitol flux due to the BMEC monolayer. For the permeable support (membrane) alone, the initial ^{3}H-mannitol flux is 24.98% / hour while in the presence of a BMEC monolayer this falls to 3.52% / hour. The BMEC monolayer provides a barrier to ^{3}H-mannitol transport such that passage across the BMEC monolayer is an important rate-limiting step. In further transport studies, ^{14}C- or ^{3}H-mannitol transport was measured, in addition to the labelled compound under study, to assess individual monolayer integrity. Variations in mannitol transport were noticed between individual monolayers. It can be seen from the following pyruvate and tyrosine experiments that mannitol flux varies between different experiments. This did not appear to be related to different isolations as mannitol fluxes varied between cells seeded from the same isolation. Mannitol flux of 1.5-5.0% / hour was deemed to be acceptable. Monolayers showing flux rates in excess of 5.0% / hour were

disregarded. Within the range of 1.5-5.0% / hour, only monolayers that varied by up to 0.5% from the mean mannitol flux were considered comparable. Audus and Borchardt use labelled sucrose as an indicator of monolayer integrity of bovine BMEC grown on cellulose membranes. These typically have a sucrose flux of 1.5% / hour.[103] As mannitol exhibits approximately 1.5 times greater paracellular diffusion than sucrose,[137] the paracellular fluxes of the two models appear comparable. A further comparison of the permeabilities of the two systems is given in Table 3.6. Human intestinal epithelial (Caco-2) cell monolayers grown on Millicell-HA 0.45μm cell culture inserts have a typical mannitol flux of less than 1% / hour.[138] This indicates a lack of tight junction integrity in the BMEC model compared with Caco-2 monolayers and indeed with the BBB *in vivo*. Audus and Borchardt[103] correct their transport data for the 'leakiness' of the model using the simultaneous flux of labelled sucrose and the following equation:

$$\text{corrected transport of test substance A (cpm)} = \text{observed transport of A (cpm)} - \left[\text{total A (cpm)} \times K \times \frac{\text{sucrose transport (cpm)}}{\text{total sucrose (cpm)}}\right]$$

$$\text{where } K = \frac{\text{molecular weight of sucrose}^{1/2}}{\text{molecular weight of A}^{1/2}}$$

The constant K reflects the difference in permeabilities between sucrose and the test substance A. Using mannitol, as a marker of monolayer integrity, the above correction did not to hold true for the transport of tyrosine. The molecular weights of ^{3}H-L-tyrosine and ^{14}C-mannitol are 185 and 184 respectively, such that K = 1.00. However, from transport data (see Table 3.18) it was apparent that a permeability difference between ^{3}H-L-tyrosine and ^{14}C mannitol does exist. A more direct measure of K is provided by:

$$K = \frac{\text{diffusion of A across a permeable support}}{\text{diffusion of mannitol across a permeable support}}$$

Using Falcon Cyclopore membranes and the above equation, K was determined to be 0.90 for ^{3}H-L-tyrosine / ^{14}C-mannitol (data from Table 3.18)) and 1.40 for ^{14}C-pyruvate / ^{3}H-mannitol (data from Table 3.9), compared to values of 1.00 and 1.45, respectively, using the method of Audus and Borchardt.[103] In the following experiments, corrections were performed using the directly measured values of K.

3.2.5 Electrical Resistance

Cell monolayer integrity may also be assessed using electical resistance (ER) measurements. A high ER for a cell monolayer is related to a high degree of monolayer integrity and resistance to the flux of hydrophilic solutes. The ER of 7-day old confluent BMEC monolayers at 37°C was measured as described in section 5.4.5.

Table 3.2 - Electrical Resistance Measurement of Three BMEC Monolayers

BMEC Monolayer	Mean Resistance of BMEC monolayer and membrane (Ω)	Corrected for Membrane Resistance and Area (Ω cm^2)	^{14}C-Mannitol Transport (%/hour)
1	230.83 (12.09)	278.74	4.02
2	240.67 (18.83)	327.06	3.31
3	232.67 (21.26)	287.78	3.91

Standard Deviations in Parentheses, n=6.
Mean Membrane Resistance is 174.06 Ω (7.41), n=18, Membrane Area is 4.91cm^2.

It can be seen from Table 3.2 that large standard deviations are associated with resistance measurements such that there is no statisical difference between the ER of the three monolayers. Wide variations and a lack of reproducability are evident in the ER values produced by different workers.[131] Values of 157-783 Ω cm^2 have been reported for BMEC monolayers. Such variations are a reflection of the different techniques and apparatus used by different workers.[131] Caco-2 monolayers typically have an ER of 400 Ω cm^2 at 37°C [138] and the ER of the BBB, *in vivo*, has been estimated to be 2000 Ω cm^2 [139] indicating a comparable lack of tight junction integrity in BMEC monolayers. Due to the variations encountered with ER measurements, mannitol flux was used routinely to assess monolayer integrity.

3.2.6 Testosterone Transport

Testosterone is highly lipophilic (log P ~ 3) and exhibits transcellular diffusion. The transport of ^{3}H-testosterone across 7-day old BMEC monolayers was investigated and the data are recorded in Table 3.3.

Table 3.3 - The Effect of BMEC Monolayers on ^{3}H-Testosterone Transport

Time (minutes)	% Testosterone Transport Across BMEC Monolayer	% Testosterone Transport Across Membrane Alone
30	9.09 (0.17)	7.59 (0.42)
60	18.90 (0.39)	16.52 (0.27)
90	27.32 (0.41)	24.56 (0.87)
120	35.24 (0.66)	32.67 (0.68)
150	42.11 (1.04)	40.36 (0.75)
180	48.27 (1.28)	46.96 (0.89)

Standard deviations in parentheses, n=3 for all time points.

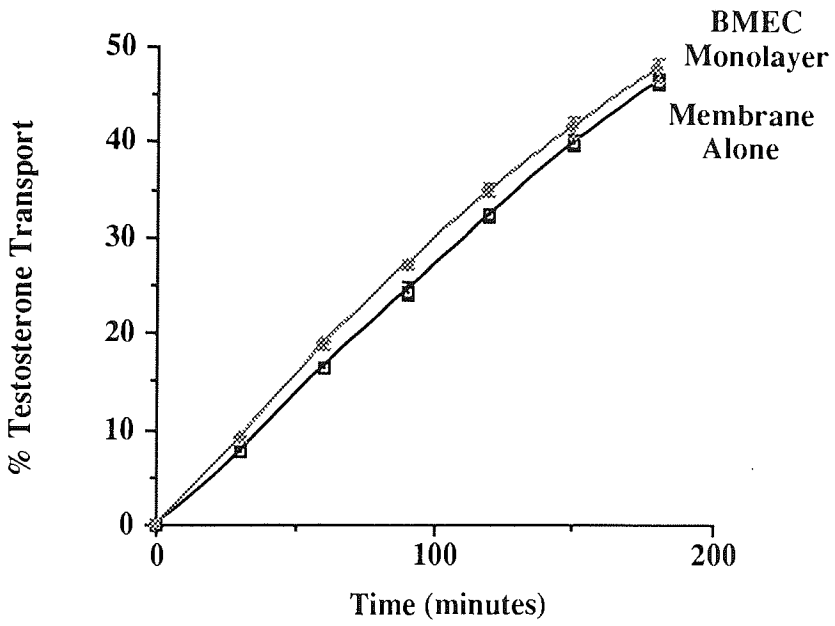

Figure 3.10 - The Effect of BMEC Monolayers on ^{3}H-Testosterone Transport

From Figure 3.10 it can be seen that the BMEC monolayer shows little resistance to ^{3}H-testosterone transport greater than that of the permeable support (membrane). Passage across the permeable support appears to be a rate-limiting step. It can be seen that the rate of ^{3}H-testosterone flux, across the permeable support alone, is less than that of ^{3}H-mannitol (see Figure 3.9) indicating that diffusion across an aqueous diffusion layer may also be a rate-limiting step.[118] The higher molecular weight of testosterone, in comparison to mannitol, may also reduce its transport through the pores of the permeable support.

3.2.7 Monolayer Permeability with Days in Culture

The optimum period for transport experiments is when the monolayer provides the greatest barrier to paracellular transport. In order to determine this period, the transport of ^{14}C-mannitol and another hydrophilic marker, ^{14}C-sucrose, was followed across BMEC monolayers cultured for progressively longer periods of time and the data are recorded in Tables 3.4 and 3.5 and illustrated in Figures 3.11 and 3.12.

Table 3.4 - The Effect of Days in Culture on Transport of ^{14}C-Mannitol over 3 Hours

Days in Culture	% Mannitol Transport
0 (no cells)	55.11 (0.45)
5	45.12 (1.97)
6	31.84 (3.72)
7	22.44 (1.21)
9	19.47 (1.13)
10	30.11 (1.59)
12	36.60 (2.03)

Standard deviations in parentheses, n=3 for all time points.

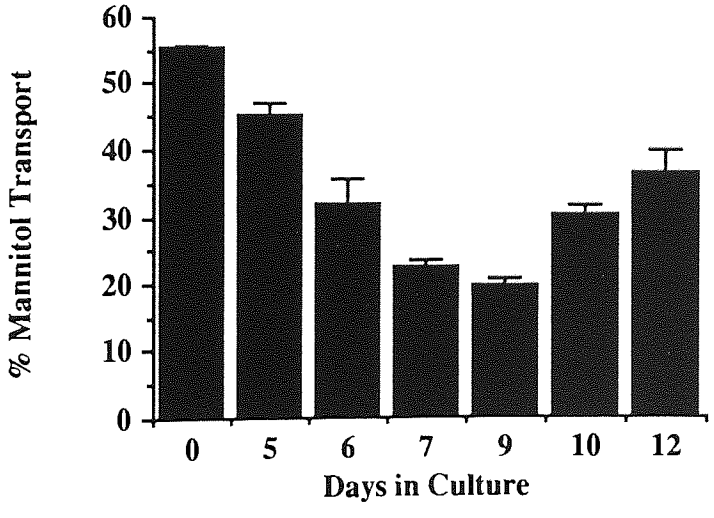

Figure 3.11 - The Effect of Days in Culture on Transport of ^{14}C-Mannitol over 3 Hours

Table 3.5 - The Effect of Days in Culture on Transport of ^{14}C-Sucrose over 3 Hours

Days in Culture	% Sucrose Transport	
	After 3 hours	After 1 hour*
0 (no cells)	46.14 (1.13)	16.11 (0.23)
3	33.46 (0.85)	
5	12.79 (1.47)	
6	11.83 (0.64)	
7	8.87 (0.66)	3.15 (0.25)
8	13.01 (0.66)	
9	10.84 (2.41)	
10	12.86 (2.04)	
12	14.30 (2.81)	

Standard deviations in parentheses, n=3 for all time points. *One hour data shown for use in calculation of permeability coefficients (see Table 3.6).

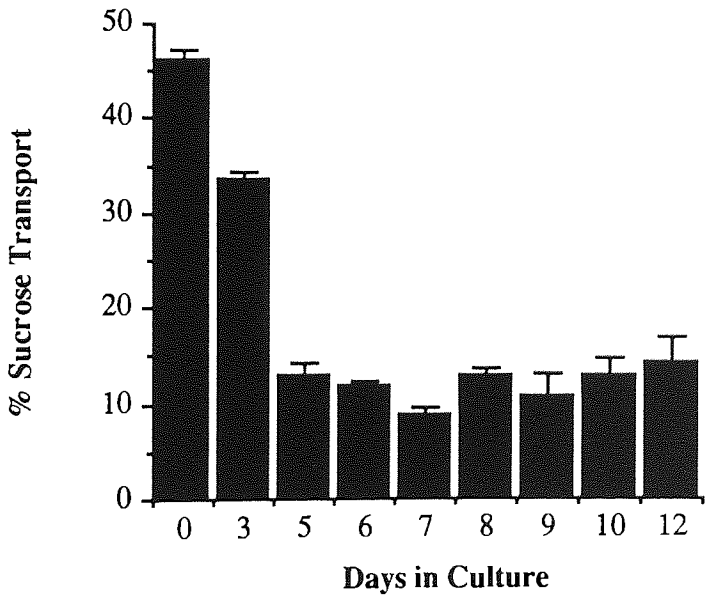

Figure 3.12 - The Effect of Days in Culture on Transport of ^{14}C-Sucrose over 3 Hours

It is apparent that from the two sets of data that the flux of the hydrophilic markers initially decreases with days in culture to an optimum around day seven and then monolayer integrity appears to fall. Also, it can be seen that sucrose transport is less than that of mannitol which is in general agreement with Rim *et al.*[137] This would be expected due to the larger molecular size of sucrose. Visual examination of the

monolayers had indicated that the optimum monolayer integrity was between day 6-7. After this time in culture, the monolayer had been complete for about 2 days, cell growth was apparent up to the edges of the membrane, no holes were detectable and no deterioration in the monolayer could be observed. This was confirmed by Figures 3.11 and 3.12 and transport studies were performed normally on day 7 and certainly within a window of day 6 to day 9 of culture. In order to compare the permeability of BMEC monolayers with those of other workers, permeability coefficients (Kp) were calculated for sucrose transport data using equations analogous to those used by Audus and Borchardt[120] and derived from Fick's Law:

For a membrane-controlled diffusion process Fick's Law provides:

$$J = \frac{K' \times D \times A \times (C_o - C_r)}{h}$$

Where:

J = Flux (nmol / min)

K' = Partition Coefficient

D = Membrane Diffusion Coefficient (cm^2 / min)

A = Cross-Sectional Area of Membrane (cm^2)

C_o = Concentration in Donor Chamber (nmol / cm^3)

C_r = Concentration in Receiver Chamber (nmol / cm^3)

h = Membrane Thickness (cm)

A permeability coefficient may be defined as $Kp = \frac{K' \times D}{h}$ (cm / min)

and if C_r is negligible in comparison to C_o

$$\text{therefore: } Kp = \frac{J}{A \times C_o}$$

if: a = Amount of Solute Transported

b = Total Solute in Donor Chamber

t = Duration of Transport

V = Volume of Donor Chamber

$$\text{then:} \quad Kp = \frac{a/t}{A \times b/V}$$

$$\text{rearrange:} \quad Kp = \frac{a \times V}{b \times t \times A}$$

$$Kp = \frac{\%\ \text{transported}}{100} \times \frac{V}{t \times A}$$

also for two barriers in series: $1 / Kp_c = 1 / Kp_t - 1 / Kp_m$

where: Kp_c = permeability coefficient of cell monolayer

Kp_t = total permeability coefficient

Kp_m = permeability coefficient of permeable support (membrane)

Table 3.6 - Comparison of Permeability Coefficients Calculated from Data from the work of Audus and Borchardt[103] and Data taken from Table 3.5

	V (ml)	A (cm^2)	J_m (%/hr)	J_t (%/hr)	Kp_m ($x10^{-3}$) (cm/min)	Kp_t ($x10^{-3}$) (cm/min)	Kp_c ($x10^{-3}$) (cm/min)
From Audus and Borchardt	**3.0**	**0.636**	**12.00**	**1.50**	**9.43**	**1.18**	**1.35**
From Table 3.5	**1.5**	**4.91**	**16.11**	**3.15**	**0.82**	**0.16**	**0.20**

J_m = ^{14}C-Sucrose flux across membrane alone.

J_t = ^{14}C-Sucrose flux across membrane and BMEC monolayer (total).

From Table 3.6 it can be seen that the permeability of the cellulose support (9.43×10^{-3} cm/min) used by Audus and Borchardt is greater than the Falcon Cyclopore membrane

(0.82×10^{-3} cm/min). The pore sizes of these two membranes are comparable and the difference in permeabilities is thought to be due to a lower density of pores in the Cyclopore membrane. This result emphasises the need to perform control experiments across the Cyclopore membrane alone to ensure solute permeability.[118] The permeability of the porcine BMEC monolayers used in this research (0.20×10^{-3} cm/min) is smaller and the barrier is, therefore, less leaky than the bovine BMEC monolayers of Audus and Borchardt (1.35×10^{-3} cm/min). Pardridge *et al.* have calculated the permeability coefficient of sucrose across BMEC monolayers grown in continuous culture to be 5.1×10^{-3} cm/min.[122] This is 25-fold more permeable than our porcine BMEC monolayers. Pardridge *et al.* then compared this value with a value obtained from *in vivo* brain perfusion studies. The *in vivo* permeability coefficient for sucrose was found to be $< 1.0 \times 10^{-5}$ which is < 20-fold less permeable than the value produced from our porcine monolayers. In summary, the system used in this research compares favourably with other *in vitro* systems in the literature but is more permeable than the *in vivo* situation.

3.3 *In Vitro* Studies on α-Keto Acid Transport

The carrier-mediated transport of short chain monocarboxylic acids (MCA) across the BBB has been characterised *in vivo* using the brain uptake index technique.[105] The saturable nature of the carrier and, in the case of lactate, stereospecificity was shown. Cross-inhibition was demonstrated between pyruvate (**31**) and acetate, propionate, L-lactate and butyrate but not for octanoate and decanoate or di- and tricarboxylic acids. Cross-inhibition was not shown between pyruvate and L-phenylalanine, L-arginine or D-glucose indicating the carrier system to be distinct from amino acid and monosaccharide transporters. It has been shown that α-keto acids such as pyruvate show a high affinity for the MCA carrier system.[105-107] Aromatic, for example phenylpyruvate (**99**), and dicarboxylic α-keto acids were shown not to inhibit the transport of other α-keto acids showing that these are not substrates for the carrier.[106,107] A non-saturable component (approximately 15% for pyruvate) of MCA transport is present *in vivo*.[107] This causes a large variation in the transport constants reported (see Table 3.7).[70] This may be due to the different methods with which the non-saturable component has been manipulated in the calculation of kinetic parameters.[70]

Table 3.7 - Transport Constants for Monocarboxylic Acids

MCA	K_m (mM)	V_{max} (nmol min^{-1} g^{-1})	K_d (ml min^{-1} g^{-1})
L-Lactate	1.8 ± 0.6	91 ± 35	0.019 ± 0.004
Pyruvate	0.57 ± 0.16	88 ± 26	0.034 ± 0.008
Butyrate	0.70 ± 0.20	86 ± 11	0.041 ± 0.002

The biological importance of the MCA transport system is not certain. It may function to increase the flux of monocarboxylic acids into the brain where they may serve as metabolic substrates or it may be a bidirectional system to allow efflux of organic acids, for example L-lactate (**97**), from the brain in normal or hypoxic states.[105] Tsuji *et al.* have investigated the role of this carrier in the BBB transport of therapeutic agents *in vivo*.[140] They have recently repeated this work *in vitro* using bovine BMEC in primary culture. Valproate (**98**) and salicylate (**100**) were shown to inhibit the uptake of ^{3}H-acetic acid, a model substrate, into BMEC cells, suggesting carrier-mediated transport of these drugs at the BBB.[104]

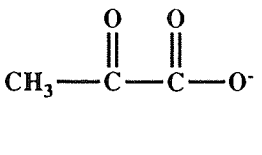

Pyruvate (31)

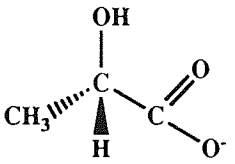

L-Lactate (97)

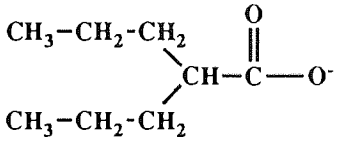

Valproate (98)

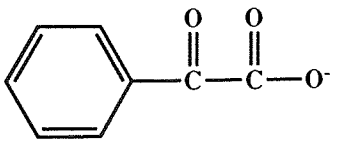

Phenylpyruvate (99)

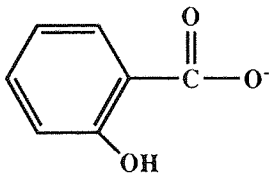

Salicylate (100)

In order to assess the possibility of esters of PFA utilising the MCA carrier system, it was first necessary to demonstrate the presence of such a system in porcine BMEC monolayers.

3.3.1 Identification of ^{14}C-Pyruvate Post-Transport using Radio-TLC

The stability of ^{14}C-pyruvate under transport conditions was investigated, to show that the ^{14}C-pyruvate was not significantly metabolised and that the ^{14}C-label detected in the basolateral chamber was ^{14}C-pyruvate. A sample from the basolateral chamber was taken after a three hour transport experiment and compared with a ^{14}C-pyruvate reference, by radio TLC, as described in section 5.5.1.

Table 3.8 - The Identification of ^{14}C-Pyruvate Post-Transport using Radio-TLC

Migration Distance	Sample (dpm)	Reference (dpm)
3mm	26	34
6mm	28	27
9mm	30	39
12mm	51	44
15mm	29	40
18mm	42	85
21mm	231	502
24mm	545	1408
27mm	442	1047
30mm	33	36

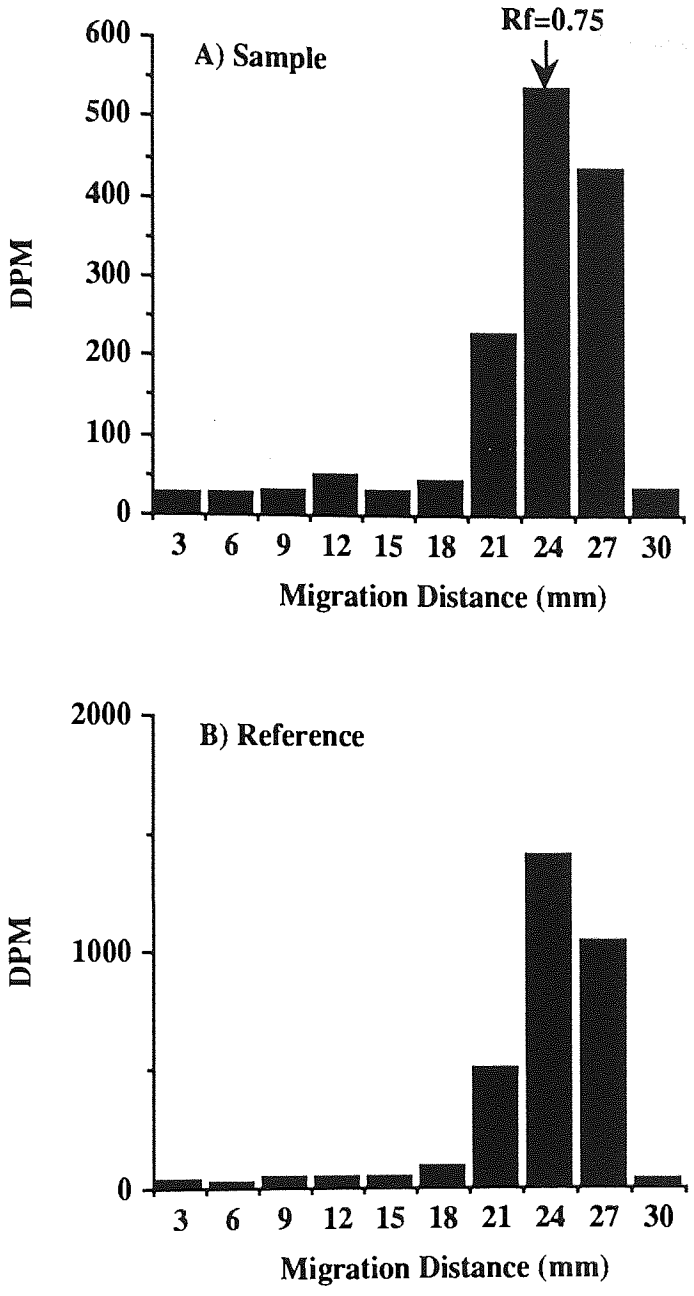

Figure 3.13 -The Identification of ^{14}C-Pyruvate Post-Transport using Radio-TLC

The ^{14}C-label entering the basolateral chamber was positively identified as ^{14}C-pyruvate by TLC. This was shown by the high degree of coincidence between the histograms for the sample taken from the basolateral chamber, after a three hour transport experiment at 37°C, and a ^{14}C-pyruvate reference. As controls, acetate and L-lactate were run on the same TLC system and found to have R_f values of 0.18 and 0.32 respectively. As little activity is apparent at these values, metabolism of pyruvate to acetate or lactate was not observed.

3.3.2 The Effect of BMEC Monolayers on ^{14}C-Pyruvate Transport

^{14}C-Pyruvate transport across 7-day old BMEC monolayers was studied and compared with diffusion across the permeable support alone.

Table 3.9 - The Effect of BMEC Monolayers on ^{14}C-Pyruvate Transport

Time (minutes)	% Pyruvate Transport Across BMEC Monolayer	% Pyruvate Transport Across Membrane Alone
30	4.08 (0.30)	18.28 (1.73)
60	8.35 (0.57)	34.44 (1.97)*
90	12.23 (0.56)	47.67 (2.52)
120	15.97 (0.59)	58.37 (3.11)
150	19.35 (0.72)	68.01 (2.90)
180	22.94 (0.57)	73.96 (2.78)

Standard deviations in parentheses, n=3 for all time points. *For calculation of K (see section 3.24), %mannitol transport across the membrane alone at 60 minutes was 24.65 (1.24).

% Mannitol transport after 180 minutes across the BMEC monolayer and the permeable support (membrane) alone were 10.31 (0.13) and 58.99 (2.94) respectively.

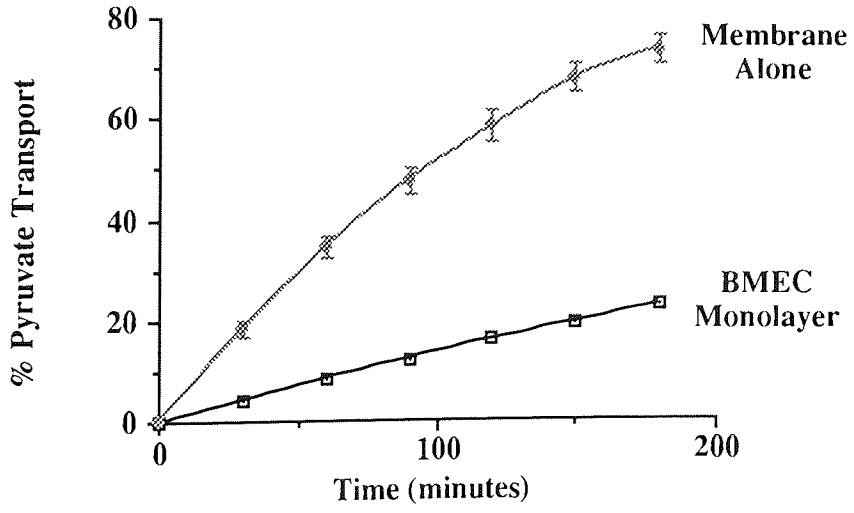

Figure 3.14 - The Effect of BMEC Monolayers on ^{14}C-Pyruvate Transport

From Figure 3.14 it can be seen that the BMEC monolayer restricts the transport of pyruvate. This is an effect similar to that seen for mannitol and is expected for a

hydrophilic molecule. The initial flux of pyruvate across BMEC monolayers is 8.35% / hour compared with 3.52% / hour for mannitol. This is due to pyruvate being a smaller molecule than mannitol and possibly due to an active transport component for pyruvate.

3.3.3 Effect of Temperature

Active transport processes are inhibited by lowering the temperature of the system from 37°C. Performing transport experiments at 4°C is commonly used to depress active transport.[103] A comparison of ^{14}C-pyruvate transport at 37°C and at 4°C was made. ^{14}C-Pyruvate transport was corrected for the 'leakiness' of the BMEC monolayers using the simultaneous transport of ^{3}H-mannitol and the following equation:

corrected % pyruvate transport =

observed % pyruvate transport - (% mannitol transport x K)

As discussed in section 3.2.4, the factor K represents the relative diffusions of ^{14}C-pyruvate and ^{3}H-mannitol. The relative diffusion of ^{14}C-pyruvate with respect to ^{3}H-mannitol across a Cyclopore membrane was determined to be 1.4.

Table 3.10 - ^{14}C-Pyruvate Transport at 37°C

Time (minutes)	% Pyruvate Transport	% Mannitol Transport	Corrected % Pyruvate Transport
30	4.08 (0.30)	1.90 (0.24)	1.42 (0.45)
60	8.35 (0.57)	3.52 (0.30)	3.42 (0.23)
90	12.23 (0.56)	5.14 (0.31)	5.04 (0.25)
120	15.97 (0.59)	6.82 (0.41)	6.42 (0.29)
150	19.35 (0.72)	8.46 (0.39)	7.51 (0.38)
180	22.94 (0.57)	10.31 (0.13)	8.50 (0.42)

Standard deviations in parentheses, n=3 for all time points.

Table 3.11 - ^{14}C-Pyruvate Transport at 4°C

Time (minutes)	% Pyruvate Transport	% Mannitol Transport	Corrected % Pyruvate Transport
30	2.58 (0.33)	1.31 (0.16)	0.74 (0.11)
60	4.97 (0.63)	2.55 (0.34)	1.41 (0.16)
90	7.77 (1.05)	4.00 (0.60)	2.17 (0.23)
120	10.23 (1.43)	5.36 (0.91)	2.72 (0.24)
150	13.30 (1.56)	7.26 (0.87)	3.32 (0.33)
180	16.46 (1.77)	8.93 (1.08)	3.95 (0.40)

Standard deviations in parentheses, n=3 for all time points.

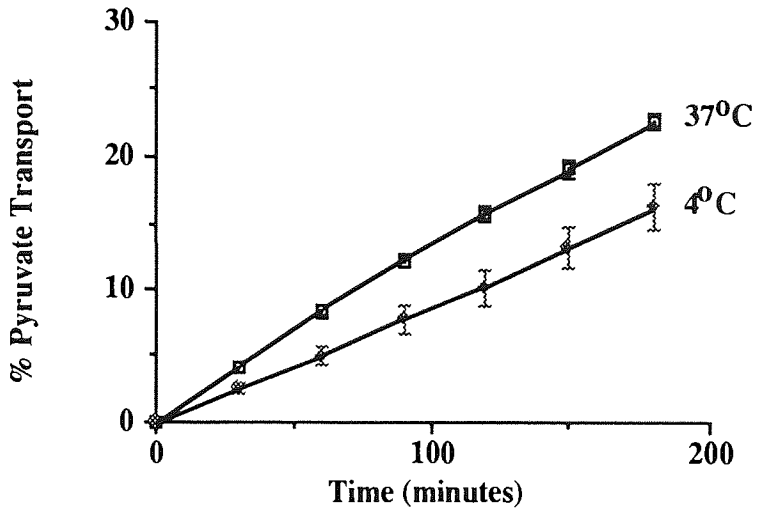

Figure 3.15 - Effect of Temperature on ^{14}C-Pyruvate Transport (Uncorrected Data)

From the uncorrected data (Figure 3.15) it can be seen that the reduction in transport observed at 4°C after 60 minutes is approximately 40%. It is suggested that a significant component (~40%) of pyruvate transport is mediated by a temperature-dependent carrier, while due to the small, highly diffusable nature of pyruvate, paracellular diffusion contributed approximately 60% of transport.

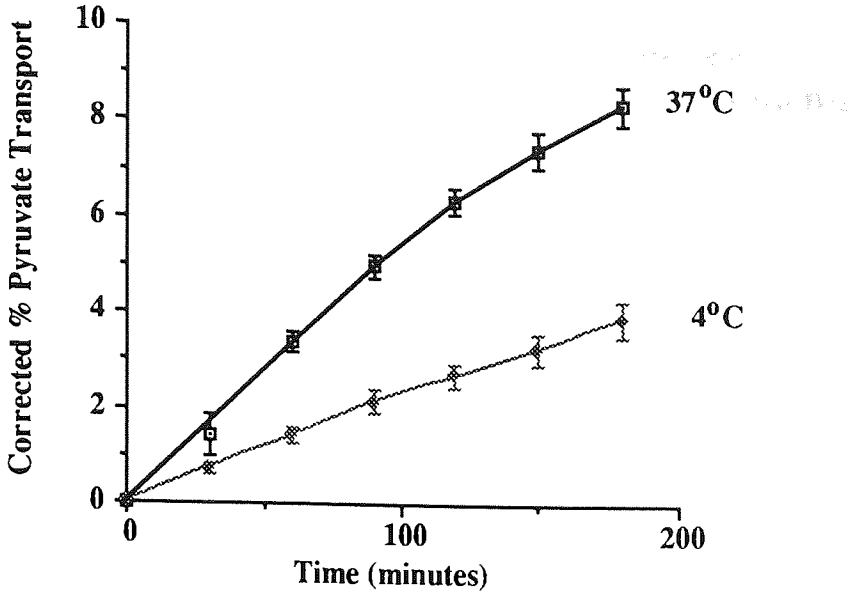

Figure 3.16 - The Effect of Temperature on ^{14}C-Pyruvate Transport (Corrected Data)

The corrected data (Figure 3.16) emphasises the reduction in transport at 4°C by removing a paracellular transport component due to the 'leakiness' of the BMEC monolayer.

3.3.4 Effect of Concentration

Carrier-mediated transport processes have been shown to be saturable. That is, only a certain number of transporters are present and the amount of substrate transported in a given time is limited. This has been demonstrated by increasing the concentration of unlabelled substrate in the apical chamber. Competition with the labelled substrate is then seen as a reduction in its transport.[103] ^{14}C-Pyruvate transport was observed with increasing concentrations of unlabelled pyruvate over a one hour period without changing the basolateral buffer. The ^{14}C-pyruvate and ^{3}H-mannitol content of the apical and basolateral chambers was then determined using liquid scintillation spectroscopy. The results are expressed as % ^{14}C-pyruvate transport in Table 3.12 and also in terms of nmol transported per hour in Table 3.13. The latter results have been corrected as discussed in section 3.2.4.

Table 3.12 - The Effect of Increasing Pyruvate Concentration Upon % ^{14}C-Pyruvate Transport Over One Hour (Uncorrected Data)

Concentration (mM)	% Pyruvate Transport	% Mannitol Transport
0.025	6.05 (0.25)	1.50 (0.29)
0.05	5.65 (0.29)	1.35 (0.06)
0.10	5.41 (0.29)	1.34 (0.16)
0.25	4.97 (0.00)	1.35 (0.01)
0.50	5.09 (0.38)	1.64 (0.26)
0.75	4.90 (0.69)	1.60 (0.26)
1.00	4.61 (0.16)	1.67 (0.16)
2.00	3.49 (0.10)	1.33 (0.10)

Standard deviations in parentheses, n=3 for all time points.

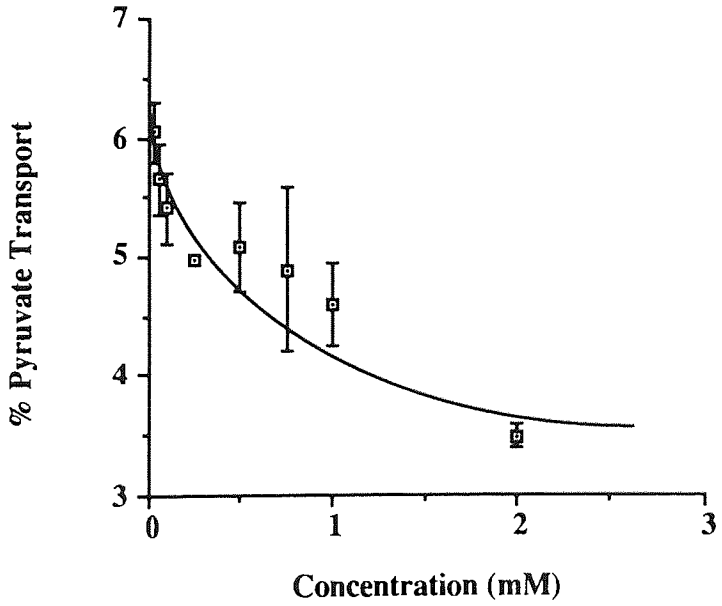

Figure 3.17- The Effect of Increasing Pyruvate Concentration Upon % ^{14}C-Pyruvate Transport Over One Hour (Uncorrected Data)

From Figure 3.17 it can be seen that ^{14}C-pyruvate transport decreases with increasing concentration of unlabelled pyruvate while Table 3.12 shows that mannitol flux remained constant. It is suggested that this is due to increasing competition for a finite number of transporters.

The amount of pyruvate transported was calculated from the dpm transported and the specific activity of the solution of lowest concentration, as follows:

specific activity of 0.025 mM solution = 0.06667 μCi / ml

therefore there is 66.67 μCi in 0.025 mmol

1 Ci in 0.025 x 1,000,000 / 66.67

1 Ci in 375 mmol

substituting in the equation $1\ Ci = 2.22 \times 10^{12}$ dpm

2.22×10^{12} dpm = 375mmol

1 dpm = 1.69×10^{-4} nmol

For each concentration the amount transported is given by:

$$\text{dpm transported} \times 1.69 \times 10^{-4}\ \text{nmol} \times \frac{\text{pyruvate concentration (mM)}}{0.025\text{mM}}$$

This calculation was repeated using dpm corrected using mannitol transport, as discussed in section 3.2.4, to give corrected pyruvate transport. The results are given in Table 3.13.

Table 3.13 - The Effect of Increasing Pyruvate Concentration Upon Amount of Pyruvate Transported Over One Hour

Concentration (mM)	Pyruvate Transport (nmol/ hour)	Corrected Pyruvate Transport (nmol/hour)
0.025	1.66 (0.07)	1.14 (0.09)
0.05	3.07 (0.02)	2.14 (0.24)
0.10	5.83 (0.20)	3.83 (0.03)
0.25	13.70 (0.30)	8.79 (0.52)
0.50	27.53 (0.50)	16.25 (1.71)
0.75	39.60 (4.17)	21.41 (2.27)
1.00	50.80 (2.00)	25.95 (1.35)
2.00	82.67 (9.68)	36.68 (1.12)

Standard deviations in parentheses, n=3 for all time points.

The kinetics of active transport are fundamentally the same as enzymatic reactions. The enzyme combining with substrate and releasing product is analogous to a transport protein combining with substrate on one side of a membrane and releasing it upon the opposite side. The Michaelis-Menten equation can be applied to biological transport and modified to accomodate non-saturable transport.

$$v = \frac{V_{max} \times [S]}{K_m + [S]} + K_d \times [S]$$

Where: v = rate of transport

K_m = concentration of substrate that will produce a half-maximal rate

V_{max} = maximum rate of transport that can be obtained

K_d = non-saturable diffusion constant

The uncorrected pyruvate transport data was manipulated using non-linear regression analysis (Fig P, Biosoft Limited) directly fitting the transport data to the above equation. However, the analysis failed to give a stable iteration. The data was then corrected as described in section 3.2.4. The corrected pyruvate transport data were plotted against concentration and gave a curve characteristic of Michaelis-Menten or saturation kinetics [see Figure 3.18 (a)]. This data was linearly transformed using Lineweaver-Burk [see Figure 3.18 (b)], Eadie-Hofstee [see Figure 3.19 (c)] and Hanes-Woolf plots [see Figure 3.19 (d)] in order to obtain estimations of K_m and V_{max}. Estimations of K_m and V_{max} were also obtained by the direct linear method (Enzpack, Biosoft Limited) and non-linear regression analysis (Fig P, Biosoft Limited). A summary of the estimated values are given in Table 3.14.

Table 3.14 - Estimated Kinetic Parameters for Pyruvate Transport

Method	Vmax (nmol/hour)	Km (mM)	Correlation Coefficient
Lineweaver-Burk	**42.0**	**0.91**	**0.999**
Eadie-Hoftsee	**61.1**	**1.39**	**0.982**
Hanes-Woolf	**63.8**	**1.48**	**0.996**
Direct Linear	**62.6**	**1.41**	*
Non-Linear Regression+	**64.5**	**1.50**	**

*** 68% Confidence Limits, 60.0-64.4 and 1.31-1.58 respectively.**

**** Standard Deviations, 3.25 and 0.13 respectively.**

+ Direct fitting of data to Michaelis-Menten Equation, K_d was set at zero.

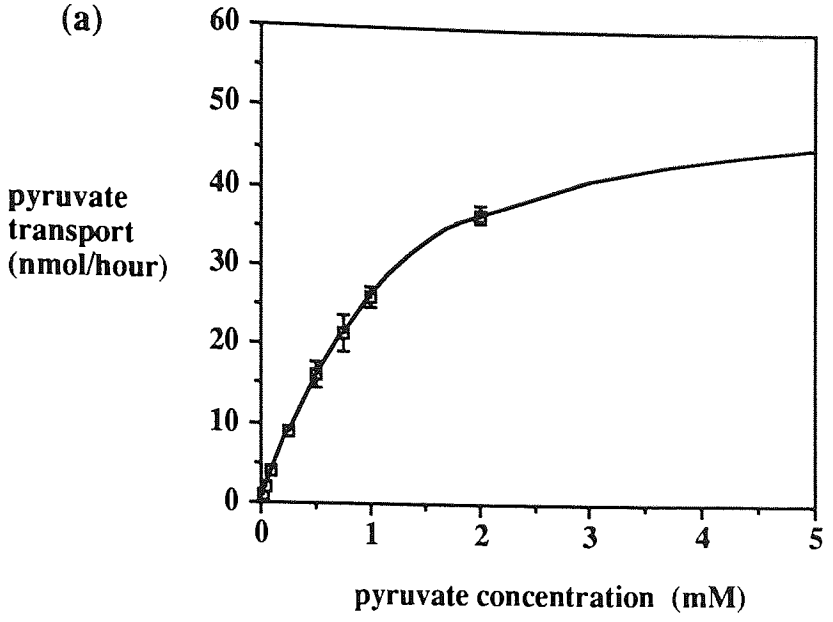

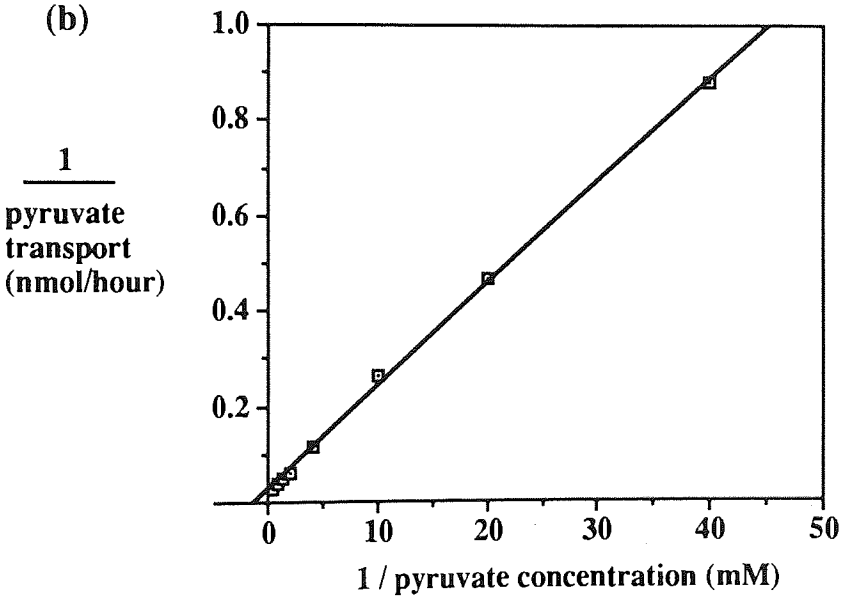

Figure 3.18 - (a) Corrected Pyruvate Transport against Concentration
(b) Lineweaver-Burk plot of data presented in (a)
K_m = 0.907 mM
V_{max}= 42 nmol/hour
Correlation = 0.999
Values from Enzpack, Biosoft Limited.

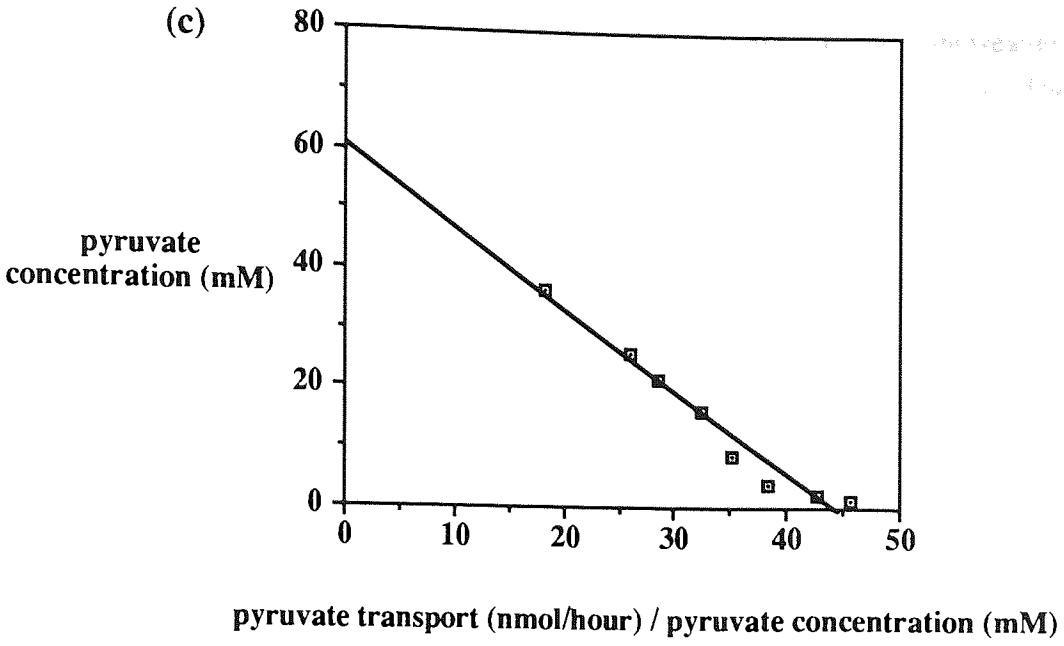

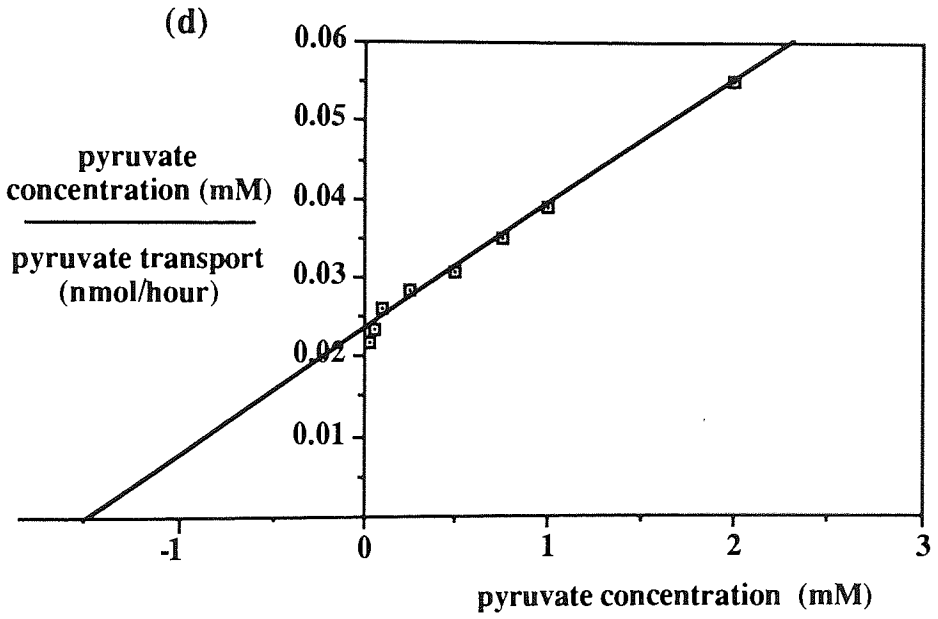

Figure 3.19 - (c) Eadie-Hofstee plot of data presented in (a)

K_m = 1.39 mM

V_{max} = 61.1 nmol/hour

Correlation = 0.982

(d) Hanes-Woolf plot of data presented in (a)

K_m = 1.48 mM

V_{max} = 63.8 nmol/hour

Correlation = 0.996

Values from Enzpack, Biosoft Limited.

From Table 3.14 it can be seen that the kinetic values, calculated by the Lineweaver-Burk plot, show some variance from the values calculated by other methods. The Lineweaver-Burk plot is considered inferior to other linear transformations, as it compresses the smaller data points and gives an unfair weighting to the larger points, as seen in Figure 3.18 (b). The K_m values calculated for pyruvate transport (mean of data from Table 3.14 = 1.34 mM) are higher than the value of 0.57 mM calculated from *in vivo* brain studies.[70] This could possibly be due to a to a non-saturable diffusion component present in the data, although this was not apparent from non-linear regression analysis of the data.

3.3.5 Inhibiton Profile

Substrates for a carrier-mediated system have been shown to compete for transport and therefore inhibit the transport other substrates.[105] This cross-inhibition provides an inhibition profile characteristic of a particular substrate and transport system. This can be used to identify and differentiate between carrier systems with similar substrates. For example, the A (alanine-preferring) and the L (leucine-preferring) amino acid carrier systems can be distiguished by their inhibition profiles. The effect of 10mM of various compounds on pyruvate transport was investigated. Pyruvate data was corrected as in section 3.3.3 and presented in Table 3.15 and Figure 3.20.

Table 3.15 - The Effect of 10mM of Various Potenetial Inhibitors on ^{14}C-Pyruvate Transport Over One Hour

Potential Inhibitor	% Pyruvate Transport	% Mannitol Transport	n	Corrected % Pyruvate Transport	Corrected % Inhibition
No Inhibitor	4.55 (0.28)	1.58 (0.25)	6	2.34 (0.21)	-
Pyruvate	2.97 (0.33)	1.54 (0.17)	3	0.81 (0.10)	65.24 (4.21)
L-Lactate	3.63 (0.13)	1.58 (0.21)	4	1.41 (0.20)	39.64 (8.46)
D-Lactate	4.48 (0.13)	1.57 (0.19)	4	2.27 (0.31)	2.89 (13.30)
Valproate	3.10 (0.31)	1.71 (0.14)	3	0.71 (0.12)	69.80 (4.92)
Phenylpyruvate	3.44 (0.13)	2.00 (0.11)	3	0.64 (0.12)	72.65 (4.92)
Acetate	3.97 (0.27)	1.47 (0.32)	4	1.92 (0.23)	18.16 (9.87)
PFA	4.97 (0.28)	1.78 (0.13)	3	2.47 (0.11)	-5.70 (4.57)
PFA diester (43)	4.97 (0.32)	1.77 (0.12)	3	2.49 (0.28)	-6.55 (11.81)
L-Phenylalanine	4.63 (0.14)	1.61 (0.07)	3	2.26 (0.12)	3.27 (5.13)

Standard deviations in parentheses.

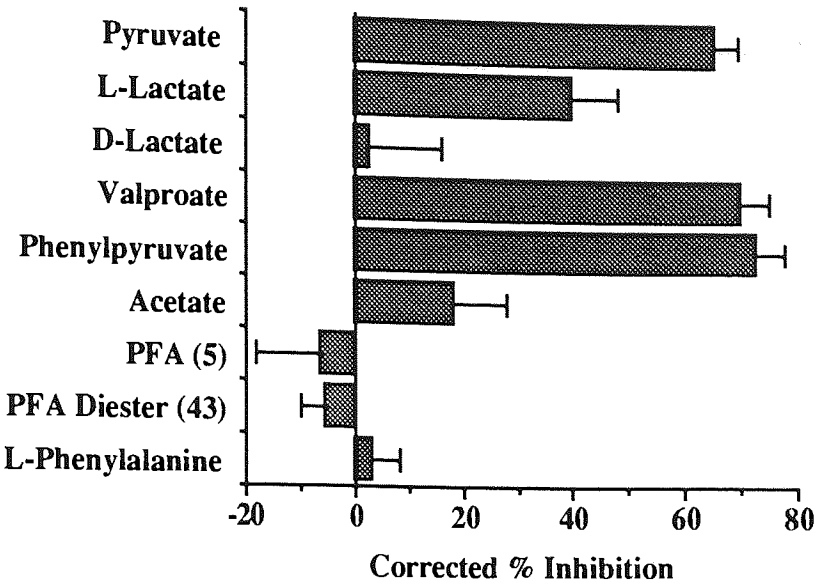

Figure 3.20 - The Effect of 10mM of Various Potential Inhibitors on Corrected ^{14}C-Pyruvate Transport Over One Hour

Figure 3.20 demonstrates that pyruvate inhibits its own transport. That is, the large excess of unlabelled pyruvate saturates the MCA carriers preventing the transport of the labelled pyruvate. Stereospecificity can be seen as L-lactate inhibits transport while D-lactate does not. This is in agreement with results *in vivo* [105] and *in vitro* using bovine BMEC[104] where the naturally occuring isomer has a greater affinity for the carrier system. The anti-epileptic drug valproate inhibited ^{14}C-pyruvate transport to a similar extent as pyruvate, an observation consistent with valproate being transported by the monocarboxylic acid system. Tsuji *et al.* demonstrated the inhibition of ^{3}H-acetic acid uptake by valproate to be twice that seen with pyruvate.[104,140] It has previously been suggested that the active transport of valproate *in vivo* occurs at a higher rate in the brain to blood direction than blood to brain.[91] As BMEC monolayers have been reported to be polar with the apical surface in culture being equivalent to the lumenal surface *in vivo*[118] the direction of valproate transport could be examined in the cell culture model by repeating the inhibition experiment following transport from the basolateral chamber to the apical chamber. It has been reported that aromatic α-keto acids such as phenylpyruvate are not substrates for the carrier system and do not inhibit the transport of other α-keto acids[106], but phenylpyruvate was shown to inhibit pyruvate transport. Other work *in vivo*[140] and *in vitro*[104] has shown inhibition of monocarboxylic acid transport by aromatic acids such as benzoic and salicylic acid. PFA and the PFA diester sodium methyl methoxycarbonyl phosphonate (**43**) showed no inhibition of pyruvate transport and are therefore unlikely to be substrates for a pyruvate carrying system. Phenylalanine also showed no inhibition of pyruvate transport consistent with previous reports that the monocarboxylic acid system is distinct from the L-amino acid carrier.[104,105]

When viewed together the effect of temperature, concentration and the inhibition profile of pyruvate transport across porcine BMEC monolayers provides evidence for a short-chain monocarboxylic acid carrier similar to those previously described *in vivo* and *in vitro*. It can be seen that PFA and the PFA diester **(43)** show no affinity for this carrier and are therefore not transported by the MCA carrier.

3.4 *In Vitro* Amino Acid Transport

The carrier-mediated transport of amino acids across the BBB has been characterised *in vivo*. Four distinct carrier systems have been characterised.[72] Large neutral amino acids (LNAA) have been shown to be transported by the sodium-independent L-(leucine-preferring) system while small neutral amino acids are transported by the sodium-dependent A-(alanine-preferring) system.[94,141] The L-system is bidirectional and present in the luminal and abluminal membranes of BMEC while the A-system is only present in the abluminal membane and unidirectional in the direction of brain to blood.[141] A separate transport system for basic amino acids at the BBB is documented as is a very low capacity transporter for the efflux of acidic amino acids from the brain.[72] The L-system has been extensively characterised and is of particular interest in the transport of amino acid drugs into the brain. The saturable nature and stereospecificity of the L-system has been shown.[94,142] Large hydrophobic amino acids show the highest affinities for the carrier. Some small amino acids such as L-alanine have a lower affinity while others such as glycine do not appear to be transported by the carrier. The basic amino acid L-histidine has an affinity for the carrier comparable to other large amino acids while the other basic and the acidic amino acids are not transported. Kinetic parameters for the transport of LNAA have been calculated.[72]

Table 3.16 - Transport Constants for Large Neutral Amino Acids

LNAA	K_m (mM)	V_{max} (nmol min^{-1} g^{-1})	K_d (ml min^{-1} g^{-1})
Leucine	0.10 ± 0.01	22 ± 3	0.018 ± 0.004
Phenylalanine	0.11 ± 0.01	28 ± 7	0.014 ± 0.008
Tyrosine	0.15 ± 0.01	31 ± 8	0.016 ± 0.004
Methionine	0.18 ± 0.08	29 ±12	0.019 ± 0.011
Histidine	0.24 ± 0.03	29 ± 4	0.012 ± 0.003
L-Dopa	0.43 ± 0.15	63 ± 22	0

The Michaelis-Menten constants (K_m) for the transport of LNAAs in brain endothelium are much lower than in non-brain tissue. As the K_m values observed in brain capillaries are similar to plasma levels of LNAAs, the brain is uniquely sensitive to transport competition effects.[70] L-Dopa (**65**), used in the treatment of Parkinsons disease, is known to be transported by this carrier. Due to the sensitivity of the BBB to LNAA competition effects, a decrease in response to L-dopa has been observed with rises in circulating LNAAs.[74] The centrally acting antihypertensive methyl dopa is also known to utilise the L-system.[73] Melphalan (phenylalanine mustard) (**66**) was synthesised in an attempt to deliver an alkylating agent to the brain.[75] It was found to be transported by the L-system but to have an affinity for the carrier far less than that of endogenous LNAA and therefore does not achieve therapeutic concentrations in the brain. D, L-NAM (**67**), a derivative of melphalan, has been shown to have an affinity for the carrier greater than other LNAAs and appears to be a promising brain-directed cytotoxic agent.[76] The L-system has been studied *in vitro* using isolated brain capillaries.[101] L-Leucine (**62**) showed cross-inhibition with L-phenylalanine, L-tyrosine (**64**), L-methionine, L-histidine (**63**), and to a lesser extent, with L-alanine. Little or no cross-inhibition was observed with glycine or L-proline. This is in agreement with the inhibition profile observed *in vivo*. Using cultured BMEC, the A- and L-system have been characterised in terms of sodium dependence and independence respectively.[143] Audus and Borchardt have produced an inhibition profile and a K_m of 0.18mM for L-leucine transport across BMEC monolayers in line with observations *in vivo*.

In order to assess the possibility of an amino acid-linked PFA prodrug utilising the L-system it was first necessary to demonstrate the presence of this system in porcine BMEC monolayers.

3.4.1 The Identification of ^{3}H-L-Tyrosine Post-Transport using Radio-TLC

The stability of ^{3}H-L-tyrosine under transport conditions was investigated, to show that the ^{3}H-L-tyrosine was not significantly metabolised and that the ^{3}H-label detected in the basolateral chamber was ^{3}H-L-tyrosine. A sample from the basolateral chamber was taken after a three hour transport experiment and compared with a ^{3}H-L-tyrosine reference.

Table 3.17 - The Identification of ^{3}H-L-Tyrosine Post-Transport using Radio-TLC

Migration Distance	Sample (DPM)	Reference (DPM)
2.5mm	66	105
5.0mm	68	83
7.5mm	79	121
10.0mm	90	878
12.5mm	307	1551
15.0mm	510	6194
17.5mm	106	129
20.0mm	75	92
22.5mm	77	83
25.0mm	74	82

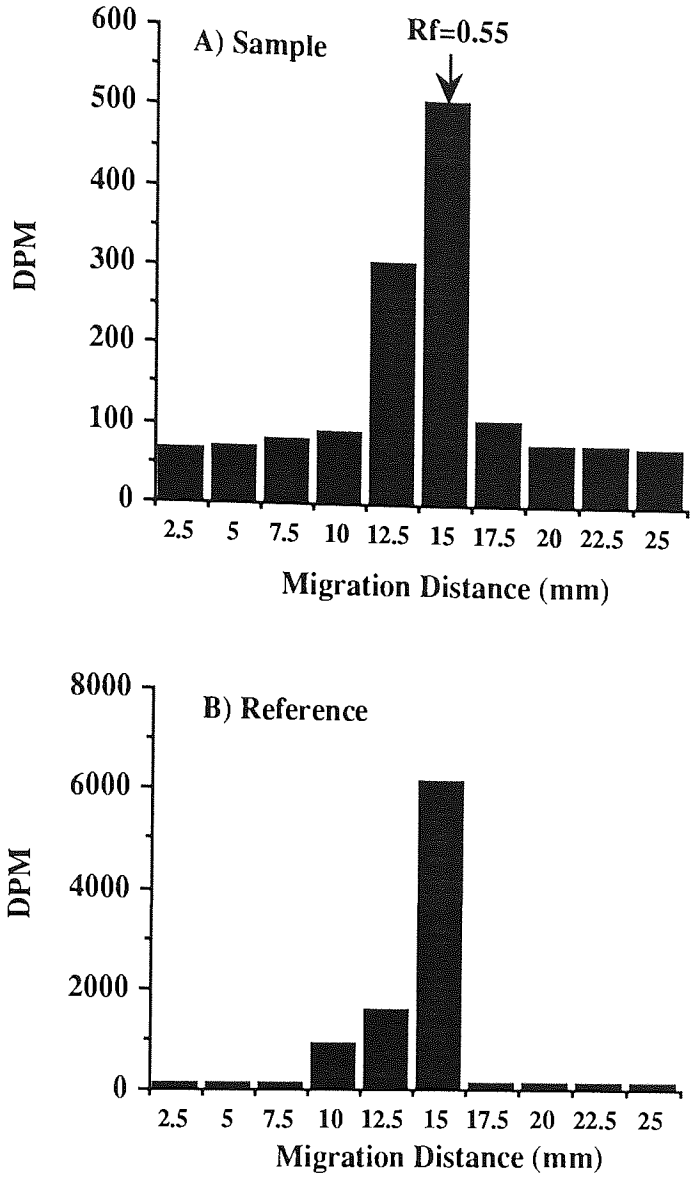

Figure 3.21 - The Identification of ^{3}H-L-Tyrosine Post-Transport using Radio-TLC

The ^{3}H-label entering the basolateral chamber was positively identified as ^{3}H-L-tyrosine by TLC. This was shown by the high degree of coincidence between the histograms for the sample taken from the basolateral chamber, after a three hour transport experiment at 37°C, and a ^{3}H-L-tyrosine reference.

3.4.2 The Effect of BMEC Monolayers on ^{3}H-L-Tyrosine Transport

^{3}H-L-Tyrosine transport across 7-day old BMEC monolayers was studied and compared with diffusion across the permeable support alone.

Table 3.18 - The Effect of BMEC Monolayers on ^{3}H-L-Tyrosine Transport

Time (minutes)	% Tyrosine Transport Across BMEC Monolayer	% Tyrosine Transport Across Membrane Alone
30	3.99 (0.17)	10.30 (1.07)
60	7.30 (0.28)	19.48 (1.18)*
90	10.44 (0.48)	27 90 (1.40)
120	12.90 (0.57)	35.20 (1.35)
150	14.89 (0.88)	41.97 (1.87)
180	16.68 (1.04)	48.38 (1.84)

Standard deviations in parentheses, n=3 for all time points. *For calculation of K %mannitol transport across membrane alone after 60 minutes was 21.43 (0.65).

% Mannitol transport after 180 minutes across the BMEC monolayer and the membrane alone were 13.20 (1.20) and 53.59 (2.09) respectively.

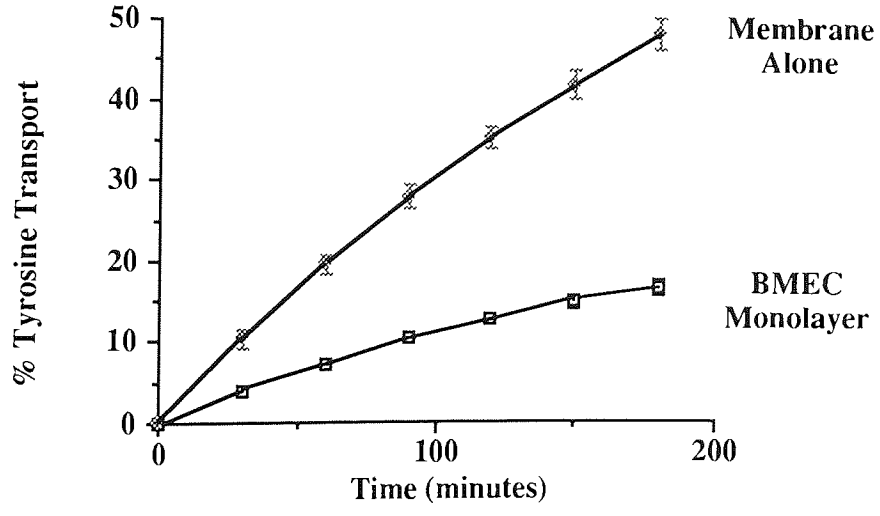

Figure 3.22 - The Effect of BMEC Monolayers on ^{3}H-L-Tyrosine Transport

From Figure 3.22 it can be seen that the BMEC monolayer restricts the transport of L-tyrosine. This is an effect similar to that seen for mannitol and pyruvate and is

expected of a hydrophilic molecule. The initial flux of L-tyrosine across BMEC monolayers is 7.30% / hour compared with 3.52% / hour for mannitol. The larger flux of L-tyrosine in comparison to mannitol may be due to an active component in the transport of L-tyrosine.

3.4.3 Effect of Temperature

In order to identify any temperature-dependent component of ^{3}H-L-tyrosine flux, a comparison of transport at 4°C and 37°C was made. Data was corrected as in section 3.3.3. The value of K was calculated to be 0.9 as discussed in section 3.2.4.

Table 3.19 - ^{3}H-L-Tyrosine Transport at 37°C

Time (minutes)	% Tyrosine Transport	% Mannitol Transport	Corrected % Tyrosine Transport
30	3.99 (0.17)	2.42 (0.30)	1.81 (0.20)
60	7.30 (0.28)	4.37 (0.30)	3.36 (0.06)
90	10.44 (0.48)	6.39 (0.30)	4.69 (0.04)
120	12.90 (0.57)	8.46 (0.64)	5.28 (0.02)
150	14.89 (0.88)	10.75 (0.90)	5.21 (0.08)
180	16.68 (1.04)	13.20 (1.19)	4.80 (0.15)

Standard deviations in parentheses, n=3 for all time points.

Table 3.20 - ^{3}H-L-Tyrosine Transport at 4°C

Time (minutes)	% Tyrosine Transport	% Mannitol Transport	Corrected % Tyrosine Transport
30	1.34 (0.43)	1.39 (0.27)	-0.02 (0.02)
60	2.84 (0.59)	2.91 (0.61)	0.25 (0.08)
90	4.56 (0.74)	4.77 (0.63)	0.21 (0.02)
120	6.14 (0.99)	6.27 (0.78)	0.42 (0.08)
150	7.97 (1.18)	8.45 (0.84)	0.24 (0.16)
180	9.73 (1.45)	10.04 (1.41)	0.58 (0.11)

Standard deviations in parentheses, n=3 for all time points.

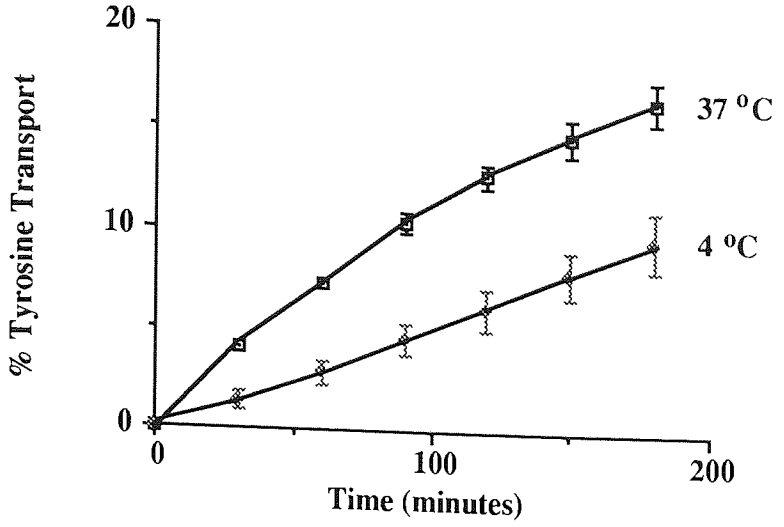

Figure 3.23 - Effect of Temperature on ^{3}H-L-Tyrosine Transport (Uncorrected Data)

The reduction in transport at 4°C was 61% after 60 minutes. Despite a small tightening of the monolayer as shown by the respective mannitol fluxes it appears clear that there is a temperature dependent component of L-tyrosine transport.

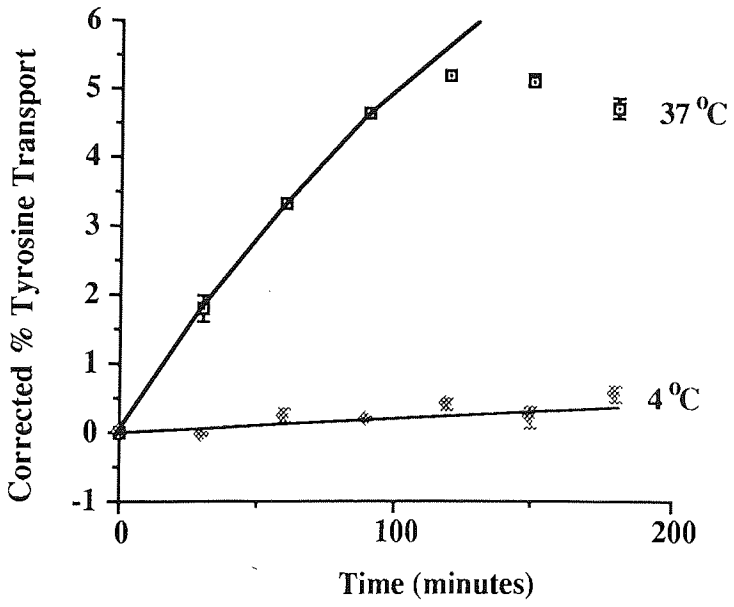

Figure 3.24 - Effect of Temperature on ^{3}H-L-Tyrosine Transport (Corrected Data)

The corrected data in Figure 3.24 show the abolition of active transport at 4°C. An anomaly occurs after 90 minutes in the 37°C transport data. Transport appears to reach a plateau, as if active transport has ceased. It is unclear whether this is an artifact or a real event possibly reflecting the viability or metabolic status of the cells after this period. Further tyrosine transport studies were restricted to 60 minutes.

3.4.4 Effect of Concentration

In order to identify any saturable component of ^{3}H-L-tyrosine transport, the effect of increasing tyrosine concentration upon transport was studied. The results are expressed as % ^{3}H-L-tyrosine transport in Table 3.21 and also in terms of nmol transported per hour in Table 3.22. The latter results have been corrected as discussed in section 3.2.4.

Table 3.21 - The Effect of Increasing Tyrosine Concentration Upon % ^{3}H-L-Tyrosine Transport Over One Hour

Concentration (mM)	% Tyrosine Transport	% Mannitol Transport
0.005	7.33 (0.38)	4.60 (0.19)
0.010	5.94 (0.20)	4.68 (0.04)
0.020	5.87 (0.41)	4.55 (0.60)
0.050	5.48 (0.57)	4.59 (0.87)
0.100	4.90 (0.33)	4.20 (0.47)
0.200	4.74 (0.40)	4.41 (0.37)
0.500	4.40 (0.44)	4.41 (0.64)
1.000	3.69 (0.49)	3.80 (0.24)

Standard deviations in parentheses, n=3 for all concentrations.

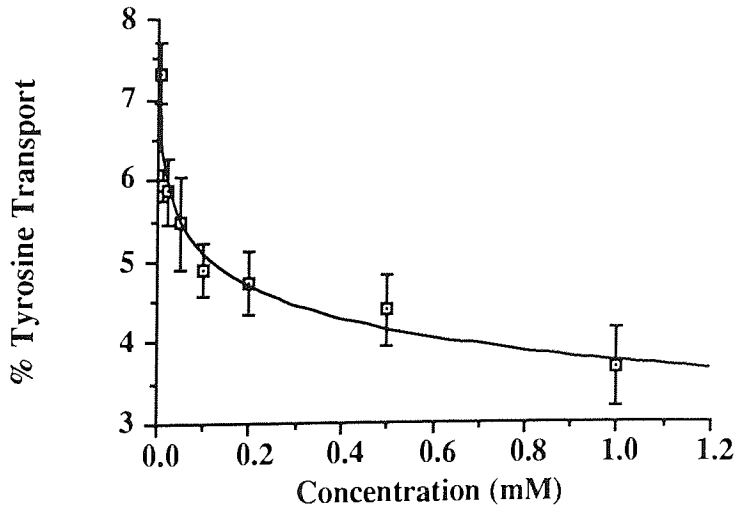

Figure 3.25 - The Effect of Increasing Tyrosine Concentration Upon Transport

From Figure 3.25 it can be seen that ^{3}H-L-tyrosine transport decreases with increasing concentration of unlabelled pyruvate while Table 3.21 shows that mannitol flux

remained constant. It is suggested that this is due to increasing competition for a finite number of transporters.

Table 3.22 - The Effect of Increasing Tyrosine Concentration Upon Transport Over One Hour (Uncorrected and Corrected Data)

Concentration (mM)	Tyrosine Transport (nmol/hour)	Corrected Tyrosine Transport (nmol/hour)
0.005	0.41 (0.02)	0.15 (0.05)
0.010	0.67 (0.02)	0.20 (0.02)
0.020	1.31 (0.10)	0.40 (0.07)
0.050	3.05 (0.32)	0.76 (0.17)
0.100	6.20 (1.02)	1.21 (0.16)
0.200	16.52 (1.01)	1.76 (0.16)
0.500	24.05 (1.80)	2.37 (0.83)
1.000	42.37 (3.91)	5.57 (0.77)

Standard deviations in parentheses, n=3 for all concentrations.

The uncorrected tyrosine transport data was manipulated using non-linear regression analysis (Fig P, Biosoft Limited). The analysis produced the graph and values shown in Figure 3.26.

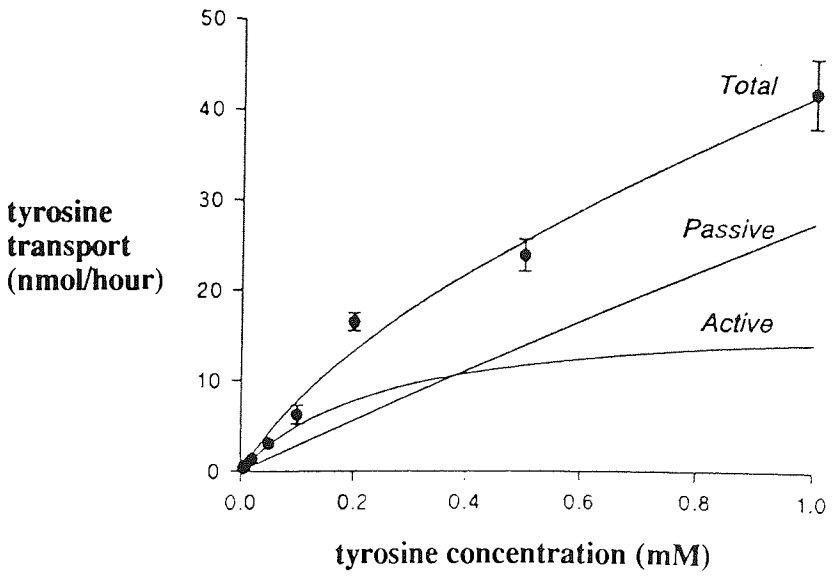

Figure 3.26 - Non-Linear Regression Analysis of Uncorrected Tyrosine Transport against Tyrosine Concentration.
K_m = 0.26 mM (1.05), V_{max} = 17.91 nmol/hour (56.85),
K_d = 27.83 x 10^{-3} ml/ hour (35.86), standard deviations in parentheses

Large errors were apparent in the figures produced by non-linear regression analysis of the uncorrected data fitted to the modified Michaelis-Menten equation (see section 3.3.4). Therefore, the data were corrected as described in section 3.2.4. The corrected tyrosine transport data were plotted against concentration and gave a curve characteristic of Michaelis-Menten or saturation kinetics [see Figure 3.27 (a)]. This data was linearly transformed using Lineweaver-Burk [see Figure 3.27 (b)], Eadie-Hofstee [see Figure 3.28 (c)] and Hanes-Woolf plots [see Figure 3.28 (d)] in order to obtain estimations of K_m and V_{max}. Estimations of K_m and V_{max} were also obtained by the direct linear method (Enzpack, Biosoft Software) and non-linear regression analysis (Fig P, Biosoft Software). A summary of the estimated values are given in Table 3.23.

Table 3.23 - Estimated Kinetic Parameters for Tyrosine Transport

Method	Vmax (nmol/hour)	Km (mM)	Correlation Coefficient
Lineweaver-Burk	**1.80**	**0.06**	**0.977**
Eadie-Hofstee	**3.82**	**0.16**	**0.850**
Hanes-Woolf	**6.33**	**0.39**	**0.743**
Direct Linear	**3.01**	**0.14**	*
Non-Linear Regression+	**3.07**	**0.15**	**

*** 68% Confidence Limits, 2.79-3.14 and 0.12-0.16 respectively.**

**** Standard Deviations, 0.18 and 0.02 respectively.**

+ Direct fitting of data to Michaelis-Menten equation, K_d was set at zero and the 1 mM data point omitted.

It can be seen from Table 3.23 that the Lineweaver-Burk plot gives kinetic values lower than those of other methods. This difference was also seen in the calculation of parameters for pyruvate transport and the limitations of the Lineweaver-Burk plot are discussed in section 3.3.4. The values produced from the Eadie-Hofstee plot, the direct linear method and non-linear regression analysis are in close agreement with each other. The K_m values from these three methods also show very close agreement to the K_m for L-tyrosine transport *in vivo* (0.15 mM).[72]

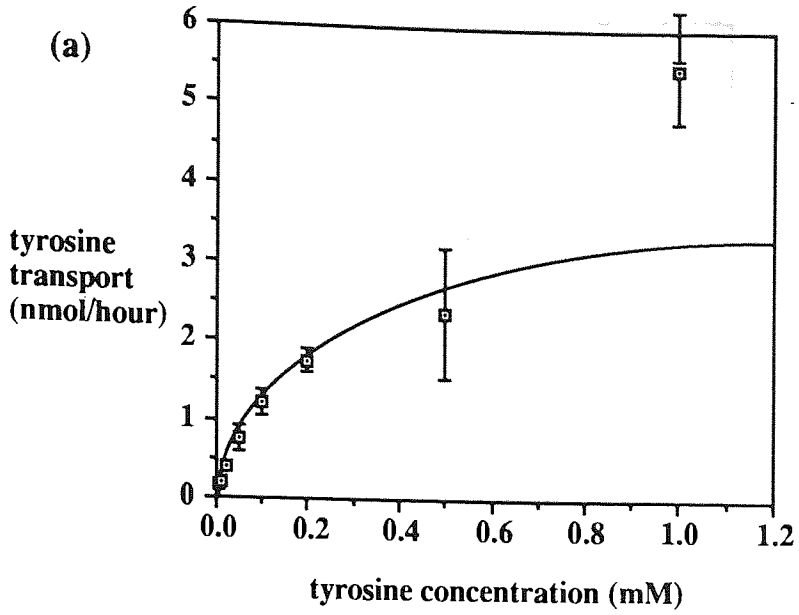

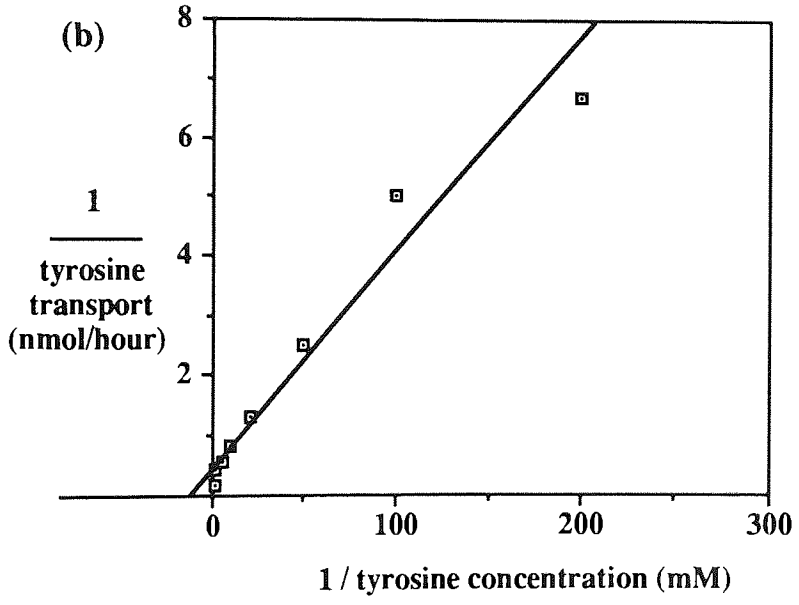

Figure 3.27 - (a) Corrected Tyrosine Transport against Concentration
(b) Lineweaver-Burk plot of data presented in (a)
K_m = 0.0604 mM
V_{max} = 1.8 nmol/hour
Correlation = 0.977
Values from Enzpack, Biosoft Limited.

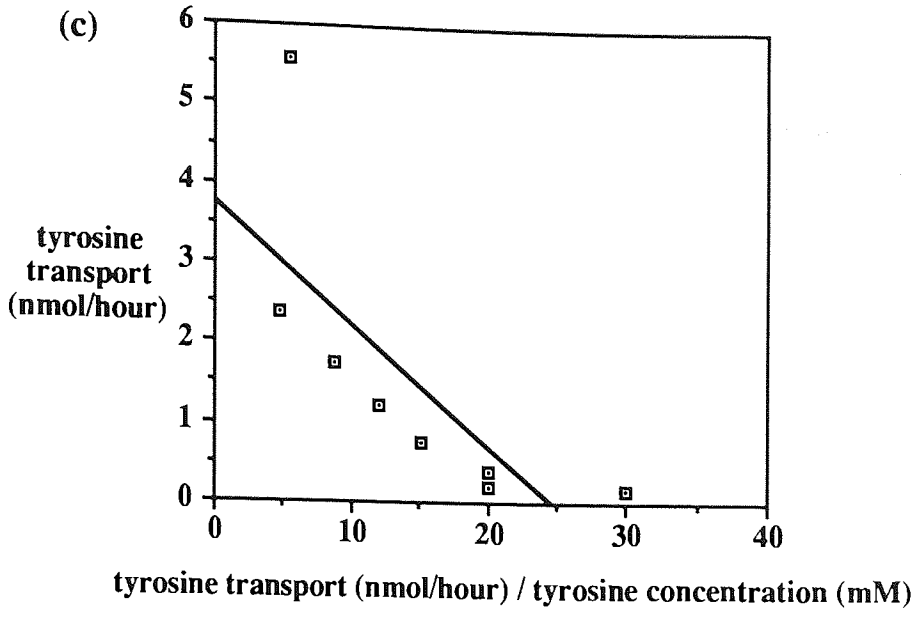

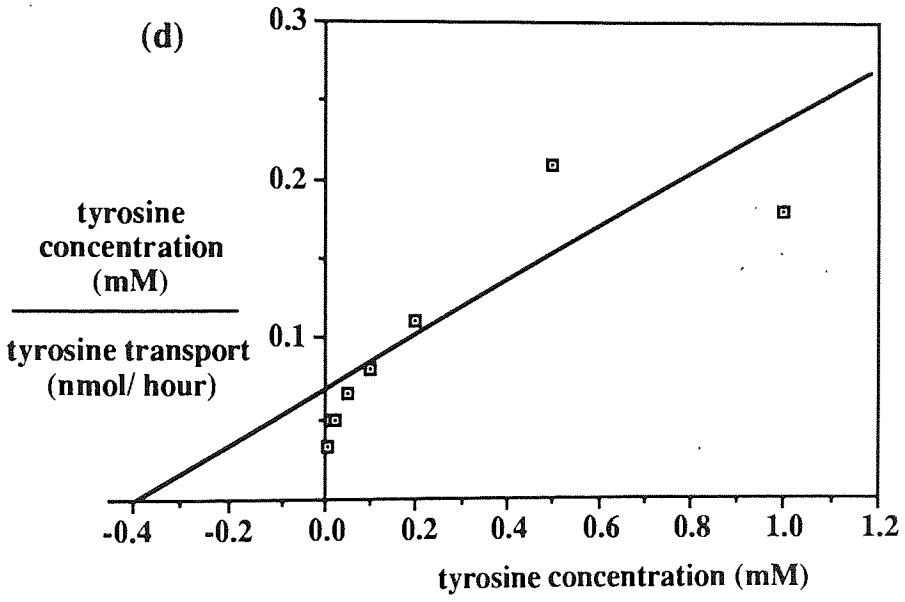

Figure 3.28 - (c) Eadie-Hofstee plot of data presented in (a)

K_m = 0.156 mM

V_{max} = 3.82 nmol/hour

Correlation = 0.743

(d) Hanes-Woolf plot of data presented in (a)

K_m = 0.386 mM

V_{max} = 6.33 nmol/hour

Correlation = 0.85 Values from Enzpack, Biosoft Limited.

3.4.5 Inhibiton Profile

An inhibition profile (as discussed in section 3.3.5) was constructed for L-tyrosine. The effect of 2mM of various amino acids on ^{3}H-L-tyrosine transport was investigated. Transport data was corrected as described in section 3.33 and presented in Table 3.24 and Figure 3.29.

Table 3.24 - The Effect of 2mM of Various Potential Inhibitors on ^{3}H-L-Tyrosine Transport

Potential Inhibitor	% Tyrosine Transport	% Mannitol Transport	n	Corrected % Tyrosine Transport	Corrected % Inhibition
No Inhibitor	5.47 (0.53)	2.29 (0.44)	6	3.38 (0.47)	-
L-Tyrosine	1.92 (0.35)	1.85 (0.61)	3	0.36 (0.14)	89.25 (4.21)
D-Tyrosine	3.70 (0.29)	1.81 (0.24)	3	2.07 (0.18)	38.75 (5.43)
L-Phenylalanine	2.34 (0.31)	2.23 (0.35)	5	0.33 (0.04)	90.18 (1.31)
D-Phenylalanine	2.51 (0.11)	2.10 (0.18)	5	0.62 (0.09)	81.66 (2.57)
L-Dopa	2.75 (0.19)	2.60 (0.31)	3	0.41 (0.09)	87.77 (2.92)
D-Dopa	5.52 (0.39)	2.54 (0.23)	3	3.23 (0.20)	4.54 (5.98)
L-Histidine	2.41 (0.13)	2.32 (0.11)	3	0.32 (0.04)	90.61 (1.12)
L-Methionine	2.56 (0.47)	2.56 (0.56)	3	0.25 (0.04)	92.61 (1.07)
L-Alanine	4.45 (0.20)	2.17 (0.25)	3	2.50 (0.17)	42.21 (6.67)
Tyrosine-PFA Diester (68)	3.13 (0.28)	2.21 (0.26)	3	1.11 (0.02)	67.26 (0.61)

Standard deviations in parentheses.

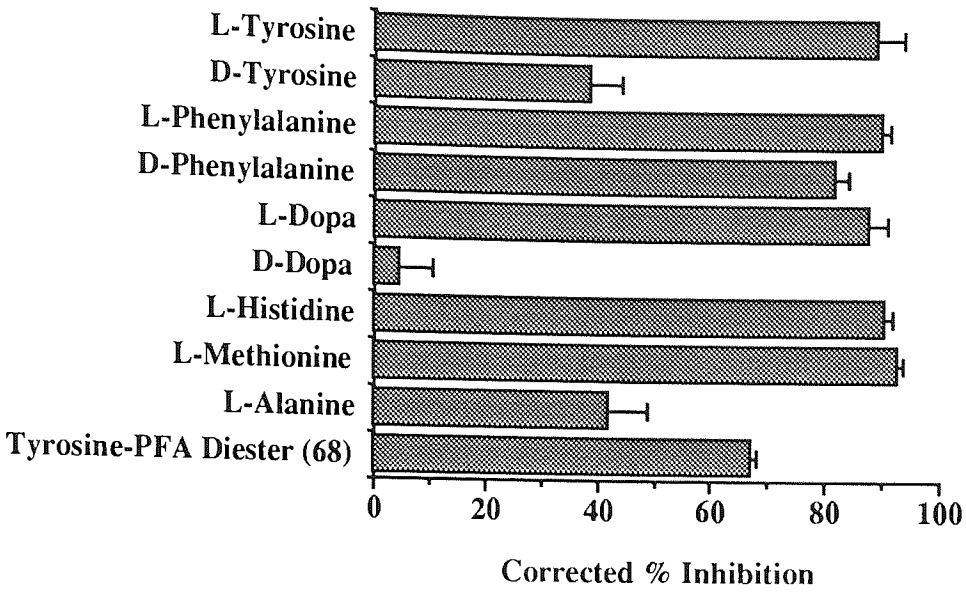

Figure 3.29 - The Effect of 2mM of Various Potential Inhibitors on ^{3}H-L-Tyrosine Transport

Figure 3.29 shows that L-tyrosine inhibits its own transport. Stereospecificity can be seen with dopa and tyrosine, in agreement with previous work *in vivo*[142] and *in vitro*.[103] Stereospecifity could not be demonstrated with phenylalanine in contrast with previous studies.[103] However, the relative order of stereospecificity observed for dopa, tyrosine and phenylalanine is consistant with the work of Oldendorf, who showed transport of dopa to be highly L-enantiomer-specific while that of tyrosine and phenylalanine was progressively less stereospecific.[142] The large basic amino acid L-histidine and the sulphur containing L-methionine showed inhibition of ^{3}H-L-tyrosine transport. This, and the partial inhibition by the small amino acid L-alanine is in agreement with previous work.[94,101]

3.5 Conclusions

An *in vitro* cell culture model of the blood-brain barrier (BBB), consisting of brain microvessel endothelial cell (BMEC) monolayers, was established. Although this model was successfully used to study BBB transport, two main problems were encountered with this system:

1) Variation in BMEC monolayer permeability resulted in difficulties in the comparison of data. The degree of paracellular diffusion, as indicated by mannitol flux, was not consistent between experiments; therefore, making direct comparison of data from separate experiments inappropiate. Furthermore, on occasions, monolayers were shown to be unusually permeable (mannitol flux > 5% / hour). This resulted in data being discarded and experiments being repeated.

2) The ability to detect concentrations of less than 50μM was required for the elucidation of concentration-dependent transport processes. The lack of chromophores in some of the molecules under study required the use of radio-labelled solutes for the accurate quantification of transport across BMEC monolayers. As appropriate radio-labelled precursors (for example ^{14}C-phosgene) are not commercially available, the radio-synthesis of PFA diesters was considered impractical. This prevented the direct study of the transport of PFA diesters. The interaction of PFA diesters with transport systems was studied by competition with the facilitated transport of ^{14}C-pyruvate and ^{3}H-L-tyrosine.

The facilitated transport of monocarboxylic acids and amino acids was studied using ^{14}C-pyruvate and ^{3}H-L-tyrosine as model substrates. The simple PFA diesters (**43-49**) were synthesised as possible substrates for the monocarboxylic acid transporter. However, no interaction between sodium methyl methoxycarbonylphosphonate (**43**) and the transport of ^{14}C-pyruvate could be demonstrated. This indicated that (**43**) was not a substrate for the monocarboxylic acid transporter. Therefore, it was considered unlikely that similar PFA diesters (**44-49**) would be substrates and they were not utilised in the cell culture system.

The diesters (**43-49**) showed no activity in anti-HIV testing suggesting that hydrolysis of these esters to active PFA did not occur in the anti-HIV cell culture test. This is in agreement with the observed chemical stability of the diester (**43**), which was shown to be stable at pH 7.4, at 37°C, for 24 hours. Also, it is considered unlikely that the phosphonate ester of diesters (**43-49**) would be substrates for any hydrolytic enzyme found *in vivo*. To produce a diester that would hydrolyse to PFA *in vivo* would require the use of either acyloxymethyl or acyloxybenzyl esters, similar to those described in

section 1.3. An acyloxybenzyl diester with the potential ability to regenerate PFA *in vivo* is proposed (**97**).

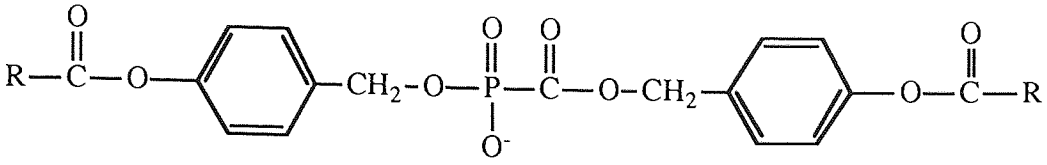

(**97**)

Acyloxybenzyl esters provide good substrates for esterases and are cleaved to give unstable p-hydroxybenzyl esters. The nature of the R groups in (**97**) may be varied to control the half-lives of the esters. For example, tertiary-butyl groups would decrease the affinity of the ester for the esterase and increase the half-life compared to an ethyl group.

The inhibition of ^{3}H-L-tyrosine transport by the tyrosine-linked PFA diester (**68**) indicates that it could be a substrate for the large amino acid transporter at the BBB. However, three further important considerations exist before (**68**) could be considered a brain-directed prodrug:

1) The possibility exists that (**68**) may be an inhibitor of the amino acid carrier but not a substrate for transport. This cannot be investigated, using the BBB model, without the radiolabelling of (**68**).or the development of a sensitive HPLC assay.

2) A high affinity for the amino acid carrier would be required if (**68**) were to achieve therapeutic concentrations in the brain. For example, melphalan (**66**) has insufficient affinity for the carrier to achieve significant brain uptake.[76] Modifying melphalan to give D,L-NAM (**67**) has enhanced affinity and achieved a greater brain uptake.[76,144] A similar modification using a 2-amino-1,2,3,4-tetrahydro-2-naphthoic acid moiety in place of a conventional α-amino acid structure, as shown in (**98**), may increase the affinity of (**68**) for the BBB carrier.

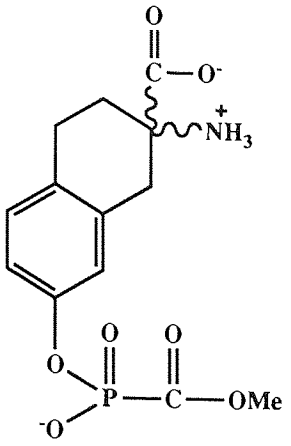

(98)

3) As (**68**) is inactive against HIV, hydrolysis to PFA within the brain is required. Therefore, the rate of hydrolysis of (**68**) in plasma would have to be sufficiently slow to allow the prodrug to gain access to the brain but not so slow that it would remain inactive within the brain. The stability of (**68**) in transport experiment conditions has been confirmed post-transport. The stability *in vivo* and in particular in plasma has to be established. The structure (**98**) may be modified to incorporate acyloxybenzyl esters to facilitate the enzymatic regeneration of phosphonoformate. The structure (**99**) is proposed.

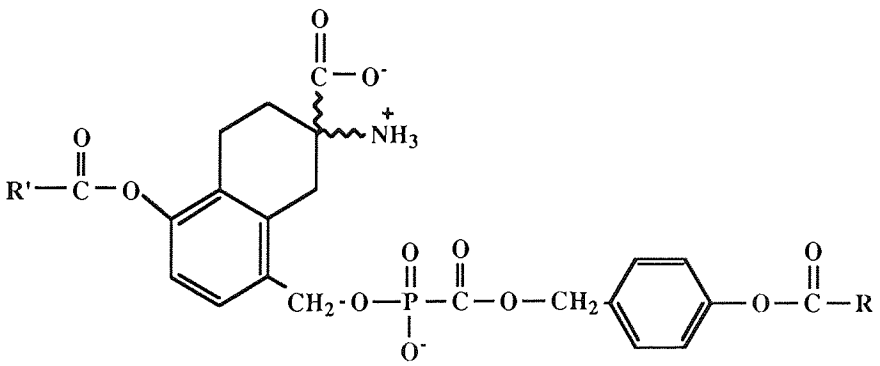

(99)

CHAPTER 4 - CHEMISTRY EXPERIMENTAL

4.1 Synthetic Chemistry

Low-field ^{1}H NMR spectra were recorded on a Varian EM-360 60 MHz spectrometer. High-field NMR spectra, ^{1}H (300 MHz or 250 MHz), ^{31}P (121.5 MHz or 101 MHz) and ^{13}C (75.5 MHz or 63 MHz), were recorded on Bruker AC spectrometers. ^{1}H and ^{13}C NMR spectra were referenced to tetramethylsilane and ^{31}P NMR spectra were referenced to 85% H_3PO_4; positive chemical shifts are downfield from the reference. All ^{13}C NMR are ^{1}H decoupled. ^{31}P NMR are ^{1}H decoupled or ^{1}H coupled as stated. Accurate mass data were recorded by the SERC mass spectrometry service at Swansea University on a VG 7070E instrument under EI, CI and positive ion FAB (nitrobenzyl alcohol matrix) techniques. Infrared spectra were recorded on a Perkin-Elmer 1310 infrared spectrometer. Melting points were measured on an Gallenkamp electrothermal melting point apparatus and are not corrected. TLC was performed using Kieselgel 60 silica gel plates containing a fluorescent indicator. Spots were visualised under 254 nm UV light or with the aid of iodine. Flash chromatography[114] was performed using Sorbsil C60 silica gel. Elemental analyses were recorded by Butterworth Laboratories Ltd. of Teddington, Middlesex. Tetrahydrofuran was dried by refluxing with sodium, using benzophenone as an indicator, followed by distillation. Dichloromethane, acetonitrile and methanol were dried by refluxing with calcium hydride followed by distillation. Chemicals were obtained from Aldrich or Sigma Chemical Company.

4.1.1 Synthesis of Triesters of PFA

Dimethyl Methoxycarbonylphosphonate (34) was prepared analogously to the method of Noren *et al.*[60] for the preparation of diethyl 4-methoxyphenoxy-carbonylphosphonate. The procedure was performed in a fume cupboard. Trimethyl phosphite (50 g, 0.40 mol) was heated at 120°C in a two-necked 250 ml round-bottomed flask fitted with a reflux condenser. Methyl chloroformate (41.58 g, 0.44 mol) was added dropwise over 30 minutes and fumes of methyl chloride were released. The mixture was then heated at 120°C for a further 1.5 hours. Vacuum distillation (0.5 mm Hg) afforded the title compound as a colourless liquid: 86% (58 g, 0.34 mol); bp 70-74°C (0.5 mm Hg), [lit. bp 86-92°C (1 mm Hg)][60]; ^{1}H NMR (300 MHz, $CDCl_3$) δ 3.91 (6H, d, J_{PH}=11 Hz, 2x$POCH_3$), 3.82 (3H, d, J_{PH}=1 Hz, $COCH_3$); ^{31}P NMR (121.5 MHz, ^{1}H decoupled, $CDCl_3$) δ -2.75 (s); ^{31}P NMR (121.5 MHz, ^{1}H coupled, $CDCl_3$) δ -2.75 (sept q, J_{PH}=11 Hz, J_{PH}=1 Hz); ^{13}C NMR (75.5 MHz, $CDCl_3$) δ 54.52 (d, J_{PC}=6 Hz, 2x$PO\underline{C}H_3$), 52.49 (d, J_{PC}=4 Hz, $CO\underline{C}H_3$),C=O not observed; IR (liquid film) 1720 cm^{-1} (C=O), 1280 (P=O), 1040 (P-O).

Dimethyl Ethoxycarbonylphosphonate (35). Trimethyl phosphite (50 g, 0.40 mol) and ethyl chloroformate (43 g, 0.40 mol) were reacted in a similar way to that described for the preparation of dimethyl methoxycarbonylphosphonate to give the title compound as a colourless liquid: 85% (57 g, 0.31 mol); bp 86-90°C (1 mm Hg); ^{1}H NMR (300 MHz, $CDCl_3$) δ 4.34 (2H, q d, J_{HH}=7 Hz, J_{PH}=1 Hz, OCH_2), 3.91 (6H, d, J_{PH}=11 Hz, 2xOCH_3), 1.35 (3H, t d, J_{HH}=7 Hz, J_{PH}=1 Hz, CH_3); ^{31}P NMR (121.5 MHz, ^{1}H decoupled, $CDCl_3$) δ -2.62 (s); ^{31}P NMR (121.5 MHz,^{1}H coupled, $CDCl_3$) δ -2.62 (sept q t , J_{PH}=11 Hz, J_{PH}=1 Hz, J_{PH}=1 Hz, observed as sept sext); ^{13}C NMR (75.5 MHz, $CDCl_3$) δ 62.13 (d, J_{PC}=4 Hz, OCH_2), 54.41 (d, J_{PC}=6 Hz, 2xOCH_3), 13.98 (s, CH_3), C=O not observed; IR (liquid film) 1720 cm^{-1} (C=O), 1280 (C=O), 1040 (P-O).

Dimethyl Propyloxycarbonylphosphonate (36). Trimethyl phosphite (25 g, 0.20 mol) and propyl chloroformate (24.5 g, 0.20 mol) were reacted in a similar way to that as described for the preparation of dimethyl methoxycarbonylphosphonate to give the title compound as a colourless liquid: 88% (34.5 g, 0.17 mol); bp 91-95°C (1 mm Hg); ^{1}H NMR (300 MHz, $CDCl_3$) δ 4.23 (2H, t d, J_{HH}=7 Hz, J_{PH}=1 Hz, OCH_2), 3.91 (6H, d, J_{PH}=11 Hz, 2xOCH_3), 1.78 (2H, q t d, J_{HH}=7 Hz, J_{HH}=7 Hz, J_{PH}=1 Hz, observed as sext d, CH_2), 0.76 (3H, t, J_{HH}=7 Hz, CH_3); ^{31}P NMR (121.5 MHz, ^{1}H decoupled, $CDCl_3$) δ -2.56 (s); ^{31}P NMR (121.5 MHz, ^{1}H coupled, $CDCl_3$) δ -2.56 (sept t, J_{PH}=11 Hz, J_{PH}=1 Hz); ^{13}C NMR (75.5 MHz, $CDCl_3$) δ 67.57 (d, J_{PC}=4 Hz, OCH_2), 54.46 (d, J_{PC}=6 Hz, 2xOCH_3), 21.79 (s, CH_2), 10.27 (s, CH_3), C=O not observed; IR (liquid film) 1720 cm^{-1} (C=O), 1280 (P=O), 1040 (P-O).

Dimethyl Butyloxycarbonylphosphonate (37). Trimethyl phosphite (50 g, 0.40 mol) and butyl chloroformate (54.6 g, 0.40 mol) were reacted in a similar way to that as described for the preparation of dimethyl methoxycarbonylphosphonate to give the title compound as a colourless liquid: 88% (74 g, 0.35 mol); bp 94-98°C (1 mm Hg), [lit. bp 97-100°C (1 mm Hg)][60]; ^{1}H NMR (300MHz, $CDCl_3$) δ 4.28 (2H, t, J_{HH}=7 Hz, OCH_2), 3.92 (6H, d, J_{PH}=11 Hz, 2xOCH_3), 1.73 (2H, t t, J_{HH}=7 Hz, J_{HH}=7 Hz, observed as pent, CH_2), 1.45 (2H, q t, J_{HH}=7 Hz, J_{HH}=7 Hz, observed as sext, CH_2), 0.95 (3H, t, J_{HH}=7 Hz, CH_3); ^{31}P NMR (121.5 MHz, ^{1}H decoupled, $CDCl_3$) δ -2.57 (s); ^{31}P NMR (121.5 MHz, ^{1}H coupled, $CDCl_3$) δ -2.57 (sept t, J_{PH}=11 Hz, J_{PH}=1 Hz); ^{13}C NMR (75.5 MHz, $CDCl_3$) δ 65.90 (d, J_{PC}=4 Hz, OCH_2), 54.38 (d, J_{PC}=6 Hz, 2xOCH_3), 30.30 (s, CH_2), 18.94 (s, CH_2), 13.50 (s, CH_3), C=O not observed; IR (liquid film) 1720 cm^{-1} (C=O), 1280 (P=O), 1040 (P-O).

Dimethyl (2-Methylpropyl)oxycarbonylphosphonate (38). Trimethyl phosphite (25 g, 0.20 mol) and 2-methylpropyl chloroformate (27.3 g, 0.20 mol) were reacted in a similar way to that as described for the preparation of dimethyl

methoxycarbonylphosphonate to give the title compound as a colourless liquid: 63% (26.6 g, 0.13 mol); bp 95-100°C (1 mm Hg); ^{1}H NMR (300 MHz, $CDCl_3$) δ 4.05 (2H, d d, J_{HH}=7 Hz, J_{PH}=1 Hz, OCH_2), 3.91 (6H, d, J_{PH}=11 Hz, 2xOCH_3), 2.07 (1H, sept t, J_{HH}=7 Hz, J_{HH}=7 Hz, observed as a nine line pattern, CH), 0.95 (6H, d, J_{HH}=7 Hz, 2xCH_3); ^{31}P NMR (121.5 MHz, ^{1}H decoupled, $CDCl_3$) δ -2.54 (s); ^{31}P NMR (121.5 MHz, ^{1}H coupled, $CDCl_3$) δ -2.54 (sept t, J_{PH}=11 Hz, J_{PH}=1 Hz); ^{13}C NMR (75.5 MHz, $CDCl_3$) δ 71.83 (d, J_{PC}=4 Hz, OCH_2), 54.45 (d, J_{PC}=6 Hz, 2xOCH_3), 27.56 (s, CH), 18.88 (s, 2xCH_3), C=O not observed; IR (liquid film) 1720 cm^{-1} (C=O), 1280 (P=O), 1040 (P-O).

Dimethyl Octyloxycarbonylphosphonate (39). Trimethyl phosphite (15 g, 0.12 mol) and octyl chloroformate (23 g, 0.12 mol) were reacted in a similar way to that as described for the preparation of dimethyl methoxycarbonylphosphonate to give the title compound as a colourless liquid: 72% (23.8 g, 0.09 mol); bp 130-135°C (1 mm Hg); ^{1}H NMR (300 MHz, $CDCl_3$) δ 4.25 (2H, t d, J_{HH}=7 Hz,J_{PH}=1 Hz, OCH_2), 3.90 (6H, d, J_{PH}=11 Hz, 2xOCH_3), 1.72 (2H, t t, J_{HH}=7 Hz, J_{HH}=7 Hz, observed as a pent, $OCH_2\underline{CH_2}$), 1.4-1.2 (10H, m, 5xCH_2), 0.86 (3H, t, J_{HH}=7 Hz, CH_3); ^{31}P NMR (121.5 MHz, ^{1}H decoupled, $CDCl_3$) δ -2.56 (s); ^{31}P NMR (121.5 MHz, ^{1}H coupled, $CDCl_3$) δ -2.56 (sept t, J_{PH}=11 Hz, J_{PH}=1 Hz), ^{13}C NMR (75.5 MHz, $CDCl_3$) δ 66.20 (d, J_{PC}=4 Hz, OCH_2), 54.40 (d, J_{PC}=6 Hz, 2xOCH_3), 31.63 (s, CH_2), 29.00 (s, CH_2), 28.97 (s, CH_2), 28.29 (s, CH_2), 25.66 (s, CH_2), 2.52 (s, CH_2), 13.97 (s, CH_3), C=O not observed; IR (liquid film) 1720 cm^{-1} (C=O), 1280 (P=O), 1040 (P-O).

Dimethyl Benzyloxycarbonylphosphonate (40). Trimethyl phosphite (15 g, 0.12 mol) and benzyl chloroformate (20.4 g, 0.12 mol) were reacted in a similar way to that as described for the preparation of dimethyl methoxycarbonylphosphonate to give the title compound as a colourless liquid: 84% (25 g, 0.10 mol); bp 136-138°C (1 mm Hg), [lit. bp 135-136°C (1 mm Hg)][60]; ^{1}H NMR (300 MHz, $CDCl_3$) δ 7.3-7.1 (5H, m, aromatic), 5.08 (2H, d, J_{PH}=1 Hz, OCH_2), 3.68 (6H, d, J_{PH}=11 Hz, 2xOCH_3); ^{31}P NMR (121.5 MHz, ^{1}H decoupled, $CDCl_3$) δ -2.90 (s); ^{31}P NMR (121.5 MHz, ^{1}H coupled, $CDCl_3$) δ -2.90 (sept t, J_{PH}=11 Hz, J_{PH}=1 Hz); ^{13}C NMR (75.5 MHz, $CDCl_3$) δ 167.25 (d, J_{PC}=270 Hz, C=O), 133.84 (s, aromatic C), 127.85 (s, aromatic CH), 127.83 (s, aromatic CH), 127.58 (s, aromatic CH), 66.83 (d, J_{PC}=9 Hz, OCH_2), 53.83 (d, J_{PC}=6 Hz, 2xOCH_3); IR (liquid film) 1720 cm^{-1} (C=O), 1500 (C=C), 1280 (P=O), 1040 (P-O).

Dimethyl Phenoxycarbonylphosphonate (41). Trimethyl phosphite (25 g, 0.20 mol) and phenyl chloroformate (31.3 g, 0.20 mol) were reacted in a similar way to that as described for the preparation of dimethyl methoxycarbonylphosphonate to give the title compound as a colourless liquid: 42% (19.4 g, 0.08 mol); bp 155-160°C (1 mm

Hg), [lit. bp 125-127°C (0.5 mm Hg)][60]; ^{1}H NMR (300 MHz, $CDCl_3$) δ 7.3-6.9 (5H, m, aromatic), 3.90 (6H, d, J_{PH}=11 Hz, 2xOCH_3); ^{31}P NMR (121.5 MHz, ^{1}H decoupled, $CDCl_3$) δ -3.18; ^{31}P NMR (121.5 MHz, ^{1}H coupled, $CDCl_3$) δ -3.18 (sept, J_{PH}=11 Hz); ^{13}C NMR (75.5 MHz, $CDCl_3$) δ 166.23 (d, J_{PC}=275 Hz, C=O), 149.33 (s, aromatic C), 129.31 (s, aromatic CH), 125.93 (s, aromatic CH), 120.52 (s, aromatic CH), 54.52 (d, J_{PC}=6 Hz, 2xOCH_3); IR (liquid film) 1720 cm^{-1} (C=O), 1590 and 1500 (C=C), 1280 (P=O), 1040 (P-O).

Dimethyl (4-Nitrophenoxy)carbonylphosphonate (42) was prepared analogously to the method of Noren *et al.*[60] 4-Nitrophenyl chloroformate (4.0 g, 0.02 mol) was dissolved in trimethyl phosphite (5 g, 0.04 mol) and warmed gently, in a fume cupboard, until crystals formed. Excess trimethyl phosphite was evaporated. The title compound was recrystallised from toluene: 90% (5.0 g, 0.018 mol); mp 82-85°C with decomposition, [lit. mp 89-91°C][60]; ^{1}H NMR (60 MHz, $CDCl_3$) δ 8.3 (2H, d, J_{HH}=8 Hz, aromatic), 7.3 (2H, d, J_{HH}=8 Hz, aromatic), 3.9 (6H, d, J_{HH}=11 Hz, 2xOCH_3); IR (Nujol mull) 1720 cm^{-1} (C=O), 1580 (C=C), 1280 (P=O), 1040 (P-O). (Further characterisation was difficult due to ready decomposition).

4.1.2 Synthesis of Diesters of PFA

Sodium Methyl Methoxycarbonylphosphonate (43) was prepared analogously to the method of Noren *et al.*[60] for the preparation of sodium methyl benzyloxycarbonyl phosphonate. Dimethyl methoxycarbonylphosphonate (0.31 g, 1.8 mmol) was dissolved in dry tetrahydrofuran (10 ml). Sodium iodide (0.27 g, 1.8 mmol) in dry tetrahydrofuran (50 ml) was added dropwise and the reaction stirred at room temperature for 24 hours. The precipitate was filtered and then washed with dry tetrahydrofuran to give the title compound as a white powder: 60% (0.19 g, 1.0 mmol); mp 180-182°C; ^{1}H NMR (300 MHz, D_2O) δ 3.58 (3H, s, $COCH_3$), 3.47 (3H, d, J_{PH}=11 Hz, $POCH_3$); ^{31}P NMR (121.5 MHz, ^{1}H decoupled, D_2O) δ -1.11 (s); ^{31}P NMR (121.5 MHz, ^{1}H coupled, D_2O) δ -1.11 (q, J_{PH}=11 Hz); ^{13}C NMR (75.5 MHz, D_2O) δ 55.87 (d, J_{PC}=6 Hz, $POCH_3$), 54.57 (d, J_{PC}=4 Hz, $CO\underline{C}H_3$), C=O not observed; IR (Nujol mull) 1720 cm^{-1} (C=O), 1280 (P=O), 1040 (P-O); (Found: C, 20.44; H, 3.40%; $C_3H_6O_5PNa$ requires C, 20.47; H, 3.44%).

Sodium Methyl Ethoxycarbonylphosphonate (44). Dimethyl ethoxycarbonyl phosphonate (0.33 g, 1.8 mmol) and sodium iodide (0.27 g, 1.8 mmol) were reacted in a similar way to that as described for the preparation of sodium methyl methoxycarbonylphosphonate to give the title compound as a white powder: 65% (0.22 g, 1.1 mmol); mp 129-130°C; ^{1}H NMR (300 MHz, D_2O) δ 4.11 (2H, q, J_{HH}=7 Hz, OCH_2), 3.48 (3H, d, J_{PH}=11 Hz, OCH_3), 1.12 (3H, t, J_{HH}=7 Hz, CH_3); ^{31}P NMR

(121.5 MHz, ^1H decoupled, D_2O) δ -0.99 (s); ^{31}P NMR (121.5 MHz, ^1H coupled, D_2O) δ -0.99 (q, J_{PH}=11 Hz); ^{13}C NMR (75.5 MHz, D_2O) δ 64.59 (d, J_{PC}=4 Hz, OCH_2), 55.85 (d, J_{PC}=6 Hz, OCH_3), 16.07 (s, CH_3), C=O not observed; IR (Nujol mull) 1720 and 1690 cm^{-1} (C=O), 1280 (P=O), 1040 (P-O); (Found: C, 25.01; H, 4.09%; $C_4H_8O_5PNa$ requires C, 25.28; H, 4.24%).

Sodium Methyl Propyloxycarbonylphosphonate (45). Dimethyl propyloxycarbonylphosphonate (0.35 g, 1.8 mmol) and sodium iodide (0.27 g, 1.8 mmol) were reacted in a similar way to that as described for the preparation of sodium methyl methoxycarbonylphosphonate to give the title compound as a white powder: 62% (0.23 g, 1.1 mmol); mp 120-121°C; ^1H NMR (300 MHz, D_2O) δ 4.02 (2H, t d, J_{HH}=7 Hz, J_{PH}=1 Hz, OCH_2), 3.49 (3H, d, J_{PH}=11 Hz, OCH_3), 1.56 (2H, q t, J_{HH}=7 Hz, J_{HH}=7 Hz, observed as sext, CH_2), 0.76 (3H, t, J_{HH}=7 Hz, CH_3); ^{31}P NMR (121.5 MHz, ^1H decoupled, D_2O) δ -0.96 (s); ^{31}P NMR (121.5 MHz, ^1H coupled, D_2O) δ -0.96 (q, J_{PH}=11 Hz); ^{13}C NMR (75.5 MHz, D_2O) δ 69.90 (d, J_{PC}=4 Hz, OCH_2), 55.86 (d, J_{PC}=6 Hz, OCH_3), 24.09 (s, CH_2), 12.33 (s, CH_3), C=O not observed, IR (Nujol mull) 1690 and 1720 cm^{-1} (C=O), 1280 (P=O), 1040 (P-O); (Found; C, 29.50; H, 4.94%; $C_5H_{10}O_5PNa$ requires C, 29.42; H, 4.94%).

Sodium Methyl Butyloxycarbonylphosphonate (46). Dimethyl butyloxycarbonyl phosphonate (0.39 g, 1.8 mmol) and sodium iodide (0.27 g, 1.8 mmol) were reacted in a similar way to that as described for the preparation of sodium methyl methoxycarbonyl phosphonate to give the title compound as a waxy white solid: 68% (0.27 g, 1.2 mmol); mp 97-98°C; ^1H NMR (300 MHz, D_2O) δ 4.06 (2H, t d, J_{HH}=7 Hz, J_{PH}=1 Hz, OCH_2), 3.47 (3H, d, J_{PH}=11 Hz, OCH_3), 1.51 (2H, t t, J_{HH}=7 Hz, J_{HH}=7 Hz, observed as a pent, $OCH_2\underline{CH_2}$), 1.23 (2H, t q, J_{HH}=7 Hz, J_{HH}=7 Hz, CH_2), 0.72 (3H, t, J_{HH}=7 Hz, CH_3); ^{31}P NMR (121.5 MHz, ^1H decoupled, D_2O) δ -0.98 (s); ^{31}P NMR (121.5 MHz, ^1H coupled, D_2O) δ -0.98 (q, J_{PH}=11 Hz); ^{13}C NMR (75.5 MHz, D_2O) δ 68.14 (d, J_{PC}=4 Hz, OCH_2), 55.86 (d, J_{PC}=6 Hz, OCH_3), 32.57 (s, $OCH_2\underline{CH_2}$), 21.21 (s, CH_2), 15.56 (s, CH_3), C=O not observed; IR (Nujol mull) 1690 and 1720 cm^{-1} (C=O), 1280 (P=O), 1040 (P-O); (Found: C, 32.92; H, 5.73%; $C_6H_{12}O_5PNa$ requires C, 33.04; H, 5.55%).

Sodium Methyl (2-Methylpropyl)oxycarbonylphosphonate (47). Dimethyl (2-methylpropyloxy)carbonylphosphonate (0.40 g, 1.8 mmol) and sodium iodide (0.27 g, 1.8 mmol) were reacted in a similar way to that described for the preparation of sodium methyl methoxycarbonylphosphonate to give the title compound as a white powder: 72% (0.28 g, 1.3 mmol); mp 156-158°C; ^1H NMR (300 MHz, D_2O) δ 3.84 (2H, d, J_{HH}=7 Hz, OCH_2), 3.49 (3H, d, J_{PH}=11 Hz, OCH_3), 1.85 (1H, sept t, J_{HH}=7 Hz, J_{HH}=7 Hz, observed as a nine line pattern, CH), 0.74 (6H, d, J_{HH}=7 Hz, 2xCH_3);

^{31}P NMR (121.5 MHz, ^{1}H decoupled, D_2O) δ -0.96 (s); ^{31}P NMR (121.5 MHz, ^{1}H coupled, D_2O) δ -0.96 (q, J_{PH}=11 Hz); ^{13}C NMR (75.5 MHz, D_2O) δ 74.04 (d, J_{PC}=4 Hz, OCH_2), 55.89 (d, J_{PC}=6 Hz, OCH_3), 29.91 (s, CH), 20.88 (s, 2xCH_3), C=O not observed; IR (Nujol mull) 1690 and 1720 cm^{-1} (C=O), 1280 (P=O), 1040 (P-O); (Found: C, 33.12; H, 5.42%; $C_6H_{12}O_5PNa$ requires C, 33.04; H, 5.55%).

Sodium Methyl Octyloxycarbonylphosphonate (48). Dimethyl octyloxycarbonyl phosphonate (0.48 g, 1.8 mmol) and sodium iodide (0.27 g, 1.8 mmol) were reacted in a similar way to that described for the preparation of sodium methyl methoxycarbonylphosphonate to give the title compound as a waxy white solid: 69% (0.34 g, 1.2 mmol); mp 90-92°C; ^{1}H NMR (300 MHz, D_2O) δ 4.06 (2H, t, J_{HH}=7 Hz, OCH_2), 3.48 (3H, d, J_{PH}=11 Hz, OCH_3), 1.51 (2H, t t, J_{HH}=7 Hz, J_{HH}=7 Hz, observed as a pent, $OCH_2\underline{CH_2}$), 1.3-0.9 (10H, m, 5xCH_2), 0.67 (3H, t, J_{HH}=7 Hz, CH_3); ^{31}P NMR (121.5 MHz, ^{1}H decoupled, D_2O) δ -0.97 (s); ^{31}P NMR (121.5 MHz, ^{1}H coupled, D_2O) δ -0.97 (q, J_{PH}=11 Hz); ^{13}C NMR (75.5 MHz, D_2O) δ 68.44 (d, J_{PC}=4 Hz, OCH_2), 55.94 (d, J_{PC}=6 Hz, OCH_3), 33.74 (s, CH_2), 30.99 (s, CH_2),30.92 (s, CH_2), 30.46 (s, CH_2), 27.74 (s, CH_2), 24.68 (s, CH_2), 16.07 (s, CH_3), C=O not observed; IR (Nujol mull) 1720 cm^{-1} (C=O), 1280 (P=O), 1040 (P-O); (Found: C, 43.45; H, 7.51%; $C_{10}H_{20}O_5PNa$ requires C, 43.80; H, 7.35%).

Sodium Methyl Benzyloxycarbonylphosphonate (49). Dimethyl benzyloxy-carbonylphosphonate (0.44 g, 1.8 mmol) and sodium iodide (0.27 g, 1.8 mmol) were reacted by the method of Noren *et al.*[60], to give the title compound as a white powder: 55% (0.25 g, 1.0 mmol); mp 122-124°C, [lit mp 120- 122°C][60]; ^{1}H NMR (300 MHz, D_2O) δ 7.3-7.1 (5H, m, aromatic), 5.09 (2H, s, OCH_2), 3.44 (3H, d, J_{PH}=11 Hz, OCH_3); ^{31}P NMR (121.5 MHz, ^{1}H decoupled, D_2O) δ -1.37 (s); ^{31}P NMR (121.5 MHz, ^{1}H coupled, D_2O) δ -1.37 (q, J_{PH}=11 Hz); ^{13}C NMR (75.5 MHz, D_2O) δ 139.15 (s, aromatic C), 131.50 (s, aromatic CH), 131.28 (s, aromatic CH), 130.86 (s, aromatic CH), 69.44 (d, J_{PC}=4 Hz, OCH_2), 55.95 (d, J_{PC}=6 Hz, OCH_3), C=O not observed; IR (Nujol mull) 1720 cm^{-1} (C=O), 1500 (C=C), 1280 (P=O), 1040 (P-O); (Found: C, 42.23,; H, 4.03%; $C_9H_{10}O_5PNa$ requires C, 42.86; H, 3.97%).

Sodium Methyl Phenoxycarbonylphosphonate (50). Dimethyl phenoxycarbonyl phosphonate (0.42 g, 1.8 mmol) and sodium iodide (0.27 g, 1.8 mmol) were reacted in a similar way to that described for the preparation of sodium methyl methoxycarbonylphosphonate to give the title compound as a white powder: 68% (0.29 g, 1.2 mmol); mp 69-70°C with decomposition, [lit mp 79-81°C with decomposition][60]; ^{1}H NMR (300 MHz, DMSO-d_6) δ 7.5-7.0 (5H, m, aromatic), 3.57 (3H, d, J_{PH}=11 Hz, OCH_3); ^{31}P NMR (121.5 MHz, ^{1}H decoupled, DMSO-d_6) δ -1.89 (s); ^{31}P NMR (121.5 MHz, ^{1}H coupled, DMSO-d_6) δ -1.89 (q, J_{PH}=11 Hz); ^{13}C NMR

(75.5 MHz, DMSO-d_6) δ 174.46 (d, J_{PC}=225 Hz,C=O), 150.74 (d, J_{PC}=6 Hz, aromatic C), 128.98 (s, aromatic CH), 125.52 (s, aromatic CH), 121.80 (s, aromatic CH), 52.41 (d, J_{PC}=6 Hz, OCH_3); IR (Nujol mull) 1720 cm^{-1} (C=O), 1600 and 1500 (C=C), 1280 (P=O), 1040 (P-O).

Sodium Methyl (4-Nitrophenoxy)carbonylphosphonate (51). Dimethyl (4-Nitrophenoxy)carbonylphosphonate (0.28 g,1.0 mmol) and sodium iodide (0.15 g, 1.0 mmol) were reacted in a similar way to that as described for the preparation of sodium methyl methoxycarbonylphosphonate to give the title compound as a yellow powder: 60% (0.17 g, 0.6 mmol); mp 55-58°C with decomposition; ^1H NMR (300 MHz, DMSO-d_6) δ 8.28 (2H, d, J_{HH}=9 Hz, aromatic), 7.40 (2H, d, J_{HH}=9 Hz, aromatic), 3.59 (3H, d, J_{PH}=11 Hz, OCH_3); ^{31}P NMR (121.5 MHz, ^1H decoupled, DMSO-d_6) δ -2.52; ^{31}P NMR (121.5 MHz, ^1H coupled, DMSO-d_6) δ -2.52 (q, J_{PH}=11 Hz); ^{13}C NMR (75.5 MHz, DMSO-d_6) δ 173.58 (d, J_{PC}=225 Hz, C=O), 155.89 (d, J_{PC}=6 Hz, aromatic C), 144.81 (s, aromatic C), 125.22 (s, aromatic CH), 123.38 (s, aromatic CH), 52.58 (d, J_{PC}=6 Hz, OCH_3); IR (Nujol mull) 1720 cm^{-1} (C=O), 1600 and 1500 (C=C), 1280 (P=O), 1040 (P-O).

4.1.3 Synthesis of Carboxyl Monoesters of PFA

Disodium Methoxycarbonylphosphonate (52) was prepared analogously to the method of Noren *et al.* for the preparation of disodium ethoxycarbonylphosphonate.[60] A mixture of dimethyl methoxycarbonylphosphonate (5 g, 0.03 mol) and bromotrimethylsilane (11.5 g, 0.075 mol) was stirred under argon, at room temperature, for 3 hours. The reaction was performed in a fume cupboard especially as methyl bromide is liberated. Volatile components were removed *in vacuo* (1 mm Hg) to give bis(trimethylsilyl) methoxycarbonyphosphonate **(66)** which was then stirred with 25 g of Amberlite IRC 50 resin (sodium form) in water (40 ml) for one hour. The resin was then removed by filtration and washed with water (40 ml). The filtrate and washings were combined and the water removed *in vacuo* (1 mm Hg). The residue was washed with tetrahydrofuran to give the title compound as a white powder: 90% (5.0 g, 0.027 mol); mp >300°C; ^1H NMR (300 MHz, D_2O) δ 3.46 (3H, s, OCH_3); ^{31}P NMR (121.5 MHz, ^1H decoupled, D_2O) δ -1.37 (s); ^{31}P NMR (121.5 MHz, ^1H coupled, D_2O) δ -1.37 (s); ^{13}C NMR (75.5 MHz, D_2O) δ 183.22 (d, J_{PC}=218 Hz, C=O), 53.36 (d, J_{PC}=2.5 Hz, OCH_3); IR (Nujol mull) 1690 cm^{-1} (C=O).

Disodium Ethoxycarbonylphosphonate (53). Dimethyl ethoxycarbonyl phosphonate (1.21 g, 6.64 mmol) and bromotrimethylsilane (2.50 g, 16.34 mmol) were reacted by the method of Noren *et al.*,[60] as described above, to give the title compound as a white powder: 88% (1.16 g,5.85 mmol); mp >300°C, [lit mp >300°C][60]; ^1H NMR

(300 MHz, D_2O) δ 3.97 (2H, q d, J_{HH}=7 Hz, J_{PH}=1 Hz, OCH_2), 1.08 (3H, t d, J_{HH}=7 Hz, J_{PH}=1 Hz, CH_3); ^{31}P NMR (121.5 MHz, ^1H decoupled, D_2O) δ -1.33 (s); ^{31}P NMR (121.5 MHz, ^1H coupled, D_2O) δ -1.33 (s); ^{13}C NMR (75.5 MHz, D_2O) δ 180.01 (d, J_{PC}=218 Hz, C=O), 62.84 (d, J_{PC}=2.5 Hz, OCH_2), 16.28 (s, CH_3); IR (Nujol mull) 1690 cm^{-1} (C=O).

Disodium Propyloxycarbonylphosphonate (54). Dimethyl propyloxycarbonyl phosphonate (1.30 g, 6.63 mmol) and bromotrimethylsilane (2.50 g, 16.34 mmol) were reacted in a similar way to that described for the preparation of disodium methoxycarbonylphosphonate to give the title compound as a white powder: 89% (1.25 g, 5.90 mmol); mp >300°C; ^1H NMR (300 MHz, D_2O) δ 3.86 (2H, t, J_{HH}=7 Hz, OCH_2), 1.56 (2H, q t, J_{HH}=7 Hz, J_{HH}=7 Hz, observed as a sext, CH_2), 0.78 (3H, t, J_{HH}=7 Hz, CH_3); ^{31}P NMR (121.5 MHz, ^1H decoupled, D_2O) δ -1.30 (s); ^{31}P NMR (121.5 MHz, ^1H coupled, D_2O) δ -1.30 (s); ^{13}C NMR (75.5 MHz, D_2O) δ 73.98 (d, J_{PC}=2.5 Hz, OCH_2), 24.74 (s, CH_2), 12.20 (s, CH_3), C=O not observed; IR (Nujol mull) 1690 cm^{-1} (C=O).

Disodium Butyloxycarbonylphosphonate (55). Dimethyl butyloxycarbonyl phosphonate (1.20 g, 5.71 mmol) and bromotrimethylsilane (2.18 g, 14.28 mmol) were reacted in a similar way to that described for the preparation of disodium methoxycarbonylphosphonate to give the title compound as a white powder: 81% (1.05 g, 4.65 mmol); mp >300°C, [lit. mp >300°C][60]; ^1H NMR (300 MHz, D_2O) δ 3.93 (2H, t, J_{HH}=7 Hz, OCH_2), 1.49 (2H, t t, J_{HH}=7 Hz, J_{HH}=7 Hz, observed as a pent, $OCH_2\underline{CH_2}$), 1.23 (2H, q t, J_{HH}=7 Hz,J_{HH}=7 Hz, observed as a sext, $\underline{CH_2}CH_3$), 0.73 (3H, t, J_{HH}=7 Hz, CH_3); ^{31}P NMR (121.5 MHz, ^1H decoupled, D_2O) δ -1.28 (s); ^{31}P NMR (121.5 MHz, ^1H coupled, D_2O) δ -1.28 (s); ^{13}C NMR (75.5 MHz, D_2O) δ 183.08 (d, J_{PC}=218 Hz, C=O), 66.63 (d, J_{PC}=3 Hz, OCH_2), 32.80 (s, $OCH_2\underline{CH_2}$), 21.26 (s, $\underline{CH_2}CH_3$), 15.70 (s, CH_3); IR (Nujol mull) 1690 cm^{-1} (C=O).

Disodium (2-Methylpropyl)oxycarbonylphosphonate (56). Dimethyl (2-methylpropyl)oxycarbonylphosphonate (1.20 g, 5.71 mmol) and bromotrimethylsilane (2.18 g, 14.28 mmol) were reacted in a similar way to that described for the preparation of disodium methoxycarbonylphosphonate to give the title compound as a white powder: 85% (1.10 g, 4.86 mmol); mp >300°C; ^1H NMR (300 MHz, D_2O) δ 3.70 (2H, d, J_{HH}=7 Hz, OCH_2), 1.81 (1H, sept t, J_{HH}=7 Hz, J_{HH}=7 Hz,observed as a nine line pattern, CH), 0.82 (6H, d, J_{HH}=7 Hz, 2xCH_3); ^{31}P NMR (121.5 MHz, ^1H decoupled, D_2O) δ -1.26 (s); ^{31}P NMR (121.5 MHz, ^1H coupled, D_2O) δ 1.26 (s); ^{13}C NMR (75.5 MHz, D_2O) δ 183.08 (d, J_{PC}=218 Hz, C=O), 72.71 (d, J_{PC}=2.5 Hz, OCH_2), 29.95 (s,CH), 21.12 (s, 2xCH_3); IR (Nujol mull) 1690 cm^{-1} (C=O).

Disodium Octyloxycarbonylphosphonate (57). Dimethyl octyloxycarbonyl phosphonate (1.34 g, 5.02 mmol) and bromotrimethylsilane (2.30 g, 15.03 mmol) were reacted in a similar way to that described for the preparation of disodium methoxycarbonylphosphonate to give the title compound as a white powder: 85% (1.20 g, 4.24 mmol); mp >300°C; ^{1}H NMR (300 MHz, D_2O) δ 3.91 (2H, t, J_{HH}=7 Hz, OCH_2), 1.50 (2H, t t, J_{HH}=7 Hz, J_{HH}=7 Hz, observed as a pentet, $OCH_2\underline{CH_2}$), 1.3-0.9 (10H, m, 5xCH_2), 0.67 (3H, t, J_{HH}=7 Hz, CH_3); ^{31}P NMR (121.5 MHz, ^{1}H decoupled, D_2O) δ -1.27 (s); ^{31}P NMR (121.5 MHz, ^{1}H coupled, D_2O) δ -1.27 (s); ^{13}C NMR (75.5 MHz, D_2O) δ 183.05 (d, J_{PC}=218 Hz, C=O), 66.94 (d, J_{PC}=2.5 Hz, OCH_2), 33.80 (s, CH_2), 31.11 (s, CH_2), 31.06 (s, CH_2), 30.70 (s, CH_2), 27.83 (s, CH_2), 24.70 (s, CH_2), 16.08 (s, CH_3); IR (Nujol mull) 1690 cm^{-1} (C=O).

Disodium Benzyloxycarbonylphosphonate (58). Dimethyl benzyloxycarbonyl phosphonate (1.22 g, 5.00 mmol) and bromotrimethylsilane (2.30 g, 15.03 mmol) were reacted in a similar way to that described for the preparation of disodium methoxycarbonylphosphonate to give the title compound as a white powder: 77% (1.00 g, 4.23 mmol); mp >300°C, [lit. mp >300°C][60]; ^{1}H NMR (300 MHz, D_2O) δ 7.4-7.1 (5H, m, aromatic), 4.60 (2H, s, OCH_2); ^{31}P NMR (121.5 MHz, ^{1}H decoupled, D_2O) δ -1.50 (s); ^{31}P NMR (121.5 MHz, ^{1}H coupled, D_2O) δ -1.50 (s); ^{13}C NMR (75.5 MHz, D_2O) δ 182.41 (d, J_{PC}=215 Hz, C=O), 139.15 (s, aromatic C), 132.45 (s, aromatic CH), 130.88 (s, aromatic CH), 130.54 (s, aromatic CH), 67.94 (s, CH_2); IR (Nujol mull) 1690 cm^{-1} (C=O).

Disodium Phenoxycarbonylphosphonate (59). Dimethyl phenoxycarbonyl phosphonate (1.50 g, 6.50 mmol) and bromotrimethylsilane (2.30 g, 15.03 mmol) were reacted in a similar way to that described for the preparation of disodium methoxycarbonylphosphonate to give the title compound as a white powder: 78% (1.25 g, 5.06 mmol); mp >300°C, [lit. mp >300°C][60]; ^{1}H NMR (300 MHz, D_2O) δ 7.3-6.8 (m, aromatic); ^{31}P NMR (121.5 MHz, ^{1}H decoupled, D_2O) δ -1.71 (s); ^{31}P NMR (121.5 MHz, ^{1}H coupled, D_2O) δ -1.71 (s); ^{13}C NMR (75.5 MHz, D_2O) δ 181.87 (d, J_{PC}=197 Hz, C=O), 153.18 (d, J_{PC}=6 Hz, aromatic C), 132.52 (s, aromatic CH), 129.00 (s, aromatic CH), 124.72 (s, aromatic CH); IR (Nujol mull) 1690 cm^{-1} (C=O).

4.1.4 Synthesis of a Phosphonate Monoester of PFA

Methyl Disodium Carboxyphosphonate (61). Dimethyl butyloxycarbonyl phosphonate (4.0 g, 0.019 mol) and sodium carbonate (2.0 g, 0.019 mol) in water (100 ml) were heated at reflux for two hours. The solution was then evaporated *in vacuo*. The residue was then redissolved in water (10 ml) and methanol (80 ml) was added which caused precipitation of the title compound: 80% (2.8 g, 0.015 mol); mp >300°C,

[lit. mp >300°C][60]; ^{1}H NMR (300 MHz, D_2O) δ 3.40 (d, J_{PH}=11 Hz, OCH_3); ^{31}P NMR (121.5 MHz, ^{1}H decoupled, D_2O) δ 4.79 (s); ^{31}P NMR (121.5 MHz, ^{1}H coupled, D_2O) δ 4.79 (q, J_{PH}=11 Hz); ^{13}C NMR (75.5 MHz, D_2O) δ 180.23 (d, J_{PC}=230 Hz, C=O), 54.86 (d, J_{PC}=5 Hz, OCH_3); IR (KBr) 1565 cm^{-1} (C=O), 1080 (P-O), 1040 (P=O).

4.1.5 Synthesis of a Tyrosine Ester of PFA

Phenyl Chloroformate was prepared analogously to the method of Zabik and Schuetz[109] for the preparation of p-methoxyphenyl chloroformate but replacing liquid phosgene with triphosgene. A solution of phenol (1.0 g, 10 mmol) and triphosgene (1.0 g, 3.3 mmol) in dichloromethane (50ml) was stirred. N,N-Dimethylaniline (1.2 g, 10 mmol) was added dropwise over 30 minutes and the reaction stirred at room temperature for three hours. The solution was washed with 0.1 M hydrochloric acid (2x30 ml), 0.1 M sodium hydroxide (2x30 ml) and water (2x30 ml). The organic solution was dried with anhydrous sodium sulphate and the dichloromethane evaporated *in vacuo* to give the title compound as a colourless liquid: 60% (0.95 g, 6.0 mmol); IR (liquid film) 1780 cm^{-1} (C=O), 1590 and 1490 (C=C), absence of OH stretch, finger print region of IR consistent with that of a commercial sample.

5-Ethyloxy-4-(4'-hydroxyphenylmethyl)-2-methyl Oxazole (74). N-Acetyl tyrosine ethyl ester (3.1 g, 11.50 mmol) and triphosgene (2.3 g, 3.83 mmol) were dissolved in dichloromethane (100 ml) and N,N-dimethylaniline (1,4 g, 11.57 mmol) was added dropwise. The reaction was stirred at room temperature for three hours. The solution was then washed with 0.1 M hydrochloric acid (2x50 ml) and then with 0.1 M sodium hydroxide (2x50 ml). The alkaline washings were then neutralised and the resultant precipitate filtered off and dried. Recrystallization from hexane - ethyl acetate gave the title compound as white crystals: 41% (1.10 g, 4.72 mmol); mp 115°C; ^{1}H NMR (300 MHz, $CDCl_3$) δ 6.87 (2H, d, J_{HH}=8 Hz, aromatic), 6.43 (2H, d, J_{HH}=8 Hz, aromatic), 4.14 (2H, q, J_{HH}=7 Hz, $O\underline{CH_2}CH_3$), 3.56 (2H, s, CH_2), 2.31 (3H, s, CH_3), 1.36 (3H, t, J_{HH}=7 Hz, $CH_2\underline{CH_3}$); ^{13}C NMR (75.5 MHz, $CDCl_3$) δ 155.24 (s, aryl C), 153.79 (s, oxazole C), 153.20 (s, oxazole C), 129.54 (s, aryl C), 129.40 (s, aryl CH), 116.27 (s, oxazole C), 115.57 (s, aryl CH), 70.70 (s, OCH_2), 29.59 (s, CH_2), 15.02 (s, CH_3), 13.96 (s, CH_3); IR (Nujol mull) 3200-3000 cm^{-1} (OH), 1660 (C=N), 1580 and 1500 (C=C); (Found: C, 66.95; H, 6.44; N, 6.00%; $C_{13}H_{15}NO_3$ requires C, 67.00; H, 6.69; N, 5.90%); m/z (EI) 233 (M^+, 21%), 107 (27%), 94 (40%), 43 (100%); m/z (CI, NH_3) 234 (M^++1, 100%);

Methoxycarbonylphosphonic Dichloride (75) was prepared analogously to the method of Morita *et al.*[111] for the preparation of other phosphonic dichlorides. A

mixture of dimethyl methoxycarbonylphosphonate (12.6 g, 0.075 mol) and bromotrimethysilane (25 g, 0.163 mol) was stirred under argon at 0°C for 3 hours. The volatile components were removed *in vacuo* (5 mm Hg) and the residue added dropwise to phosphorus pentachloride (31.3 g, 0.15 mol) suspended in dichloromethane (50 ml) with stirring. After one hour, the volatile components were removed *in vacuo* (20 mm Hg and then 5 mm Hg). Distillation (2 mm Hg) afforded the title compound as a colourless liquid: 82% (10.8 g, 0.061 mol); bp 50-54°C (2 mm Hg), [lit. bp 105-109°C (20 mm Hg)][145]; ^{1}H NMR (250 MHz, $CDCl_3$) δ 3.92 (s, OCH_3); ^{31}P NMR (101 MHz, ^{1}H decoupled, $CDCl_3$) δ 11.73 (s); ^{31}P NMR (101 MHz, ^{1}H coupled, $CDCl_3$) δ 11.73 (s); ^{13}C NMR (63 MHz, $CDCl_3$) δ 162.26 (d, J_{PC}=252.5 Hz, C=O), 55.67 (d, J_{PC}=5.5 Hz, OCH_3); IR (liquid film) 1735 cm^{-1} (C=O), 1280 (P=O).

Diphenyl Methoxycarbonylphosphonate (77). Methoxycarbonylphosphonic dichloride (2.0 g, 11.4 mmol) was added dropwise to a stirred solution of phenol (2.15 g, 22.8 mmol) in dichloromethane (50 ml). After 4 hours the dichloromethane was removed *in vacuo* (20 mm Hg). Vacuum distillation (0.1 mm Hg) gave the title compound as a colourless liquid: 73% (2.42 g, 8.3 mmol); bp 165-170°C (0.1 mm Hg); ^{1}H NMR (250 MHz, $CDCl_3$) δ 7.25-7.05 (10H, m, aromatic), 3.85 (3H, s, OCH_3); ^{31}P NMR (101 MHz, ^{1}H decoupled, $CDCl_3$) δ -13.10 (s); ^{31}P NMR (101 MHz, ^{1}H coupled, $CDCl_3$) δ -13.10 (s); ^{13}C NMR (63 MHz, $CDCl_3$) δ 165.20 (d, J_{PC}=282 Hz, C=O), 149.55 (d, J_{PC}=8.5 Hz, aromatic C), 129.86 (s, aromatic CH), 125.92 (s, aromatic CH), 120.47 (s, aromatic CH), 53.07 (d, J_{PC}=5 Hz, OCH_3); IR (liquid film) 1720 cm^{-1} (C=O), 1580 and 1490 (C=C).

Sodium 4-(2'-Ethoxycarbonyl-2'-acetamido-ethyl)phenyl Methoxycarbonyl phosphonate (79). N-Acetyl tyrosine ethyl ester monohydrate was dried by dissolving in dry tetrahydrofuran and evaporating to dryness *in vacuo* (1 mm Hg). This was repeated and the solid left in a vacuum desiccator for 24 hours (1 mm Hg) over phosphorus pentoxide. A solution of methoxycarbonylphosphonic dichloride (350 mg, 2.0 mmol) in dichloromethane (5 ml) was added dropwise to a stirred solution of N-acetyl tyrosine ethyl ester (500 mg, 2.0 mmol) in dichloromethane (10 ml). After 4 hours, the dichloromethane was removed *in vacuo* and the residue dissolved in acetone (10 ml). This was added to 10 g of Amberlite IRC 50 resin (sodium form) in water (40 ml) and stirred for one hour. The resin was filtered off and washed with water (10 ml). The filtrate and washings were combined and the acetone and water removed *in vacuo*. The residue was purified by preparative thin layer chromatograghy eluting with methanol - dichloromethane (1:3). A band of R_f 0.1-0.3 was scraped from the plate and the silica extracted with methanol (50 ml). The methanol was removed in vacuo and the residue dissolved in water. Freeze drying gave the title compound as a white solid: 38% (300 mg, 0.76 mmol); mp 70-72°C; ^{1}H NMR (250MHz, D_2O) δ 7.18

(2H, d, J_{HH}=8.5 Hz, aromatic), 7.07 (2H, d, J_{HH}=8.5 Hz, aromatic), 4.57 (1H, d d d, J_{HNH}=8 Hz,J_{HH}=6 Hz, J_{HH}=6 Hz, appears as d t, CH), 4.12 (2H, q, J_{HH}=7 Hz, $\underline{CH_2}CH_3$), 3.76 (3H, s, OCH_3), 3.11 (1H, d d, J_{gem}=13.5 Hz, J_{HH}=6 Hz, $ArCH_2C$), 2.98(1H, d d, J_{gem}=13.5 Hz, J_{HH}=6 Hz, $ArCH_2C$), 1.92 (3H, s, $O=CCH_3$), 1.16 (3H, t, J_{HH}=7 Hz, $CH_2\underline{CH_3}$); ^{31}P NMR (101 MHz, ^1H decoupled, D_2O) δ -7.38 (s); ^{31}P NMR (101 MHz, ^1H coupled, D_2O) δ –7.38 (s); ^{13}C NMR (63 MHz, D_2O) δ 176.94 (s, C=O), 176.30 (s, C=O), 152.91 (d, J_{PC}=8 Hz, aromatic C), 135.81 (s, aromatic C), 133.40 (s, aromatic CH), 123.84 (s, aromatic CH), 65.62 (s,OCH_2), 57.39 (s, CH), 55.14 (d, J_{PC}=4.5 Hz, OCH_3), 38.89 (s, $ArCH_2$), 24.42 (s, CH_3), 16.17 (s, CH_3), (P-C=O not observed); IR (Nujol mull) 1720cm^{-1} (C=O, esters), 1660 (C=O, amide); (Found C, 43.30; H, 4.92; N, 3.40%; $C_{15}H_{19}O_8NNaP$ requires C, 40.62; H, 4.00; N, 4.31%; $C_{15}H_{19}O_8NNaP.H_2O$ requires C, 43.58; H, 5.08; N, 3.39%).

N-Carbonyloxybenzyl L-Tyrosine (81) was prepared by the method of Bodanszky and Bodanszky.[112] L-Tyrosine (5.0 g, 27.6 mmol) was dissolved in 2 M sodium hydroxide (150 ml) and cooled in ice, with stirring. Benzyl chloroformate (4.7 g, 27.6 mmol) was added dropwise along with sufficient 2 M sodium hydroxide to maintain the pH above 12. Stirring was continued for 30 minutes and the solution was acidified with dilute hydrochloric acid.The product was then extracted with ether (3x100 ml).The ether layer was dried with anhydrous sodium sulphate and evaporated *in vacuo*. Recrystallisation from ethyl acetate - hexane gave the title compound as white crystals: 47% (4.1 g, 13 mmol); mp 97-98°C; ^1H NMR (300 MHz, DMSO-d_6) δ 13.5-11.5 (1H, bs, COOH), 9.7-8.8 (1H, bs, ArOH), 7.55 (1H, d, J_{HH}=8 Hz, NH), 7.40-7.10 (5H, m, aromatic), 7.02 (2H, d, J_{HH}=8 Hz, aromatic), 6.64 (2H, d, J_{HH}=8 Hz, aromatic), 4.96 (2H, s, $O\underline{CH_2}Ph$), 4.06 (1H, d d d, J_{HNH}=8 Hz, J_{HH}=6 Hz, J_{HH}=6 Hz, appears as d t, $ArCH_2CHNH$), 3.50-3.20 (2H, bs, H_2O), 2.92 (1H, d d, J_{gem}=13.5 Hz, J_{HH}=6 Hz, $ArCH_2C$), 2.67 (1H, d d, J_{gem}=13.5 Hz, J_{HH}=6 Hz, $ArCH_2C$); ^{13}C NMR (75.5 MHz, DMSO-d_6) δ 173.49 (s, COOH), 155.99 (s, NHCO), 155.88 (s, aromatic C), 137.05 (s, aromatic C), 130.03 (s, aromatic CH), 128.30 (s, aromatic CH), 127.92 (s, aromatic C), 127.70 (s, aromatic CH), 127.48 (s, aromatic CH), 114.96 (s, aromatic CH), 65.21 (s, OCH_2), 55.93 (s, CH), 35.79 (s, $Ar\underline{CH_2}$); IR (Nujol mull) 3400-3100 cm^{-1} (OH), 3340 (NH), 1710 (C=O, carboxylic acid), 1680 (C=O, carbamate), 1600 and 1500 (C=C).

L-Tyrosine N-Carboxyanhydride. (4-[4'-Hydroxyphenylmethyl] Oxazolidine-2-5-dione) (82). N-Carbonyloxybenzyl L-tyrosine (1.0 g, 3.2 mmol), benzyl alcohol (0.35 g, 3.2 mmol) and thionyl chloride (0.38 g, 3.2 mmol) were heated at reflux in dichloromethane (40 ml) for three hours. The resultant precipitate was filtered and dried *in vacuo*: 70% (0.46 g, 2.2 mmol); mp 180-185°C decomp.; ^1H NMR (60 MHz, DMSO-d_6) δ 8.9 (1H, s, OH), 7.3 (1H, d, J_{HH}=8 Hz, NH), 7.1 (2H, d,

J_{HH}=8 Hz, aromatic), 6.8 (2H, d, J_{HH}= 8 Hz, aromatic), 4.6 (1H, d t, J_{HH}=8 Hz, J_{HH}=8 Hz, observed as a quartet, CH), 3.0 (2H, d, J_{HH}=8 Hz, CH_2); IR (Nujol mull) 3400-3100 cm^{-1} (OH), 3300 (NH), 1820 and 1750 (C=O,anhydride), 1590 and 1500 (C=C).

L-Tyrosine Benzyl Ester (83) was prepared by a similar method to that of Erlanger and Hall[113] for the preparation of L-tyrosine benzyl ester hydrochloride. Polyphosphoric acid (5 g) and benzyl alcohol (25 ml) were stirred together at 90-95°C until the mixture was homogeneous. L-Tyrosine (2.0 g, 11 mmol) was added and the reaction stirred at 90-95°C for four hours. The reaction mixture was poured into 2M hydrochloric acid (200 ml) and then washed with ether (100 ml). The ether layer was washed with 2 M hydrochloric acid (2x50 ml). All aqueous layers were collected and the pH adjusted to 10 using solid sodium carbonate. The product was then extracted into ether (3x100 ml). The combined ether extracts were dried with anhydrous sodium sulphate and evaporated *in vacuo* to leave a yellow oil. The title compound was crystallised from ethyl acetate - hexane as white crystals: 60% (1.8 g, 6.6 mmol); mp 119-120°C; ^{1}H NMR (300 MHz, $CDCl_3$) δ 7.40-7.20 (5H, m, aromatic), 6.92 (2H, d, J_{HH}=8 Hz, aromatic), 6.62 (2H, d, J_{HH}=8 Hz, aromatic), 5.16 (1H, d, J_{gem}=12 Hz,CC(O)OCH_2Ph), 5.11 (1H, d, J_{gem}=12 Hz, CC(O)OCH_2Ph), 3.73 (1H, d d t, J_{HH}=6 Hz, J_{HH}=6 Hz, J_{HNH}=8 Hz, observed as d t,ArCH_2CHNH_2), 3.05-2.45 (4H, bs, NH_2 and H_2O), 3.00 (1H, d d, J_{gem}=13.5 Hz, J_{HH}=6 Hz, ArCH_2C), 2.81 (1H, d d, J_{gem}=13.5 Hz, J_{HH}=6 Hz, ArCH_2C); ^{13}C NMR (75.5 MHz, $CDCl_3$) δ 174.77 (s, C=O), 155.09 (s, aromatic C), 135.37 (s, aromatic C),130.35 (s, aromatic CH), 128.58 (s, aromatic CH), 128.44 (s, aromatic CH), 127.97 (s, aromatic C), 115.61 (s, aromatic CH), 66.89 (s, OCH_2), 55.60 (s, CH), 39.89 (s, CH_2), one aromatic CH not observed or overlapping; IR (Nujol mull) 1720 cm^{-1} (C=O), 1600 (C=C).

N-Carbonyloxybenzyl L-Tyrosine Benzyl Ester (80). Tyrosine benzyl ester (1.0 g, 3.7 mmol) and triethylamine (0.36 g, 3.5 mmol) were dissolved in dry acetonitrile (40 ml) and cooled in ice. A solution of benzyl chloroformate (0.60 g, 3.5 mmol) in acetonitrile (10 ml) was added dropwise, with stirring, over 30 minutes. After a further two hours, the TLC [ethyl acetate-hexane (2:1)] of the reaction mixture showed two spots above the baseline with R_f 0.21 and R_f 0.34 which were separated by flash chromatography.[114] The fractions corresponding to the compound with R_f 0.21, after evaporation *in vacuo* and recrystallization from ethyl acetate-hexane gave the title compound as white crystals: 42% (0.45 g, 1.5 mmol); mp 117-118°C; ^{1}H NMR (300 MHz, $CDCl_3$) δ 7.45-7.25 (10H, m, aromatic), 6.87 (2H, d, J_{HH}=8 Hz, aromatic), 6.67 (2H, d, J_{HH}=8 Hz, aromatic), 5.50 (1H, bs, OH), 5.30 (1H, d, J_{HH}=8 Hz, NH), 5.22 (1H, d, J_{gem}=12 Hz, CC(O)OCH_2Ph), 5.15 (1H, d, J_{gem}=12 Hz, CC(O)OCH_2Ph, half of this doublet is hidden under the singlet at 5.13), 5.13 (2H, s,

HNC(O)O$\underline{CH_2}$Ph), 4.69 (1H, d d d, J_{HNH}=8 Hz, J_{HH}=6 Hz, J_{HH}=6 Hz, appears as quartet, ArCH$_2\underline{CH}$NH), 3.09 (1H, d d, J_{gem}=13.5 Hz, J_{HH}=6 Hz, Ar$\underline{CH_2}$C), 3.03 (1H, d d, J_{gem}=13.5 Hz, J_{HH}=6 Hz, Ar$\underline{CH_2}$C); ^{13}C NMR (75.5 MHz, $CDCl_3$) δ 171.46 (s, C=O), 155.67 (s, C=O), 154.82 (s, aromatic C), 136.06 (s, aromatic C), 134.96 (s, aromatic C), 130.41 (s, aromatic CH), 128.54 (s, aromatic CH), 128.48 (s, aromatic CH), 128.15 (s, aromatic CH), 128.03 (s, aromatic CH), 127.22 (s, aromatic C), 115.42 (s, aromatic CH), 67.23 (s, OCH_2), 67.00 (s, OCH_2), 54.90 (s, CH), 37.30 (s, CH_2), two aromatic CH not observed or overlapping; IR (Nujol mull) 1720 cm^{-1} (C=O, ester), 1680 (C=O, carbamate), 1600 and 1500 (C=C); (Found: C, 70.81; H, 5.79; N, 3.60%; $C_{24}H_{23}O_5N$ requires C, 71.11; H, 5.68; N, 3.46%).

The fractions corresponding to the compound with R_f 0.34, after evaporation *in vacuo* and recrystallisation from ethyl acetate-hexane, gave **N-carbonyloxybenzyl L-tyrosine benzyl ester O-benzyl carbonate (84)** as white crystals: 10% (0.20 g, 0.37 mmol); mp 85-89°C; ^{1}H NMR (300 MHz, $CDCl_3$) δ 7.50-7.20 (15H, m, aromatic), 7.01 (2H, d, J_{HH}=8 Hz, aromatic), 6.96 (2H, d, J_{HH}=8 Hz, aromatic), 5.40-5.00 (6H, m, 3xOCH_2), 4.67 (1H, d d d, J_{HNH}=8 Hz, J_{HH}=6 Hz, J_{HH}=6 Hz, observed as d t, CH), 3.10 (1H, d d, J_{gem}=13.5 Hz, J_{HH}=6 Hz, Ar$\underline{CH_2}$C), 3.03 (1H, d d, J_{gem}=13.5 Hz, J_{HH}=6 Hz, Ar$\underline{CH_2}$C); ^{13}C NMR (75.5 MHz, $CDCl_3$) δ 171.10 (s, C=O), 155.55 (s, C=O), 153.49 (s, C=O), 150.14 (s, aromatic C), 136.20 (s, aromatic C), 134.93 (s, aromatic C), 134.73 (s, aromatic C), 133.39 (s, aromatic C), 130.33 (s, aromatic CH), 128.75 (s, aromatic CH), 128.65 (s, aromatic CH), 128.58 (s, aromatic CH), 128.51 (s, aromatic CH), 128.17 (s, aromatic CH), 128.09 (s, aromatic CH), 121.03 (s, aromatic CH), 70.31 (s, OCH_2), 67.31 (s, OCH_2), 66.98 (s, OCH_2) 54.70 (s, CH), 37.43 (s, CH_2), three aromatic CH not observed or overlapping; IR (Nujol mull) 1740 cm^{-1} (C=O, carbonate), 1680 (C=O, carbamate).

Sodium 4-[2'-(benzyloxycarbonyl)-2'-(N-carbonyloxybenzylcarbamate)-ethyl]phenyl Methoxycarbonylphosphonate (85).

A solution of Methoxycarbonylphosphonic dichloride (440 mg, 2.5 mmol), in dichloromethane (5 ml) was added dropwise to a stirred solution of N-carbonyloxybenzyl L-tyrosine benzyl ester (1g, 2.5 mmol) in dichloromethane (25 ml). After 4 hours the dichloromethane was removed *in vacuo* and the residue taken up into acetone (10 ml). This was then added to 10 g of Amberlite IRC 50 resin (sodium form) in water (50 ml) and stirred for 1 hour. The resin was filtered off and washed with water (10 ml). The filtrate and washings were combined and the acetone and water removed *in vacuo* . The residue was purified by preparative thin layer chromatography eluting with methanol-dichloromethane (3:17). A band R_f 0.25 to 0.45 was scraped from the plate and the silica extracted with methanol (50 ml). The methanol was removed *in vacuo* and the residue dissolved in water (30 ml). Freeze drying gave the title compound as a white solid: 40% (550 mg, 1.0 mmol); mp 70-75°C; ^{1}H NMR (250 MHz, CD_3OD) δ 7.40-

7.10 (10H, m, aromatic), 7.08 (2H, d, J_{HH}=10Hz, aromatic), 7.04 (2H, d, J_{HH}=10Hz, aromatic), 5.10 (2H, s, CC(O)O$\underline{CH_2}$Ph), 4.96 (2H, s, NC(O)O$\underline{CH_2}$Ph), 4.43 (1H, ddd, ArCH$_2\underline{CH}$NH, J_{HNH}=6 Hz, J_{HH}=9 Hz, J_{HH}=6 Hz, appears as quartet), 3.68 (3H, s, OCH_3), 3.07 (1H, dd, J_{gem}=14 Hz, J_{HH}=6 Hz, Ar$\underline{CH_2}$C), 2.89 (1H, dd, J_{gem}=14 Hz, J_{HH}=9 Hz, Ar$\underline{CH_2}$C); ^{31}P NMR (101 MHz, ^{1}H decoupled, CD_3OD) δ –6.96 (s), ^{31}P NMR (101 MHz, ^{1}H coupled, CD_3OD) δ –6.96 (s), ^{13}C NMR (63 MHz, CD_3OD) δ 173.45 (s, C=O), 152.68 (d, J_{PC}=8 Hz, aromatic C), 138.27 (s, aromatic C), 137.23 (s, aromatic C), 133.79 (s, aromatic C), 131.28 (s, aromatic CH), 129.78 (s, aromatic CH),129.66 (s, aromatic CH), 129.54 (s, aromatic CH), 129.17 (s, aromatic CH), 128.89 (s, aromatic CH), 122.21 (s, aromatic CH), 122.14 (s, aromatic CH), 68.19 (s, OCH_2), 67.79 (s, OCH_2), 57.33 (s, CH), 51.84 (d, J_{PC}=4.5 Hz, OCH_3), 37.88 (s, CH_2), (P-C=O and C=O not observed); IR (Nujol mull) 1730cm^{-1} (C=O, benzyl ester), 1710 (C=O, methyl ester), 1690 (C=O, carbamate), 1600 and 1510 (C=C); (Found C, 53.01; H, 4.59; N, 2.36%; $C_{26}H_{25}O_9NPNa$ requires C, 56.83; H, 4.55, N, 2.55%; $C_{26}H_{25}O_9NPNa.2H_2O$ requires C, 53.33; H, 4.96; N, 2.39).

Sodium 4-(2'-Carboxyl-2'-aminoethyl)phenyl Methoxycarbonyl-phosphonate (68).

Sodium 4-[2'-(benzyloxycarbonyl)-2'-(N-carbonyloxybenzylcarbamate)ethyl]phenyl methoxycarbonylphosphonate (500mg, 0.91 mmol) was dissolved in dry methanol. Palladium 10% on activated carbon (50mg) was added and the mixture shaken under an atmosphere of hydrogen for 4 hours. The catalyst was filtered off and the methanol removed *in vacuo*. The residue was dissolved in water (30ml) and freeze dried to give the title compound as a white solid: 84% (250mg, 0.77mmol); mp 190-195°C with decomposition; ^{1}H NMR (250 MHz, D_2O) δ 7.33 (2H, d, J_{HH}=8.5 Hz, aromatic), 7.19 (2H, d, J_{HH}=8.5 Hz, aromatic), 3.99 (1H, dd, J_{HH}=5 Hz, J_{HH}=8 Hz, CH), 3.86 (3H, s, OCH_3), 3.32 (1H, dd, J_{gem}=14.5 Hz, J_{HH}=5 Hz, CH_2), 3.11 (1H, dd, J_{gem}=14.5 Hz, J_{HH}=8.5 Hz, CH_2); ^{31}P NMR (101 MHz, ^{1}H decoupled, D_2O) δ –7.35 (s); ^{31}P NMR (101 MHz, ^{1}H coupled, D_2O) δ –7.35 (s); ^{13}C NMR (63 MHz, D_2O) δ 176.99 (s, C=O), 175.67 (d, J_{PC}=251 Hz, P-C=O), 153.31 (d, J_{PC}=8 Hz, aromatic C), 134.72 (s, aromatic C), 133.66 (s, aromatic CH),124.34 (s, aromatic CH), 59.02 (s, CH), 55.23 (d, J_{PC}=4.5 Hz, OCH_3), 38.72 (s, CH_2); IR (Nujol mull) 1700cm^{-1} (C=O, ester), 1610 (C=O, carboxyl and C=C), 1500 (C=C); (Found C, 34.83; H, 4.50; N, 3.58; $C_{11}H_{13}O_7NPNa$ requires C, 40.62; H, 4.00; N, 4.31; $C_{11}H_{13}O_7NPNa.3H_20$ requires C, 34.83; H, 5.01; N, 3.69); m/z (FAB, nitrobenzyl alcohol matrix) 348 ($M+Na^+$, 69%), 326 ($M+H^+$, 100), 255 (64). Observed accurate FAB m/z on ($M+H^+$) gives 326.0406. $C_{11}H_{14}O_7NPNa$ requires 326.0374.

4.1.6 Synthesis of a Dipalmitoyl Glycerol Ester of PFA

1-Benzyl-2,3-isopropylidene-*rac*-glycerol (89) was prepared analogously to the method of Vogel[115] for the preparation of benzyl ethers. Solketal (1,2-isopropylidene-*rac*-glycerol) (**76**) (5.0 g, 37.0 mmol), benzyl chloride (5.0 g, 39.0 mmol) and tetrabutylammonium sulphate (0.5 g, 1.5 mmol) were dissolved in dichloromethane (20 ml). Sodium hydroxide (6 g, 150 mmol) was dissolved in water (6 ml) and added to the mixture which was heated at reflux for 2 hours. Water (50 ml) and dichloromethane (20 ml) were then added with stirring. The dichloromethane layer was separated and washed with water (2x50 ml), dried with anhydrous sodium sulphate and evaporated *in vacuo*. Vacuum distillation of the residue afforded the title compound as a colourless liquid: 84% (7.0 g, 31.4 mmol); bp 84-86°C (0.05 mm Hg), [lit. bp 95-97°C (0.3 mm Hg)][116]; R_f 0.26 (hexane - ethyl acetate, 5:1); ^1H NMR (250 MHz, $CDCl_3$) δ 7.33-7.28 (5H, m, aromatic), 4.58 (1H, d, J_{gem}=14.8 Hz, CH_2Ph), 4.53 (1H, d, J_{gem}=14.8 Hz, CH_2Ph), 4.28 (1H, d d d d, J_{HH}=6.5 Hz, J_{HH}=6.3 Hz, J_{HH}=5.6 Hz, J_{HH}=5.4 Hz, appears as pent with J_{HH}=6.0 Hz, $CH_2\underline{CH}CH_2$), 4.03 (1H, d d, J_{gem}=8.3 Hz, J_{HH}=6.5 Hz, 3-CH_2), 3.73 (1H, d d, J_{gem}=8.3 Hz, J_{HH}=6.3 Hz, 3-CH_2), 3.54 (1H, d d, J_{gem}=9.7 Hz, J_{HH}=5.6 Hz, $\underline{CH_2}OCH_2Ph$), 3.45 (1H, d d, J_{gem}=9.7 Hz, J_{HH}=5.4 Hz, $\underline{CH_2}OCH_2Ph$), 1.42 (3H, s, CH_3), 1.35 (3H, s, CH_3); ^{13}C NMR (63 MHz, $CDCl_3$) δ 138.05 (s, aromatic C), 128.48 (s, aromatic CH), 128.21 (s, aromatic CH), 127.78 (s, aromatic CH), 109.57 [s, $\underline{C}$ $(CH_3)_2$], 74.67 (s, CH), 73.55 (s, $Ph\underline{CH_2}O$), 71.14 (s, CH_2O), 66.92 (s, CH_2O), 26.85 (s, CH_3), 25.47 (s, CH_3); IR (liquid film) 1100-1050 cm^{-1} (ether, C-O), 740 and 690 (monosubstituted aromatic).

1-Benzyl-*rac*-glycerol (90) was prepared analogously to the method of Sowden and Fischer.[116] 1-Benzyl-2,3-isopropylidene-*rac*-glycerol (5 g, 22.4 mmol) was added to 0.2 M sulphuric acid (150 ml) and heated at reflux overnight. The solution was made alkaline with sodium bicarbonate and saturated with sodium chloride. The solution was then extracted with ether (3x50 ml). The extract was dried with anhydrous sodium sulphate and evaporated *in vacuo*. The residue was purified by flash chromatography[114] eluting with ethyl acetate. The fractions having an R_f of 0.26, upon evaporation *in vacuo*, gave the title compound: 74% (3.0 g, 16.5 mmol); ^1H NMR (250 MHz, $CDCl_3$) δ 7.39-7.29 (5H, m, aromatic), 4.52 (2H, s, CH_2Ph), 3.89 (1H, d d d d, J_{HH}=5.4 Hz, J_{HH}=5.8 Hz, J_{HH}=5.4 Hz, J_{HH}=6.5 Hz, appears as pent with J_{HH}=6.0 Hz, $CH_2\underline{CH}CH_2$) 3.67 (1H, d d, J_{gem}=11.5 Hz, J_{HH}=5.4 Hz, CH_2OH), 3.58 (1H, d d, J_{gem}=11.5 Hz, J_{HH}=5.8 Hz, CH_2OH), 3.54 (1H, d d, J_{gem}=10.3 Hz, J_{HH}=5.4 Hz, $\underline{CH_2}OCH_2Ph$), 3.50 (1H, d d, J_{gem}=10.3 Hz, J_{HH}=6.5 Hz, $\underline{CH_2}OCH_2Ph$), 2.86 (2H, bs, exchanges with D_2O, 2xOH); ^{13}C NMR (63 MHz, $CDCl_3$) δ 137.74 (s, aromatic C), 128.57 (s, aromatic CH), 127.98 (s, aromatic CH), 127.89 (s, aromatic CH), 73.62

(s, Ph$\underline{CH_2}$O), 71.78 (s, CH), 70.79 (s, CH_2O), 64.08 (s, CH_2O); IR (liquid film) 3380 cm^{-1} (OH), 1100-1050 (ether, C-O), 740 and 690 (monosubstituted aromatic).

1-Benzyl-2,3-dipalmitoyl-*rac*-glycerol (91) was prepared analogously to the method of Sowden and Fischer.[116] Palmitoyl chloride (15.5 g, 56.4 mmol) was added dropwise to 1-benzyl-*rac*-glycerol (5.0 g, 27.5 mmol) and pyridine (4.5 g, 56.4 mmol) in dry dichloromethane (50 ml) under argon. The mixture was stirred at 20°C for 48 hours. The dichloromethane was then removed *in vacuo* and ether (100 ml) added. Undissolved material was filtered off and the solution washed with 0.1 M hydrochloric acid (2x20 ml), water (20 ml), saturated sodium bicarbonate solution (2x20 ml) and water (20 ml). The ether solution was dried over sodium sulphate and concentrated *in vacuo*. Recrystallisation from ether gave the title compound as white crystals: 81% (14.6 g, 22.2 mmol); mp 42.5-43°C, (lit. mp 42-42.5°C)[116]; ^{1}H NMR (250 MHz, $CDCl_3$) δ 7.33-7.27 (5H, m, aromatic), 5.22 (1H, d d t, J_{HH}=5.2 Hz, J_{HH}=6.2 Hz, J_{HH}=5.2 Hz, appears as sext with J_{HH}=5.5 Hz, $CH_2\underline{CH}CH_2$), 4.55 (1H, d, J_{gem}=14.8 Hz, Ph$\underline{CH_2}$O),4.50 (1H, d, J_{gem}=14.8 Hz, Ph$\underline{CH_2}$O), 4.34 (1H, d d, J_{gem}=12.0 Hz, J_{HH}=5.2 Hz, CH_2OCO), 4.17 (1H, d d, J_{gem}=12.0 Hz,J_{HH}=6.2 Hz, CH_2OCO), 3.57 (2H, d, J_{HH}=5.2 Hz, $\underline{CH_2}OCH_2Ph$), 2.31 (2H, t, J_{HH}=7.5 Hz, CH_2COO), 2.27 (2H, t, J_{HH}=7.5 Hz, CH_2COO), 1.66-1.48 (4H, m, 2x$\underline{CH_2}CH_2COO$), 1.39-1.18 (48H, m, 24xCH_2), 0.89 (6H, t, J_{HH}=6.8 Hz, 2xCH_3); ^{13}C NMR (63 MHz, $CDCl_3$) δ 173.31 (s, C=O), 173.02 (s, C=O), 137.60 (s, aromatic C), 128.31 (s, aromatic CH), 127.68 (s, aromatic CH), 127.52 (s, aromatic CH), 73.20 (s, Ph$\underline{CH_2}$O), 69.89 (s, CH), 68.15 (s, CH_2O), 62.55 (s, CH_2O), 34.24 (s, CH_2), 34.02 (s, CH_2), 31.83 (s, CH_2), 29.61 (s, CH_2), 29.58 (s, CH_2), 29.40 (s, CH_2), 29.28 (s, CH_2), 29.20 (s, CH_2), 29.03 (s, CH_2), 28.99 (s, CH_2), 28.94 (s, CH_2), 24.86 (s, CH_2), 24.79 (s, CH_2), 22.60 (s, CH_2), 14.03 (s, CH_3); IR (liquid film) 1740 cm^{-1} (C=O, ester), 740 and 690 (monosubstituted aromatic).

1,2-Dipalmitoyl-*rac*-glycerol (92). 1-Benzyl-2,3-dipalmitoyl-*rac*-glycerol (8.0 g, 12.1 mmol) was dissolved in dry ethanol (200 ml) by heating to 40°C. Palladium 10% on activated carbon (800mg) was then added. The mixture was shaken in a water bath at 40°C under an atmosphere of hydrogen for 24 hours. While the mixture was still warm the catalyst was filtered off and the solution concentrated *in vacuo* until crystallisation occurred. Recrystallisation from hexane gave the title compound as white crystals: 87% (6.0 g, 10.6 mmol); mp 60-62°C, (lit. mp 67-67.5°C)[116]; ^{1}H NMR (250 MHz, $CDCl_3$) δ 5.06 (1H, d d t, J_{HH}=4.5 Hz, J_{HH}=5.7 Hz, J_{HH}=5.0 Hz, appears as pent with J_{HH}=5.0 Hz, $CH_2\underline{CH}CH_2$), 4.30 (1H, d d, J_{gem}=12.0 Hz, J_{HH}=4.5 Hz, CH_2OC), 4.21 (1H, d d, J_{gem}=12.0 Hz, J_{HH}=5.7 Hz, CH_2OC), 3.71 (2H, d, J_{HH}=5.0 Hz, CH_2OH), 2.33 (2H, t, J_{HH}=5.7 Hz, CH_2COO), 2.28 (2H, t, J_{HH}=5.7 Hz, CH_2COO), 1.75-1.50 (4H, m, 2x$\underline{CH_2}CH_2COO$), 1.45-1.20 (48H, m, 24xCH_2), 0.89 (6H, t,

J_{HH}=6.8 Hz, 2xCH_3); ^{13}C NMR (63 MHz, $CDCl_3$) δ 173.70 (s, C=O), 173.34 (s, C=O), 71.99 (s, CH), 61.91 (s, CH_2O), 61.43 (s, CH_2O), 34.19 (s, CH_2), 34.00 (s, CH_2), 31.82 (s, CH_2), 29.60 (s, CH_2), 29.56 (s, CH_2), 29.52 (s, CH_2), 29.38 (s, CH_2), 29.26 (s, CH_2), 29.17 (s, CH_2), 29.02 (s, CH_2), 28.99 (s, CH_2), 24.84 (s, CH_2), 24.79 (s, CH_2), 22.59 (s, CH_2), 14.02 (s, CH_3); IR (Nujol mull) 3430 cm^{-1} (OH), 1715 (C=O, ester).

1-Chloroformyl-2,3-dipalmitoyl-*rac*-glycerol (93). 1,2-Dipalmitoyl-*rac*-glycerol (5.0 g, 8.8 mmol) and triphosgene (870 mg, 2.9 mmol) were dissolved in dry dichloromethane (20 ml). Triethylamine (880 mg, 8.8 mmol) in dry dichloromethane (10 ml) was then added dropwise under an atmosphere of argon. The solution was stirred for 3 hours and then washed with 0.1M hydrochloric acid (2x30 ml), 0.1 M sodium hydroxide (2x30 ml) and water (2x30 ml). The dichloromethane layer was dried using anhydrous sodium sulphate and evaporated *in vacuo* to give the title compound as a viscous colourless liquid: 63% (3.5 g, 5.6 mmol); IR (liquid film) 1775 cm^{-1} (C=O, chloroformate), 1740 (C=O, ester).

Dimethyl (2,3-Dipalmitoyl-*rac*-glycero)carbonylphosphonate (94). 1-Chloroformyl-2,3-dipalmitoyl-*rac*-glycerol (2.0 g, 3.2 mmol) and trimethyl phosphite (400 mg, 3.2 mmol) were heated together at 80°C for 2 hours under argon. Upon cooling a solid formed which was purified by flash chromatography[114] eluting with ethyl acetate-hexane (1:1). The fractions having an R_f of 0.42 were concentrated *in vacuo* until crystallisation occurred. Recrystallisation from hexane gave the title compound as a white solid: 66% (1.5 g, 2.1 mmol); mp 49.5-51°C; ^1H NMR (250 MHz, $CDCl_3$) δ 5.30 (1H, d d d d d, J_{HH}=4.0 Hz, J_{HH}=5.9 Hz, J_{HH}=4.8 Hz, J_{HH}=5.7 Hz, J_{PH}=1.0 Hz, appears as m with character of pent d with J_{HH}=5.0 Hz, J_{PH}=1.0 Hz,$CH_2\underline{CH}CH_2$), 4.45 [1H, d d d, J_{gem}=11.9 Hz, J_{HH}=4.0 Hz, J_{PH}=1.1 Hz, $CH_2OC(O)P$], 4.33 [1H, d d d, J_{gem}=11.9 Hz, J_{HH}=5.9 Hz, J_{PH}=1.1 Hz, $CH_2OC(O)P$], 4.30 [1H, d d, J_{gem}=11.9 Hz, J_{HH}=4.8 Hz, $CH_2OC(O)C$), 4.13 (1H, d d, J_{gem}=11.9 Hz, J_{HH}=5.7 Hz, $CH_2OC(O)C$], 3.91 (3H, d, J_{PH}=11.1 Hz, $POCH_3$), 3.90 (3H, d, J_{PH}=11.1 Hz, $POCH_3$), 2.29 (4H, t, J_{HH}=7.5 Hz, 2xCH_2COO), 1.58 (4H, m, 2x$\underline{CH_2}CH_2COO$), 1.20-1.40 (48H, m, 24xCH_2), 0.85 (6H, t, J_{HH}=6.5 Hz, 2xCH_3); ^{31}P NMR (101 MHz, ^1H decoupled, $CDCl_3$) δ -2.85 (s); ^{31}P NMR (101 MHz, ^1H coupled, $CDCl_3$) δ -2.85 (sept t d, J_{PH}=11 Hz, J_{PH}=1 Hz, J_{PH}=1 Hz, appears as sept q with J_{PH}=11 Hz, J_{PH}=1 Hz); ^{13}C NMR (63 MHz, $CDCl_3$) δ 173.07 (s, C=O), 172.65 (s, C=O), 68.16 (s, CH), 63.24 [d, J_{PC}=5.0 Hz, $\underline{CH_2}OC(O)P$], 61.60 (s, CH_2O), 54.57 [d, J_{PC}=8.0 Hz, $P(OCH_3)_2$], 33.99 (s, CH_2), 33.88 (s, CH_2), 31.81 (s, CH_2), 29.58 (s, CH_2), 29.55 (s, CH_2), 29.52 (s, CH_2), 29.36 (s, CH_2), 29.25 (s, CH_2), 29.16 (s, CH_2), 29.00 (s, CH_2), 28.96 (s, CH_2), 24.72 (s, CH_2), 24.69 (s, CH_2), 22.58 (s, CH_2), 14.00 (s, CH_3), PC=O not observed; IR (liquid film) 1730 cm^{-1} (C=O, ester), 1285

(P=O); (Found: C, 64.98; H, 10.45%; $C_{38}H_{73}O_9P$ requires C, 64.77; H, 10.37%); m/z (CI, ammonia carrier gas) 722 (M^++NH_4, 54%), 551 (37), 128 (100); observed accurate CI m/z on (M^++NH_4) gives 722.5336.$C_{38}H_{77}O_9NP$ requires 722.5288.

Di(cyclohexylammonium) (2,3-Dipalmitoyl-*rac*-glycero)carbonyl-phosphonate (87). Dimethyl (2,3-dipalmitoyl-*rac*-glycero)carbonylphosphonate (200 mg, 0.28 mmol) was dissolved in dichloromethane (3 ml). Bromotrimethylsilane (130 mg,0.85 mmol) was added and the solution stirred under an atmosphere of argon, in a fume cupboard, for 4 hours. ^{31}P NMR spectroscopy was used to ensure that the reaction had gone to completion, with the bis(trimethylsilyl) ester having a shift of δ -23.44. The dichloromethane, excess bromotrimethylsilane and methyl bromide were evaporated *in vacuo*. The cyclohexylamine salt was then prepared by the method of Freeman *et al.*[117] Cyclohexylamine (56 mg, 0.56 mmol) and water (10 mg, 0.56 mmol) in dioxane (5 ml) was added to the residue and stirred for 10 minutes. The dioxane was removed *in vacuo*, and the residue recrystallised from acetone-water to yield the title compound as a white solid: 81% (200 mg, 0.23 mmol); mp 60-62°C; ^1H NMR (250 MHz, $CDCl_3$) δ 5.18 (1H, m, $CH_2\underline{CH}CH_2$), 4.38 [1H, d, J_{gem}=9.5 Hz, $CH_2OC(O)P$], 4.12 [3H, m, $CH_2OC(O)C$ and 1H of $CH_2OC(O)P$], 2.84 (2H, m, 2x$CHNH_3^+$), 2.25 (4H, t, J_{HH}=7.5 Hz, 2xCH_2COO), 1.99 (4H, m, cyclohexyl), 1.70 (4H, m, cyclohexyl), 1.56 (6H, m, 2x$\underline{CH_2}CH_2COO$ + 2H cyclohexyl), 1.23 (58H, m, 24xCH_2 + 10H cyclohexyl), 0.86 (6H, t, J_{HH}=6.5 Hz, 2xCH_3); ^{31}P NMR (101 MHz, ^1H decoupled, $CDCl_3$) δ -8.46 (s); ^{31}P NMR (101 MHz, ^1H coupled, $CDCl_3$) δ -8.46 (bs); ^{13}C NMR (63 MHz, $CDCl_3$) δ 172.92 (s, C=O), 172.52 (s, C=O), 69.15 (s, CH), 62.06 (s, CH_2O, no coupling observed due to broad peak), 59.92 (s, CH_2O), 49.78 (s, $CHNH_3^+$), 34.02 (s, CH_2), 33.94 (s, CH_2), 31.80 (s, CH_2), 30.84 (s, CH_2), 29.59 (s, CH_2), 29.55 (s, CH_2), 29.42 (s, CH_2), 29.24 (s, CH_2), 29.06 (s, CH_2), 29.04 (s, CH_2), 25.04 (s, CH_2), 24.79 (s, CH_2), 24,74 (s, CH_2), 24.49 (s, CH_2), 22.56 (s, CH_2), 13.97 (s, CH_3), 3xCH_2 not observed or overlapping, PC=O not observed; IR (liquid film) 2800-2200 cm^{-1} (primary amine salt), 1735 (C=O, ester), 1695 (PC=O, ester), (Found: C, 63.90%; H, 11.12; $C_{48}H_{95}O_9PN_2$ requires C, 65.90%; H, 10.87; $C_{48}H_{95}O_9PN_2.1\,1/2\,H_2O$ requires C, 63.93%; H, 10.88).

Sodium Methyl (2,3-Dipalmitoyl-*rac*-glycero)carbonylphosphonate (86). A solution of sodium iodide (4.2 mg, 0.028 mmol) in dry tetrahydrofuran (2 ml) was added to a solution of dimethyl (2,3-dipalmitoyl-*rac*-glycero)carbonylphosphonate (20 mg, 0.028 mmol) in dry tetrahydrofuran (1 ml). The mixture was stirred for 7 days at 20°C in a flask fitted with a anhydrous calcium chloride tube to exclude moisture. The reaction was followed by ^{31}P NMR spectroscopy to ensure completion. The tetrahydrofuran was removed *in vacuo* to give the title compound as a white solid: 85% (17 mg, 0.024 mmol); mp 54-56°C; ^1H NMR (250 MHz, $CDCl_3$) δ 5.4-5.3 (1H, m,

$CH_2\underline{CH}CH_2$), 4.5-4.1 [4H, m, $CH_2OC(O)P$ and $CH_2OC(O)C$], 3.59 (3H, d, J_{PH}=10.8 Hz, $POCH_3$), 2.28 (4H, t, J_{HH}=7.1 Hz, $2xCH_2COO$), 1.7-1.5 (4H, m, $\underline{CH_2}CH_2COO$), 1.4-1.2 (48H, m, $24xCH_2$), 0.87 (6H, t, J_{HH}=6.6 Hz, $2xCH_3$); ^{31}P NMR (101 Hz, ^1H decoupled, $CDCl_3$) δ -3.62 (s); ^{31}P NMR (101 Hz, ^1H coupled, $CDCl_3$) δ -3.62 (q, J_{PH}=10.8 Hz); ^{13}C NMR (63 MHz, $CDCl_3$) δ 173.28 (s, C=O), 173.15 (s, C=O), 68.38 (s, CH), 63.45 [s, $\underline{CH_2}OC(O)P$, no coupling observed due to broad peak], 61.84 (s, CH_2O), 54.80 (s, $POCH_3$, no coupling observed due to broad peak), 34.12 (s, CH_2), 33.93 (s, CH_2), 31.83 (s, CH_2), 29.66 (s, CH_2), 29.59 (s, CH_2), 29.53 (s, CH_2), 29.29 (s, CH_2), 29.13 (s, CH_2), 24.76 (s, CH_2), 22.59 (s, CH_2), 14.01 (s, CH_3), $4xCH_2$ not observed or overlapping, PC=O not observed; IR (liquid film) 1730-1700 cm^{-1} (C=O, ester), 1260 (P=O); (Found: C, 60.77; H, 9.59%; $C_{37}H_{70}O_9PNa$ requires: C, 62.36; H, 9.83%; $C_{37}H_{70}O_9PNa.H_2O$ requires: C, 60.82; H, 9.59%).

4.2 Stability Studies

4.2.1 Hydrolysis of Dimethyl Phenoxycarbonylphosphonate Monitored by ^{31}P NMR Spectroscopy

A solution of dimethyl phenoxycarbonylphosphonate (**41**) (80mg, 0.35mmol) in acetonitrile (4 ml) was added to a 10mm NMR tube, containing a 5mm NMR tube with a D_2O inner lock. After the ^{31}P NMR spectrum was recorded [^{31}P NMR (121.5 MHz, ^1H decoupled) δ 1.9 (s)], phosphate buffer (4 ml, pH 7.4, 0.1M) was added to initiate the hydrolysis. After 5 minutes the mixture was monitored by ^{31}P NMR which showed only dimethyl phosphite [^{31}P NMR (121.5 MHz, ^1H coupled) δ 14.6 (d sept, J_{PH}=718 Hz, J_{PH}=12 Hz)], which slowly hydrolysed to methyl phosphite [^{31}P NMR (121.5 MHz, ^1H coupled) δ 8.2 (d q, J_{PH}=626Hz, J_{PH}=12Hz)]. To confirm the identity of the product, dimethyl phosphite was added to the sample and the ^{31}P NMR spectrum was repeated and the peak for this compound increased in intensity.

4.2.2 Stability of Sodium Methyl Methoxycarbonylphosphonate Monitored by ^{31}P NMR Spectroscopy

Sodium methyl methoxycarbonylphosphonate (**43**) (8mg, 0.045mmol) was dissolved in phosphate buffer (1ml, pH 7.4, 0.1M) and added to a 5mm NMR tube, containing a D_2O inner lock in a capillary tube. The ^{31}P NMR spectrum was recorded [^{31}P NMR (101 MHz, ^1H decoupled) δ -2.60 (s)] After one hour and 24 hours at room temperature the mixture was monitored by ^{31}P NMR spectroscopy and no change in the original spectrum was observed.

4.2.3 Stability of Sodium 4-[2'-(benzyloxycarbonyl)-2'-(N-carbonyl-oxybenzylcarbamate)ethyl]phenyl Methoxycarbonylphosphonate Monitored by ^{31}P NMR Spectroscopy

Sodium 4-[2'-(benzyloxycarbonyl)-2'-(N-carbonyloxybenzylcarbamate)ethyl]phenyl methoxycarbonylphosphonate **(68)** (10mg, 0.031mmol) was dissolved in phosphate buffer (1ml, pH 7.4, 0.1M) and added to a 5mm NMR tube, containing a D_2O inner lock in a capillary tube. The ^{31}P NMR spectrum was recorded [^{31}P NMR (101 MHz, ^{1}H decoupled) δ -7.37 (s)]. After one hour and 24 hours the mixture was monitored by ^{31}P NMR spectroscopy and no change in the original spectrum was observed.

4.3 Anti-HIV Testing

The method used by the Mill Hill testing centre is summarised below.[146] The inhibitory effect of compounds on HIV replication in infected C8166 T-lymphoblastoid cells was expressed as a reduction in the viral p24 antigen or gp120 antigen as compared with HIV replication in infected cells without any potentially inhibitory compound. The HIV antigen was assayed using a commercial ELISA (enzyme-linked immunoabsorbent assay). Briefly, the antigen is captured from a detergent lysate of virions onto a polyclonal antibody adsorbed onto a solid phase. The bound antigen is then detected with an alkaline phosphatase-conjugated anti-p24 or anti-gp120 monoclonal antibody. The cytotoxic effect of compounds was expressed as a reduction in cell growth as compared with cells without any potentially cytotoxic compound. Cell viability was measured by a colourimetric assay (MTT-Formazan method). Briefly, viable cells are determined by their ability to reduce a tetrazolium compound to a blue formazan product which is measured at 540 nm.

CHAPTER 5 - BBB - EXPERIMENTAL

5.1 Preparation of Solutions used in the Isolation, Culture and Characterisation of Porcine Brain Microvessel Endothelial Cells.

5.1.1 Preparation of Amphotericin B Stock Solution

Sterile distilled water (10ml) was aseptically added to a vial of amphotericin B (100mg, Sigma). The solution was stored at -20°C.

5.1.2 Preparation of Polymyxin B Stock Solution

Polymyxin B sulphate (200mg, Sigma) was dissolved in distilled water (10ml) and sterile-filtered into a 25ml sterile vial. The solution was stored at 4°C.

5.1.3 Preparation of Gentamicin Stock Solution

Gentamicin sulphate (500mg, Sigma) was dissolved in distilled water (10ml) and sterile-filtered into a 25ml sterile vial. The solution was stored at 4°C.

5.1.4 Preparation of Heparin Stock Solution

Heparin (500mg, Sigma) was dissolved in distilled water (10ml) and sterile-filtered into a 25ml sterile vial. The solution was stored at 4°C.

5.1.5 Preparation of 1M HEPES pH 7.4

HEPES (N-[2-hydroxyethyl]piperazine-N'-[2-ethanesulphonic acid], 47.6g, Sigma) was dissolved in distilled water (100ml), the pH was adjusted to 7.4 with 2M sodium hydroxide solution and made up to 200ml in a volumetric flask. The solution was sterile-filtered and stored at 4°C.

5.1.6 Preparation of Minimum Essential Medium (MEM)

The following components were dissolved in distilled water (900ml):

MEM (Gibco)	powder sufficient for 1000ml
HEPES (Sigma)	11.9g
Polymyxin B sulphate (Sigma)	50mg
Gentamicin sulphate (Sigma)	50mg

The pH was adjusted to 7.4 using 2M sodium hydroxide and the solution made up to 1000ml in a volumetric flask. The solution was sterile-filtered into two 500ml sterile bottles. Amphotericin B stock solution (0.125ml) was aseptically added to each 500ml bottle. The solution was stored at 4°C.

5.1.7 Preparation of MEM without antibiotics

This was prepared as for MEM but polymyxin B sulphate, gentamicin sulphate and amphotericin B stock solution were omitted.

5.1.8 Preparation of MEM pH 9-10

This was prepared as for MEM but the pH of the solution was adjusted to between 9 and 10 by the addition of 2M sodium hydroxide.

5.1.9 Preparation of Concentrated MEM (x10) Solution

A tub of autoclavable MEM (Gibco) sufficient for 5L was dissolved in distilled water and made up to 500ml in a volumetric flask. The solution was transferred to a 500ml bottle and autoclaved at 120°C for 20 minutes. The solution was stored at 4°C.

5.1.10 Preparation of Dispase Solution

Dispase (2.5g, Boehringer Mannheim) was mixed with MEM without antibiotics (15ml) and incubated in a water bath at 37°C for 30 minutes. The suspension was centrifuged at 2800rpm (approximately 1000g) for 30 minutes in a Sarstedt LC1 centrifuge and the supernatant sterile-filtered into a 25ml sterile tube. This was stored at -20°C and thawed in a water bath at 37°C when required.

5.1.11 Preparation of Dispase/Collagenase Solution

Dispase/collagenase (20mg, Boehringer Mannheim) was dissolved in MEM without antibiotics (5ml) and incubated in a water bath at 37°C for 30 minutes. The solution was sterile-filtered into a sterile 5ml tube and stored at -20°C. This was thawed in a water bath at 37°C and diluted to 20ml with MEM without antibiotics immediately prior to use.

5.1.12 Preparation of 13% Dextran Solution

Dextran (65g, mw 60-90,000 Daltons, Sigma) was dissolved in distilled water (422ml) in a 500ml bottle and autoclaved at 120°C for 20 minutes The solution was stored at 4°C and the following components added aseptically prior to use:

Polymyxin B stock solution	1.25ml
Amphotericin B stock solution	0.125ml
Gentamicin stock solution	1.00ml
Concentrated MEM (x10) solution	50ml
1M HEPES pH 7.4 solution	25ml

5.1.13 Preparation of Percoll Gradient Tubes

The following solutions were aseptically mixed:

Percoll (Sigma)	75ml
Concentrated MEM (x10) solution	15ml
1M HEPES pH 7.4	7.5ml
Sterile distilled water	52ml
Polymyxin B stock solution	0.4ml
Gentamicin stock solution	0.3ml
Polymyxin B stock solution	0.1ml

To each of four 40ml sterile centrifuge tubes, 35ml of the resulting solution was added and centrifuged at 18,200rpm (approximately 20,000g) for 60 minutes at 4°C in a JA-20 rotor in a Beckman J2-21 centrifuge. These tubes were prepared immediately prior to use.

5.1.14 Preparation of Basic Culture Medium

The following components were dissolved in distilled water (1800ml):

MEM (Gibco)	powder sufficient for 1000ml
Ham's F12 nutrient (Gibco)	powder sufficient for 1000ml
HEPES (Sigma)	4.76g
Sodium bicarbonate (Sigma)	2.18g
Gentamicin sulphate (Sigma)	100mg

The pH of the solution was adjusted to 7.4 with 2M sodium hydroxide and the solution made up to 2000ml in a volumetric flask. The solution was then sterile-filtered into four 500ml bottles and stored at 4°C.

5.1.15 Preparation of Culture Medium No.1

To 500ml of basic culture medium the following were aseptically added:

Plasma-derived horse serum (Hyclone)	55ml
Polymyxin B stock solution	1.25ml
Amphotericin B stock solution	0.125ml

The solution was stored at 4°C.

5.1.16 Preparation of Culture Medium No.2

To 500ml of basic culture medium the following were aseptically added:

Plasma-derived horse serum (Hyclone)	55ml
Heparin stock solution	1.1ml
Amphotericin B stock solution	0.125ml

The solution was stored at 4°C.

5.1.17 Preparation of Freezing Medium

The following were added to 28ml of culture medium no.1:

Plasma-derived horse serum (Hyclone)	8ml
Dimethyl sulphoxide	4ml

The solution was made immediately prior to use.

5.1.18 Preparation of Plating Medium

The following was added to 50ml of culture medium no.1:

Heparin stock solution	0.1ml

The solution was made immediately prior to use.

5.1.19 Preparation of Fibronectin Stock Solution

Sterile distilled water (12.5ml) was added to a vial of fibronectin from bovine plasma (1mg, Sigma). The solution was then withdrawn from the vial and added to a further 12.5ml of sterile distilled water in a 25ml sterile tube. The solution was stored at -20°C. The solution may be re-used twice, again with storage at -20°C.

5.1.20 Preparation of Rat-Tail Collagen

Aqueous acetic acid (0.1M, 300ml) was sterile-filtered into a 500ml bottle. Four rat tails were stripped of skin and clean collagen fibres removed, washed in ethanol and dried. Collagen (900mg) was collected and added to the 0.1M acetic acid and stirred for 48 hours. The suspension was centrifuged at 2800rpm (approximately 1000g) for 30 minutes in a Sarstedt LC1 centrifuge. The supernatant was poured into 25ml sterile tubes and stored at 4°C.

5.1.21 Preparation of Transport Medium

The following components were added to distilled water (900ml):

Hanks Balanced Salts (Gibco)	sufficient for 1000ml
1M HEPES pH 7.4	14ml

The solution was then made up to 1000ml in a volumetric flask and sterile-filtered into two 500ml sterile bottles. The solution was stored at 4°C.

5.1.22 Preparation of Crystal Violet Solution

Trisodium citrate monohydrate (2.94g, Sigma) was dissolved in distilled water and made up to 100ml in a volumetric flask. Crystal violet (100mg, Sigma) was dissolved in the 100ml of trisodium citrate monohydrate solution and filtered through Whatman no.1 filter paper. This solution was made immediately prior to use.

5.1.23 Preparation of Phosphate-Buffered Saline pH 7.4

One phosphate-buffered saline (PBS) tablet (Sigma) was dissolved in distilled water and made up to 100ml in a volumetric flask. This solution was stored at 4°C.

5.1.24 Preparation of Trypan Blue Solution

Trypan blue (40mg, Sigma) was dissolved in 10ml of PBS. This solution was made up immediately prior to use.

5.1.25 Preparation of 10% Formalin in Phosphate Buffered Saline

Formalin (formaldehyde solution 38-40%, 10ml) was diluted to 100ml in a volumetric flask with PBS. This solution was stored at 4°C.

5.1.26 Preparation of Alkaline Dye Mixture and Control Solution

The contents of one capsule of fast blue RR salt (Sigma) was dissolved in distilled water (48ml). To this naphthol AS-MX phosphate alkaline solution (2ml, Sigma) was added. For the control solution the naphthol AS-MX alkaline solution was substituted with distilled water (2ml). These solutions were made immediately prior to use.

5.1.27 Preparation of γ-Glutamyl Transpeptidase Staining Solution and Control Solution

Using a sonication bath, the following were dissolved in 8ml of PBS containing 2 drops of dimethyl sulphoxide:

γ-Glutamyl-4-methoxy-2-naphthylamide (Sigma)	2mg
Glycylglycine (Sigma)	5mg
Fast blue BB salt (Sigma)	5mg

For the control solution, γ-glutamyl-4-methoxy-2-naphthylamide was omitted. These solutions were made immediately prior to use.

5.1.28 Preparation of 0.3% Hydrogen Peroxide Solution

30% hydrogen peroxide solution (1ml, Sigma) was diluted to 100ml with distilled water in a volumetric flask. This solution was made immediately prior to use.

5.1.29 Preparation of Primary Antibody Solution

Stock blocking serum (3 drops, Vector) was added to PBS (10ml). To this, Von Willebrand factor antibody (50µl, Dako) was added. This solution was made immediately prior to use.

5.1.30 Preparation of Biotinylated Secondary Antibody Solution

Stock blocking serum (3 drops, Vector) was added to PBS (10ml). To this, stock biotinylated antibody (50µl, Vector) was added. This solution was made immediately prior to use.

5.1.31 Preparation of Avidin Biotin Complex (ABC) Reagent

Vectastain Elite ABC reagent A (2 drops, Vector) was added to PBS (5ml), followed by reagent B (2 drops). This was immediately mixed and allowed to stand for 30 minutes before use.

5.1.32 Preparation of Peroxidase Substrate Solution

To distilled water (5ml) the following were added from the Vector Peroxidase Substrate kit and the solution mixed after each addition:

Buffer stock solution	2 drops
DAB (diaminobenzidene) stock solution	4 drops
Hydrogen peroxide solution	2 drops
Nickel solution	2 drops

This solution was made immediately before use.

5.2 Isolation of Porcine Brain Microvessel Endothelial Cells

Porcine brain microvessel endothelial cells (BMEC) were isolated by a method similar to that described by Audus[102] for the isolation of bovine BMEC. Porcine brains were obtained from a local abattoir, where the pigs were electrocuted and briefly immersed in boiling water. Thirty to sixty minutes after death, seven brains were removed and transported in MEM packed in ice. The brains were transferred into a beaker of ice cold MEM in a Gelaire BSB 4A cell culture cabinet. Under sterile conditions, the meninges and surface blood vessels were removed, using forceps, and discarded. The grey matter of the cerebral cortex was scraped away with a sterile razor blade and placed in a beaker

containing 50ml of MEM. The grey matter was then minced into 1 to 2mm cubes using four razor blades glued together. Approximately 200ml of minced gray matter was collected and placed in a sterile 500ml plastic bottle. To this, the dispase solution was added and the bottle placed in a shaking water bath at 37°C. After 30 minutes the bottle was removed and 100ml of MEM pH 9-10 was added, in order to adjust the pH to 7.4. The bottle was then returned to the water bath for a further 2 hours. The cell suspension was then poured into two sterile 250ml centrifuge tubes and centrifuged at 3200rpm (approximately 1000g) for 10 minutes at 4°C in a JA-14 rotor, in a Beckman J2-21 centrifuge. The top brown solution was then discarded leaving semi-solid material behind, which was then mixed thoroughly with 500ml of 13% dextran solution and divided into four 250ml sterile centrifuge tubes. The tubes were then centrifuged as before, but at 7700rpm (approximately 6000g). The red pellet and surrounding material was retained and the floating matter and dextran solution were discarded. The four red pellets were each resuspended in 5ml of collagenase/dispase solution. These were combined in a sterile 50ml tube and placed in a shaking water bath at 37°C for $4^1/_2$ hours. After the incubation, the cell suspension was diluted to 50ml with MEM and centrifuged at 2800rpm (approximately 1000g) for 10 minutes in a Sarstedt LC1 centrifuge. The pellet was resuspended in a total volume of 8ml with MEM. A 2ml portion of this suspension was carefully layered on top of four Percoll gradient tubes and centrifuged at 2800rpm for 10 minutes as before. The portion of the Percoll containing the endothelial cells (see Figure 5.1 and Photograph 3.7) was then removed with a pipette. This retained portion was diluted 50% with Culture Medium No.1 and centrifuged at 2800rpm for 10 minutes as before. The pellet was resuspended in 40ml of freezing medium and 1.5ml portions placed in Cryovials and frozen in a liquid nitrogen cell bank.

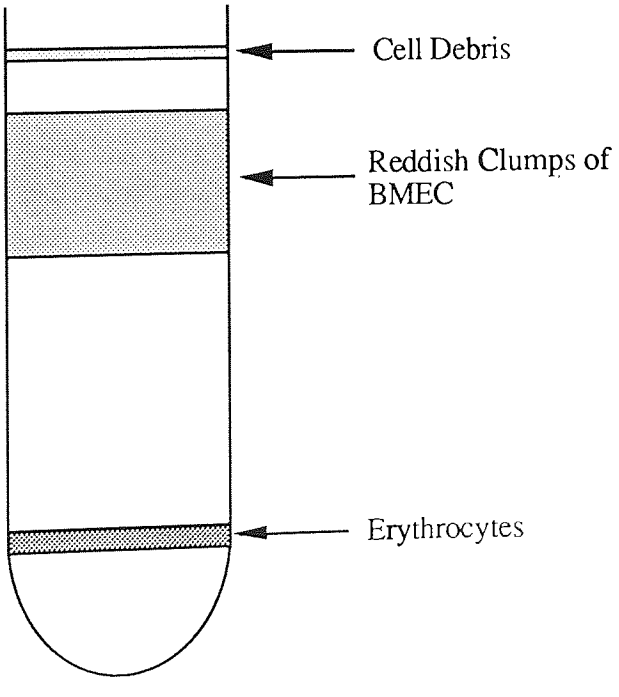

Figure 5.1 - Percoll Tube Showing the Position of BMEC

5.3 Culture of Porcine Microvessel Endothelial Cells

5.3.1 Cell Count

One Cryovial of cell suspension was thawed in a water bath at 37°C. Cell suspension (200µl) was mixed with crystal violet solution (400µl) and incubated at 37°C for 30 minutes. A cell count was performed using a haemocytometer and the cell concentration calculated.

5.3.2 Cell Viability

One Cryovial of cell suspension was thawed in a water bath at 37°C. The suspension was diluted to 5ml with basic culture medium and centrifuged at 2800rpm (approximately 1000g) for 10 minutes in a Sarstedt LC1 centrifuge. The pellet was resuspended in 5ml of basic culture medium and the centrifugation repeated. The pellet was resuspended in 5ml of basic culture medium. A 500µl portion of this supension was mixed with trypan blue solution (500µl). After 10 minutes, a cell count of viable (those having excluded stain) and non-viable (those having taken up stain) cells was performed using a haemocytometer and a percentage viability calculated.

5.3.3 Coating of Growth Surfaces

The following procedure was performed under aseptic conditions. Six Falcon 25mm cell culture inserts (Becton Dickinson) were removed from their packaging and inserted into a six-well plate (Nunc). Rat-tail collagen (1ml) was added to each insert. The collagen was swirled around the insert to ensure complete coverage of the membrane. After removing the excess collagen, using an aspirator, the inserts were placed in an atmosphere of ammonia for 5 minutes and were then exposed to ultraviolet light for 60 minutes. Fibronectin stock solution (0.5ml) was added to each insert and swirled to ensure coverage. The fibronectin was allowed to stand for 30 minutes with occasional swirling before being removed by aspiration. Culture medium no.1 (1ml) was added to each insert, swirled and removed by aspiration. The inserts were then exposed to ultraviolet light for a further 60 minutes.

5.3.4 Seeding of Cell Culture

Sufficient cell suspension, to allow seeding at 250,000 cells per insert, was removed from the liquid nitrogen cell bank and thawed in a water bath at 37°C. The cell suspension was diluted to 10ml with culture medium no.1 and centrifuged at 1800rpm (approximately 415g) in a Sarstedt LC1 centrifuge for 10 minutes. The pellet was

resuspended in 10ml of culture medium no.1 and the centrifugation repeated. The pellet was resuspended in plating medium to give a concentraion of 100,000 cells per ml. A 2.5ml portion of the suspension was added to each insert and 2.5ml of plating medium was added to each well containing an insert.

5.3.5 Maintenance of Cell Culture

The cells were incubated at 37°C in 100% humidity in 5% carbon dioxide in air. The cells were left undisturbed for 3 days, then the plating medium was removed and replaced with culture medium no.2. After a further 2 days this was replaced with fresh culture medium no.2. If monolayers were to be maintained for longer than seven days, culture medium no.2 was replaced at 2-day intervals.

5.4 Characterisation of Porcine Microvessel Endothelial Cell Monolayers on Falcon 25mm Cell Culture Inserts

5.4.1 Detection of Alkaline Phosphatase Activity

A Falcon 25mm insert, with a 7-day old confluent BMEC monolayer growing on its membrane, was removed from its six-well plate and the medium removed from it with an aspirator. A solution of 10% formalin in phosphate buffered saline (PBS, 2ml) was added and left to stand at room temperature for 30 minutes. The membrane was washed with PBS, the membrane removed from the insert with a scalpel and the membrane cut in half. Half of the membrane was placed in alkaline dye mixture and the other half in alkaline dye mixture without naphthol AS-MX phosphate (substrate) to serve as a control. Both solutions were allowed to stand in darkness at room temperature for 30 minutes. The half membranes were removed from the solutions, washed with PBS and mounted on a microscope slide in glycerol gelatin (Sigma). The slides were viewed and photographed under a Nikon TMS inverted phase-contrast microscope using x100 magnification.

5.4.2 Detection of γ–Glutamyl Transpeptidase Activity

A 7-day old confluent BMEC monolayer in a Falcon 25mm insert was removed from its six-well plate and the medium removed by aspiration. A solution of 10% formalin in PBS (2ml) was added and left to stand at room temperature for 30 minutes. The membrane was washed with PBS, the membrane was removed from the insert with a scalpel and the membrane cut in half. Half of the membrane was placed in γ-glutamyl transpeptidase staining solution and the other half in staining solution without γ-

glutamyl-4-methoxy-2-naphthylamide (substrate) to serve as a control. Both solutions were incubated for 1 hour at 37°C. The half membranes were removed from the solutions, washed with PBS and mounted on a microscope slide using glycerol gelatin. The slides were viewed under a phase-contrast microscope, as before.

5.4.3 Detection of Factor VIII Antigen

A 7-day old confluent BMEC monolayer in a Falcon 25mm insert was removed from its six-well plate and the medium removed by aspiration. A solution of 10% formalin in phosphate buffered saline (2ml) was added and left to stand at room temperature for 30 minutes. The membrane was washed with PBS, removed from the insert with a scalpel and placed in 0.3% hydrogen peroxide solution for 30 minutes. The membrane was cut in half. One half was incubated in primary antibody solution at 37°C, in a humid atmosphere for 10 minutes, while the other half was incubated in PBS to serve as a control. The two half membranes were washed with PBS and both incubated in biotinylated secondary antibody solution under the previous conditions. The two half-membranes were then washed with PBS and incubated in ABC reagent under the previous conditions. Finally, the two half membranes were washed with PBS and incubated in peroxidase substrate solution for 2 minutes. They were then washed with PBS and mounted on a microscope slide using glycerol gelatin. The slides were viewed and photographed under a phase contrast microscope.

5.4.4 Mannitol Transport

Three 6 to 8-day old confluent BMEC monolayers in Falcon 25mm inserts were removed from their six-well plate and the medium removed by aspiration. Transport medium (1.5ml) containing 0.2μCi of ^{14}C-mannitol (60 mCi / mmol, Amersham) was added to each insert. Each insert was placed in a six-well plate containing transport medium (2.5ml) in each well. The six-well plates were then incubated at 37°C. The insert was moved into the next numbered well at 30 minute intervals. After 3 hours, the insert was removed and the solution from the insert was added to Optiphase HiSafe 3 scintillation cocktail (10ml). The membrane was removed from the insert with a scalpel and added to scintillation cocktail (10ml). The transport medium from the wells in the six well plates was individually added to scintillation cocktail (10ml). All samples were then counted using a Packard Tri-Carb 1600TR liquid scintillation counter and the cummulative transport of ^{14}C-mannitol over the 3 hours as a percentage of the total DPM was then calculated. The experiment was repeated using coated Falcon 25mm inserts without cells to act as a control.

5.4.5 Electrical Resistance Measurements

The electrical resistance of each monolayer was measured using an Evom voltmeter, (World Precision Instruments, USA) at 37°C. The average of six readings was taken and the resistance of the coated Falcon inserts subtracted from this, to give monolayer resistance. This was corrected for surface area (4.91 cm^2) and expressed as ohms cm^2.

5.4.6 Testosterone Transport

Testosterone transport experiments were performed as descibed in section 5.4.4, except that 0.2μCi of ^{3}H-testosterone (45 Ci / mmol, NEN) was substituted for ^{14}C-mannitol .

5.4.7 Transport with Days in Culture

Transport experiments were performed 5, 6, 7, 9, 10 and 12 days after seeding with ^{14}C-mannitol as described in section 5.4.4. This was repeated using 0.2μCi of ^{14}C-sucrose (632 mCi / mmol, NEN) on days 3, 5, 6, 7, 8, 9, 10 and 12 after seeding.

5.5 *In Vitro* Studies on α-Keto Acid Transport

5.5.1 Identification of ^{14}C-Pyruvate Post-Transport using Radio-TLC

A 6-8 day old confluent BMEC monolayer on a Falcon 25mm insert was removed from its six-well plate and the medium removed by aspiration. Transport medium (1.5ml) containing 1.0μCi of ^{14}C-pyruvate (28.9 mCi / mmol, Amersham)was added to the insert. The insert was placed in a well of a six-well plate containing transport medium (2.5ml). The six-well plate was incubated at 37°C for three hours. A sample of medium from the basolateral chamber was taken and spotted on a Merck aluminium-backed cellulose TLC plate (3.5cm wide and 4.5cm long). The sample was repeatedly spotted along a horizontal base line across the width of the TLC plate, 1cm from the bottom. After drying, the plate was stood vertically in a solvent tank with a 0.75cm depth of solvent (isopropanol - 5% formic acid, 13:7). The solvent was allowed to run 3cm up the plate before it was removed from the solvent tank and dried. The plate was then cut into ten 3mm horizontal strips from the base line to the solvent front. Each strip was individually added to Optiphase HiSafe 3 scintillation cocktail (10ml) and counted using a Packard Tri-Carb 1600TR liquid scintillation counter. Distance from the base line was then plotted against DPM. This was repeated using ^{14}C-Pyruvate, not subjected to transport, for use as a reference.

5.5.2 The Effect of BMEC Monolayers on ^{14}C-Pyruvate Transport

Pyruvate transport experiments were performed as descibed in section 5.4.4, except that 0.2μCi of ^{3}H-mannitol (19.1 Ci / mmol, Sigma) and 0.2μCi of ^{14}C-pyruvate were used.

5.5.3 The Effect of Temperature

Experiments to evaluate the effect of temperature on pyruvate transport were performed as described in section 5.4.4 except that 0.2μCi of ^{3}H-mannitol and 0.2μCi of ^{14}C-pyruvate were used and incubations were maintained at 4°C. This was then compared with incubatiions at 37°C in section 5.5.2.

5.5.4 The Effect of Concentration

Twenty-four confluent BMEC monolayers in Falcon 25mm inserts, 6 to 8-days old, were removed from their six-well plates and the medium removed by aspiration. Transport medium (1.5ml) containing 0.2μCi of ^{3}H-mannitol, 0.2μCi of ^{14}C-pyruvate and a given concentration of unlabelled sodium pyruvate was added to each insert. The concentrations of sodium pyruvate used were 0.05, 0.1, 0.5, 1.0, 2.5, 5.0, 7.5 and 10.0mM; each concentration being added to three inserts. Each insert was placed in a six-well plate containing transport medium (2.5ml) in each well. The six-well plates were then incubated at 37°C. After 1 hour, the inserts were removed and the solution from the inserts individually added to Optiphase HiSafe 3 scintillation cocktail (10ml). The membranes were removed from the inserts with a scalpel and added individually to scintillation cocktail (10ml). The transport medium from the wells in the six-well plates was individually added to scintillation cocktail (10ml). All samples were then counted using a Packard Tri-Carb 1600TR liquid scintillation counter and the transport of ^{3}H-mannitol and ^{14}C-pyruvate over one hour as a percentage of the total DPM was then calculated.

5.5.5 Inhibition Profile

Thirty confluent BMEC monolayers in Falcon 25mm inserts, 6 to 8-days old, were removed from their six-well plates and the medium removed by aspiration. Transport medium (1.5ml) containing 0.2μCi of ^{3}H-mannitol, 0.2μCi of ^{14}C-pyruvate and 10mM of a potential inhibitor of pyruvate transport was added to each insert. The potential inhibitors used were sodium pyruvate, sodium L-lactate, lithium D-lactate, sodium valproate, sodium phenylpyruvate, sodium acetate, trisodium phosphonofomate hexahydrate, sodium methyl methoxycarbonylphosphonate (**43**) and L-phenylalanine; each one being added to three inserts. A control containing 0.2μCi of ^{3}H-mannitol,

0.2μCi of ^{14}C-pyruvate and 0.05mM sodium pyruvate was also added to three inserts. Each insert was placed in a six-well plate containing transport medium (2.5ml) in each well. The six-well plates were then incubated at 37°C. After 1 hour, the inserts were removed and the solution from the inserts individually added to Optiphase HiSafe 3 scintillation cocktail (10ml). The membranes were removed from the inserts with a scalpel and added individually to scintillation cocktail (10ml). The transport medium from the wells in the six-well plates was individually added to scintillation cocktail (10ml). All samples were then counted using a Packard Tri-Carb 1600TR liquid scintillation counter and the transport of ^{3}H-mannitol and ^{14}C-pyruvate over one hour as a percentage of the total DPM was then calculated. From this, the percentage inhibition of each potential inhibitor, as compared with the control, was calculated.

5.6 *In Vitro* Studies on Amino Acid Transport

5.6.1 Identification of ^{3}H-L-Tyrosine Post-Transport using Radio-TLC

The experiment to test the stability of ^{3}H-L-tyrosine (57 Ci / mmol, Amersham) was as described in section 5.5.1, except that 1.0μCi ^{3}H-L-tyrosine was substituted for ^{14}C-pyruvate and the solvent system used was pyridine - n-butanol - water (1:1:1). The solvent was allowed to run 2.5cm and the TLC plate cut into ten horizontal 2.5mm strips. This was repeated for ^{3}H-L-Tyrosine, not subjected to transport, for use as a reference.

5.6.2 The Effect of BMEC Monolayers on ^{3}H-L-Tyrosine Transport

L-Tyrosine transport experiments were performed as described in section 5.4.4, except that 0.2μCi of ^{14}C-mannitol and 0.2μCi of ^{3}H-L-tyrosine were added to the transport medium.

5.6.3 The Effect of Temperature

Experiments to evaluate the effect of temperature on L-tyrosine transport were performed as described in section 5.4.4 except that 0.2μCi of ^{14}C-mannitol and 0.2μCi of ^{3}H-L-tyrosine were added to the transport medium and incubations were maintained at 4°C. This was then compared with incubatiions at 37°C in section 5.6.2.

5.6.4 The Effect of Concentration

Experiments to evaluate the effect of concentration on L-tyrosine transport were performed as described in 5.5.4 except that 0.2μCi of ^{14}C-mannitol, 0.2μCi of ^{3}H-L-tyrosine were used to the transport medium and the following concentrations of unlabelled L-tyrosine were used: 0.005mM, 0.01mM, 0.02mM, 0.05mM, 0.1mM, 0.2mM, 0.5mM and 1mM.

5.6.5 Inhibition Profile

Experiments to evaluate the effect of potential inhibitors were performed as described in section 5.5.5 except that 0.2μCi of ^{14}C-mannitol, 0.2μCi of ^{3}H-L-tyrosine and the following potential inhibitors at a concentration of 2mM were used: L-tyrosine, D-tyrosine, L-phenylalanine, D-phenylalanine, L-dopa, D-dopa, L-histidine, L-methionine, L-alanine and the tyrosine-linked PFA diester (68).

REFERENCES

1. A.R. Moss, Clinical Epidemiology of AIDS and HIV Infection: What do we Expect in the Second Decade of the Epidemic?, in AIDS and the New Viruses, 1-10, A.G. Dalgleish, R.A. Weiss, Eds., Academic Press, London, 1990.
2. Weekly Epidemiological Record, 2nd July 1992, World Health Organization, Geneva, **67**, 97-104.
3. P.D. Minor, Strategies for the Development of Vaccines against HIV, *J. Antimicrob. Chemother.*, 1989, **23**, suppl. A, 55-62.
4. W.A. Haseltine, Molecular Biology of HIV-1, in AIDS and the New Viruses, 11-40, A.G. Dalgleish, R.A. Weiss, Eds., Academic Press, London, 1990.
5. G.L. Ada, Strategies in the Quest for a HIV Vaccine, in AIDS and the New Viruses, 81-110, A.G. Dalgleish, R.A. Weiss, Eds., Academic Press, London, 1990.
6. J. Sattentau, Molecular Interactions between CD4 and the HIV Envelope Glycoproteins, in Aids and the New Viruses, 41-54, A.G. Dalgleish, R.A. Weiss, Eds., Academic Press, London, 1990.
7. J. Weber, The Biology and Epidemiology of HIV Infection, *J. Antimicrob. Chemother.*, 1989, **23**, suppl. A, 1-7.
8. A. Traunecker, W. Luke and K. Karjalainen, Soluble CD4 Molecules Neutralise Human Immunodeficiency Virus Type 1, *Nature*, 1988, **331**, 84-86.
9. D.J. Capon, S.M. Chamow, J. Mordenti, S.A. Marsters, T. Gregory, H. Mitsuya, R.A. Byrn, C. Lucas, F.M. Wurm, J.E. Groopman, Designing CD4 Immunoadhesins for AIDS Therapy, *Nature*, 1989, **337**, 525-531.
10. J. Palca, New AIDS Drugs Take Careful Aim, *Science*, 1989, **246**, 1559-1560.
11. A.B.P.I. Data Sheet Compendium 1991-92, Datapharm Publications Limited, London, 1991.
12. E. De Clercq, Potential Drugs for the Treatment of AIDS, *J. Antimicrob. Chemother.*, 1989, **23**, suppl.A, 35-46.
13. D. Wilks and A.G. Dalgleish, Antiretroviral Therapy, in AIDS and the New Viruses, 55-80, A.G. Dalgleish, R.A. Weiss, Eds., Academic Press, London, 1990.
14. M. Muckenthaler, N. Gunkel, P. Levantis, K. Broadhurst, B. Goh, B. Colvin, G. Forster, G.G. Jackson and J.S. Oxford, Sequence Analysis of an HIV-1 Isolate Which Displays Unusually High-Level AZT Resistance *In Vitro*, *J. Med. Virol.*, 1992, **36**, 79-83.
15. E. De Clercq, Targets and Strategies for the Antiviral Chemotherapy of AIDS, *Trends. Pharmacol. Sci.*, 1990, **11**, 198-205.
16. B. Oberg, Antiviral Effects of Phosphonoformate (PFA, Foscarnet Sodium), *Pharmac. Ther.*, 1989, **40**, 213-285.

17. R. Pauwels, K. Andries, J. Desmyter, D. Schols, M.J. Kukla, H.J. Breslin, A. Raeymaekers, J. Van Gelder, R. Woestenborghs, J. Heykants, K. Schellekens, M.A. Janssen, E. de Clercq and P.A. Janssen, Potent and Selective Inhibition of HIV-1 Replication *In Vitro* by a Novel Series of TIBO Derivatives, *Nature*, 1990, **343**, 470-474.

18. K. de Vreese, Z. Debyser, A. Vandamme, R. Pauwels, J. Desmyter, E. de Clercq and J. Anne, Resistance of Human Immunodeficiency Virus Type I Reverse Transcriptase to TIBO Derivatives Induced by Site-Directed Mutagenesis, *Viriol.*, 1992, **188**, 900-904.

19. J.R. Huff, HIV Protease: A Novel Chemotherapeutic Target for AIDS, *J. Med. Chem.*, 1991, **34**, 2305-2314, and references therein.

20. A.S. Tyms, E.M. Berrie, T.A. Ryder, R.J. Nash, M.P. Hegarty, D.L. Taylor, M.A. Mobberley, J.M. Davies, E.A. Bell, D.J. Jeffries, D. Taylor-Robinson and L.E. Fellows, Castanospermine and other Plant Alkaloid Inhibitors of Glucosidase Activity Block the Growth of HIV, *Lancet*, 1987, 1025-1026.

21. G.W. Fleet, A. Karpas, R.A. Dwek, L.E. Fellows, A.S. Tyms, S. Petursson, S.K. Namgoong, N.G. Ramsden, P.W. Smith, J.C. Son, F. Wilson, D.R. Witty, G.S. Jacob and T.W. Rademacher, Inhibition of HIV Replication by Amino-Sugar Derivatives, *FEBS Letters*, 1988, **237**, 128-132.

22. P.C. Zamecnik, J. Goodchild, Y. Yaguchi and P.S. Sarin, Inhibition of Replication and Expression of Human T-Cells Lymphotrophic Virus Type III in Cultured Cells by Exogenous Synthetic Oligonucleotides Complementary to Viral RNA, *Proc. Natl. Acad. Sci.*, 1986, **83**, 4143-4146.

23. S. Akhtar and R.L. Juliano, Antisense DNA Oligonucleotides as Potential Therapeutic Agents, *Pharm. J.*, 1991, July 20, 89-92.

24. S. Akhtar and R.L. Juliano, Cellular Uptake and Intracellular Fate of Antisense Oligonucleotides, *Trends Cell Biol.*, 1992, **2**, 139-144.

25. A.S. Fauci, The Human Immunodeficiency Virus: Infectivity and Mechanisms of Pathogenesis, *Science*, 1988, **239**, 617-622.

26. M. Youle, J. Clarbour, P. Wade and C. Farthing, AIDS, Therapeutics in HIV Disease, Churchill Livingstone, England, 1988.

27. R.W. Price, B. Brew, J. Sidtis, M. Rosenblum, A.C. Scheck and P. Cleary, The Brain in AIDS: Central Nervous System HIV-1 Infection and AIDS Dementia Complex, *Science*, 1988, **39**, 586-592.

28. G.A. Elder and J.L. Sever, Neurologic Disorders with AIDS Retroviral Infection, *Rev. Infect. Dis.*, 1988, **10**, 286-302.

29. T.P. Bridge and L.J. Ingraham, Central Nervous System Effects of HIV-1, *Annu. Rev. Med.*, 1990, **41**, 159-168.

30. J. Sidtis and R.W. Price, Early HIV-1 Infection and the AIDS Dementia Complex, *Neurol.*, 1990, **40**, 323-326.

31. M.E. Gurney, Mechanisms of Brain Damage by HIV-1, *Pharmacol. Bull.*, 1988, **24**, 311-314.

32. E. Helgstrand, B. Eriksson, B. Johansson, B. Lannero, A. Larsson, A. Misiorny, J.O. Noren, B. Sjoberg, K. Stenberg, G. Stening, S. Stridh, B. Oberg, S. Alenius and L. Philipson, Trisodium Phosphonoformate, a New Antiviral Compound, *Science*, 1978, **201**, 819-820.

33. E.G. Sandstrom, J.C. Kaplan, R.E. Byington and M.S. Hirsch, Inhibition of Human T-Cell Lymphotrophic Virus Type III *In Vitro* by Phosphonoformate, *Lancet*, 1985, **1**, 1480-1482.

34. A. Tsuji and I. Tamai, Sodium and pH Dependent Transport of Foscarnet *via* the Phosphate Carrier System across Intestinal Brush-Border Membrane, *Biochem. Pharmacol.*, 1985, **38**, 1022-1025.

35. R. Koshida, L. Vrang, G. Gilljam, J.Harmenberg, B. Oberg and B. Wahren, Inhibition of Human Immunodeficiency Virus *In Vitro* by Combinations of 3'-Azido-3'-Deoxythymidine and Foscarnet, *Antimicrob. Agents Chemother.*, 1989, **33**, 778-780.

36. M.A. Jacobson, S. Crowe, J. Levy, F. Aweeka, J, Gambertoglio, N. McManus and J. Mills, Effect of Foscarnet Therapy on Infection with Human Immunodeficiency Virus in Patients with AIDS, *J. Infect. Dis.*, 1988, **158**, 862-865.

37. Foscavir Product Summary, 1991, Astra Pharmaceuticals Ltd, Kings Langley.

38. J. Gilquin, L. Weiss and M.D. Kazatchkine, Genital and Oral Erosions Induced by Foscarnet, *Lancet*, 1990, **335**, 287.

39. P.A. Pizzo, J. Eddy, J. Falloon, F.M. Balis, R.F. Murphy, H. Moss, P. Wolters, P. Brouwers, P. Jarowsinski, M. Rubin, S. Broder, R. Yarchoan, A. Brunetti, M. Maha, S. Nusinoff-Lehrman and D.G. Poplack, Effect of Continuous Intravenous Infusion of Zidovudine (AZT) in Children with Symptomatic HIV Infection, *N. Eng. J. Med.*, 1988, **319**, 889-896.

40. T. Terasaki and W. Pardridge, Restricted Transport of 3'-Azido-3'-Deoxythymidine and Dideoxynucleosides Through the Blood-Brain Barrier, *J. Infect. Dis.*, 1988, **158**, 630-632.

41. S.S. Good and P. de Miranda, Species Differences in the Metabolism and Disposition of Antiviral Nucleoside Analogues: 2. Zidovudine, *Antiviral Chem. Chemother.*, 1992, **3**, 65-77.

42. R. Yarchoan, G. Berg, P. Brouwers, M.A. Fischl, A.R. Spitzer, A. Wichman, J. Grafman, R.V. Thomas, B. Safai and A. Brunetti, Response of Human Immunodeficiency Virus Associated Neurological Disease to 3'-Azido-3'-Deoxythymidine, *Lancet*, 1987, **1**, 132-135.

43. S. Warren and M.R. Williams, The Acid-Catalysed Decarboxylation of Phosphonoformic Acid, *J. Chem. Soc. B*, 1971, 618-621.

44. V.J. Stella, T.J. Mikkelson and J.D. Pipkin, Prodrugs: The Control of Drug Delivery *via* Bioreversible Chemical Modification, in Drug Delivery Systems, Characteristics and Biochemical Applications, R. Juliano Ed., Oxford University Press, New York, 1980.

45. N.H. Greig, Drug Delivery to the Brain by Blood-Brain Barrier Circumvention and Drug Modification, in Implications of the Blood-Brain Barrier and its Manipulation, 311-368, E.A. Neuwelt, Ed., Plenum Medical Book Company, New York, 1989.

46. I. den Daas, P.G. Tepper and A.S. Horn, Improvement of the Oral Bioavailability of the Selective Dopamine Agonist N-0437 in Rats: the *in vitro* and *in vivo* activity of Eight Ester Prodrugs, *Naunyn-Schmiedeberg's Arch. Pharmacol.*, 1990, **341**, 186-191.

47. N.M. Nielson and H. Bundgaard, Prodrugs as Delivery Systems. Chemical and Plasma-Catalysed Hydrolysis of Various Esters of Benzoic Acid: A Reference System for Designing Prodrug Esters of Carboxylic Acid Agents, *Int. J. Pharm.*, 1987, **39**, 75-85.

48. N. Bodor, E. Shek and T. Higuchi, Delivery of a Quaternary Pyridinium Salt Across the Blood-Brain Barrier by its Dihydropyridine Derivative, *Science*, 1975, **190**, 155-156.

49. N. Bodor, R.G. Roller and S.J. Selk, Elimination of a Quaternary Pyridinium Salt Delivered as its Dihydropyridine Derivative from the Brain of Mice, *J. Pharm. Sci.*, 1978, **67**, 685-687.

50. N. Bodor and M.E. Brewster, Problems of Delivery of Drugs to the Brain, *Pharmac.Ther.*, 1983, **19**, 337-386.

51. C.K. Chu, V.S. Bhadti, K.J. Doshi, J.T. Etse, J.M. Gallo, F.D. Boudinot and R.F. Schinazi, Brain Targeting of Anti-HIV Nucleosides: Synthesis and *In Vitro* and *In Vivo* Studies of Dihydropyridine Derivatives of 3'-Azido-2',3'-dideoxyuridine and 3'-Azido-3'-deoxythymidine, *J. Med. Chem.*, 1990, **33**, 2188-2192.

52. P.F. Torrence, J. Kinjo, K. Lesiak, J. Balzarini and E. de Clerk, AIDS Dementia: Synthesis and Properties of a Derivative of 3'-Azido-3'-deoxythymidine (AZT) that may become 'Locked' in the Central Nervous System, *FEBS Letters*, 1988, **234**, 135-140.

53. E. Palomino, D. Kessel and J.P. Horwitz, A Dihydropyridine Carrier System for Sustained Delivery of 2',3'-Dideoxynucleosides to the Brain, *J. Med. Chem.*, 1989, **32**, 622-625.

54. D. Farquhar, D.N. Srivastva, N.J. Kuttesch and P.P. Saunders, Biologically Reversible Phosphate-Protective Groups, *J. Pharm. Sci.*, 1983, **72**, 324-325.

55. D.N. Srivastva and D. Farquhar, Bioreversible Phosphate Protective Groups: Synthesis and Stability of Model Acyloxymethyl Phosphates, *Bioorg. Chem.*, 1984, **12**, 118-129.

56. J.K. Sastry, P.N.Nehete, S. Khan, B.J. Nowak, W. Plunkett, R.B. Arlinghaus and D. Farquhar, Membrane-Permeable Dideoxyuridine 5'-Monophosphate Analogue Inhibits Human Immunodeficiency Virus Infection, *Mol. Pharmacol.*, 1992, **41**, 441-445.

57. S. Freeman, W.J. Irwin, A.G. Mitchell, D. Nicholls and W. Thomson, Bioreversible Protection for the Phospho Group: Chemical Stability and Bioactivation of Di(4-Acetoxybenzyl) Methylphosphonate with Carboxyesterase, *J. Chem. Soc., Chem. Commun.*, 1991, 875-877.

58. A.G. Mitchell, W. Thomson, D. Nicholls, W.J. Irwin and S. Freeman, Bioreversible Protection for the Phospho Group: Bioactivation of the Di(4-acyloxybenzyl) and Mono(4-acyloxybenzyl) Phosphoesters of Methylphosphonate and Phosphonoacetate, *J. Chem. Soc., Perkin Trans. I*, 1992, 2345-2353.

59. W. Thomson, D. Nicholls, J.S. Al-Mushadani, W.J. Irwin, S.Freeman and A. Karpas, Prodrugs of the Phospho Group: Synthesis, Bioactivation and Antiviral Testing of the 4-Acetyloxybenzyl Esters of the Phosphate of AZT, *J. Pharm. Pharmacol.*, 1992, **44**, 77P.

60. J.O. Noren, E. Helgstrand, N.G. Johansson, A. Misiorny and G. Stening, Synthesis of Esters of Phosphonoformic Acid and their Antiherpes Activity, *J. Med. Chem.*, 1983, **26**, 264-270.

61. M.M. Vaghefi, P.A. McKernan and R.K. Robins, Synthesis and Antiviral Activity of Certain Nucleoside 5'-Phosphonoformate Derivatives, *J. Med. Chem.*, 1986, **29**, 1389-1393.

62. H. Griengl, W. Hayden, G. Penn, E.D. Clercq and B. Rosenwirth, Phosphonoformate and Phosphonoacetate Derivatives of 5'-Substituted 2'-Deoxyuridines: Synthesis and Antiviral Activity, *J. Med. Chem.*, 1988, **31**, 1831-1839.

63. R.W. Lambert, J.A. Martin, G.J. Thomas, I.B. Duncan, M.J. Hall and E.P. Heimer, Synthesis and Antiviral Activity of Phosphonoacetic and Phosphonoformic Acid Esters of 5-Bromo-2'-Deoxyuridine and Related Pyrimidine Nucleosides and Acyclonucleosides, *J. Med. Chem.*, 1989, **32**, 367-374.

64. A. Rosowsky, J. Saha, F. Fazely, J. Kock and R.M. Ruprecht, Inhibition of HIV-1 Replication by Phosphonoformate Esters of 3'-Azido-3'-deoxythymidine, *Biochem. Biophys. Res. Commun.*, 1990, **172**, 288-294.

65. R.P. Iyer, L.R. Phillips, J.A. Biddle, D.R. Thakker, W. Egan, S. Aoki and H. Mitsuya, Synthesis of Acyloxyalkyl Acylphosphonates as Potential Prodrugs of the Antiviral, Trisodium Phosphonoformate (Foscarnet Sodium), *Tetrahedron Lett.*, 1989, **30**, 7141-7144.

66. A.G. Mitchell, D. Nicholls, I. Walker, W.J.Irwin and S. Freeman, Prodrugs of Phosphonoformate: Products , Kinetics and Mechanisms of Hydrolysis of Dibenzyl (Methoxycarbonyl)phosphonate, *J. Chem. Soc. Perkin Trans. 2*, 1991, 1297-1303.

67. A.G. Mitchell, D. Nicholls, W.J.Irwin and S. Freeman, Prodrugs of Phosphonoformate: The Effect of Para-substituents on the Products, Kinetics and Mechanism of Hydrolysis of Dibenzyl (Methoxycarbonyl)phosphonate, *J. Chem. Soc., Perkin Trans. 2*, 1992, 1145-1151.

68. E.S. Krol, J.M. Davis and G.R.J. Thatcher, Hydrolysis of Phosphonoformate Esters: Product Distribution and Reactivity Patterns, *J. Chem. Soc., Chem. Commun.*, 1991, 118-119.

69. C.C. Neto, J.M. Steim, P.S. Sarin, D.K. Sun, N.N. Bhongle, R.K. Piratla and J.G. Turcotte, Lipid Conjugates of Antiretroviral Agents. II. Disodium Palmityl Phosphonoformate: Anti-HIV Activity, Physical Properties and Interaction with Plasma Proteins, *Biochem. Biophys. Res. Comm.*, 1990, **171**, 458-464.

70. W.M. Pardridge, Brain Metabolism: A Perspective from the Blood-Brain Barrier, *Physiol. Rev.*, 1983, **63**, 1481-1535.

71. W.H. Oldendorf, The Blood-Brain Barrier, *Exp. Eye Res.*, 1977, Suppl., 177-190.

72. W.M. Pardridge, Recent Advances in Blood-Brain Barrier Transport, *Ann. Rev. Pharmacol. Toxicol.*, 1988, **28**, 25-39.

73. D.C. Markovitz and J.D. Fernstrom, Diet and Uptake of Aldomet by the Brain: Competition with Natural Large Neutral Amino Acids, *Science*, 1977, **197**, 1014-1015.

74. J.G. Nutt, W.R. Woodward, J.P. Hammerstad, J.H. Carter and J.L. Anderson, The 'On-Off' Phenomenon in Parkinson's Disease - Relation to Levodopa Absorption and Transport, *N. Engl. J. Med.*, 1984, **310**, 483-488.

75. N.H. Greig, S. Momma, D.J. Sweeney, Q.R. Smith and S.I. Rapoport, Facilitated Transport of Melphalan at the Rat Blood-Brain Barrier by the Large Neutral Amino Acid Carrier System, *Cancer Res.*, 1987, **47**, 1571-1576.

76. Y. Takada, N.H. Greig, D.T. Vistica, S.I. Rapoport and Q.R. Smith, Affinity of Antineoplastic Amino Acid Drugs for the Large Neutral Amino Acid Transporter of the Blood-Brain Barrier, *Cancer Chemother. Pharmacol.*, 1991, **29**, 89-94.

77. A. Garzon-Aburbeh, J.H. Poupaert, M. Claesen and P. Dumont, A Lymphotropic Prodrug of L-Dopa: Synthesis, Pharmacological Properties and Pharmacokinetic Behavior of 1,3-Dihexadecanoyl-2-[(s)-2-amino-3-(3,4-dihydroxyphenyl)propanoyl]propane-1,2,3-triol, *J. Med. Chem.*, 1986, **29**, 687-691.

78. M. Maccoss, J.J. Edwards, P.Lagocki and Y.E. Rahman, Phospholid-Nucleoside Conjugates. The Interaction of Selected 1-B-D-Arabinofuranosylcytosine-5' Diphosphate-L-1,2-Diacylglycerols with Serum Lipoproteins. *Biochem. Biophys. Res. Commun.*, 1983, **116**, 368-372.

79. M.W. Brightman, The Anatomical Basis of the Blood-Brain Barrier, in Implications of the Blood-Brain Barrier and its Manipulation, 53-78, E.A. Neuwelt, Ed., Plenum Medical Book Company, New York, 1989.

80. J.N. Jacob, V.E. Shashoua, A. Campbell and R.J. Baldessarini, γ-Aminobutyric Acid Esters. 2. Synthesis, Brain Uptake, and Pharmacological Properties of Lipid Esters of γ-Aminobutyric Acid, *J. Med. Chem.*, 1985, **28**, 106-110.

81. J.N. Jacob, G.W. Hesse and V.E. Shashoua, γ-Aminobutyric Acid Esters. 3. Synthesis, Brain Uptake, and Pharmacological Properties of C-18 Glyceryl Lipid Esters of GABA with Varying Degree of Unsaturation, *J. Med. Chem.*, 1987, **30**, 1573-1576.

82. J.N. Jacob, G.W. Hesse and V.E. Shashoua, Synthesis, Brain Uptake, and Pharmacological Properties of a Glyceryl Lipid Containing GABA and the GABA-T Inhibitor γ-Vinyl-GABA, *J. Med. Chem.*, 1990, **33**, 733-736.

83. S. Spanner, R.C. Hall and G.B. Ansell, Arterio-Venous Differences of Choline and Choline Lipids across the Brain of Rat and Rabbit, *Biochem. J.*, 1976, **154**, 133-140.

84. J.N. Hawthorne and G.B. Ansell, Phospholipids, 28-32, Elsevier Biomedical Press, Amsterdam, New York, Oxford, 1982.

85. J.M. Steim, C.C. Neto, P.S. Sarin, D.K. Sun, R.K. Sehgal and J.G. Turcotte, Lipid Conjugates of Antiretroviral Agents. I. Azidothymidine-Monophosphate-Diglyceride: Anti-HIV Activity, Physical Properties and Interaction with Plasma Proteins, *Biochem. Biophys. Res. Comm.*, 1990, **171**, 451-457.

86. J.R. Deverre, Y. Letourneux, P.Couvreur and J.P. Benoit, 1,3-Dipalmitoyl-2-(4'[bis{2-chloroethyl}amino]phenylalaninoyl) a Stable and Lymphotrophic Prodrug of Melphalan, *Proceed. Intern. Symp. Control. Rel. Bioact. Mater.*, 1991, **18**, 215-216.

87. Y. Henin, C. Gouyette, O. Schwartz, J. Debouzy, J. Neumann and T. Huynh-Dinh, Lipophilic Glycosyl Phosphotriester Derivatives of AZT: Synthesis, NMR Transmembrane Study and Antiviral Activity, *J. Med. Chem.*, 1991, **34**, 1830-1837.

88. W.M. Pardridge, Strategies for Delivery of Drugs Through the Blood-Brain Barrier, in Annual Reports in Medicinal Chemistry 20, 305-313, Academic Press, USA, 1985.

89. K. Yagi and M. Naoi, Glycolipid Insertion into Liposomes for their Targeting to Specific Organs, in Medical Applications of Liposomes, 91-97, K. Yagi, Ed., Japan Scientific Societies Press, Tokyo, 1986..

90. C. Crone, The Permeability of Brain Capillaries to Non-Electrolytes, *Acta. Physiol. Scand.*, 1965, **64**, 407-417.

91. E.M. Cornford, C.P. Diep, and W.M. Pardridge, Blood-Brain Barrier Transport of Valproic Acid, *J. Neurochem.*, 1985, **44**, 1541-1550.

92. W.M. Pardridge and W.H. Oldendorf, Kinetic Analysis of Blood-Brain Barrier Transport of Amino Acids, *Biochim. Biophys. Acta*, 1975, **401**, 128-136.

93. W.H. Oldendorf, Blood-Brain Barrier Permeability to Lactate, *Europ. Neurol.*, 1972, **6**, 49-55

94. W.H. Oldendorf, Brain Uptake of Radiolabelled Amino Acids, Amines and Hexoses after Arterial Injection, *Am. J. Physiol.*, 1971, **221**, 1629-1639.

95. M.E. Raichle, J.O. Eichling and M.G. Straatmann, Blood-Brain Barrier Permeability of ^{11}C-Labelled Alcohols and ^{15}O-Labelled Water, *Am. J. Physiol.*, 1976, **230**, 543-522.

96. D.J. Brooks, R.P. Beaney and A.A. Lammertsma, Glucose Transport Across the Blood-Brain Barrier in Normal Human Subjects and Patients with Cerebral Tumours Studied Using (^{11}C)-3-O-Methyl-D-Glucose and Positron Emission Tomograghy, *J. Cereb. Blood Flow Metab.*, 1986, **6**, 230-239.

97. Y. Takasato, S.I. Rapoport and Q.R. Smith, An *In Situ* Brain Perfusion Technique to Study Cerebrovascular Transport in the Rat, *Am. J. Physiol.*, 1984, **247**, H484-H493.

98. Q.R. Smith, S. Momma, M. Aoyagi and S.I. Rapoport, Kinetics of Neutral Amino Acid Transport across the Blood-Brain Barrier, *J. Neurochem.*, 1987, **49**, 1651-1658.

99. Y. Tsukada, Y. Nagata, S. Hirano and T. Matsutani, Active Transport of Amino Acid into Cerebral Cortex Slices, *J. Neurochem.*, 1963, **10**, 241-256.

100. K.M. Hargreaves and W.M. Pardridge, Neutral Amino Acid Transport at the Human Blood-Brain Barrier, *J. Biol. Chem.*, 1988, **263**, 19392-19397.

101. A.L. Betz and G.W. Goldstein, Polarity of the Blood-Brain Barrier: Neutral Amino Acid Transport into Isolated Brain Capillaries, *Science*, 1978, **202**, 225-226.

102. K.L. Audus and R.T. Borchardt, Characterisation of an *In Vitro* Blood-Brain Barrier Model System For Studying Drug Transport and Metabolism, *Pharm. Res.*, 1986, **3**, 81-87.

103. K.L. Audus and R.T. Borchardt, Characteristics of the Large Neutral Amino Acid Transport System of Bovine Brain Microvessel Endothelial Cell Monolayers, *J. Neurochem.*, 1986, **47**, 484-488.

104. T. Terasaki, S. Takakuwa, S. Moritani and A. Tsuji, Transport of Monocarboxylic Acids at the Blood-Brain Barrier: Studies with Monolayers of Primary Cultured Bovine Brain Capillary Endothelial Cells, *J. Pharm. Exp. Ther.*, 1991, **258**, 932-937

105. W.H. Oldendorf, Carrier-Mediated Blood-Brain Barrier Transport of Short Chain Monocarboxylic Acids, *Am. J. Physiol.*, 1973, **224**, 1450-1453.

106. R.D. Steele, Blood-Brain Barrier Transport of the α-Keto Acid Analogues of Amino Acids, *Fed. Proc.*, 1986, **45**, 2060-2064.

107. A.R. Conn and R.D. Steele, Transport of the α-Keto Acid Analogues of Amino Acids Across the Blood-Brain Barrier in Rats, *Am. J. Physiol.*, 1982, **243**, E272-E277.

108. C.F. Bigge, G. Johnson, D.F. Ortwine, J.T. Drummond, D.M. Retz, L.J. Brahce, L.L. Coughenour, F.W. Marcoux and A.W. Probert, Exploration of N-Phosphonoalkenyl-, and N-(Phosphononalkyl)phenyl-Spaced α-Amino Acids as Competitive N-Methyl-D-aspartic Acid Antagonists, *J. Med. Chem.*, 1992, **35**, 1371-1384.

109. M.J. Zabik and R.D. Schuetz, Product and Rate Studies on the Reactions of Selected Aryl Chloroformates with Silver Nitrate, *J. Med. Chem.*, 1967, **32**, 300-304.

110. G.R. Newkome and W.W. Paudler, Contemporary Heterocyclic Chemistry, John Wiley and Sons, New York, Chichester, Brisbane, Toronto, Singapore, 1982.

111. T. Morita, Y. Okamoto and H. Sakurai, A Mild and Facile Synthesis of Alkyl- and Arylphosphonyl Dichlorides under Neutral Conditions. Reaction of Bis(trimethylsilyl) Phosphonates with PCl_5, *Chem. Letts.*, 1980, 435-438.

112. M. Bodanszky and A. Bodanszky, The Practice of Peptide Synthesis, Springer-Verlag, Berlin, Heidelberg, New York, Tokyo, 1984.

113. B.F. Erlanger and R.M. Hall, The Improved Synthesis of Amino Acid Benzyl Esters, *J. Am. Chem. Soc.*, 1954, **76**, 5781-5782.

114. W.C. Still, M. Kahn and A. Mitra, Rapid Chromatographic Technique for Preparative Separations with Moderate Resolution, *J. Org. Chem.*, 1978, **43**, 2923-2925.

115. Vogel's Textbook of Practical Organic Chemistry, 4th Edition, A. Vogel, Longman, London and New York, 1978.

116. J.C. Sowden and H.O.L. Fischer, Optically Active α,β-Diglycerides, *J. Am. Chem. Soc.*, 1941, **63**, 3244-3248.

117. S. Freeman, W.J. Irwin and C.H. Schwalbe, Synthesis and Hydrolysis Studies of Phosphonopyruvate, *J. Chem. Soc. Perkin Trans. 2*, 1991, 263-267.

118. K.L. Audus, R.L. Bartel, I.J. Hidalgo and R.T. Borchardt, The Use of Cultured Epithelial and Endothelial Cells for Drug Transport and Metabolism Studies, *Pharm. Res.*, 1990, **7**, 435-451.

119. K.L. Audus and R.T. Borchardt, Bovine Brain Microvessel Endothelial Cell Monolayers as a Model System for the Blood-Brain Barrier, *Ann. N. Y. Acc. Sci.*, 1987, **507**, 9-18.

120. M.V. Shah, K.L. Audus and R.T. Borchardt, The Application of Bovine Brain Microvessel Endothelial-Cell Monolayers Grown onto Polycarbonate Membranes *In Vitro* to Estimate the Potential Permeability of Solutes Through the Blood-Brain Barrier, *Pharm. Res.*, 1989, **6**, 624-627.

121. J.B. van Bree, A.G. de Boer, M. Danhof, L.A. Ginsel and D.D. Breimer, Characterisation of an *In Vitro* Blood-Brain Barrier: Effects of Molecular Size and Lipophilicity on Cerebrovascular Endothelial Transport Rates of Drugs, *J. Pharm. Exp. Ther.*, 1988, **247**,1233-1239.

122. W.M. Pardridge, D. Triguero, J. Yang and P.A. Cancilla, Comparison of *In Vitro* and *In Vivo* Models of Drug Transcytosis Through the Blood-Brain Barrier, *J. Pharm. Exp. Ther.*, 1990, **253**, 884-891.

123. G.W. Goldstein, The Blood-Brain Barrier: Interactions Between Endothelial Cells and Astrocytes, *Mead Johnson Symposium on Perinatal and Developmental Medicine*, 1987, **29**, 15-17.

124. L.E. DeBault and P.A. Cancilla, γ-Glutamyl Transpeptidase in Isolated Brain Endothelial Cells: Induction by Glial Cells *In Vitro*, *Science*, 1980, **207**, 653-655.

125. M.P. Dehouck, S. Meresse, P. Delorme, J.C. Fruchart and R. Cecchelli, An Easier, Reproducible, and Mass-Production Method to Study the Blood-Brain Barrier *In Vitro*, *J. Neurochem.*, 1990, **54**, 1798-1801.

126. F.E. Arthur, R.R. Shivers and P.D. Bowman, Astrocyte-Mediated Induction of Tight Junctions in Brain Capillary Endothelium: An Efficient *In Vitro* Model, *Dev. Brain Res.*, 1987, **36**, 155-159.

127. T.J. Raub, S.L. Kuentzel and G.A. Sawada, Permeability of Bovine Brain Microvessel Endothelial Cells *In Vitro*: Barrier Tightening by a Factor Released by Astroglioma Cells, *Exp. Cell Res.*, 1992, **199**, 330-340.

128. K. Maxwell, J.A. Berliner and P.A. Cancilla, Stimulation of Glucose Analogue Uptake by Cerebral Microvessel Endothelial Cells by a Product Released by Astrocytes, *J. Neuropath. Exp. Neurol.*, 1989, **48**, 69-80.

129. Y. Takakura, A.M. Trammel, S.L. Kuentzel, T.J. Raub, A. Davies, S.A. Baldwin and R.T. Borchardt, Hexose Uptake in Primary Cultures of Bovine Brain Microvessel Endothelial Cells. Effects of Conditioned Media from Astroglial and Glioma Cells, *Biochim. Biophys. Acta.*, 1991, **1070**, 11-19.

130. M.P. Dehouck, P. Jolliet-Riant, F. Bree, J.C. Fruchart, R. Cecchelli and J.P. Tillement, Drug Transfer Across the Blood-Brain Barrier: Correlation Between *In Vitro* and *In Vivo* Models, *J. Neurochem.*, 1992, **58**, 1790-1797.

131. M.P. Dehouck, S. Meresse, B. Dehouck, J.C. Fruchart and R. Cecchelli, *In Vitro* Reconstituted Blood-Brain Barrier, *J. Cont. Rel.*, 1992, **21**, 81-92.

132. L.L. Rubin, S. Porter, H.C. Horner and T.A. Yednock, Blood-Brain Barrier Model, International Patent, WO91/05038, 18th April 1991.

133. U. Mischeck, J. Meyer and H.J. Galla, Characterisation of γ-Glutamyl Transpeptidase Activity of Cultured Endothelial Cells from Porcine Brain Capillaries, *Cell Tissue. Res.*, 1989, **256**, 221-226.

134. W. Risau, A. Dingler, U. Albrecht, M. Dehouck and R. Cecchelli, Blood-Brain Barrier Pericytes are the Main Source of γ-Glutamyl Transpeptidase Activity in Brain Capillaries, *J. Neurochem.*, 1992, **58**, 667-672.

135. H. Kukushima, M. Fujimoto and M. Ide, Quantitative Detection of Blood-Brain Barrier-Associated enzymes in Cultured Endothelial cells of Porcine Brain Microvessels, *In Vitro Cell. Dev. Biol.*, 1990, **26**, 612-620

136. J. Meyer, U. Mischeck, M. Veyhl, K. Henzel and H. Galla, Blood-Brain Barrier Characteristic Enzymatic Properties in Cultured Brain Capillary Endothelial Cells, *Brain Res.*, 1990, **514**, 305-309.

137. S. Rim, K.L. Audus and R.T. Borchardt, Relationship of Octanol / Buffer and Octanol / Water Partition Coefficients to Transcellular Diffusion across Brain Microvessel Endothelial Cell Monolayers, *Int. J. Pharm.*, 1986, **32**, 79-84.

138. Paul Nicklin, Aston University, Personal Communication.

139. W.M. Scheld, Drug Delivery to the Central Nervous System: General Principles and Relevance to Therapy for Infections of the Central Nervous System, *Rev. Infect. Dis.*, 1989, **11**, S1669-S1690.

140. Y.S. Kang, T. Terasaki and A. Tsuji, Acidic Drug Transport *In Vivo* Through the Blood-Brain Barrier. A Role of the Transport Carrier for Monocarboxylic Acids, *J. Pharmacobio-Dyn*, 1990, **13**, 158-163.

141. A.L. Betz and G.W. Goldstein, The Basis for Active Transport at the Blood-Brain Barrier, *Adv. Exp. Med. Biol.*, 1980, **131**, 5-16

142. W.H. Oldendorf, Stereospecificity of Blood-Brain Barrier Permeability to Amino Acids, *Am. J. Physiol.*, 1973, **224**, 967-969.

143. P.A. Cancilla and L.E. DeBault, Neutral Amino Acid Transport Properties of Cerebral Endothelial Cells *In Vitro*, *J. Neuropath. Exp. Neurol.*, 1983, **42**, 191-199.

144. Y. Takada, D.T. Vistica, N.H. Greig, D. Purdon, S.I. Rapoport and Q.R. Smith, Rapid High-Affinity Transport of a Chemotherapeutic Amino Acid Across the Blood-Brain Barrier, *Cancer Res.*, 1992, **52**, 2191-2196.

145. A.G. Mitchell, Ph.D. Thesis, Aston University, 1991.

146. H.C. Holmes, N. Mahmood, A. Karpas, J.Petrik, D. Kinchington, T. O'Conner, D.J. Jeffries, J. Desmyter, E. De Clercq, R. Pauwels and A. Hay, Screening of Compounds for Activity against HIV: A Collaborative Study, *Antiviral Chem. Chemother.*, 1991, **2**, 287-293.